

The 18kDa translocator protein in human glioma

A thesis Submitted to the University of Manchester

For the degree of Doctor of Philosophy

in the Faculty of Biology, Medicine and Health

PhD Medicine

2020

Bahiya Mohammed Osrah

School of Biological Sciences

Faculty of Biology, Medicine and Health

Blank page

| | |
|------------------------------------|-----------|
| LIST OF CONTENTS | 4 |
| LIST OF FIGURES..... | 10 |
| LIST OF TABLES..... | 14 |
| LIST OF ABBREVIATIONS | 16 |
| ABSTRACT | 18 |
| DECLARATION | 19 |
| COPYRIGHT | 19 |
| ACKNOWLEDGEMENTS | 22 |

LIST OF CONTENTS

| | |
|-------------------------------------------------------------------|-----------|
| Chapter1: Introduction..... | 24 |
| 1.1. General overview..... | 24 |
| 1.1.1. TSPO gene..... | 24 |
| 1.1.2. TSPO protein structure | 25 |
| 1.1.3. TSPO history..... | 30 |
| 1.1.4. TSPO expression in normal and pathological conditions..... | 31 |
| 1.1.5. TSPO expression in gliomas..... | 32 |
| 1.2. TSPO's function..... | 34 |
| 1.3. TSPO expression regulation..... | 38 |
| 1.3.1. Genes involved in the regulation of TSPO expression | 38 |
| 1.3.2. Epigenetic regulation..... | 42 |
| 1.3.2.1. Definition..... | 42 |
| 1.3.2.2. Promoter Methylation in different cancers..... | 44 |
| 1.4. Gliomas..... | 45 |
| 1.4.1. Introduction..... | 45 |
| 1.4.2. WHO classification..... | 46 |
| 1.4.3. Epigenetic methylation in gliomas..... | 52 |
| 1.4.4. Oligodendrogliomas..... | 54 |
| 1.4.5. Imaging and Diagnosis of oligodendrogliomas..... | 54 |
| 1.4.6. Histopathological analysis..... | 55 |
| 1.4.7. Oligodendrogliomas treatment and follow-up..... | 56 |
| 1.4.7.1. Chemotherapy and radiotherapy..... | 56 |
| 1.5. Molecular Imaging of gliomas..... | 58 |
| 1.5.1. Positron Emission Tomography (PET) scan..... | 58 |

| | | |
|-----------------|--------------------------------------------------------------------------------|----|
| 1.5.2. | Development of PET tracers..... | 59 |
| 1.5.3. | PET and TSPO tracers..... | 61 |
| 1.6. | TSPO expression in neurovascular unit at the blood brain barrier (BBB)..... | 64 |
| 1.6.1. | The neuro-vascular Unit (NVU)..... | 64 |
| 1.6.1.1. | Endothelial cells..... | 64 |
| 1.6.1.2. | Astrocytes..... | 65 |
| 1.6.1.3. | Pericytes..... | 66 |
| 1.6.1.4. | microglia/macrophage..... | 67 |
| 1.6.2. | Glioma-associated microglia and macrophage..... | 69 |
| 1.6.3. | Vascular pathology and inflammatory contributions in glioma growth..... | 71 |
| 1.6.4. | PET imaging and inclusion of vascular components in the kinetic modelling..... | 74 |
| 1.7. | Current study insights and purposes | 75 |
| Chapter 2 | | 77 |
| 2.1. | Hypothesis..... | 77 |
| 2.2. | Study rationale and background..... | 77 |
| 2.3. | Material and methods..... | 81 |
| 2.3.1. | Primary endothelial cells (PBECS) isolation and culture | 81 |
| 2.3.2. | Astrocyte isolation from porcine brains..... | 82 |
| 2.3.3. | Porcine immortalised macrophage cell line culture..... | 84 |
| 2.3.4. | Mitotracker for isolated primary cells and cell lines..... | 84 |
| 2.3.5. | Immunocytochemistry for primary cells..... | 85 |
| 2.3.6. | Western Blot | 86 |
| 2.3.7. | RNA isolation of cultured cells..... | 88 |

| | |
|------------------------------------------------------------------------------------------------------------------|------------|
| 2.3.8. RT-qPCR..... | 89 |
| 2.3.9. Scatchard analysis..... | 89 |
| 2.4. Results..... | 92 |
| 2.4.1. TSPO subcellular expression in porcine <i>in vitro</i> cell culture..... | 92 |
| 2.4.1.1. TSPO and Iba1 colocalisation in macrophage cell lines..... | 93 |
| 2.4.1.2. TSPO and mitotraker colocalisation in macrophage..... | 94 |
| 2.4.1.3. TSPO and GFAP colocalisation in porcine astrocytes..... | 95 |
| 2.4.1.4. TSPO and mitotracker colocalisation in porcine astrocytes..... | 97 |
| 2.4.1.5. TSPO and GFAP in rat astrocytes..... | 99 |
| 2.4.1.6. TSPO and CD31 colocalisation in porcine endothelial cells (PBECs)..... | 100 |
| 2.4.1.7. TSPO and mitotraker colocalisation in porcine endothelial cells (PBECs)..... | 101 |
| 2.4.2. TSPO subcellular expression in porcine brain cell lines by protein extraction and western blotting..... | 102 |
| 2.4.3. TSPO subcellular expression in porcine astrocytes, macrophage and PBECs by RNA extraction and RTqPCR..... | 103 |
| 2.4.4. [¹⁸ F] DPA-714 specific binding and affinity bindings in PBECs and macrophages..... | 104 |
| 2.5. Discussion..... | 112 |
| 2.6. Conclusion..... | 116 |
| Chapter 3..... | 118 |
| 3.1. Hypotheses..... | 118 |

| | |
|-----------------------------------------------------------------------------------------------------------------------|------------|
| 3.2. Study rationale and background..... | 122 |
| 3.3. Material and methods..... | 125 |
| 3.3.1. Immunohistochemistry of FFPE tissue sections for oligodendrogliomas..... | 125 |
| 3.3.2. Evaluation of peroxidase immunohistochemistry..... | 126 |
| 3.3.3. Tissue microarrays (TMA)..... | 128 |
| 3.3.3.1. The TMA construction process..... | 128 |
| 3.3.3.2. TMA 3D analysis for TSPO in neoplastic, GAMMs, and endothelial cells..... | 131 |
| 3.3.4. Mass Cytometry Analysis..... | 133 |
| 3.3.5. DNA isolation for polymorphism | 134 |
| 3.3.6. [¹¹C]-(R)PK11195 PET Imaging..... | 138 |
| 3.4. Results..... | 145 |
| 3.4.1. TSPO is a biomarker for oligodendroglioma progression..... | 145 |
| 3.4.2. TSPO expression analysis in neoplastic, GAMMs and endothelial cells (3D tissue analysis)..... | 157 |
| 3.4.3. TSPO can predict the overall survival of oligodendrogliomas patients but not the progression free | 162 |
| 3.4.4. TSPO polymorphism (rs6971) in oligodendrogliomas | 162 |
| 3.5. Discussion..... | 173 |
| 3.6. Conclusion..... | 178 |
| Chapter 4..... | 180 |
| 4.1. Hypothesis..... | 180 |
| 4.2. Study rationale and background..... | 181 |
| 4.3. Material and methods..... | 183 |
| 4.3.1. RNA isolation from frozen brain samples of oligodendroglioma..... | 183 |

| | |
|--------------------------------------------------------------------------------------------------------------------------------|------------|
| 4.3.2. RNA sequencing: Illumina Truseq RNA libraries..... | 184 |
| 4.3.3. RNAseq data analysis..... | 185 |
| 4.3.4. TSPO promoter methylation analysis..... | 186 |
| 4.3.5. In-silico candidate genes expression analysis from The Cancer Genome Atlas Programme database..... | 194 |
| 4.4. Results..... | 196 |
| 4.4.1. RNA sequencing (RNA-seq) data selection..... | 196 |
| 4.4.2. RNA sequencing (RNA-seq) analysis..... | 198 |
| 4.4.3. RNA-seq for oligodendroglioma cases with high vs low TSPO transcriptome expression level in (frozen brain tissues)..... | 204 |
| 4.4.3.1. IPA adjusted to p-value <0.05, Fold-change >1, CNS and cancer..... | 207 |
| 4.4.3.2. IPA adjusted to p-value <0.05, Fold-change >1, FDR<0.05 CNS and cancer..... | 209 |
| 4.4.4. The Cancer Genome Atlas program online database (TCGA)..... | 211 |
| 4.4.4.1. Oligodendrogliomas cases with high TSPO transcriptome expression level..... | 212 |
| 4.4.4.2. Oligodendrogliomas cases with low TSPO transcriptome expression level..... | 214 |
| 4.4.4.3. Astrocytomas cases with high TSPO transcriptome expression level..... | 217 |
| 4.4.4.4. Astrocytomas cases with low TSPO transcriptome expression level..... | 218 |
| 4.4.4.5. Synopsis of the results..... | 228 |

| | |
|-------------------------------------------|-----|
| 4.4.5. Methylation analysis results | 231 |
| 4.5. Discussion..... | 234 |
| 4.6. Conclusion..... | 239 |
| Chapter 5..... | 241 |
| 5.1. General discussion..... | 241 |
| 5.2. General conclusion..... | 245 |
| 5.2.1. Synopsis of the main findings..... | 245 |
| 5.2.2. Future direction..... | 246 |
| References..... | 248 |
| Appendix..... | 274 |

LIST OF FIGURES

| | |
|-------------------------------------------------------------------------------------------------------------------------------------------------------------------------------------------|------------|
| Figure 1: The TSPO amino acid sequence homology..... | 26 |
| Figure 2: TSPO protein structure..... | 27 |
| Figure 3: TSPO in the outer mitochondrial membrane as part of a heterooligometric complex..... | 28 |
| Figure 4: Summary of the genes studied in the literature and their roles in regulating TSPO expression..... | 40 |
| Figure 5: Neurovascular unit cellular composition in brain (NVU). Biorender software..... | 64 |
| Figure 6: Representative images for TSPO/Iba1 immunofluorescence staining in Macrophage cell line. 40x original magnification..... | 93 |
| Figure 7: Representative images for TSPO/mitotracker immunofluorescence staining in Porcine primary macrophage cells. 40x original magnification..... | 94 |
| Figure 8: Representative images for TSPO/GFAP immunofluorescence staining showing TSPO basal level in Porcine primary isolated astrocytes cells..... | 95 |
| Figure 9: Representative images for TSPO/Mitotracker immunofluorescence staining showing TSPO mitochondrial subcellular location in porcine primary isolated astrocytes cells..... | 97 |
| Figure 10: Representative images for TSPO/GFAP immunofluorescence staining in rat astrocytes cell line. 40x original magnification..... | 99 |
| Figure 11: Representative images for TSPO/CD31 immunofluorescence staining in PBECs. 40x original magnification..... | 100 |
| Figure 12: Representative images for TSPO and Mitotracker in PBECs..... | 101 |
| Figure 13: TSPO expression in PBECs, macrophage, and astrocytes cell lines as assessed using western blotting..... | 102 |
| Figure 14: RT-qPCR of TSPO expression level in three different cell types, Macrophages, PBECs and Astrocytes..... | 103 |
| Figure 15: The Scatchard plots and saturation curves showing the estimated Bmax and Kd values for both PBECs and macrophages..... | 107 |
| Figure 16: Flow chart summarising three different cohorts in TSPO expression study..... | 121 |

| | |
|-----------------------------------------------------------------------------------------------------------------------------------------------------------------------------------------------------------------------------|------------|
| Figure 17: ImageJ thresholding to quantify the TSPO expression..... | 127 |
| Figure 18: TMA construction process and staining process..... | 130 |
| Figure 19: TSPO colocalisation algorithm protocol for 3D quantification..... | 132 |
| Figure 20: TSPO homo sapiens polymorphism rs6971..... | 137 |
| Figure 21: Segmentation process..... | 141 |
| Figure 22: Manual correction of the inaccurate brain boundaries by Analyze software..... | 143 |
| Figure 23: Steps of generating binding potential map. | 144 |
| Figure 24: TSPO expression in low-grade (LGO) and anaplastic (AO) oligodendrogliomas by immunohistochemistry..... | 148 |
| Figure 25: TSPO expression in oligodendrogliomas (LGO and AO) by immunohistochemistry..... | 149 |
| Figure 26: TSPO expression (IHC) quantification by ImageJ in oligodendroglioma (LGO and AO) and astrocytomas (LGA and AA). | 152 |
| Figure 27: Anaplastic oligodendroglioma (AO) showing areas with increased [¹¹ C]- (R)PK11195 uptake, (transverse- coronal -sagittal). | 153 |
| Figure 28: Low grade oligodendroglioma (LGO) showing areas with [¹¹ C]- (R)PK11195 uptake, (transverse- coronal –sagittal) | 154 |
| Figure 29: Anaplastic astrocytoma (AA) showing areas with increased [¹¹ C]- (R)PK11195 uptake, (transverse- coronal -sagittal) | 155 |
| Figure 30: Low grade astrocytoma (LGA) showing areas with [¹¹ C]- (R)PK11195 uptake, (transverse- coronal sagittal)..... | 156 |
| Figure 31: Quantification of TSPO expression from endothelial cells, neoplastic and GAMMs in constructed TMA of biopsies taken from high [¹¹ C]- (R)PK-11195 binding potential in PET imaging..... | 161 |
| Figure 32: Kaplan-Meier survival analysis of overall survival in oligodendroglioma cases (n=50)..... | 165 |

| | |
|---------------------------------------------------------------------------------------------------------------------------------------------------------------------------------------|------------|
| Figure 33: Kaplan-Meier survival analysis of progression-free in oligodendroglioma cases (n=50). | 168 |
| Figure 34: Kaplan-Meier overall survival in oligodendroglioma cases with A147T polymorphism | 171 |
| Figure 35: Infinium HD methylation protocol workflow..... | 193 |
| Figure 36: mRNA normalized counts generated from RNA-seq..... | 197 |
| Figure 37: Candidate genes from RNA-seq with IPA analysis adjusted to p-value <0.05, Fold-change >1, CNS and cancer..... | 207 |
| Figure 38: Candidate genes from RNA-seq with IPA adjusted to p-value <0.05, Fold-change >1, FDR<0.05, CNS and cancer..... | 209 |
| Figure 39: FPKM values extracted from TCGA database..... | 211 |
| Figure 40: Candidate genes for oligodendroglioma cases (n=25) extracted from TCGA that has high level of TSPO expression more than the 75th percentiles in cancer and CNS..... | 219 |
| Figure 41: Candidate genes for oligodendroglioma cases (n=24) extracted from TCGA that has low level of TSPO expression less than the 25th percentile..... | 220 |
| Figure 42: Candidate genes for oligodendroglioma cases (n=24) subcellular compartment view of the gene candidate's subcellular distribution in cancer and CNS field..... | 221 |
| Figure 43: Candidate genes for astrocytomas cases (n=26) extracted from TCGA that has high level of TSPO expression more than the 75th percentiles..... | 225 |
| Figure 44: Candidate genes for astrocytomas cases (n=23) extracted from TCGA that has low level of TSPO expression less than the 25th percentile..... | 226 |
| Figure 45: Synopsis of the previously suggested candidate genes in the literature..... | 229 |
| Figure 46: Synopsis of the main candidate genes after comparing TCGA with RNA-seq analysis..... | 230 |

Figure 47: The average mean beta pattern difference between two groups (TSPO low and high protein expression level) along the CpG island. 232

Figure 48: DNA methylation (beta value) across the TSPO CpG sequence BLAT matched to hg19 = chr22:43,547,320-43,548,169.....233

Figure 49: Summary for the main findings in the thesis.....247

LIST OF TABLES

| | |
|------------------------------------------------------------------------------------------------------------------------------------------------------------------------------------------------------------------|------------|
| Table 1: Summary of the histological and genotypic hallmarks of different gliomas histotypes | 49 |
| Table 2: Primer sequences and PCR conditions..... | 136 |
| Table 3: List of oligodendrogliomas cohort used in methylation, RNA-seq, TSPO expression and survival curve..... | 146 |
| Table 4: List of twenty-six patients of astrocytomas and oligodendroglioma. | 151 |
| Table 5: Statistical analysis of the TSPO expression in LGO, AO, LGA, and AA..... | 152 |
| Table 6: Statistical analysis summary for the studied cases. Statistical Multiple ANOVA with Tukey's test for anaplastic oligodendrogliomas (AO) | 161 |
| Table 7: Chi-square and statistical analysis of Kaplan-Meier overall survival (OS) | 166 |
| Table 8: Chi-square and statistical analysis of Kaplan-Meier progression-Free..... | 169 |
| Table 9: Chi-square and statistical analysis of Kaplan-Meier overall-survival (OS) between group of A147T (mutated) and normal TSPO groups..... | 172 |
| Table 10: Genes from RNA-seq dataset and their corresponding interactive pathways..... | 204 |
| Table 11: A summary of the candidate genes from RNA-seq dataset with IPA knowledge base in both cancer and central nervous system fields, p-value<0.05,Log2>1 | 208 |
| Table 12: A summary of candidate genes from RNA seq dataset that have been filtered based on the knowledge base in both cancer and central nervous system (CNS) fields, p-value<0.05,Log2>1 FDR<0.05..... | 210 |
| Table 13: A summary of candidate genes in oligodendroglioma cases with low and high TSPO transcriptome expression level in CNS and cancer..... | 222 |

Table 14: A summary of candidate genes from TCGA dataset in oligodendroglioma cases with low and high TSPO expression level in cancer field.
.....**223**

Table 15: A summary of candidate genes from TCGA dataset in astrocytomas cases with low and high TSPO expression level in cancer and CNS.....**227**

LIST OF ABBREVIATIONS

| | |
|---------------|----------------------------------------------------------------------------------------------------------------------------------------------|
| 1p/19q | Short arm chromosome 1 (1p) and long arm chromosome 19 (19q) co-deletion |
| α -SMA | Smooth Muscle Alpha-actin |
| AA | Anaplastic Astrocytoma |
| ADC | Apparent Diffusion Coefficient |
| ANT | Adenine Nucleotide Transporter |
| AO | Anaplastic Oligodendroglioma |
| Apaf-1 | Apoptotic protease-activating factor 1 |
| AR/PR | Androgen receptor/progesterone receptor |
| ATRX | Alpha-thalassemia/mental retardation X-linked |
| BBB | Blood brain barrier |
| BPND | Binding Potential Non-Displaceable ratio at equilibrium of specifically bound Radioligand to that of non-displaceable radioligand in tissue. |
| CBV | Cerebral Blood Volume |
| CIMP | CpG island methylator phenotype |
| CMT | Carrier-mediated transport |
| CNS | Central Nervous System |
| CORT | Corticosteroid |
| CRAC | Conserved Cholesterol Recognition Amino acid Consensus |
| CSF | Cerebrospinal Fluid |
| CYP11A1 | Cytochrome p450 family member |
| D-2HG | D-2-hydroxyglutarate |
| DIF | Double Immunofluorescence |
| Ets1/2 | E26 oncogene homologue |
| FDG | [18F]-fluoro-deoxyglucose |
| FET | Fluoro-Ethyl-Tyrosine |
| FISH | Fluorescence In Situ Hybridization |
| FLAIR | Fluid Attenuation Inversion Recovery |
| FZD9 | Frizzled receptor family |
| GABAA | Gamma-aminobutyric acid type A |
| GAMM | Glioma Associated Macrophages and Microglia |
| GBM | Glioblastoma Multiforme |
| GFAP | Glial fibrillary acidic protein |
| GLUT1 | Glucose transporter 1 |
| GM | Grey Matter |
| HAT | Histone acetyltransferase |
| HE | Hematoxylin-Eosin |
| HGG | High Grade Glioma |
| HK2 | Hexokinase-2 |
| HRRT | High Resolution Research Tomography |
| IDH | Isocitrate Dehydrogenase |

| | |
|----------------|---------------------------------------------------------------------------|
| IHC | Immunohistochemistry |
| IL-8 | Interleukin-8 |
| KM | Kaplan-Meier |
| LAT | Large Amino acid Transporter |
| LDH | lactate dehydrogenase |
| LGA | Low Grade Astrocytoma |
| LGG | Low Grade Glioma |
| LGO | Low Grade Oligodendroglioma |
| M1/M2 | pro-inflammatory phenotypes/anti-inflammatory |
| MMP | Matrix metallopeptidases |
| mPTP | Mitochondrial permeability transition pore |
| NOX2 | NADPH oxidase 2 |
| NVU | The neurovascular unit |
| PBR | Peripheral-type benzodiazepine receptor). |
| PDGFR β | Platelet derived growth factor receptor- β |
| PET | Positron emission tomography |
| PK 11195 | 1-(2-chlorophenyl)-N-methyl-N-(1-methylpropyl)23-isoquinoline-carboxamide |
| PKC ϵ | Protein kinase C family |
| PMA | Phorbol-12-myristate 13-acetate |
| ROS | Reactive oxygen species |
| SLC | Solute carriers |
| StAR | Steroidogenic acute regulatory protein |
| TMA | Tissue microarray |
| TNFRSF10 | Tumour necrosis factor receptor superfamily ten |
| TP53 | Tumour Protein p53 |
| VDAC | Voltage dependent anion channel |
| VEGF-A | Vascular endothelial growth factor A |
| α -KG | α -ketoglutarate |

Abstract

The translocator protein (TSPO) is a mitochondrial protein with five transmembrane domains. It is involved in many biological functions including cholesterol transport, cell proliferation and apoptosis. TSPO is expressed at a low level in normal brain tissues but its expression is up-regulated in brain tumours and many inflammatory diseases. A positive correlation has been identified between TSPO and proliferation in brain tumours suggesting a possible role for TSPO in tumour progression. Vascular endothelial cells and glial cells have been shown to express TSPO in many neuropathological conditions, including tumours of the central nervous system (CNS). Therefore, studying the contribution of neurovascular unit (NVU) cellular components to TSPO expression warrants further research. Here, TSPO expression was examined for several cell types of the NVU via immunohistochemistry (IHC) and immunofluorescence (IF). TSPO was found to be expressed by astrocytes, macrophages and endothelial cells in normal condition. Additionally, TSPO expression levels in glioma associated macrophages/microglia (GAMMs) and vascular tissues in oligodendroglioma has not been previously studied. This perhaps represents a missed opportunity to utilize TSPO expression as a diagnostic marker or predictor of tumour behaviour. Therefore, tissue microarray (TMA) and Mass Cytometry have been used to examine the vascular, GAMMs and neoplastic TSPO expression in oligodendrogliomas. It was noted in TMA analysis that neoplastic cell contribution to overall TSPO expression levels was greater compared to the vascular (CD31) and inflammatory cell (GAMMs) components. Next, tissue from fifty oligodendrogliomas was examined by IHC to discern whether TSPO expression varied significantly between low (WHO II) and high grade (WHO III) tumours. TSPO expression was significantly increased in high-grade oligodendrogliomas compared to low-grade. Furthermore, TSPO was found to be a predictor of prognosis for oligodendroglioma patients. High TSPO expression levels correlated with poor outcome in terms of disease progression and mean survival time. Furthermore, the regulation of TSPO expression is very poorly understood. This thesis has studied the epigenetic regulatory mechanism that might control TSPO expression in oligodendroglioma. For that purpose, DNA was isolated from thirty-eight cases of oligodendrogliomas and the methylation status of the TSPO gene and its promoter examined by using the Infinium methylation EPIC beadChip. No difference within the promoter methylation state was seen between samples showing high or low TSPO expression. As an alternative mechanism, RNA sequencing for oligodendroglioma frozen tissues RNA samples was done to identify possible candidate's genes which might regulate TSPO expression.

In conclusion, this thesis has identified TSPO as a possible biomarker of oligodendroglioma progression and patient's survival. It provided a wide coverage of the possible cellular components that contributed to TSPO expression in NVU and oligodendrogliomas. Moreover, TSPO expression was not found to be regulated by promoter methylation suggesting other alternative mechanism which might be involved.

Declaration

No portion of the work referred to in the thesis has been submitted in support of an application for another degree or qualification of this or any other university or other institute of learning.

Copyright statement

i. The author of this thesis (including any appendices and/or schedules to this thesis) owns certain copyright or related rights in it (the “Copyright”) and she has given The University of Manchester certain rights to use such Copyright, including for administrative purposes.

ii. Copies of this thesis, either in full or in extracts and whether in hard or electronic copy, may be made only in accordance with the Copyright, Designs and Patents Act 1988 (as amended) and regulations issued under it or, where appropriate, in accordance with licensing agreements which the University has from time to time. This page must form part of any such copies made.

iii. The ownership of certain Copyright, patents, designs, trademarks and other intellectual property (the “Intellectual Property”) and any reproductions of copyright works in the thesis, for example graphs and tables (“Reproductions”), which may be described in this thesis, may not be owned by the author and may be owned by third parties. Such Intellectual Property and Reproductions cannot and must not be made available for use without the prior written permission of the owner(s) of the relevant Intellectual Property and/or Reproductions.

iv. Further information on the conditions under which disclosure, publication and commercialisation of this thesis, the Copyright and any Intellectual Property and/or Reproductions described in it may take place is available in the University IP Policy (see <http://documents.manchester.ac.uk/DocuInfo.aspx?DocID=24420>), in any relevant Thesis

restriction declarations deposited in the University Library, The University Library's regulations (see <http://www.library.manchester.ac.uk/about/regulations/>) and in The University's policy on Presentation of Theses.

I dictate my PhD thesis to:

My precious parents

and

my lovely sisters Hifa and Hibah

for their love, supports and strong belief in me

Acknowledgements

I would like to thank my supervisor, professor Federico Roncaroli and my co-supervisors, professor Karl Herholz and Dr David Coope, for giving me the opportunity to work on this project. I wish to express my gratitude to professor Nigel Hooper, professor Jeff Penny, and professor David Brough groups for their cooperation and supports during my PhD lab work. My special thanks would go to Dr Kate Fisher and Monica Seif from professor Nigel Hooper group for all their sincere supports during my PhD. I would not be able to accomplish my lab work without their advices and emotional supports.

My sincere gratitude and appreciation would go to my lovely parents (Mohammed Osrah and Najat Zawawi) and sisters, Haifa and Hibah, who were always there for me with a strong belief and love. I passed all the difficult times with your warm prayers and continuous strong faith. I'm lucky to have you in my life. I would also like to thank my best friend and brother, Nadeem Osrah, for his sincere support and encouragement. I'm blessed to have you all in my life.

My warm thanks to my best friends who were always there for me with emotional support during the hard times, Sarah Alnajar, Fatimah Zawawi, Hadeer Mattar, Anwar Kerdawi and Hana Sonbol.

Finally, special thanks would go to King Abdulaziz University for supporting this research.

CHAPTER 1

INTRODUCTION

INTRODUCTION

1.1. General overview

The translocator protein (TSPO) is an outer mitochondrial protein with five transmembrane domains. It was discovered in 1977 by Braestrup as a peripheral binding site for benzodiazepines that is distinct from the central nervous system (CNS) receptor (gamma-aminobutyric acid type A [GABA_A]) [1]. It is expressed at low basal levels in normal brain tissues, but its expression is dramatically induced in Alzheimer disease (AD), multiple sclerosis (MS), Huntington disease (HD), Parkinson disease and brain tumours [2-10]. Therefore, enormous studies were invested to study using TSPO as a diagnostic target in different brain diseases, including brain tumours with positron emission tomography (PET) imaging technique.

1.1.1. The TSPO gene

The human TSPO gene is localised on the long arm of chromosome 22 (22q) and band 22q13.2 [11, 12]. It is composed of four exons with a total size of 11729 bp [13]. Lin et al. indicated that exon 1 contains a 5' untranslated region (5'-UTR) and is separated from the other exons by a large intron with an approximate size of 6 kb. The sizes of introns 2 and 3 were determined to be about 1.8 and 0.9 kb, respectively. Sequence analysis of the TSPO promoter conducted by Batarseh et al. indicates that the human TSPO promoter lacks the TATA and CCAAT elements. The TSPO gene is situated within a CpG island about 470 bp upstream and 615 bp downstream of the TSPO transcription initiation site, which may be an important region for TSPO expression regulation. The proximal TSPO promoter is GC rich and contains six copies of G(A)GGCGG(A) that serve as binding sites for several

transcription factors, including erythroblastosis virus E26 oncogene homologue (Ets, v-ets), activating protein-1 (Ap1), specificity protein 1/specificity protein 3 (SP1/SP3), activating protein 2 (Ap2), I kappa 2 (Ik2, a member of the I kappa B kinase family), GATA consensus sequence DNA binding transcription factor (GATA), Sry related HMG box (SOX) and SRY, which may also play important roles in the regulation of TSPO expression [14].

1.1.2. TSPO protein structure

The TSPO protein is composed of 169 amino acids and has a molecular weight of 18 kDa with five transmembrane helices [15, 16]. The N-terminus is expanded into the intermembrane space, and the C-terminus is expanded into the cytoplasm [17]. The TSPO protein structure shows a relatively evolutionarily conserved amino acid sequence between *Homo sapiens* and other species: The sequence homologies of *Homo sapiens* TSPO to TSPO from *Rhodobacter sphaeroides* (Proteobacteria), *Drosophila melanogaster*, *Danio rerio* (zebrafish, native to South Africa), *Xenopus laevis* (a species of African aquatic frog), *Gallus gallus* (a chicken species), *Mus musculus* (mouse) and porcine species are 33.5%, 42.6%, 54.3%, 57.3%, 60.4%, 81.1% and 84.40%, respectively [18, 19] (Figure 1). The mammalian TSPO is composed of five transmembrane (TM) helices, with the N-terminus extending to the intramitochondrial region and the C-terminus pointing towards the extra-mitochondrial membrane.

Translocator protein (TSPO) - amino acid sequence homology

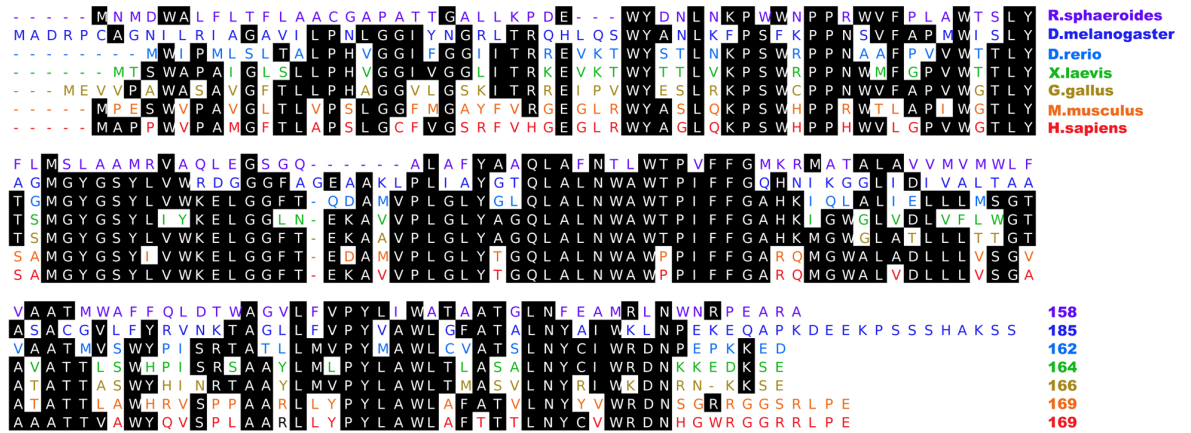


Figure 1: The TSPO amino acid sequence homology. The amino acid sequence homologies of *Homo sapiens* TSPO with TSPO from *Rhodobacter sphaeroides* (Proteobacteria), *Drosophila melanogaster*, *Danio rerio* (zebrafish, native to South Africa), *Xenopus laevis* (a species of African aquatic frog), *Gallus gallus* (a chicken species) and *Mus musculus* (mouse; 33.5%, 42.6%, 54.3%, 57.3%, 60.4% and 81.1%, respectively) [19]. The shaded regions are conserved amino acid sequences.

Many endogenous molecules bind to TSPO for specific biological processes, including cholesterol and porphyrin transport. In TSPO, a conserved cholesterol recognition amino acid consensus sequence (CRAC) motif (residues 147–159) close to the C-terminus binds with high affinity to cholesterol. The synthetic ligand 1-(2-chlorophenyl)-N-methyl-N-(1-methylpropyl)23-isoquinoline-carboxamide (PK11195) binds to the hydrophobic region formed between TM1 and TM2 of the TSPO helices and comes into indirect contact with many amino acid residues, including alanine at position 147 (Figure 2).

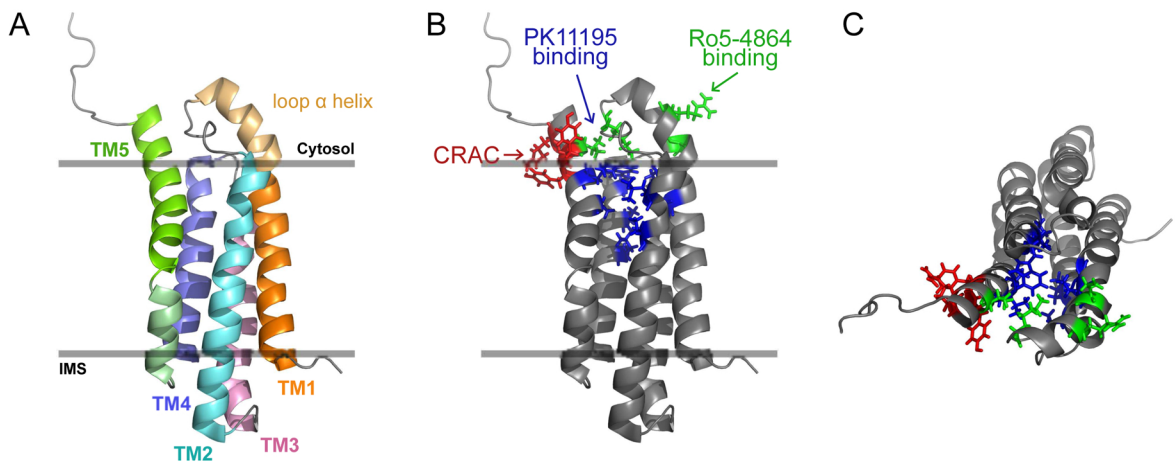


Figure 2: TSPO protein structure. TSPO protein structure showing its distinct binding sites for cholesterol (at CRAC), [^{11}C]-(*R*)PK11195 and Ro5-4864. (A) Side view of the five transmembrane helices (TM1–TM5) in TSPO. (B) Side view of the different ligands that bind to different sites of TSPO, including cholesterol (red), [^{11}C]-(*R*)PK11195 (blue) and Ro5-4864 (green). Cholesterol (red) binds at the CRAC motif exposed to the cytosol. [^{11}C]-(*R*)PK11195 (blue) binds to the TSPO pocket without the involvement of CRAC residues. Ro5-4864 (green) is distinct from the binding pocket of [^{11}C]-(*R*)PK11195 and is involved with different contact residues [19].

A single nucleotide polymorphism is a single nucleotide substitution leading to an amino acid substitution at the alanine-147 residue (the rs6971 polymorphism). This polymorphism leads to a reduction in the binding affinity of TSPO for porphyrins, cholesterol and second-generation synthetic radioligands, while [^{11}C]-(*R*)PK11195 binds with similar affinity [20-22]. A147T is a missense mutation that causes substitution of alanine (A) with threonine (T) [23]. This amino acid substitution affects the stability of the structure and its ligand-binding affinity. The A147T TSPO polymorphism in oligodendrogliomas is discussed in Chapter 3.

TSPO interacts with many proteins and receptors in the outer mitochondrial membrane to perform its functions. TSPO forms a complex with a 32-kDa voltage-dependent anion channel (VDAC) at the outer mitochondrial membrane and with the 30-kDa adenine nucleotide transporter (ANT) at the inner mitochondrial membrane (Figure 3)

[24, 25]. Steroidogenic acute regulatory protein (StAR) interacts with a multi-protein complex to transport cholesterol from the outer mitochondrial membrane into the inner mitochondrial membrane for steroid hormone biosynthesis [26, 27]. However, no evidence yet supports a direct interaction between StAR and TSPO, and this possibility is still under debate [28]. Many studies have suggested that different protein complexes function in cooperation with TSPO in cholesterol transport and steroidogenesis, and these complexes are called transduceosomes [29-32]. VDAC is located in the outer mitochondrial membrane and is involved in many biological functions, including the transport of metabolites (with molecular weight up to 5 kDa), ions (Ca^{+2} , Mg^{+2} and Zn^{+2}), cholesterol, fatty acids and acyl CoA across the outer mitochondrial membrane and into the inner mitochondrial membrane for β -oxidation [33].

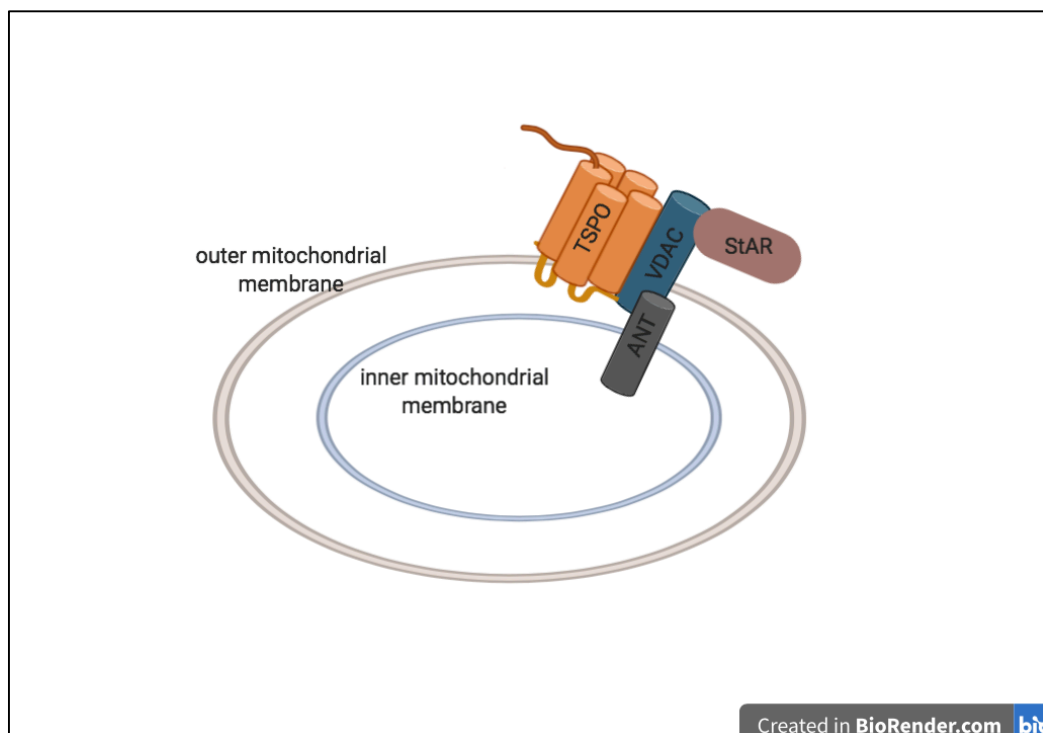


Figure 3: TSPO in the outer mitochondrial membrane as part of a heterooligomeric complex.

TSPO locating in the outer mitochondrial membrane as part of a hetero-oligomeric complex with voltage-dependent anion channel (VDAC), adenine nucleotide transporter (ANT) and steroidogenic acute regulatory protein (StAR).

Image created by Biorender.

VDAC, ANT and TSPO were previously considered to form the core component of the mitochondrial permeability transition pore (mPTP). Subsequent studies suggested that these proteins are regulators of mitochondrial permeability rather than indispensable components of the mPTP. Further, they play an important role as inducers of pro-apoptotic mitochondrial membrane permeabilisation [34, 35]. The induction of mitochondrial membrane permeability leads to the release of the apoptogenic factor cytochrome c from the inner mitochondrial space into the cytoplasm. Cytochrome c forms an apoptosome with apoptotic protease-activating factor 1 (Apaf-1) and caspase-9 to initiate apoptosis. Therefore, the interaction between TSPO and VDAC is considered to play an important role in the apoptosis initiation process. VDAC1 allows cytochrome c release from mitochondria and apoptotic cell death [36]. More interestingly, VDAC1 depletion has been found to lead to an 80% reduction in TSPO expression, which indicates the regulatory role of VDAC1 in TSPO expression in glioblastoma multiforme (GBM) [37, 38]. The physical interaction between TSPO and all three isoforms of VDAC is suggestive of the collaborative interaction between these proteins in many functions, including steroidogenesis, mitochondrial autophagy inhibition and apoptosis [38-41]. In addition, a recent study has suggested that the interaction of TSPO with endoplasmic reticulum NADPH oxidase 2 (NOX2; subunits gp91^{Phox} and P22^{Phox}) might modulate cytochrome b₅₅₈ formation and reactive oxygen species (ROS) production [42].

The mammalian TSPO can form monomer, dimer and higher oligomeric structures, but the underlying mechanism is not fully understood [43]. Cholesterol binding to TM5 of TSPO could contribute to TSPO oligomerisation [44, 45]. In addition, ROS might mediate the formation of covalent bonds between tyrosine residues within the monomeric TSPO structure to form multimers [46]. The TSPO dimer structure was first illustrated in *R. sphaeroides* (RsTSPO), with 34% sequence homology to the human TSPO protein [47, 48].

A crystal structure of TSPO in *Bacillus cereus* TSPO (*Bc*TSPO) was reported by Youzhong et al., and they suggested that the TSPO tryptophan residues are involved in the interaction with protoporphyrin IX (PpIX), which suggests a physiological function for TSPO in protection against oxidative stress [49, 50].

1.1.3. TSPO history

TSPO was first discovered in 1977 by Braestrup et al. as a peripheral receptor for a group of psychoactive drugs, benzodiazepines are distinct from the CNS benzodiazepine receptor (the GABA_A receptor) [1, 51]. Benzodiazepines make up a class of drugs that work as muscle relaxants and neurotransmission inhibitors in anxiety disorders [52-54]. TSPO was previously named peripheral-type benzodiazepine receptor (PBR) to distinguish it from central-type benzodiazepine receptor (CBR). It was described in rat adrenal sections and heart in 1983 by Benavides et al. and Le et al., respectively [55, 56]. Benavides et al. found [³H]PK 11195 specific binding sites with high affinity in adrenal sections and *in vivo* which are independent of GABA binding sites [55, 57]. Peripheral diazepam (Benzodiazepine Drug Class) binding sites were also previously identified in rat blood platelets by Wang et al. in 1980 which are distinct than GABA binding sites [58]. Moreover, Schoemaker et al. in 1981 showed PK11195 specific binding sites in the rat cerebral cortex and kidney [59].

PBR was renamed TSPO in 2006, based on new insights about its function in cholesterol translocation from the outer to the inner mitochondrial membrane and the transport of other molecules (e.g. protoporphyrin IX and other tetrapyrroles) [51, 60-65]. Moreover, the term ‘peripheral’ did not reflect the correct TSPO distribution, which also included glial and ependymal cells in the CNS [47, 66-74]. The term ‘benzodiazepine’ was also inaccurate because other ligands can bind to this receptor, including cholesterol, porphyrine and [¹¹C]-(R)PK11195. The other alternative names for TSPO were

mitochondrial diazepam-binding inhibitor (DBI) receptor complex, [¹¹C]-(R)PK11195 binding site, isoquinoline-binding protein (IBP), 18-kDa PK (isoquinoline)-binding subunit (pk18), benzodiazepine peripheral binding site (BPBS) and mitochondrial benzodiazepine receptor (MBR) [51, 75, 76].

1.1.4. TSPO expression in normal and pathological conditions

TSPO is ubiquitously expressed in normal tissues. It is expressed at high levels in gonads, adrenal glands and placenta; at intermediate levels in renal and myocardial tissues; and at very low levels under normal conditions in liver tissues [14, 51].

In the normal brain, TSPO is expressed at low levels, where it is found in the choroid plexus, pineal gland, ependyma, meninges, olfactory epithelium and vessels [59, 77-79]. During neuroinflammation, TSPO expression increases in reactive microglia. TSPO expression has been found to be up-regulated in AD, HD, Parkinson disease, stroke and brain injury [6, 9, 10, 80-84]. Therefore, TSPO has been proposed as a biomarker of neuroinflammation and neuronal damage. In many pathological conditions of the CNS, such as MS and AD, strong positive immunohistochemical staining for TSPO has been observed in macrophages, activated microglia and reactive astrocytes [5, 69, 85-87]. In contrast, neurons and oligodendrocytes do not exhibit detectable TSPO expression in normal and diseased brains [88].

An increase in TSPO expression occurs in many types of cancer, including breast [2, 89], colon [90], ovary [91], and liver [92] carcinoma. Further, elevated TSPO expression has been found to affect cell proliferation in different cancer cell lines, including those of breast, colorectal, prostate, ovarian and brain cancers [89, 93, 94]. Accordingly, a positive correlation has been reported between TSPO levels and tumour aggressiveness in human breast cancers, colorectal carcinomas and prostate carcinomas; this further supports the

potential role of TSPO in tumour progression [2-4, 95]. In contrast, down-regulation of TSPO has been shown to reduce cell proliferation and tumour growth in breast cancer in both *in vitro* and *in vivo* conditions [2, 89, 95-97]. Therefore, based on these findings, TSPO is considered as a potential biomarker for many human cancers [98]. However, the exact mechanism of action of TSPO during tumour progression and the factors that control TSPO expression in cancer are still not well understood.

1.1.5. TSPO expression in gliomas

In gliomas, the initial studies (conducted in 1979 and 1987) reported high expression of TSPO *in vitro* and *in vivo* [99-101]. In addition, a positive correlation was observed between TSPO expression and glioma grade of malignancy in humans; this indicates that TSPO could be an important diagnostic marker for malignant tumours [102]. In 1998, Miyazawa et al. showed that radiolabelled [³H] PK11195 tracer density was higher in high-grade gliomas compared with low-grade tumours and could be used to differentiate them [103]. They also noted a higher expression of TSPO in human brain gliomas than in the normal cortex. Subsequently, Miettinen et al. confirmed these findings with immunohistochemistry and *in situ* hybridisation in 86 cases of astrocytoma [4]. They found positive correlations between TSPO expression and tumour proliferation [4]. Subsequently, studies confirmed the association of high TSPO expression levels with tumorigenicity, proliferation and invasion in glioma cells [104, 105]. In astrocytomas, a 12-fold higher TSPO expression in high-grade anaplastic astrocytomas than in the normal brain was observed [106]. Vlodaysky et al. reported consistent results for human astrocytomas, showing that TSPO expression was significantly higher in the tumours than in normal brain tissues. They also found a strong positive correlation between TSPO expression and glioma

grade, but they detected a strong negative correlation between TSPO expression and patient survival [94].

The primary location of TSPO is in the mitochondria, but some studies have found TSPO localised in the plasma membrane, endoplasmic reticulum and nucleus [42, 51, 70, 76, 83, 107]. TSPO expression, distribution and localisation within the tissues is cell-type specific. In human breast cancer cells, TSPO was found to be localised in the nucleus and perinuclear region in the most aggressive metastatic cell line, while in less aggressive metastatic cells, it was mostly localised within the cytoplasm [2, 108]. This study suggested a correlation between the aggressive phenotype of tumour cells with high TSPO expression and nuclear localisation of TSPO.

A study by Brown et al. indicated that the subcellular localisations of TSPO could affect its function in the cell. For instance, in primary tumour cells of MGM-1 human GBM, TSPO was mainly located in the perinuclear region, and a very small fraction was located in the mitochondria. In addition, it had an effect on proliferation (as measured by Bromodeoxyuridine (BrdU) incorporation assays) but did not affect steroidogenesis (as measured by tracing the production level of pregnenolone and dehydroepiandrosterone [DHEA]). In recurrent human glioblastoma cells (MGM-3), TSPO was mainly located in the mitochondria and was found to further induce steroid synthesis, but it had no effect on the proliferation of these cells [109]. These observations indicate that the TSPO localised in the mitochondria could contribute to its corresponding function in steroidogenesis, whereas the nuclear or perinuclear location would be more suitable for its role in the regulation of proliferation.

1.2. TSPO's function

TSPO is involved in many biological processes, including the regulation of mitochondrial adenosine triphosphate (ATP) production [110, 111], heme biosynthesis [112], ROS generation, Ca²⁺ modulation [113], cytochrome release from the mitochondrion [114], programmed cell death processes [115, 116], and the regulation of the mPTP [117, 118]. Furthermore, two studies have suggested that TSPO is a basic housekeeping gene [52, 119].

The role of TSPO in steroidogenesis is controversial. Some studies agree on the role of TSPO in cholesterol transportation and steroid hormone synthesis [51, 120]. Cholesterol transport from the outer mitochondrial membrane into the inner mitochondrial membrane is a rate-limiting step in steroid biosynthesis [121]. Within the mitochondrial matrix, cholesterol is converted to pregnenolone via an enzymatic reaction with CYP11A1 (a cytochrome p450 family member) for steroid biosynthesis. Further, *in vitro* studies in Leydig tumour cells have shown that a reduction in TSPO expression caused a decrease in steroid production [122, 123]. Consistent research showed that TSPO depletion decreased testosterone plasma levels and caused accumulation of cholesteryl ester-enriched lipid droplets in steroidogenic cells [29, 124]. These features reflect inefficient cholesterol metabolism and low accessibility to free cholesterol for steroid biosynthesis. Barron et al. found a significant reduction in corticosteroid (CORT) and progesterone (P4) synthesis in a TSPO-knockout (KO) model [125]. The TSPO CRAC domain is important for corticosteroid formation. The A147T TSPO polymorphism reduced the cholesterol binding affinity to TSPO and further lowered the corticosteroid production. In contrast, other studies have indicated that TSPO depletion does not affect steroidogenesis [110, 126-128]. Moreover, TSPO KO mice showed normal fertility, viability and steroid hormone production [110, 129].

Studies that have examined the role of TSPO in proliferation have also reported contradictory findings. This might indicate that TSPO has a cell-specific function or may reflect a response to the TSPO-silencing strategies conducted in these studies, for example, genetic manipulation and the use of synthetic ligands. The reduction in TSPO function by synthetic ligands is concentration-dependent, and any off-target binding effects of the used ligands could also affect the results. For instance, using different concentrations of [¹¹C]- (R)PK11195 to down-regulate TSPO function showed that a low concentration of [¹¹C]- (R)PK11195 (at the nanomolar level) stimulated cell proliferation via S-phase accumulation in aggressive breast cancer cell lines [130]. By contrast, a high concentration of the tracer (at the micromolar level) inhibited cell proliferation by inducing the cells to enter into the G2/M phase and arresting cell proliferation, leading to breast cancer cell apoptosis [131-133]. Similar results have been published on different cell types, including C6 glioma cells and Leydig tumour cells; this supports the finding that synthetic ligands have a concentration-dependent effect on proliferation [134, 135].

Rechichi et al. showed that TSPO over-expression induced the *in vitro* proliferation and migration of C6 glioma cells [105]. Numerous other studies have also shown positive correlations between TSPO expression and tumour proliferation [4, 102, 104-106]. For example, Veenman et al. showed a positive correlation between a high level of TSPO expression in glioma cell lines and induction of cell proliferation, but they found a negative correlation between TSPO expression and apoptosis [104]. Further, a rat C6 glioma cell line with the highest TSPO level showed the highest level of proliferation when compared with other cell lines with intermediate (U87MG cells) and low (T98G cells) levels of TSPO expression. Li et al. considered TSPO to be directly involved in cell cycle regulation. In their study, down-regulation of TSPO (using siRNA) led to downstream activation of

apoptosis through an increase in the p21 level (potent cyclin-dependent kinase inhibitor [CKI]), p53 phosphorylation and caspase-3 cleavage [133].

The studies mentioned above indicate a role for TSPO as a positive regulator of tumour proliferation. However, other groups found different effects of TSPO on tumour growth and malignancy. For instance, Bode et al. demonstrated that TSPO knockdown (with siRNA against TSPO and 25 $\mu\text{mol/L}$ [^{11}C]-(R)PK11195) enhanced the *in vitro* migration of U118MG glioblastoma cells through a modified Boyden chamber, as opposed to the inhibitory effect on migratory ability that had been previously reported in C6 glioma cells [136]. They showed that TSPO knockdown (via siRNA) induced *in vivo* tumour growth in a xenograft mouse model; they also showed that a larger area of the brain was invaded following implantation of U118MG cells lacking TSPO expression than implantation of U118MG cells with normal TSPO expression. Thus, their findings indicate that knockdown of TSPO induced invasion of cancer cells. In accordance with these findings, another study by Levin et al. showed similar results after stably transfecting the C6 glioma cell lines with IBP knockdown vector to down-regulate TSPO expression [137]. However, in contrast to these findings, Veenman et al. drew a different conclusion regarding the expected role of TSPO in proliferation and apoptosis, as they found a positive correlation between TSPO expression level and proliferation and a negative correlation between TSPO expression and cell death [104]. They conducted a comparative study between three different glioma cell lines that expressed different levels of TSPO (high, intermediate and low) and examined the effect of TSPO expression level on *in vitro* proliferation and apoptosis, without inducing any genetic alterations in TSPO expression. Consistent with these findings, Voldavsky et al. demonstrated that immunohistochemical TSPO expression had a positive correlation with proliferation in brain tumours of different grades, but it had a negative correlation with apoptosis [94]. The correlation study was based on the detection of proliferation in cells that

were immunohistochemically positive for TSPO in the absence of any genetic manipulation or synthetic ligand treatment.

Some questions that arose from the previous studies concerned the mechanism by which a TSPO deficiency could promote glioma growth and malignancy and the corresponding mechanism used by these cells to overcome the high-energy demand for proliferation. A TSPO deficiency could impair mitochondrial function, energy metabolism (through reduced ATP production), oxidative phosphorylation and mitochondrial metabolism, and lead to an increased demand for energy. Fu et al. indicated that a metabolic shift towards glycolysis within the tumour microenvironment could overcome the high energy demand [111]. The researchers proposed that TSPO deficiency triggers hypoxia-inducible factor-alpha (HIF- α) induction and leads to angiogenesis via the release of pro-angiogenic factors, such as vascular endothelial growth factor A (VEGF-A), matrix metalloproteinases (MMPs) and interleukin-8 (IL-8), and this subsequently results in tumour growth induction. In addition, glycolytic enzymes (e.g. glucose transporter 1 [GLUT1], hexokinase-2 [HK2] and lactate dehydrogenase [LDH]) were also likely to be induced and involved in a metabolic shift [111].

TSPO has been suggested to be involved in the anti-oxidant pathway. A study using Jurkat cell lines suggested that TSPO over-expression increased the resistance to cell damage caused by hydrogen peroxide and reduced ultraviolet (UV)-induced apoptosis and cytotoxicity; this indicates the possible role of TSPO in providing protection against mitochondrial damage and delaying cell apoptosis [138, 139].

In response to pro-inflammatory stimuli, Nicotinamide adenine dinucleotide phosphate oxidase isoform-2 (NOX2) is activated, leading to oxidative stress and increased ROS generation. TSPO has a role in counteracting oxidative stress and an increased level of ROS via interaction with NOX, leading to the release and translocation of nuclear factor

erythroid-2 (Nfr2) to the nucleus ARE element to further induce the anti-oxidative stress process [42, 140, 141].

1.3. TSPO expression regulation

1.3.1. Genes involved in the regulation of TSPO expression

Under normal conditions, TSPO is expressed at a low level in microglia. In contrast, under pathological conditions, microglial cells become activated, and TSPO protein expression is induced. Rashid et al. suggested that the Ap-1, Ets and Sp binding site elements in the TSPO promoter region are important in the regulation of TSPO expression in microglia [2, 89-92, 94, 142]. During lipopolysaccharide (LPS)-induced pathophysiological conditions, many transcription factors, including Pu.1, SP1, SP3, Sp4, c-Jun, c-Fos and Stat3, are recruited in response to LPS to its corresponding binding sites on the TSPO promoter, in order to activate TSPO transcription. Batarseh et al. studied MA-10 mouse Leydig cells (which express high levels of TSPO) and NIH/3T3 mouse embryo fibroblasts (which express low levels of TSPO) and concluded that the V-ets erythroblastosis virus E26 oncogene homologue (Ets 1, Ets 2) and androgen receptor/progesterone receptor (AR/PR) upstream of Ets1 are important positive regulatory elements of the TSPO promoter in MA-10 cells [143]. In addition, specificity protein 1 transcription factor (SP1), specificity protein 3 transcription factor (SP3) and GA-binding protein transcription factor (GABP), which is also a member of the Ets family of transcription factors, may also have crucial roles in the regulation of TSPO expression.

Batarseh et al. suggested the involvement of a member of the protein kinase C (PKC) family, PKC ϵ , in the induction of the TSPO promoter in response to phorbol-12-myristate 13-acetate (PMA) in steroidal and non-steroidal cells [144]. PKC ϵ has previously been

shown to be involved in many biological processes, including cell proliferation and differentiation [145]. PMA induces an increase in either the synthesis or the activation of downstream transcription factors (c-Jun and c-Fos [AP1 Family] and GABP α [Ets family]), leading to an increase in TSPO mRNA and protein expression levels in NIH-3T3 fibroblast cells [144]. The induction of TSPO expression by PKC ϵ is thought to occur through the mitogen-activated protein kinase (MAPK) signal transduction pathway (Raf1-MEK1/2-ERK1/2) in TSPO-rich steroidogenic cells (MA-10 Leydig) and TSPO-poor non-steroidogenic cells (NIH 3T3 fibroblasts). MAPK signal activation was found to lead to the induction of downstream transcription factors (Stat3 and c-Jun), which then bound to their corresponding binding sites on the TSPO promoter to induce TSPO expression (Figure 4) [143].

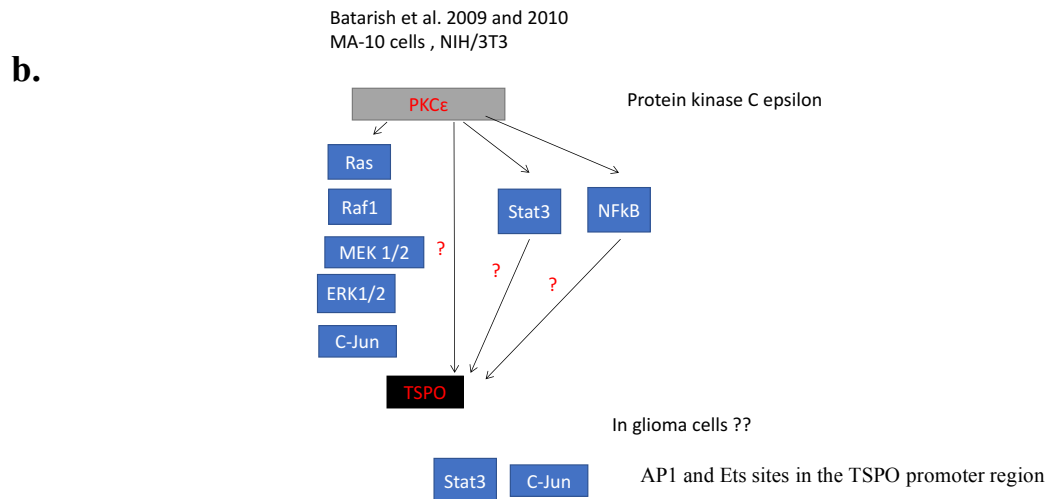
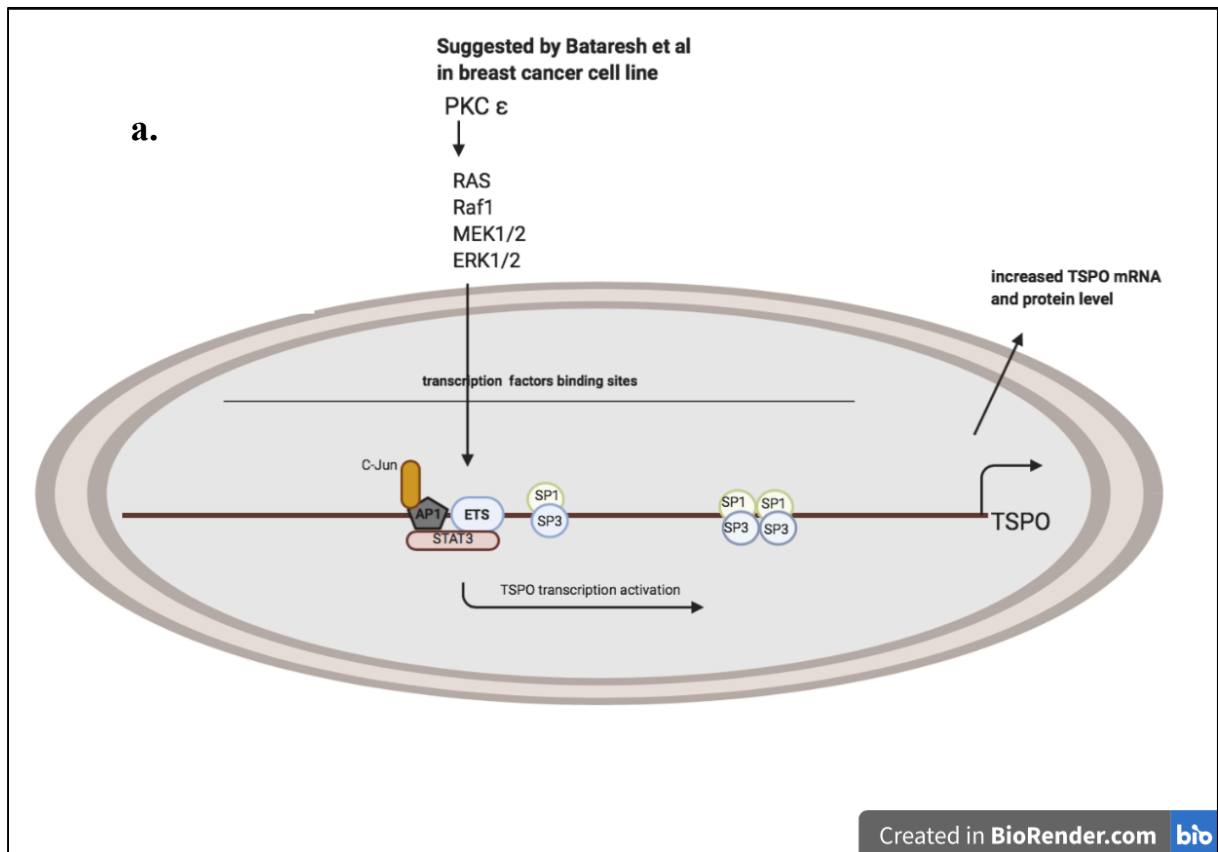


Figure 4: Summary of the genes studied in the literature and their roles in regulating TSP0 expression. Bataresh et al. suggested PKC ϵ to be upstream regulator of TSP0 expression through RAS/Raf1/MEK1/2/ERK1/2 [143]. Panel a. showed a study by Bataresh et al. in breast cancer cells and indicated that c-Jun and Stat3 bind to specific binding sites within the TSP0 promoter region between AP1 and Ets binding sites (grey and blue in panel a). SP1 and SP3 factors bind to their

specific binding sites within the TSPO promoter region (green and blue). PKC ϵ is an upstream regulator of TSPO expression that induce recruitment of c-Jun and Stat3 to bind to their corresponding sites within the promoter. c-Jun and Stat3 bindings to the promoter region lead to induce TSPO transcription level. Batarseh et al. study was performed in breast cancer cells, MA-10, NIH/3T3 and nothing is known about this pathway effect on glioma cell TSPO expression level. Panel b. showed the suggested TSPO upstream regulators in Batarseh et al. study in 2009 and 2010, including PKC ϵ , Ras, Raf1, MEK1/2, ERK1/2, c-Jun, and Stat3. c-Jun and Stat3 have a corresponding binding sites within the TSPO promoter. It is still unknown if these factors could regulate TSPO expression in glioma cells.

Another potential influencing mechanism of TSPO expression could involve a cell defence mechanism against damage induced by ROS [138]. For instance, Jurkat cells do not normally express TSPO, but after TSPO over-expression within these cells, increased resistance (by 25%) to H₂O₂-induced stress has been shown. With regard to the mechanism, increased ROS production activates PKC ϵ and, further downstream, transcription factors that have specific binding sites on the TSPO promoter (e.g. SP1/SP3, AP1, AP2 and NF κ B) leading to an increase in TSPO expression [3]. A study by Giatzakis et al. showed the involvement of two important regions on the TSPO promoter; these regions, including two proximal SP1/SP3 sites and the Ets family of transcription factors, were suggested to regulate TSPO expression. Although the level of Sp1 is the same in steroidogenic and non-steroidogenic cells, the Sp3 level is higher in steroidogenic cells and might be involved in one of the mechanisms that could explain the differences in TSPO expression [14, 138]. Another mechanism for the regulation of TSPO expression was suggested by Hardwick et al. They indicated an amplification of the TSPO gene in aggressive metastatic MDA-MB-231 human breast cancer cells could be involved in the progression of aggressive metastatic breast cancer cells [95, 97].

1.3.2. Epigenetic regulation

1.3.2.1. Definition

The term ‘epigenetic’ refers to the heritable alteration of the expression pattern of genes without any changes within the gene sequence [146, 147]. Epigenetic changes include methylation of the gene promoter region where transcription is initiated. The methylation process involves the addition of a methyl group from *S*-adenosyl-methionine by the enzyme DNA methyltransferase (DNMT) to the fifth cytosine base of the cytosine pyrimidine ring

of a CpG dinucleotide, which precedes the guanosine base within the CpG dinucleotide [148]. Constituent repetitive CpG dinucleotides form a CG-rich region (0.5–4 kb in length) that is usually within the promoter; this is called a CpG island [146, 149]. The methylation of the cytosine base within the CpG island results in gene silencing, which means the attenuation of gene transcription, and therefore, inhibition of the expression of the corresponding gene. CpG islands span the 5' end of the UTR and usually remain unmethylated in normal cells. Another synergic modification (methylation or acetylation) could occur on the histone protein residues to remodel the chromatin, which comprises 3 billion human DNA base pairs that are organised and compacted into a condensed structure. Each chromatin structure is composed of repeated units of nucleosomes, and each nucleosome is composed of an octamer of histone proteins. Structural changes (e.g. histone deacetylation) in chromatin are associated with synergic changes in DNA methylation that lead to gene silencing. Histone modification (covalent modification with acetylation) changes the electrostatic interaction between the DNA and histones, and this makes the DNA more accessible to transcription regulatory factors.

Epigenetic modification, which includes DNA methylation, is a reversible change. Constitutively active genes within the genome (housekeeping genes) have a promoter CpG island that mainly remains unmethylated, and these islands act as regions of access for transcription proteins (e.g. transcription factors and histone acetyltransferase [HAT]), which induce transcription. Active genes usually have acetylated histones and unmethylated CpG islands within the promoter, as well as a widely spaced structure, while a silenced gene has deacetylated histones and methylated CpG islands with a tightly compacted architecture that precludes access to the transcription activator complex proteins. A transcriptionally silenced gene recruits a complex of proteins associated with DNA methylation, including histone

deacetylase (HDAC) and DNMT. Epigenetic changes lead to dysregulation of the global gene expression profile and have been suggested to be related to many diseases [150].

1.3.2.2. Promoter methylation in different cancers

Hypermethylation of CpG islands is a molecular and prognostic marker for many cancers, including lymphomas, lung tumours and gliomas. The CpG island methylator phenotype (CIMP) is generally known for genome hypermethylation at CpG islands (CGIs). Tumours that carry this hypermethylation phenotype were first identified in colon cancer as CIMP cancers; they were subsequently subdivided into high-CIMP, low-CIMP and non-CIMP colorectal cancers; importantly, the CIMP-positive cases showed a better prognosis [151]. Different pathways are disrupted as a result of gene silencing by hypermethylation of the corresponding gene promoter in different tumours. For instance, cell cycle regulator genes, such as retinoblastoma (RB) protein and p16^{Ink4a}/p14^{ARF} cyclin-dependent kinase (CDK) inhibitor, block the ability of CDK to stimulate cell cycle progression. Their silencing leads to uncontrolled cell cycle progression because the role of p16^{Ink4a}/p14^{ARF} is to attenuate RB phosphorylation and lead to the G1 checkpoint, blocking S-phase entry and cell growth.

The expression of DNA repair genes, such as O6-alkylguanine DNA alkyltransferase (O6-MGMT), breast cancer susceptibility gene (BRCA1) and MutL homologue (MLH1), can also be silenced by CpG island hypermethylation [152-154]. CpG hypermethylation was found to regulate the expression of different genes in many cancers, including ovarian, colon, leukaemia and breast cancers [155, 156].

In terms of breast cancer, Batarseh et al. studied the location of CpG islands within the TSPO promoter region in the breast cancer cell lines MCF-7 and MDA-MB-231. They reported an epigenetic methylation regulatory mechanism of the TSPO promoter in MCF-

7. They used 5-azacytidine (a DNA methyltransferase inhibitor that causes demethylation of the CpG site) in the MCF-7 cell line (which weakly expresses TSPO). Demethylation induced by the 5-azacytidine inhibitor led to a three-fold increase in TSPO expression; this is indicative of the involvement of epigenetic silencing in the regulation of TSPO expression in breast carcinoma [157]. Similarly, a deacetylase inhibitor (trichostatin A) caused a decrease in promoter methylation and led to a 120-fold increase in TSPO expression in MCF-7 cells and a 10-fold increase in MDA-MB-231 cells. Moreover, in T-cell leukaemia cell lines, 5-azacytidine treatment resulted in a 180-fold induction of TSPO mRNA expression in Jurkat cells; thus, TSPO expression in human cell lines (Jurkat) could be regulated by epigenetic silencing [156]. A low frequency of promoter methylation has been observed in other studied cells, such as Hela, HEL-293 and U87-MG GBM cells, and no post-treatment effect was observed on the level of TSPO mRNA in these cells [156]. These findings led us to ask whether oligodendrogliomas would also show a similar low frequency of hypermethylation as observed in the U87-MG GBM cells and whether TSPO expression is epigenetically regulated in this subtype of glioma.

1.4. Gliomas

1.4.1. Introduction

Gliomas are named for the glial cells from which they originate; for example, astrocytomas are named for astrocytes, oligodendrogliomas are named for oligodendrocytes and ependymomas are named for ependymal cells [158]. In the 2007 CNS World Health Organization (WHO) criteria, diagnosis of gliomas was mainly based on histological features, whereas the new 2016 CNS WHO classification combines molecular parameters (genetic changes) with histological features for more accurate diagnosis. Gliomas are graded by the WHO as grade I, grade II (low-grade), grade III (anaplastic) and grade IV

(glioblastoma). Grade I represents tumours with low proliferative activity. Grade II defines infiltrative tumours with histological features of cytological atypia and low growth potential but a tendency to transform to a higher grade at an unpredictable time interval. Grade III defines malignant tumours with rapid progression and histological evidence of malignancy, including nuclear atypia, anaplasia and high mitotic activity. Grade IV (glioblastoma) is the most aggressive form of brain tumour, and it shows high mitotic activity, a high invasion rate, high microvascular proliferation and high necrosis. Anaplastic astrocytomas (AA) and anaplastic oligodendrogliomas (AO) are grade III tumours that usually transform from lower grades. Low-grade gliomas (LGG) have a 15% incidence among the age group of 35–44 years [159]. Gliomas are heterogeneous in terms of their genetic and molecular basis and share some overlapping histological features. Understanding the molecular and genetic basis of CNS tumours can improve diagnostic accuracy and reduce the inter-observer variability that accompanies diagnosis based on histological features alone. This expanded basis will also help in predicting treatment responses and the tumour transformation potential.

1.4.2. WHO classification

The 2000 and 2007 WHO classifications were mainly based on histological features and microscopic similarities among the different tumour entities. Tumours that share a similar haematoxylin-eosin (H&E) staining appearance, immunohistochemical protein expression and microscopic morphological features were classified as the same entity. Accordingly, LGGs could be divided into two different entities, namely, astrocytomas and oligodendrogliomas.

The revised version of the fourth edition of the WHO classification published in 2016, combined and integrated phenotypic and genotypic parameters. The main molecular and genetic features in the 2016 classification are based on the status of isocitrate dehydrogenase (IDH1 or IDH2) and co-deletion of the short arm of chromosome 1 (1p) and the long arm of chromosome 19 (19q) (Table 1) [160]. The identified IDH mutation is a single amino acid missense mutation (a point mutation that causes a single nucleotide change and results in coding of a different amino acid) in IDH1 at arginine residue 132 (R132) or in IDH2 at arginine residue 172 (R172) [161]. IDH1 is the principal producer of NADPH in the brain, and cytoplasmic IDH1 and mitochondrial IDH2 enzymes are involved in the reversible oxidative decarboxylation of isocitrate into α -ketoglutarate (α -KG) and the generation of NADPH. The missense mutation R132 leads to substitution of important amino acid residues in the IDH1 and IDH2 active sites, thereby reducing the efficiency of conversion of isocitrate into α -KG. A functional analysis demonstrated that this missense mutation leads to a 15- to 30-fold increase in the generation of D-2-hydroxyglutarate (D-2HG) from α -KG, and this is thought to be associated with epigenetic deregulation and increased histone/DNA hypermethylation.

Most grade II and grade III tumours fall into the IDH-mutant category, and the absence of a mutation in the IDH1 and IDH2 genes would be diagnosed as an IDH wildtype. More than 70% of WHO grade II and III gliomas show IDH1 mutations, whereas IDH2 mutations are found in only 6% [162]. The genotype hallmarks for astrocytoma are mutations in IDH1, alpha-thalassemia/mental retardation X-linked (ATRX) and TP53. The ATRX mutation has been discovered in X-linked mental retardation (MR) syndrome (ATRX syndrome) and is involved in chromatin remodelling and DNA methylation. The ATP-dependent helicase (ATRX) gene encodes a chromatin remodelling protein; therefore, its functional impairment leads to an increase in genetic instability and epigenetic changes

[163]. TP53 is a tumour suppressor that controls cell division by regulating the DNA damage repair process; consequently, TP53 loss promotes tumour growth. The occurrence of both TP53 and ATRX mutations together promotes tumour cell survival.

Diffuse astrocytomas or low grade astrocytomas (LGA; grade II) are characterised by mild to moderate cytological atypia with low or absent mitotic activity, whereas anaplastic astrocytomas (AA; grade III) show significant proliferative activity and anaplasia. Glioblastomas are classified into IDH-wildtype (primary or de novo gliomas) and IDH-mutant (secondary glioblastomas with a prior history of lower-grade glioma) [160]. The majority of glioblastomas fall into the IDH-wildtype category (90% of cases), and only 10% are of the IDH-mutant type.

Table 1: Summary of the histological and genotypic hallmarks of gliomas

Summary of the histological and genotypic hallmarks of different glioma histotypes (oligodendrogliomas, astrocytomas and GBM), according to the WHO classification of the CNS tumours (World Health Organization Classification of Tumours book, 2016 [164]).

| <i>Tumour subtype</i> | <i>Genetic hallmarks</i> | <i>Associated mutation</i> | <i>Microscopic features</i> |
|-------------------------------------------------------------------------|----------------------------------------------------------------------|--------------------------------------------------------------------------|----------------------------------------------------------------------------------------------------------------------------------------------------------------------------------------------------------------------|
| Diffuse Astrocytomas or Low grade astrocytomas (LGA) | ATRX loss and TP53 mutation 1p/19q intact IDH1 mutant | No EGFR amplification No TERT mutation | -Glial fibrillary acidic protein processes (well-differentiated astrocytes) -Nuclear Atypia -Absence of mitotic activity -absence of microvascular proliferation -no necrosis -Ki-67 1-4% |
| Anaplastic Astrocytomas (AA) | | EGFR amplification | -Increased mitotic activity (high Ki-67 5%-10%) -Anaplasia -Nuclear morphology is more atypical and with changed size |
| Diffuse Oligodendrogliomas Or Low grade oligodendrogliomas (LGO) | 1p/19q co-deletion IDH1 mutant | CIC FUBP1 NOTCH1 TERT mutation | -Uniform Round nuclei -Perinuclear haloes (fried eggs or honeycomb appearance on FFPE tissues) -Low/absence mitotic activity -Nuclear atypia |
| Anaplastic Oligodendrogliomas (AO) | | -TERT mutation -MGMT promoter methylation -CIC -FUBP1 | - Nuclear atypia -High cell density -High mitotic activity -microvascular proliferation |

| | | | |
|---------------------------|----------------------------------------------------------------------------------------------------------------------------------------------------------------------------------------------------------------|--------------------------------------------------------------------------------------------|-----------------------------------------------------------------------------------------------------------------------------------------------------|
| Glioblastoma (GBM) | -EGFR amplification -Majority primary GBM with intact wild type (WT) IDH1 (90%) -10% mutant IDH1 (secondary developed from diffuse or anaplastic astrocytoma or oligodendrogliomas) | PTEN TP53 NF1 PIK3Ca PTPN11 PLCG1 | -Nuclear atypia -Cellular pleomorphism -High mitotic activity -Microvascular proliferation -Necrosis |
|---------------------------|----------------------------------------------------------------------------------------------------------------------------------------------------------------------------------------------------------------|--------------------------------------------------------------------------------------------|-----------------------------------------------------------------------------------------------------------------------------------------------------|

Using both histological and genotypic features, gliomas are classified into three different categories. The first is oligodendroglioma, which harbours both an IDH1/2 mutation and a 1p/19q co-deletion. The second category is the astrocytic phenotype (no necrosis and no microvasculature) that harbours an IDH1/2 mutation but no 1p/19q co-deletion and is considered an astrocytoma. The presence of an ATRX mutation and TP53 confirms this subtype. The third category consists of tumours with necrosis and high microvascular density but harbouring wild-type IDH1/2 and no 1p/19q co-deletion; these fall into the glioblastoma category. This subtype with wild-type IDH has the characteristics of a glioblastoma molecular profile, including epidermal growth factor receptor (EGFR) amplification and Phosphatase and TENSin homolog (PTEN) mutation.

1.4.3. Epigenetic methylation in gliomas

DNA methylation has been reported as one of the important mechanisms that control gene silencing in gliomas [165]. Gene silencing by promoter methylation at CpG islands can repress the expression of many genes that control different vital processes. For instance, it can repress the expression of many genes involved in apoptosis and cell invasion, such as tissue inhibitor of metalloproteinase-3 (TIMP3), the tumour necrosis factor receptor superfamily ten (TNFRSF10a) and death-associated protein kinase 1 (DAPK1). Moreover, it can repress genes involved in the cell cycle and cell division, such as Tumour Protein p53 (TP53), cyclin-dependent kinase inhibitor 2A (CDKN2A/ p16^{INK4a}), cyclin-dependent kinase inhibitor 2B (CDKN2B/p15^{INK4b}) and RB1 [166-169].

The O6-MGMT (O6-alkylguanine DNA alkyltransferase) promoter is another example of a gene regulated by promoter hypermethylation, and this epigenetic marker is a predictor of better response to alkylating therapy and better overall survival [152, 170]. The MGMT enzyme repairs the DNA damage caused by the alkylating agents (temozolomide,

TMZ) used in cancer treatment, and its silencing makes the tumour more sensitive to TMZ. CpG hypermethylation of the MGMT promoter was found in different gliomas, including diffuse astrocytomas (50% of the studied cases) and glioblastomas (39–55% of the studied cases), and it was commonly detected in 60% of the oligodendroglioma cases that harboured the 1p/19q co-deletion. Overall, CpG hypermethylation has been suggested to be an important epigenetic hallmark in oligodendroglial tumours (74% of the studied oligodendrogliomas) [171].

Hypermethylation of specific genes is associated with the development of anaplastic oligodendroglioma due to its effects on the expression of important factors in gliomagenesis. Many genes are hypermethylated in oligodendroglial tumours, including CDKN2A/p16^{INK4a}, CDKN2B/p15^{INK4b}, death-associated protein kinase (DAK) and P14^{ARF} (a mediator of cell cycle arrest and apoptosis) [172-177]. Epigenetic CpG hypermethylation is a suggested mechanism for the lack of detectable expression or low expression of these genes. In LGGs, CpG island hypermethylation has been indicated in many genes, including cyclin A1 (CCNA1), fibroblast growth factor receptor 3 (FGR3), met proto-oncogene hepatocyte growth factor receptor (MET) and transforming growth factor β 2 (TGF β 2) [178].

The CpG island methylator phenotype (CIMP) in gliomas was first described as glioma CIMP (G-CIMP) by Noushmehr et al. for GBM and was later studied and confirmed in LGG by Turcan et al. [176, 179]. Noushmehr et al. suggested that the G-CIMP phenotype in oligodendrogliomas correlates with better prognosis and improved patient survival. Turcan et al. showed that the isocitrate dehydrogenase (IDH1) mutation was sufficient to induce a *de novo* hypermethylation pattern *in vitro* in an astrocyte cell line in many genes [179-181]. Moreover, the G-CIMP-positive phenotype in GBM showed a significant association with IDH mutations and better survival [176, 179]. The findings of the study

indicate a relationship between epigenetic and genetic alterations in the human genome for different diseases that could be important for prognostics and predictive profiling of treatment responses [182, 183].

Gene deletion is another suggested mechanism of gene expression regulation that has been indicated in oligodendrogliomas for the CDKN2A/p16^{INK4a} gene [184].

1.4.4. Oligodendrogliomas

Oligodendrogliomas account for 5-20% of all gliomas [185-187]. The mean survival time (MST) is about 11.6 years for Low-grade oligodendrogliomas (LGO; WHO type II) and 4.5–3.5 years for anaplastic oligodendrogliomas (AO; WHO III) [188]. LGO can transform to a higher grade within an unpredictable timeframe. Oligodendrogliomas display mutations of isocitrate dehydrogenase (IDH1 or IDH2) and co-deletion of the short arm chromosome 1 (1p) and long arm chromosome 19 (19q; as its molecular hallmarks) [160, 189]. The associated genetic alterations with the IDH mutation and 1p/19q co-deletion are orthologues of the *Drosophila melanogaster* capicua gene (CIC), FAR upstream element binding protein 1 (FUBP1), notch 1 receptor member (NOTCH1) and telomerase reverse transcriptase (TERT) mutations [190].

1.4.5. Imaging and diagnosis in oligodendrogliomas

Magnetic resonance imaging (MRI) is the gold standard for localising the tumour region and assessing the location for surgical and radiation interventions. However, no biological information about the tumour metabolic activity or the predicted tumour progression can be obtained from these sequences. Finding non-invasive imaging techniques and modalities that complement MRI could provide more specific information about glioma progression and radiation therapy response.

Advanced imaging techniques, such as perfusion imaging using the parameter of relative cerebral blood volume (rCBV), have been proposed for distinguishing between low-grade and high-grade gliomas [191]. The rCBV is the relative ratio of the cerebral blood volume of the tissue of interest (brain tumour) to the cerebral blood volume of the reference tissue (white or grey matter). It is the most widely used perfusion parameter to distinguish between low-grade and high-grade gliomas. However, Xu et al. found no significant difference in rCBV between low- and high-grade oligodendrogliomas due to the high vascular density even within low-grade gliomas [192, 193]. Therefore, an overlap would be predicted between low and high oligodendroglioma grades. Alternatively, using [¹¹C]- (R)PK11195 positron emission tomography (PET) imaging helped to detect an increased TSPO expression in AO compared to low-grade tumours [8]. Preliminary data suggested that a threshold of 1.4 for the [¹¹C]- (R)PK11195 maximum binding potential (Bpmax) with PET imaging could help differentiate between low-grade and anaplastic oligodendrogliomas. (LGO studied cases showed Bpmax below 1.4, while a higher Bpmax was found in AO).

1.4.6. Histopathological analysis

Despite the previously discussed advantages of using imaging in the diagnosis, the tumour subtype and grade cannot be identified without histopathological examination. However, there are concerns about the inter-observer variation among neuropathologists [194]. The unique microscopic appearance of oligodendrogliomas is characterised by perinuclear haloes (referred to as a ‘fried egg’) and a chicken wire pattern of high vascular density. Grading based on histopathological appearance relates to the presence of cytological atypia, anaplasia, mitotic activity, microvascular proliferation and necrosis. Ki-67 is a marker for cell division due to its high expression during the cell cycle (G1, S, G2

and M); in contrast, its expression is low and undetected in the G0 phase (cell resting phase) and in the late stage of cell division [195]. Tumours with cytological atypia alone are considered grade II, whereas those with anaplasia and high mitotic activity (based on the level of Ki-67, a marker of proliferation and a cell division index) in addition to atypia are considered grade III. In addition to these features, grade IV tumours show high microvascular proliferation and necrosis.

1.4.7. Oligodendrogliomas treatment and follow-up

1.4.7.1. Chemotherapy and radiotherapy

Temozolomide (TMZ), procarbazine, lomustine (CCNU) and vincristine (PCV) are the most frequently used chemotherapy agents for treating gliomas [196]. TMZ is an oral methylating agent that methylates DNA at the O6 position of guanine nucleotides, and this later causes incorrect pairing with thymine during DNA replication and induces cell cycle arrest, mismatch repair and cell death [196]. Procarbazine induces alkylation at the O6 position of guanine nucleotides and induces DNA strand breaks, and this leads to inhibition of DNA synthesis. CCNU (lomustine) is lipid soluble and crosses the blood–brain barrier (BBB) to induce DNA-DNA crosslinks that inhibit DNA repair. The third component of PCV, vincristine, enters the cell via carrier-mediated transport and binds to tubulin during the S-phase, preventing tubulin polymerisation and causing metaphase arrest [197].

Many factors could predict different patient's response to the treatment, including IDH1 and 1p/19q codeletion. In previous research, patients with mutated IDH1 showed significantly better overall survival after radiotherapy (RT) plus PCV therapy compared with the wildtype IDH1/2 cohort [189, 198]. Furthermore, IDH1 mutation could be a prognostic factor of better overall survival in patients with anaplastic oligodendroglioma, but it cannot predict the patient's response to PCV chemotherapy [199, 200].

In addition to the IDH1 mutation, 1p/19q co-deletion is another prognostic factor for survival in patients with oligodendroglioma. Patients who harboured both co-deleted 1p/19q and mutated IDH1 had the highest overall survival compared with the other groups with non-co-deleted/IDH mutated or non-co-deleted/intact IDH1 after receiving RT and PCV treatments [189, 190]. Moreover, low-grade tumours with IDH mutation and 1p/19q co-deletion have a slower growth rate and gradually become more responsive and sensitive to chemotherapy. In anaplastic oligodendroglioma, cases with 1p/19q co-deletion showed better benefit from PCV plus RT compared with RT alone [200, 201]. TMZ is more suitable for treating anaplastic oligodendroglioma due to the sensitivity of these tumours to this therapy, and it is considered to be less toxic than PCV.

Sabha et al. showed that both molecular factors, IDH1 and 1p/19q, were prognostic of survival of patients with LGG [202, 203]. Moreover, 1p/19q co-deletion could be used as an indicator of tumours that have a low growth rate and more sensitivity towards chemotherapy treatment, and this molecular marker needs to be studied as a separate entity [200, 201]. Based on the previously indicated findings, all the patients selected in the present study harboured both the IDH1 mutation and 1p/19 co-deletion.

Many risk factors that indicate possible worse survival and outcome should be considered to find the most suitable treatment protocol. These factors include tumour size greater than 6 cm, incomplete resection, IDH1 and 1p/19q status, age over 40 years, histological features of astrocytes and risk factors for tumour recurrence and progression [204].

Regarding RT, one study showed that patients with high-risk LGG ($n = 251$; age higher than 40 and subtotal resection), who received post-operative RT and adjuvant PCV, had a better overall survival (13.3 years) compared with a group that received only RT (7.8 years) [198]. Immediate RT after surgery in low-grade glioma did not show any significant

difference in overall survival compared with delayed therapy according to the European Organisation for Research and Treatment of Cancer (EORTC) 22845 study [205].

Currently, post-operative follow-up is achieved using T2-weighted MRI and Fluid-attenuated inversion recovery (FLAIR) for semi-automatic contouring of the tumour size changes. In LGG, it is challenging to distinguish recurrent tumours from treatment-induced related changes (e.g. radiation necrosis) by MRI. T2-weighted MRI and FLAIR signals in the assessment of the treatment response reflect both the tumour region and gliosis (glial cells reacting in response to damage and forming scars with dense fibrous texture within the damaged area). Moreover, the time until recurrence onset is also unpredictable. After many years of quiescent/stable radiological assessment, tumour progression can be developed from lower grade tumours [206, 207]. The demand is increasing to find complementary imaging models in addition to MRI to allow better non-invasive assignment of tumour progression.

1.5. Molecular Imaging of gliomas

1.5.1. Positron Emission Tomography scan

Positron emission tomography (PET) is a promising imaging technique that uses radioactively labelled tracers and provides sensitive molecular information about the tumour cells' metabolic level, based on the knowledge that the metabolic rate (glucose uptake and protein synthesis) positively correlates with tumour grade. PET imaging involves the intravenous administration of an appropriate ligand labelled with a positron-emitting radioisotope. The selected ligands are chemical tracers that bind specifically to the desired target. The injected chemicals are labelled with well-described, short-lived radioactive nuclides (radionuclides), such as ^{11}C ($t_{1/2} = 20.4$ min) and ^{18}F ($t_{1/2} = 109.8$ min). Isotopes are unstable atoms with either extra protons or extra neutrons. The nucleus of an isotope

with an excess proton converts the excess proton into a neutron by capturing the orbital electron and emitting a positron (β^+) with high kinetic energy. The positron combines with a free electron to form positronium, which then undergoes annihilation. In the positron annihilation process, the electron collides with the positron, leading to the emission of a pair of gamma-ray photons (511 keV) that travel in an anti-parallel direction [208]. The pair of gamma-ray photons are detected by the PET scanner, which is composed of rings of radiation detectors.

1.5.2. Development of PET tracers

Molecules in circulation can access the brain via many mechanisms, including lipid-mediated free passive diffusion and carrier-mediated transport (CMT) [209]. A wide range of lipid-soluble molecules enter the brain passively, and lipophilicity (lipid solubility) is an essential factor that influences the passive entry of molecules into the brain. Passive transfer across the BBB depends on the molecular weight of the substance being less than 500 Da [210].

The main BBB glucose carrier is glucose transporter type 1 (GLUT1), which also transports other hexoses, including mannose and galactose. A classic example of a glucose PET tracer is 2- ^{18}F -fluoro-2-deoxy-D-glucose (^{18}F FDG).

^{18}F FDG is transported into the brain via the action of the glucose transporter. It can provide diagnostic information regarding the tumour grade and progression based on the glucose metabolism level in the tumour compared with normal tissues [211, 212]. ^{18}F FDG used in *in vivo* tumour PET imaging exhibits high non-specific binding because of normal tissue glucose metabolism and tracer uptake; thus, the tumour-to-background ratios in the brain are poor [213]. The high uptake of ^{18}F FDG in the grey matter (reference region) compared with the tumour region complicates the accurate definition of tumour localisation

and progression tracking [214].

Radiolabelled amino acid tracers are used in brain tumour imaging to trace amino acid metabolism to reflect high proliferative activity within the tumour region compared with normal tissue. Neutral amino acids, such as L-phenylalanine, are transported through large neutral amino acid transporter type 1 (LAT1). Arginine and other cationic amino acids, such as lysine and ornithine, can be transported via the cationic amino acid transporter type 1 (CAT1) transporter. Many amino acid tracers have been previously studied in PET imaging, including [^{11}C]-methionine ([^{11}C]MET), [^{18}F]-fluoroethyltyrosine ([^{18}F]FET), [^{11}C]-alpha-methyl-L-tryptophan ([^{11}C]AMT) and [^{18}F]-dihydroxyphenylalanine ([^{18}F]DOPA).

The [^{11}C]MET tracer is commonly used in PET imaging for gliomas. The increase in methionine uptake correlates with increasing tumour grade [215]. [^{11}C]MET is transported across the BBB via LAT [216]. [^{11}C]MET is the most prevalently studied amino acid tracer due to its low background and low uptake density by the healthy brain compared with tumour tissues [217-219]. [^{11}C]MET uptake has been indicated to correlate with glioma grade, micro-vessel density, tumour cell density and proliferation [220-222]. However, regardless of the previous advantages, the clinical utility of this tracer is limited due to the short half-life of ^{11}C . Therefore, many other tracers have been developed, including [^{18}F]FET and [^{18}F]DOPA, which show high sensitivity in high-grade recurrence diagnosis [223-225].

1.5.3. PET and TSPO tracers

Based on the previous findings, PET is also considered an effective quantitative imaging method for analysing the over-expression of TSPO in many brain diseases, including brain tumours [226, 227]. In brain tumours, the enhanced TSPO expression in astrocytomas compared with its low expression in the normal brain indicates that TSPO is a potential candidate for PET imaging. Previous research has indicated that TSPO is a promising PET imaging target for glioma grade assessment [227]. In addition, the possibility of co-registering PET and MRI has allowed for an improved prospective understanding of tumour progression.

[¹¹C]-(R)PK11195 is the first-generation ligand and is the most widely used tracer in PET imaging that binds specifically to TSPO. The [¹¹C]-(R)PK11195 tracer was first introduced for PET imaging of gliomas in 1989 and 1991. [¹¹C]-(R)PK11195 tracer is widely used as a successful tracer in many neuropathological conditions, including AD [228]. [¹¹C]-(R)PK11195 has been promising in PET neuroimaging to differentiate between LGGs and the higher grade of the same type. For instance, previous research from our group has shown that [¹¹C]-(R)PK11195 binding can be used to detect increased TSPO expression in AO compared with low-grade oligodendrogliomas, even when rCBV analysis does not show significant differences in blood flow [8]. Moreover, previous research conducted using PET imaging techniques in glioblastoma patients indicated that [¹¹C]-(R)PK11195 showed a two-fold higher binding in the tumour than in the normal grey matter [229]. A positive correlation between [¹¹C]-(R)PK11195 and tumour grading was indicated in a study by Takaya and colleagues [230]. However, despite the promising findings on the use of [¹¹C]-(R)PK11195 as a radiolabelled tracer for TSPO, [¹¹C]-(R)PK11195 has some limitations, such as its highly non-specific binding, short half-life of ¹¹C (20.4 min) and weak signal-to-noise ratio [226, 231-233].

Numerous studies have investigated alternative tracers that can overcome the limitations of [^{11}C]-(R)PK11195, and these are called second-generation and third-generation tracers. Compared with [^{11}C]-(R)PK11195, second-generation tracers, such as [^{18}F]N-fluoroacetyl-N-(2,5-dimethoxybenzyl)-2-phenoxyaniline ([^{18}F]PBR06), N-acetyl-N-(2-[^{11}C]methoxybenzyl)-2-phenoxy-5-pyridinamine ([^{11}C]PBR28), N-(2,5-Dimethoxybenzyl)-N-(5-fluoro-2-phenoxyphenyl)acetamide ([^{11}C]DAA1106), N,N-diethyl-2-[2-(4-methoxyphenyl)-5,7-dimethylpyrazolo[1,5-a]pyrimidin-3-yl]acetamide ([^{11}C]DPA-713) and N,N-diethyl-2-[4-(2-fluoroethoxy)phenyl]-5,7-dimethylpyrazolo[1,5-a]pyrimidine-3-acetamide ([^{18}F]DPA-714) have been found to have higher binding affinity for TSPO with specific binding [227, 234-236]. For example, [^{18}F]PBR06 exhibited higher specific binding in a preclinical model of glioma and 75% *in vivo* displacement with an unlabelled ligand [227]. Further, [^{18}F]PBR06, [^{11}C]PBR28 and [^{11}C]DAA1106 showed higher levels of specific binding in animal models of neuroinflammation and brain tumours than [^{11}C]-(R)PK11195 did [234-236].

[^{18}F]DPA-714 was first proposed in 2008 as a tracer with rapid BBB penetration and was considered useful for glioma tumour detection and treatment response monitoring [237]. It has been previously shown to have stronger, more specific binding to TSPO and lesser non-specific binding compared with [^{11}C]-(R)PK11195 in a rat neuroinflammation model and a rat glioma model [238-240]. Moreover, [^{18}F]DPA-714 longer half-life (109.7 minutes) than [^{11}C]-(R)PK11195, with its higher specificity and lower non-specific binding, making it more suitable for clinical use [241, 242]. A preclinical study in a rat glioma model showed the feasibility of using [^{18}F]DPA-714 as a suitable alternative TSPO radiotracer in gliomas, and a high level of TSPO expression was validated by immunohistochemistry of rat brain tissue sections [239, 240]. Moreover, [^{18}F]DPA-714 showed significantly higher uptake within the tumour region compared with the contralateral brain, with high specificity

of more than 85%, demonstrated by an *in vivo* displacement study [239]. A multi-tracer study using [¹⁸F]DPA-714, [¹⁸F]BR-351 (matrix metalloproteinase marker) and [¹⁸F]FET identified unique glioma tissue regions that could be detected by [¹⁸F]DPA-714 but not [¹⁸F]FET in a preclinical murine glioma model, which may reflect increased TSPO expression at glioma infiltrative regions [243]. Furthermore, another study indicated the earlier detection of glioma progression and infiltration compared with [¹⁸F]FET in a human GBM-derived xenograft rat model [244]. Awde et al. showed the feasibility of using [¹⁸F]DPA-714 to monitor tumour progression and glioma treatment response (administration of anti-neoplastic agent, erufosine) in a GBM rat model [240].

Third-generation TSPO PET radioligands (e.g. ER176 and GE-180) have been developed to reduce background noise and to achieve greater specificity than [¹¹C]-(R)PK11195 [245, 246]. S-N,N-diethyl-9-(2-(18F-fluoroethyl))-5-methoxy-2,3,4,9-tetrahydro-1H-carbazole-4-carboxamide ([¹⁸F]GE-180) shows good affinity for TSPO, but its low penetration through the BBB prevents its use as a tracer in LGG with intact BBB [245, 247, 248]. Its high tumour-to-background ratios were suggested to be driven by BBB breakdown [249]. However, there is a debate regarding [¹⁸F]GE-180's sensitivity/insensitivity to TSPO polymorphism and its dependence on BBB breakdown [247, 249-251]. [¹¹C]ER176 is a quinazoline analogue of [¹¹C]-(R)PK11195 that overcomes the limitations of [¹¹C]-(R)PK11195 by providing improved lipophilicity and better specificity [7, 252]. A head-to-head comparison study between [¹¹C]ER176 and [¹¹C]PBR28 showed that [¹¹C]ER176 had better time stability, lower plasma metabolism and higher BPND for the examined healthy subjects with high-affinity binders (HABs) and mixed-affinity binders (MABs), respectively [246].

1.6. TSPO expression in neurovascular unit at the blood brain barrier (BBB)

1.6.1. The neuro-vascular Unit

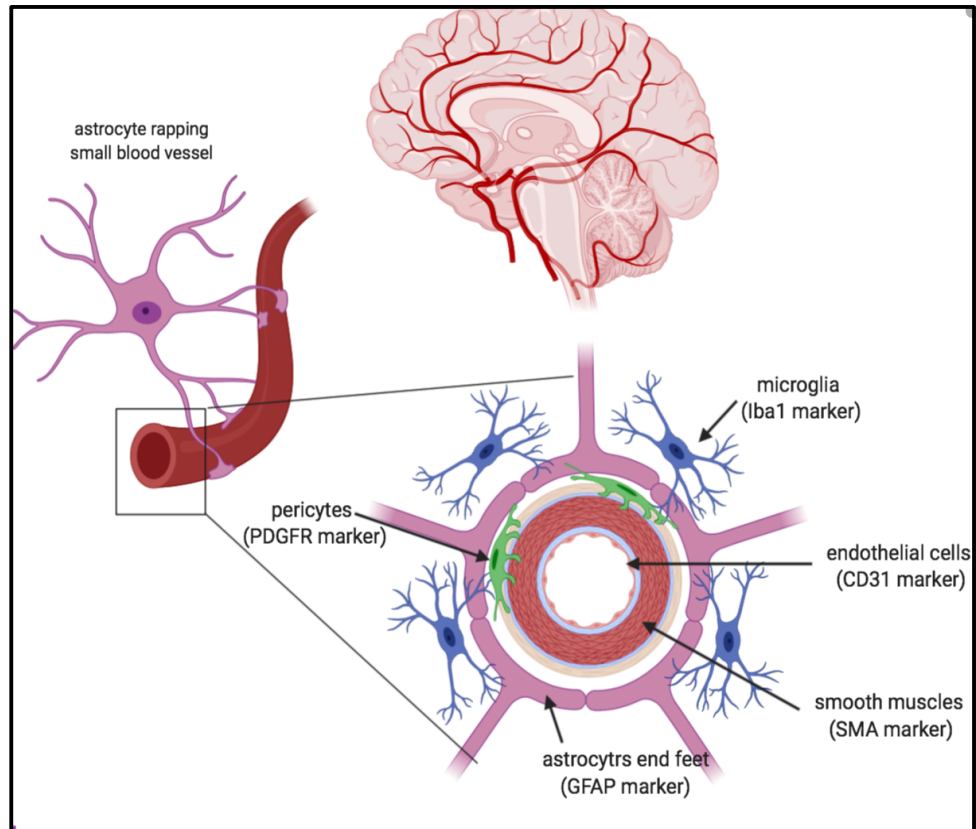


Figure 5: Neurovascular unit cellular composition in brain (NVU). Biorender software.

The neurovascular unit (NVU) is mainly composed of endothelial cells (ECs), microglia, astrocytes, and pericytes.

1.6.1.1. Endothelial cells

BBB mainly constitutes of endothelial cells (ECs) which is an important component of the neuro-vascular unit (NVU) (Figure 5). ECs form the main component lining the cerebral blood vessels, and they play an important role in creating a selective barrier for different molecules. This important barrier structure is composed of tight junctions and adherens junctions present between each EC. The luminal and abluminal membranes of the

ECs contain ion channels, transporters and metabolite-degrading enzymes that control the transport of nutrients (e.g. glucose, amino acids and electrolytes) from blood to the brain and the efflux of products to the blood. ECs express TSPO under normal conditions; therefore, it would be interesting to study their contribution to TSPO density and signal observed in tissues (immunohistochemistry, IHC) on PET images [253]. IHC analysis of ECs showed co-localisation between TSPO and CD31, a marker of ECs, and this indicates that ECs express TSPO [254]. TSPO-expressing ECs within the cortical and white matter of the normal brain accounted for 30% of the total vascular density [255]. Moreover, TSPO was found to be expressed by vascular ECs in GBM and AD brain tissue [256, 257]. Many studies have suggested the importance of including the vascular component in the quantification model of TSPO with PET imaging for more accurate estimation of TSPO signals within the target region [255, 258-262].

1.6.1.2. Astrocytes

Astrocytes are highly branched star-shaped cells that are widely distributed within the brain, between the ECs and the neurons. Astrocytes mediate synaptic activity and synaptic neurotransmitter levels, maintain ionic homeostasis around the neurons, regulate cerebral blood flow and cover the cerebral blood vessels by their end feet (processes), which are a part of the BBB [263]. They have an important role in regulating fluid homeostasis and maintaining the integrity of the BBB [264, 265]. Moreover, astrocyte processes have a vital role in maintaining ion, pH, fluid and healthy synaptic transmission [266]. TSPO expression has been shown to be up-regulated in reactive astrocytes during inflammation in many pathological conditions [267, 268], but this evidence has been debated. A study indicated that TSPO was expressed at a low level by astrocytes in neuroinflammatory disease [269], while other studies indicated a high level of TSPO [88, 270, 271]. In the

normal mouse brain, no TSPO co-localisation was observed in the astrocyte endfeet surrounding the perivascular region; this indicates that resting glial cells do not express TSPO under normal conditions [272]. However, another study indicated that astrocytes express TSPO at minimal levels during normal conditions [270]. Moreover, in gliomas, the astrocytic contribution to the total TSPO signal was found to be limited compared with glioma-infiltrating microglia/macrophage cells [239]. Liddel et al. indicated two phenotypes for activated astrocytes in neurodegenerative diseases A1 (neurotoxic) and A2 (neuroprotective) which are involved in releasing neurotrophic factors. They suggested the activated microglia's contribution to induce A1-activated astrocyte phenotype through IL-1 α , TNF- α and complement component 1,q subcomponent (C1q; protein complex component of classical complement pathway involved in innate immune response) *in vivo* and *in vitro* [273]. In glioblastoma, reactive astrocytes' A2-specific phenotype is induced by activated microglia linked to the JAK/STAT pathway, leading to the evolution of the immunosuppressive environment and anti-inflammation [274].

1.6.1.3. Pericytes

Pericytes are embedded in the basement membrane between ECs and astrocyte endfeet within the NVU, and they play an important role in BBB integrity. Pericyte coverage and density along the vessels correlates inversely with the permeability of vessels. Pericytes express some cell surface receptors (e.g. platelet-derived growth factor receptor- β [PDGFR β]) which is important to maintain BBB integrity [275]. Pericytes play an important role in BBB integrity. One study indicated that in PDGFR β -null mice, the BBB permeability to water and high-molecular-mass molecules (e.g. albumin, which has a mass of 70 kDa) increased; this indicates an impairment in BBB integrity [276]. Moreover, ECs are involved in pericyte recruitment to the vessel wall through the PDGF receptor- β . Pericytes'

contribution to TSPO expression has been previously studied in normal mouse brains; a previous study found that pericytes could express TSPO in large blood vessels in this context [272]. Another study found that TSPO was expressed by pericytes and ECs in GBM [256].

1.6.1.4. Microglia/Macrophages

Microglia are resident immune cells of the CNS that are also associated with the NVU. They remain in a quiescent (inactive) state in normal conditions, but they become activated in pathological conditions [75, 277]. TSPO is considered to be one of the molecules that is highly expressed in activated microglia during inflammation in many neurodegenerative and neuroinflammatory diseases [277-280]. Therefore, TSPO has been used as a target to measure activated microglia in the brain in [¹¹C]-(R)PK11195 PET imaging [277]. Moreover, a preliminary study in brain tumours found that glioma-associated microglia and macrophages (GAMMs) showed partial contribution to the total TSPO expression level (detected by double immunofluorescence staining) compared with the TSPO in neoplastic tissues [8, 281].

Macrophages in the CNS are differentially distributed within the perivascular region, choroid plexus and subdural meninges. Perivascular macrophages are elongated cells that are distributed in close proximity along the outer layer of brain microvessels [282]. Immunohistochemical and DIF studies of TSPO expression indicated that activated microglia and macrophages have been found to express high levels of TSPO as main contributors to TSPO expression compared with astrocytes in AD, human immunodeficiency virus encephalitis (HIVE), GBM and AA [88, 230, 256]. Rodent microglia and macrophage induced TSPO expression in response to pro-inflammatory stimulus (LPS) but no increase was not seen in human microglia and peripheral blood mononuclear cells (PBMCs) *in vitro* [283]. In mice model, pro-inflammatory stimulus

(TNF) showed increased in TSPO expression while no increase was seen in response to anti-inflammatory (IL-4) *in vitro* and *in vivo* [284, 285].

Further research indicated that TSPO expression in microglia and macrophages differ based on their pro-inflammatory or anti-inflammatory phenotypes in response to different environmental signals. A very recent study found increased TSPO expression in microglia and macrophages after *in vitro* treatment with a pro-inflammatory stimulus (LPS), while no significant increase was seen in the response to an anti-inflammatory stimulus (IL-4) [284]. Moreover, cultured astrocytes showed a significant increase in response to pro-inflammatory stimuli (LPS, TNF), while no significant increase was seen in response to the anti-inflammatory stimulus (IL-4). During anti-inflammatory stimulation (IL-4), TSPO expression remains at a low level in microglia/macrophages [286]. The exact role of TSPO in modulating M1/M2 polarisation is not fully understood, and it was recently suggested to operate via the peroxisome proliferator-activated receptor- γ (PPAR γ) pathway [286]. The proposed model by Mantovani and colleagues indicated that interferon- γ (INF- γ), LPS, TNF and GM-CSF induced the M1 phenotype of macrophages, while M2 was subdivided into M2a, M2b and M2c in response to L-4, toll-like receptor (TLR)/IL-1R and IL-10, respectively [287]. Microglia cells alternatively activated M2 phenotype also subdivided into three different classes, M2a (repair and regeneration), M2b (immune-regulatory), M2c (acquired-deactivating phenotype) in response to different inducers including, IL -4 and IL-13 for M2a; IL-1R ligands, IL-10 for M2b; TGF β and glucocorticoids for M2c [288]. The M2 phenotype switching in microglia and macrophages in the tumour microenvironment is a complex process that includes different cells' cross-talk and released factors from the glioma and tumour microenvironment that induce M2 polarisation [289].

1.6.2. Glioma-associated microglia and macrophages

GAMMs are a heterogeneous population of resident and peripherally derived inflammatory cells [290-293]. A direct correlation between glioma grade and the density of infiltrating GAMMs was suggested in 1996 by Roggendorf et al. A subsequent study indicated that the prevalence of perivascular and intra-tumoral CD68-positive microglia and macrophages are significantly higher in GBM (WHO grade IV) than in AA (WHO grade III), diffuse astrocytomas or low-grade astrocytomas (WHO grade II, LGA) and pilocytic astrocytomas (WHO grade I). The authors indicated that these differences could be related to the disturbance of the BBB in GBM, as a result of which, the BBB is more permeable to the infiltrating immune cells in GBM compared with LGGs with an intact BBB [294-296]. Glioma cells may recruit GAMMs by secreting specific factors, chemokines and chemoattractants (e.g. monocyte chemoattractant protein-1 [MCP-1] or CCL2, growth factor glial cell-derived neurotrophic factor [GDNF] and colony stimulating factor-1 [CSF1]) [297-299]. The role of GAMMs in the tumour is still not fully understood. There is ongoing debate regarding the function of GAMMs within the tumour microenvironment and whether they promote tumour growth or have an immunosuppressive role. The immunosuppressive role of GAMMs in tumour growth might be inhibited within the tumour microenvironment, or the GAMMs may have a tumour-supporting role that leads to the promotion of glioma cell survival and migration. One study suggested a tumour-supporting role of GAMMs arising by secretion of cytokines (e.g. IL-10, IL-1 β and TGF- β) and growth factors (e.g. VEGF and HGF), which further promote glioma proliferation and migration [300, 301]. Other studies have indicated that microglia play a tumour-supporting role by creating an inflammatory microenvironment that is favourable for tumour growth initiation and progression, but the exact mechanism by which microglia support tumour progression is not well understood [302, 303]. Glioma-infiltrating microglia were found to be positive for

MHCII/TLR4, but they lacked the co-stimulatory markers (CD86, CD80 and CD40) important for T-cell activation [290]. This indicates that intra-tumoral inhibitory signals may play a role in suppressing the activation of pro-inflammatory mechanisms [290]. Moreover, macrophages were found to have dual roles as tumour-rejecting and tumour-promoting actors [304-307]. However, the mechanism responsible for diminishing the level of co-stimulatory proteins is still not fully understood.

The extent and distribution of TSPO in GAMMs has become an interesting field of research. Tissue analysis of immunoperoxidase stained cells also indicated a co-localisation between Iba1 and TSPO, suggesting that intra-tumoral macrophages/microglia contribute partially to the total TSPO expression and to the [¹¹C]-(R)PK11195 PET signal within the tumour microenvironment. Although these cells were TSPO positive, the highest contribution to the total TSPO staining on tissues was from neoplastic tissues [8]. The TSPO-positive GAMM density was illustrated to be unchanged among different brain tumour histotypes and grades [8].

In AA, immunohistochemistry and microarray expression analysis indicated the expression of low levels of TSPO by glioma-infiltrating microglia. However, the mechanism that leads to the reduction in microglial TSPO expression within intra-tumoral regions is still unknown [230]. Other pathological conditions considered a decrease in TSPO in microglia and macrophage, such as small vessel disease (SVD) and AD [308, 309].

A preliminary study in a cohort of 50 patients with astrocytic and oligodendroglial gliomas indicated that there was no TSPO staining in the astrocytes, oligodendrocytes and neurons in either tumour type. Another study indicated a limited TSPO signal in astrocytes within the glioma, but macrophages and microglia made a minor contribution to the observed TSPO expression in the glioma model [239].

Based on the previous findings, we examined the contribution of GAMMs to TSPO

expression in the glioma microenvironment and compared it with the neoplastic contribution to determine which cell type contributed the most to the observed TSPO expression.

1.6.3. Vascular pathology and inflammatory contributions in glioma growth

During the early development of LGGs, there is no apparent disruption of the BBB; as the gliomas transform to a high grade, the increased proliferation and metabolic rate will induce angiogenesis. Hypoxia increases with tumour grade and creates a high demand for oxygen and nutrients within the tumour region. High levels of hypoxia alongside transforming high-grade gliomas lead to increased levels of HIF-1. High-grade gliomas start to secrete VEGF, which induces growth of new capillaries with altered structure and increased permeability. The newly formed tumoral vascular ECs express an increased level of molecular transporters to overcome the high energy demand. This newly formed barrier is called the blood–brain–tumour barrier (BBTB). In LGG, the BBTB resembles the BBB under normal physiological conditions. TSPO expression has been found to transiently increase in a mouse model of chronic hypoxia in the newly formed endothelial vessels during the early phase of vascular remodelling [310]. This could be detected with PET imaging as a sign of early vascular remodelling. A preliminary study suggested that an increasing neoplastic growing population is accompanied by increased inflammatory proliferation cells and increased vascular permeability supporting tumour growth [311]. Neoplastic cells secrete cytokines to recruit inflammatory cells. These inflammatory cells switch from a pro-inflammatory phenotype role (M1) into an anti-inflammatory tumour-supporting role (M2) in mechanisms that are still not fully understood. However, the distinct individual cellular components and the different released factors within the tumour

microenvironment participate in the development of an anti-inflammatory immunosuppressive environment. The change in the microglia and macrophage M1/M2 phenotypes is a complex process that is affected by cross-talk between distinct cellular components within the tumour microenvironment. One study indicated that astrocyte-microglia cross-talk is involved in the immunosuppression in the tumour microenvironment and is mediated by JAK-STAT activation, leading to increased IL-10, TGF β and G-CSF secretion (*in vitro* astrocyte/microglia/tumour co-culture slices) in the medium. Activated microglia induce astrocytes' activation and secretion of anti-inflammatory cytokines within the tumour microenvironment, which is involved in preventing an efficient immune response in glioblastoma [274]. Moreover, another study indicated the contribution of the vascular niche IL-6 synergistically with CSF-1 from glioma cells to the M2 alternative activation phenotype in macrophages through downstream PPAR γ and HIF-2 α favouring tumour growth [312].

A recent paper showed that pro-inflammatory M1 expressed a high level of TSPO, while in response to IL-4, TSPO expression was reduced in the M2 anti-inflammatory cells [286]. Targeting TSPO with either agonist (FGIN-1-27) or antagonist ([¹¹C]-(R)PK11195) *in vitro* for TSPO activity could be a future interesting therapeutic target to modulate tumour growth. The M1 to M2 polarisation in inflammatory cells was shown to be modulated by TSPO through PPAR γ . IL-4 induces M2 polarisation supporting glioma growth and increased PPAR γ expression. TSPO over-expression and agonist (FGIN-1-27) treatment blocked IL-4-inducing M2 polarisation by inhibiting the expression of PPAR γ . In contrast, antagonist ([¹¹C]-(R)PK11195) treatments of TSPO induced PPAR γ expression, leading to inducing M2 polarisation to support tumour growth *in vitro*. However, this study was conducted *in vitro* in microglia, which still will not reflect the complexity of the *in vivo* microenvironment but could suggest that TSPO is a possible upstream modulator of PPAR γ

expression. Further *in vivo* studies of brain tumours would be interesting.

Based on the previously indicated studies, examining both vascular and inflammatory contributions to TSPO expression levels within the glioma microenvironment would be an important future direction to better understand tumour growth. More interestingly, a very recent study by Zinnhardt et al. showed that TSPO was restrictively expressed in activated GAMMs and tumour-infiltrating myeloid-derived suppressor cells (MDSCs) [313]. MDSCs are myeloid cells that have a role in suppressing the immune response in cancer. Therefore, TSPO could be used as a non-invasive target with PET imaging to selectively image glioma-associated immunosuppressive tumour-associated microglia/macrophages [254, 313]. In agreement with these findings, TSPO is involved in creating a balance between pro-inflammatory (M1) and anti-inflammatory (M2) phenotypes.

In microglia, high level of ROS, NFkB activation, NLR family pyrin domain containing 3 (NLRP3) inflammasome (involved in processing pro-IL-1 β to release IL-1 β), lead to increase level of pro-inflammatory cytokines (e.g. IL-1 β and TNF α) downstream [314]. One study suggested that TSPO down-modulates the increased TNF α expression level in response to LPS in murine microglia, suggesting a possible TSPO role in controlling the prolonged increased pro-inflammation under stress conditions, but this suggested mechanism is still not fully understood. Moreover, a proposed mechanism in the same study involved Annexin A1 (inhibitor of development of innate inflammation that blocks the LPS-induced inflammatory cytokine secretion) in inhibiting TNF α production in a TSPO-dependent manner [315]. Glucocorticoids are positive modulators of Annexin A1 expression, which connects steroids in modulating pro-inflammation. Furthermore, in glioma, TSPO was shown to reduce oxidative stress, pro-inflammatory cytokines and pro-inflammatory enzymes (inducible nitric oxide synthase [iNOS] and COX-2) through

neurosteroid synthesis [316].

1.6.4. PET imaging and inclusion of vascular components in the kinetic modelling

Using TSPO as a PET imaging target in brain tumours is a promising but methodologically challenging approach because of TSPO's ubiquitous expression in ECs and inflammatory cells in the intra-tumoral environment [317].

Many second-generation tracers, such as [¹¹C]PBR28, have a high affinity for TSPO and are likely to show a high degree of binding to TSPO in blood vessels. This highlights the importance of including vascular compartments in the kinetic modelling of TSPO signal quantification [255, 317]. The classical standard model for TSPO quantification is the two-tissue compartmental model or 2TCM model. 2TCM is mainly based on the kinetics between two compartments the non-displaceable component (C_{nd}; non-specific and free ligands binding) and specific binding (C_s). C_s represents the specific binding of ligands from the plasma to the studied target tissue. C_{nd} represents the binding of the non-specific and free ligands to the target tissue. TSPO specific ligand binding to the brain vessels has not been previously considered in PET imaging. The first study that introduced vascular contribution to the 2TCM model (named 2TCM1K) was performed by Rizzo et al. [317]. Analysis of clinical data from healthy subjects showed a significant difference in the estimated total volume of distribution (VT) between the two models (2TCM and 2TCM1K), with poor correlation between the two ($R^2 < 0.25$).

In 2TCM-1K model, the vascular contribution of the TSPO radiotracer bindings showed better correlation with TSPO mRNA expression mapping using the Allen Human Brain Atlas (<https://portal.brain-map.org/>) compared with the estimations made with the standard 2TCM [255].

1.7. Current study insights and purposes:

Based on the previously mentioned findings and studies within the literature, this current study examined three main hypotheses that will be discussed in chapter 2 to chapter 4.

- 1) In chapter 2, the NVU different cell types contributions to TSPO expression have not been well studied in normal brain condition. This current study will present a comprehensive study of TSPO expression at the NVU in normal porcine brain tissues.
- 2) In chapter 3, four main purposes were studied. First, TSPO can be used as a biomarker to differentiate between low-grade and transforming higher grade oligodendrogliomas. Second, studying if TSPO high expression could predict a worse overall survival in oligodendrogliomas cohort of fifty patients. Third, the vascular endothelial cells, GAMMs, neoplastic contributions were mainly examined in oligodendrogliomas cases. The main purpose is to examine if the increased TSPO protein expression that has been found in high-grade oligodendrogliomas was mainly contributed by the neoplastic cells (IDH1) compared with GAMMs and vascular endothelial cells. Fourth, studying the percentage of TSPO rs6971 polymorphism among the studied cohort of fifty patients who are all diagnosed with oligodendrogliomas.
- 3) In chapter 4, the regulation of TSPO expression in gliomas was discussed. Two main mechanisms have been examined including, epigenetic regulation (TSPO promoter methylation) and suggested candidate genes that might have a regulatory role in TSPO expression through different pathways in oligodendrogliomas and astrocytomas.

CHAPTER 2

EXPRESSION AND DISTRIBUTION OF THE 18KDA TRANSLOCATOR PROTEIN IN THE GLIO-VASCULAR UNIT

CHAPTER 2

2.1. Hypothesis:

We hypothesised that porcine astrocytes, endothelial cells and macrophages express TSPO at NVU in normal porcine brains. Taking into consideration the distinct cellular contributions of the NVU to TSPO expression, in addition to vascular endothelial cells, would improve the understanding of TSPO expression in these cellular components in normal and pathological brain conditions.

2.2. Study rationale and background:

The tumour microenvironment (TME) is complex, and quantification of TSPO expression in human gliomas is challenging due to the different cell population within the TME. Understanding the complexity and cellular distinct contributions to TSPO expression in normal and pathological conditions is essential when interpreting PET imaging and tissue analysis results. Moreover, TSPO PET imaging signal quantification does not consider the different cell population within TME and their different response that may affect the TSPO expression level during the disease progression. Understanding the distribution of TSPO expression level in various cellular components is still very limited in a normal brain. One study in a normal mouse brain by Betlazar et al. showed different cellular contributions to TSPO expression including, macrophage, astrocytes, microglia and endothelial cells [257]. They indicated that TSPO was expressed at a different level in different brain regions, even in normal condition. TSPO expressed at a high level in the olfactory bulb, cerebellum, ependymal and choroid plexus. TSPO was expressed in blood vessels in large arteries, capillaries, and veins by showing strong colocalisation with CD31. No detectable TSPO

expression was found in perivascular macrophage and microglia. Therefore, it was interesting to check the basal level of TSPO expression at the NVU in a more developed model such as porcine. To our knowledge, studying different cellular contributions to TSPO expression in the porcine model is novel and was not studied before. Several immortalised BBB models showed a good expression level of BBB transporter proteins with a low ability to sustain BBB integrity (low transendothelial electrical resistance [TEER]) [318]. Primary cultured porcine endothelial cells became a reliable model that showed high TEER with a good expression level of tight junction proteins that resembles maintained integrity. The main cellular components studied in the current chapter are macrophage, astrocytes and endothelial cells (ECs) in normal porcine brain.

The neurovascular unit (NVU) consists of endothelium, astrocyte end-feet, pericytes, neurons, and axons. In normal brain conditions, microglia and macrophage express low TSPO, but this expression is dramatically induced during inflammation. During inflammation in many neurodegenerative and inflammatory CNS diseases, microglia become activated with induced TSPO expression [277-280].

In normal mouse brain astrocytes, no TSPO colocalisation was indicated in astrocytes end-feet surrounding endothelial cells [272]. In glioma, astrocytic TSPO expression was limited compared to the CD11b-positive GAMMs [239].

Studying the TSPO basal level at these cells in a normal brain model would help to better understand the TSPO expression level in similar cell types under pathological conditions, more precisely, gliomas.

In this current dissertation, the expression of TSPO receptors was examined at a cellular level in the porcine macrophage cells and primary isolated PBECs using the radiolabelled tracer [¹⁸F]DPA-714 by Scatchard binding assay. The Scatchard binding assay

was performed to estimate both cells TSPO density Bmax and Kd by using unlabelled PK11195 and DPA-714.

[¹¹C]-(R)PK11195 is the first-generation ligand and is the most widely used tracer in PET imaging that binds specifically to TSPO. [¹¹C]-(R)PK11195 tracer is widely used as a successful tracer in many neuropathological conditions, including AD [228]. There was an excellent correlation between TSPO tissue expression and [¹¹C]-(R)PK11195 binding in PET imaging in many studied diseases, including brain tumours [8].

Despite the advantages of using [¹¹C]-(R)PK11195 tracer in glioma and neuroinflammatory diseases, it has many limitations, such as its high level of non-specific binding [226], the short half-life of ¹¹C (20.4 min) and weak signal-to-noise ratio [233]. Later studies examined many tracers to overcome these limitations, and the [¹⁸F]DPA-714 tracer has shown promising outcomes to be used as an alternative to [¹¹C]-(R)PK11195.

The [¹⁸F]DPA-714 tracer showed many properties including its ¹⁸F-labelled longer half-life (109.8 minutes) and its reduced non-specific binding compared with [¹¹C]-(R)PK11195. The [¹⁸F]DPA-714 tracer showed three times higher specific bindings and lower non-specific uptake in animal models of neuroinflammation and stroke diseases [238, 319]. In preclinical 9L glioblastoma rat model, a significant higher uptake of the tracer within the tumour region compared to the contralateral normal brain hemisphere or cerebellum. Second, the unlabelled displacement of this tracer *in vivo* showed the high specificity of [¹⁸F]DPA-714 to TSPO and more than 85% displacement of tumour uptake [239]. They also referred to minor GAMMs contribution to TSPO signal compared to the neoplastic region while no TSPO expression was seen in reactive astrocytes. Moreover, other preclinical studies considered [¹⁸F]DPA-714 is a suitable tracer for targeting tumour progression and infiltration [243, 244].

In general, all TSPO used tracers have been shown to bind with different affinities to ECs in healthy subjects, indicating the importance of vascular inclusion in the TSPO density signal interpretation with PET imaging [255, 258-261]. Therefore, based on all the previously mentioned studies, the NVU cellular components' contribution to TSPO expression is a suggested important aspect examined and discussed in this chapter.

2.3. Material and methods:

2.3.1. Primary endothelial cells (PBECS) isolation and culture:

Pig brains from the domestic *Sus. Scrofa* were collected from a local abattoir and transported to the University in L-15 medium treated with antibiotics (100mg/ml⁻¹ streptomycin, 100mg/ml⁻¹ penicillin). Brain hemispheres were then washed in phosphate-buffered saline containing 1% P/S (penicillin/streptomycin). Brains were cleared of meninges and placed in ice-cold PBS containing 1% P/S. White matter was removed and grey matter placed into isolation medium (500mL high glucose Dulbecco Modified Eagle Medium, 10% foetal bovine serum, 1% PS, 2% 1M HEPES). Grey matter was chopped into small pieces using previously sterilised scissors and passed through a 50mL syringe into isolation medium.

Approximately 40mL of tissue in isolation medium was passed through a dounce tissue grinder using twenty strokes each from a loose and a tight-fitting pestle. The resulting homogenate was filtered under vacuum through a 150µm mesh and the remaining filtrate was filtered through a 60µm mesh. The 60 µm mesh filters were placed in digestion medium (Medium 199; 10% FBS, 1% P/S, 210units.mL⁻¹ Collagenase type 3, 114units.mL⁻¹ DNAase I, 91units.mL⁻¹ Trypsin) and incubated for 1 hour at 37°C with gentle shaking. Resulting medium was centrifuged at 1200 rpm for 5 minutes, the supernatant aspirated and the pellet re-suspended in isolation medium. Centrifugation at 1200rpm for 5 minutes was repeated a further three times with the pellet suspended in FBS: DMSO in a 9:1 ratio following the final spin. Isolate was stored at -80°C in isopropanol overnight and transferred to liquid nitrogen for long term storage.

Cells were cultured using six well culture plates pre-treated with collagen for 1.5 hours and fibronectin for a subsequent 24 hours. Cells were thawed to 37°C before being centrifuged for 5 minutes at 1000rpm to remove DMSO. The supernatant was re-suspended in Dulbecco

Modified Eagle Medium (glucose-, phenol red-, 1% PS, 2mM glutamine, 10 % Plasma Derived Serum, 125 µg/ml heparin). Cells were seeded onto aforementioned plates and incubated at 37°C, 5% CO₂ for 24 hours before removal of leftover media and purification for 48 hours in the same medium mix containing 4µg/mL puromycin dihydrochloride. Medium was again removed from each well before addition of growth medium (DMEM glucose-, phenol red-, 1% PS, 2mM glutamine, 10% PDS) for 48 hours in a 1:1 ratio with previously purified rat Astrocyte Conditioned Media CTX-TNA2 line (ACM). Rat cells were grown in DMEM supplemented with 10% (v/v) foetal bovine serum with 100 U.ml⁻¹ penicillin and 100 mg ml⁻¹ streptomycin until reached 75% confluent. The medium was collected and stored at -20°C until use. The isolation process has been conducted by me with Jeffery Penny group and Dominic Mosses (DM) helps at Stopford building, University of Manchester.

2.3.2. Astrocyte isolation from porcine brains:

The chosen Minipigs are aged between two to four months because older pigs would become senescent more quickly while culturing compared to younger ones. The isolation method was processed based on Bobilya DJ protocol [320]. First, brains were cleared of meninges carefully by sterile forceps. White matter was removed and grey matter placed into collection medium (Minimum Essential Eagles Medium (MEM) with Earle's salts containing 25mM HEPES, 2.2g/L sodium bicarbonate, 2% Fetal bovine serum (FBS), 5µg/ml Amphotericin B (Sigma, A2942), 50µg/ml gentamicin (Cambridge bioscience, G046), sterile filtered) and later minced into smaller chunks by using previously sterilised scissors. Then, the minced tissues were applied to loose homogenizer for 6 times and further tight homogenizer for 6 times. The homogenized tissues were further transferred to 50ml sterile syringe to be aspirated and ejected through the syringe. Then, the homogenized

tissues were applied for a wash by centrifugation at 400xg for 5 min at 4°C (3 times repeatedly). Each time 45ml of collection media were added and the supernatant was later discarded. Next, the tissues were digested enzymatically by adding equal volume (1:1) of collagenase Type IA enzyme (The effective final concentration is ~135 IU/mL) to the collection medium. The mixture was then allowed for incubation at 37°C in water bath for 60 min. The digested tissues were washed by centrifugation at 400xg for 5 min at 4°C (3 times repeatedly). Each time 45ml of collection media were added and the supernatant was discarded after centrifugation. The combined pellet from previous steps were carefully combined and applied for 25% BSA/Collection medium gradient by adding 25ml of 25%BSA to the combined pellet. Later, the mixture was centrifuged at 400xg for 15 min. Three layers were noticed after centrifugation (top layer contains fatty tissues, middle layer contains floating cakes of Myelin and fatty tissues, the bottom layer contains Astrocytes, capillary fragments, cellular debris and erythrocytes). The top and middle layers were both transferred to another clean falcon tube and vigorously mixed with 25ml fresh collection medium for further centrifugation at 400xg for 15 min. The bottom layer was saved on ice. This step was repeated (minimum 6 times) until the formed pellet could be negligible. All the saved pellets from previous steps were combined in one new falcon tube and suspended in 30 ml of fresh collection medium. The re-suspended pellet was later applied to a filtration step composed of 4 different filters with different sizes (149 µm, 60 µm, 30 µm, and 20 µm respectively) (Plastok® Associates Ltd., Birkenhead, Merseyside). The filtrate was centrifuged at 400xg for 5 min at 4°C and the supernatant was discarded.

Finally, the pellet was suspended in astrocyte growth medium (Minimum Essential Eagles Medium (MEM) with Earle's salts, 10%FBS, 5µg/ml Amphotericin B (Sigma, A2942), 50µg/ml gentamicin (Cambridge bioscience, G046), sterile filtered). Part of the suspension was transferred to a 75 flask for incubation at 37°C, 5% CO₂, and 95% humidity. The

medium was changed every 2-3 days until the development of astroglial cell growth was noticed. The remaining suspension was saved in FBS: DMSO (9:1) in liquid nitrogen for future use. The entire isolation process was conducted by me at Stopford building, University of Manchester.

2.3.3. Porcine immortalised macrophage cell line culture:

Sus. scrofa lung Macrophagic cells (3D4/2) were purchased from ATCC (ATCC, CRL-2845). Macrophages were cultured in RPMI 1640 medium (2 mM L-glutamine adjusted to contain 1.5 g/L sodium bicarbonate, 4.5 g/L glucose, 10 mM HEPES, 1.0 mM sodium pyruvate supplemented with 0.1 mM nonessential amino acids, 10% FBS) in 75 cm² cell culture flasks

2.3.4. Mitotracker for isolated primary cells and cell lines:

PEBECs, macrophages and astrocytes were cultured in six well plates and adhered to circular coverslips (13mm diameter) within each well. PEBECs plates only were previously coated for 1.5 hours with collagen and a subsequent for 24 hours with fibronectin. Mitotracker Green (Thermo Fisher Scientific, M7514) was diluted according to manufacturer's instructions in 1ml pre-warmed growth medium without serum at concentration 500nM to avoid cell toxicity. 1ml of MT solution was added to each well containing coverslip and plates were incubated at 37°C for 45 minutes followed by two washes for five minutes each in PBS containing calcium and magnesium. Later, cells were fixed with 4% formaldehyde for 20 minutes at room temperature. Cells were then permeabilised in PBS containing 0.2% Triton followed by 3 washes in PBS for 5 minutes each. Cells were blocked in 10% Donkey serum diluted in PBS for 2 h at room temperature. Later, it washed 3 times in PBS containing calcium and magnesium. A 1:250 working

dilution of anti-TSPO antibody (Abnova, Pab7095) was prepared in PBS and incubated for overnight at 4°C in humidity chamber. Following three washings in PBS, an anti-Goat IgG secondary conjugated with texas red (Abcam, ab6883) was diluted to 1:700 and coverslips containing cells incubated for 1 hour at room temperature ensuring this step was performed in darkness followed by washing in PBS three times for 5 minutes each. The last washing step was with distilled water to avoid crystallization and coverslips were allowed to dry in the dark for overnight. Finally, Coverslips containing cells were then treated with Prolong GOLD anti-fade fluorescent mounting medium with DAPI (Life Technologies, P36935).

2.3.5. Immunocytochemistry for primary cells:

Cells were cultured in six well plate and adhered on round coverslips (13mm in size). Cells were washed twice with PBS and later fixed with 4% formaldehyde for 20 minutes at room temperature. Later, cells were washed twice with PBS and permeabilised with 0.2% of Triton-X for 10 minutes at room temperature. Next, cells were blocked with donkey normal serum for 2h at room temperature. Later, primary antibody was added in blocking serum and incubated at 4 °C for overnight in humidity chamber. Next day, cells were washed twice with PBS and the secondary antibody was added for 1 hour at room temperature in the dark. The cells washed twice with PBS and twice with distal water and later allowed to dry at room temperature for overnight in the dark. Next day, the cells were mounted with prolong gold anti-fade mounting reagent with DAPI (Life Technologies, P36931).

The primary antibodies were used in this study were, TSPO at dilution 1:250 (Abnova, Pab7095). Iba1 at dilution 1:500 (Wako, 019-19741). GFAP (abcam, ab7260) at dilution 1:1000, CD31 (Abcam, ab225883) at dilution 1:1000. Secondary antibodies used are donkey anti-goat at dilution 1:700 (Abcam, ab6883) for TSPO, donkey anti-rabbit alexa

flour 488 at dilution 1:700 (Abcam, a21206) for GFAP and CD31 primary antibodies detection.

Individual contributions:

Porcine primary astrocytes cells, macrophages, rat astrocytes cell lines ICC and images were all conducted by me. PBECs ICC and images were conducted with Dominic Mosses (DM) helps.

2.3.6. Western Blot:

Cultured astrocytes, macrophages and PBECs cells were washed with iced cold PBS and homogenised in ice cold Protein Lysis Buffer (RIPA buffer, 50 mM Tris-HCl pH=7.4, 150mM NaCl, 1% NP 40, 2 mM EDTA, 0.1% SDS) with protease inhibitor cocktail ("Complete Mini", Roche Diagnostics, Ltd.). The amount of protein to be loaded into the gel was estimated by using Pierce BCA protein Assay (Thermofisher scientific, 23228).

Samples were then electrophoretically resolved by using a pre-casted 12% Tris-Glycine gel (Thermo Fisher Scientific) and using a 1X Running Buffer (pH=8.3, 25mM Tris base, 192 mM glycine, 0.1% SDS) with 100V applied for 90 minutes or MES SDS running buffer 1x from 20x (REF# B0002). Proteins were then transferred onto a nitrocellulose membrane using 1X Transfer Buffer TranspBlot Turbo (REF#170-4270) for 10 minutes at 125v high M.wt protein. Broad range molecular weight ladders (Precision Plus Protein™ Dual Color Standards, #1610374) were added to one side of each gel. The membrane was transferred using the transfer system Trans-Blot Turbo Bio Rad, #170-4155.

Following membranes transfer process, membranes were blocked with 5% skimmed milk powder in 1x TBS/T buffer for 1 hour at room temperature. The membranes were then probed with primary anti-body goat Anti-TSPO at a working dilution of 1:1000 (Abnova,

Pab7095) in 1x TBS/T buffer containing 5% BSA for 12-16 hours at 4°C while shaking. Following primary incubation, the membranes were allowed for washing, 3 times for 10 minutes each in 1x T/TBS. Next, a secondary Anti-goat IgG HRP conjugated (Dako, P0449) was diluted to 1:500 in 5% BSA and exposed to the membrane for 1 hour at room temperature while shaking. After secondary antibody incubation, the membranes were washed 3 times for 10 minutes each in 1x TBS/T. Porcine macrophage primary antibody Iba1 (Wako 019-19741) used at working dilution 1:1000 diluted in 5% BSA. The used secondary antibody for Iba1 is anti-rabbit HRP conjugated (Abcam, ab205718) at working dilution of 1:2000 in 5% BSA. Rat astrocytes primary antibody GFAP (sigma G3893) used at working dilution of 1:1000 in 5% BSA. The used secondary antibody for GFAP is anti-mouse HRP conjugated (Abcam, ab97023) at the working dilution of 1:2000 in 5% BSA. CD34 primary antibody (Abcam, ab81289) with 1:1000 dilution and anti-rabbit HRP conjugated secondary antibody (Abcam, ab205718).

A Clarity Enhanced Chemi-luminescence kit (Biorad, 1705060) was used in conjunction with syngene G:BOX gel and blot imaging system in order to visualise protein bands.

Individual contributions:

Porcine primary astrocytes cells, macrophages, rat astrocytes cell lines WB were conducted by me. PBECs WB was conducted with DM helps.

2.3.7. RNA isolation of cultured cells:

RNA isolation from cultured cells: The used kit was RNeasy Mini Kit (50), Qiagene, 74104. 10µl of beta-mercaptoethanol or BME was added per 1ml of the RLT. Cells were plated on 6-well plate and allowed to grow for 72 hours until its confluent (80%). Next, wells were washed 3 times with PBS and 600 µl RLT was added to each well. Later, the lysate collected and carefully placed in pre-labelled tube (RNase free). Next, the cells were homogenized for 10-15 min. Later, the tube was applied to centrifugation at maximum speed for 3 min. 350 µl of 70% ethanol was added to the homogenized tissues. 700 µl of the mixture was transferred into the RNeasy Mini spin column placed in a clean 2ml collection tube. Later, the column was centrifuged for 15 seconds at 9000 rpm and the flow through was discarded. 700 µl of RW1 to the column and allowed later for centrifugation for 15 seconds at 9000 rpm. Next, 500 µl of RPE to the column and allowed for centrifugation for 15 seconds at 9000 rpm. The flow through was discarded. 500 µl RPE was added again and the column was centrifuged for 2 minutes at 9000 rpm. The column next was placed in a new clean collection tube and allowed for centrifugation at full speed for 1 minute. The column was transferred to a pre-labelled Eppendorf tube 1.5ml and 30 µl was added to the spin membrane carefully. Finally, the tube was centrifuged for 1 minute at 9000 rpm to elute the RNA. RNA concentration measurement was done by nanodrop.

Individual contribution:

The RNA isolation from all three cell types was conducted by me.

2.3.8. RT-qPCR:

Total RNA was extracted using the RNeasy Mini Kit (Qiagen, Manchester, UK) and first strand cDNA was synthesized using the iScript cDNA synthesis kit (Bio-Rad Laboratories, Inc.). Quantitative polymerase chain reactions were performed with Claire Oleary (CO) help by using SYBR green and primers mix designed by Primerdesign Ltd. (primerdesign, Camberley, UK) specific for the TSPO transcript. RPL32 was used as an endogenous housekeeping gene. RPL32-F, TGGAAGAGACGTTGTGAGCAA and RPL32-R, CGGAAGTTTCTGGTACACAATGTAA.

TSPO-F GCCACACTGGACACTGGC, TSPO-R ACCACAGCCTCCTCCGAG.

2.3.9. Scatchard analysis:

Three independent cultures of the primary cells PBECs and macrophages cell line were scraped and collected in the Tris/NaCl (50mM/120mM) pH 7.4 buffer. Cells were saved at -80°C until they needed. Three independent Scatchard assay experiments was conducted for PBECs and macrophages. On the Scatchard experiment day, the cells were re-suspended in the Tris/NaCl buffer and the protein concentration were estimated by using Pierce BCA protein assay (Thermoscientific, Rockford, USA). The protein concentration was adjusted to 0.4mg/ml. Borosilicate glass test tubes (Fisher Scientific, product code: 11942198) were carefully labelled. Ten different concentrations of the radiolabelled ligands ($[^{18}\text{F}]$ DPA-714) ranging from 5.1pM to 43.4nM for PBECs and 15.0 pM to 52.4 nM for macrophages were prepared. A total of 100 tubes were prepared for each experiment including ten different tubes for each radiolabelled tracer concentration. The 100 tubes including, total binding (in duplicate), non-specific binding with unlabelled PK11195 (in duplicate), non-specific binding with unlabelled DPA-714 (in duplicate), total background (in duplicate and contain labelled $[^{18}\text{F}]$ DPA-714 without cell lysate) and non-specific background for unlabelled

PK11195 and unlabelled DPA-714. To estimate the specific radiolabelled binding (total binding tubes contain only radiolabelled [^{18}F]DPA-714 with cells without unlabelled tracers) and other tubes for non-specific binding (unlabelled PK11195 or DPA-714 tubes contain radiolabelled [^{18}F]DPA-714 with cell lysates and one unlabelled tracer). The unlabelled ligand was prepared to be at concentration 1000-fold higher than the concentration of [^{18}F]DPA-714. The ligand specific binding will be estimated by subtracting the total bound from the non-specific bound. The final volume in each tube is 1000 μl (both ligands diluted in buffer with 10% DMSO). Once all the tubes were prepared, 500 μl of cell suspension were added in each tube. Immediately, the time counted for 1 h incubation at room temperature. Once 1h incubation passed, each solution was rapidly filtered on GF/C filters (WHA1822025 Whatman® Glass microfiber filters, Grade GF/C, Sigma) and washed 4 times with 5 ml of ice-cold buffer using ten wells filtration unit connected to a vacuum pump. Next, gamma-counter (1470 Wizard Automatic Gamma Counter from Perkin Elmer, UK) was used to count the bound ligands. The specific binding was calculated by subtracting the total ([^{18}F]DPA-714 alone) and non-specific binding values (addition of either unlabelled DPA-714 or unlabelled PK11195). Saturation curves were plotted by using the specific binding (bound ligand-Y axis) against total concentration (x axis). Scatchard plot was generated by plotting (Bound/free-Y axis) against bound ligands (x axis). Bmax and Kd values were estimated for both PBECs and macrophages. GraphPad 8.1 for Windows (GraphPad Software, Inc., San Diego, California USA) was used to calculate the Bmax and Kd. unpaired Welch's t-tests was used and the statistical level of significance was set to $p < 0.05$.

Individual contributions:

PBECs, macrophage cell cultures, cell lysates preparation and BCA measurements was conducted by me and Dominic Mosses. The binding assay experiments and preparation of reagents was conducted mainly by Dr. Herve Boutin at Wolfson Molecular Imaging Center (WMIC), the University of Manchester. Dr. Herve Boutin helped with the binding assay data analysis and interpretation.

2.4. Results:

2.4.1. TSPO subcellular expression in porcine *in vitro* cell culture:

TSPO expression level was examined at the cellular level in cell cultures of primary isolated porcine brain endothelial cells (PBECs), primary isolated porcine astrocytes, immortalised macrophages and rat astrocytes. We extracted PBECs and astrocytes from porcine brains as it was previously described in the methods, while macrophage and rat astrocytes were immortalised cell lines. Macrophage cells showed TSPO/Iba1 colocalisation, indicating TSPO expressed in normal porcine macrophage (Figures 6 and 7). PBECs showed TSPO/CD31 colocalisation with TSPO, indicating that these cells express TSPO (Figures 11 and 12). Porcine and rat astrocytes (TSPO/GFAP) also showed colocalisation with TSPO (Figures 8-10). Astrocyte TSPO basal expression level was lower than PBECs and macrophage in ICC and western blotting (Figure 13).

Further immunohistochemistry staining on porcine tissue sections would be suggested to confirm this result on porcine brain tissue sections. MitoTracker is a green fluorescently labelled mitochondrial-selective marker that selectively accumulates within the mitochondrial matrix and interacts with different mitochondrial proteins through free thiol groups at cysteine residues. MitoTracker was used to show the TSPO mitochondrial location within these studied cells. Rat immortalised astrocytes cell line was used as a positive control for porcine astrocytes to validate the used GFAP antibody. The TSPO protein level expressed in each cell line was further validated by protein extraction and western blotting. PBECs and macrophage TSPO expression were detectable in cell lysates (Figure 13, a -b) and showed an approximately similar mRNA level by RT-qPCR (Figure 14). Astrocytes showed a slightly less detectable protein level in cell lysates (Figure 13, c), while the mRNA level was higher than PBECs and macrophage by RT-qPCR (Figure 14).

**I) TSPO and Iba1 colocalisation in macrophage cell lines:
a.**

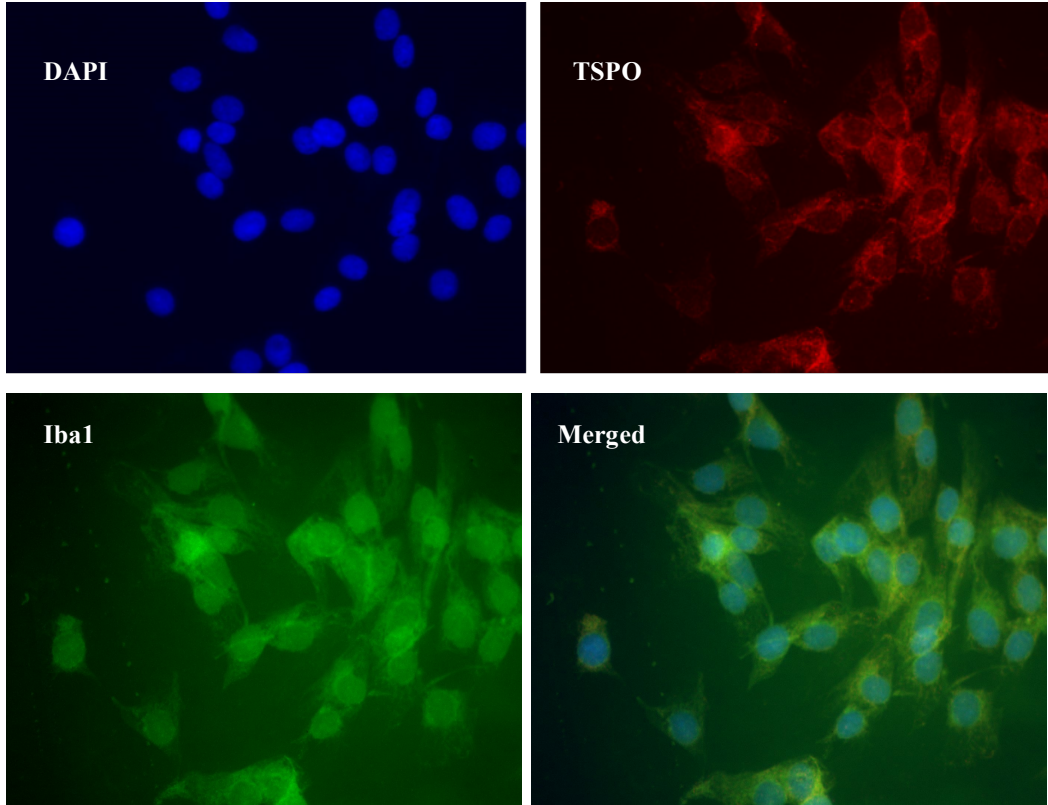


Figure 6: Representative images for TSPO/Iba1 immunofluorescence staining in macrophage cell line. 40x original magnification. ICC images showed TSPO basal expression level in porcine macrophage cells.

b. TSPO and mitotracker colocalisation showed TSPO mitochondrial subcellular location in macrophages:

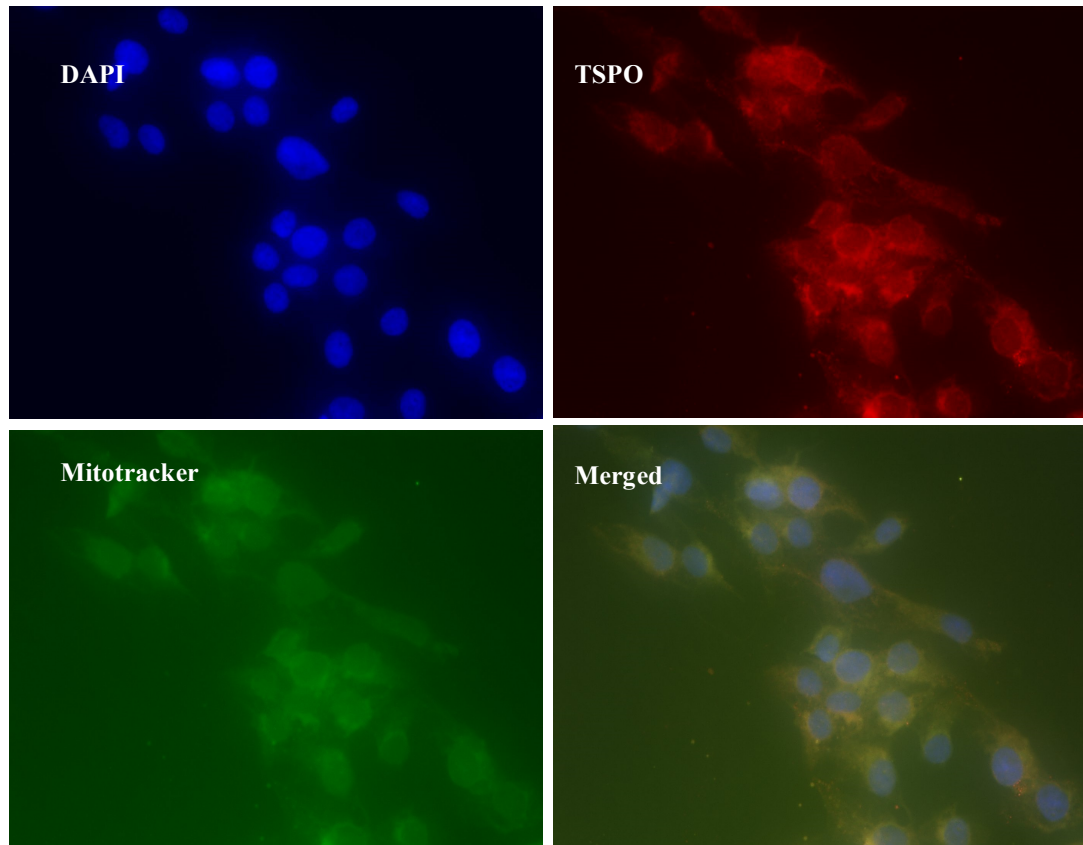
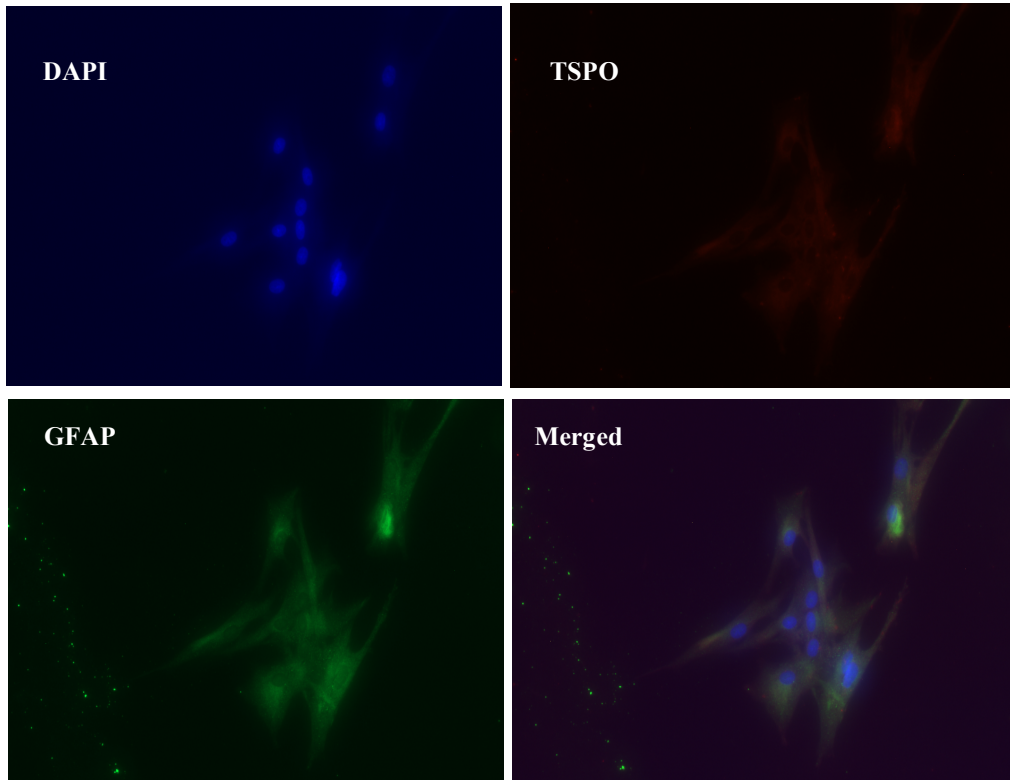


Figure 7: Representative images for TSPO/mitotracker immunofluorescence staining in macrophage cell line. 40x original magnification. TSPO basal expression level in macrophage cells and colocalisation with mitotracker (mitochondrial marker) showed TSPO subcellular location.

II) TSPO and GFAP colocalisation in Porcine Astrocytes:

a.



b.

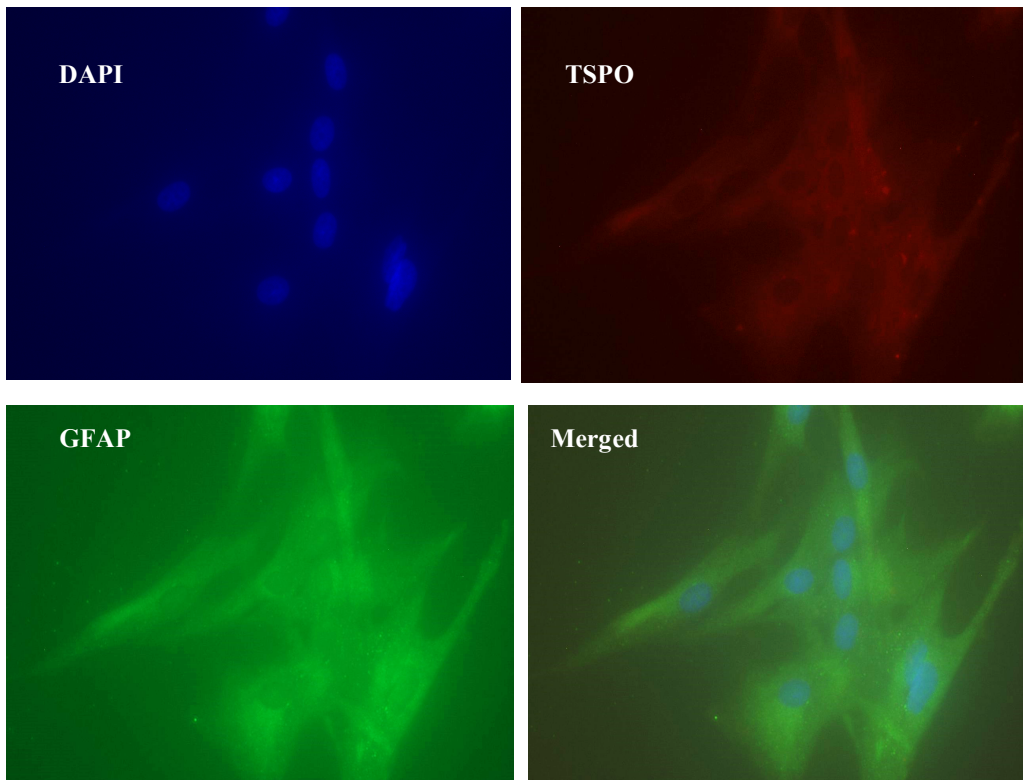
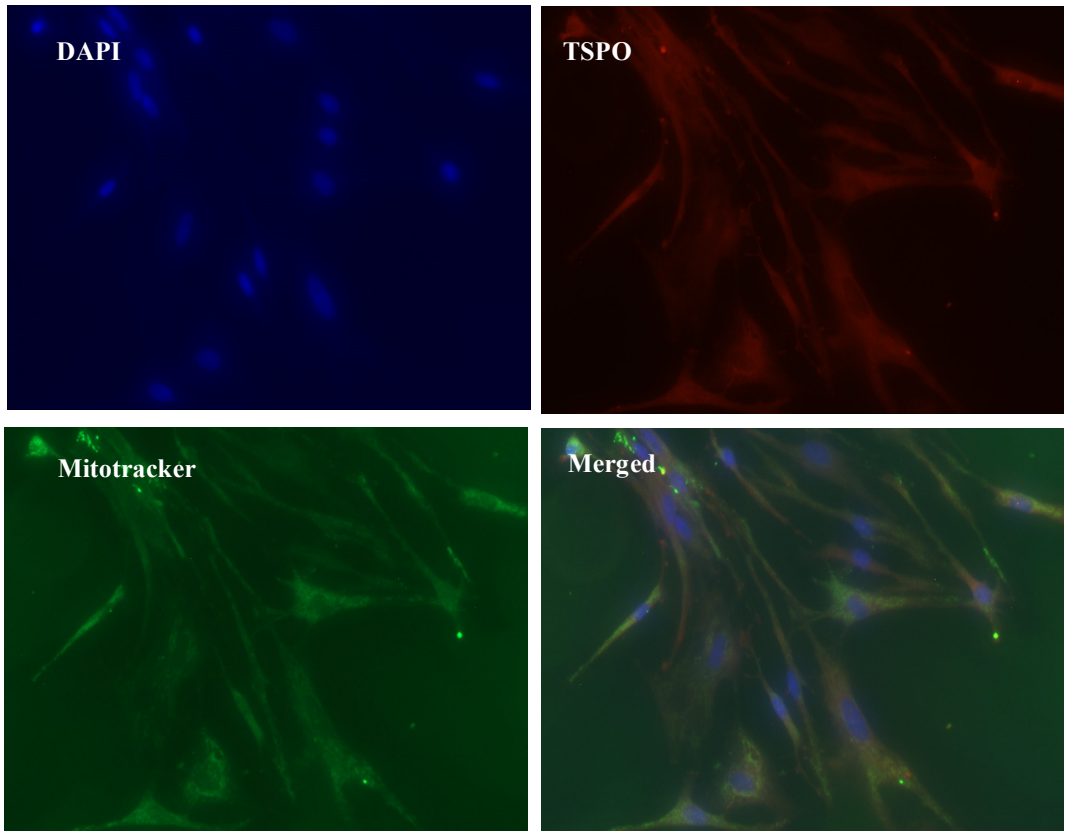


Figure 8: Representative images for TSPO/GFAP immunofluorescence staining showing TSPO basal level in porcine primary isolated astrocytes cells.

- a) Porcine astrocytes primary isolated cells basal TSPO level by ICC, GFAP was used as a positive marker for astrocytes. 20x original magnification.
- b) Porcine astrocytes primary isolated cells basal TSPO level by ICC, GFAP was used as a positive marker for astrocytes. 40x original magnification.

III) TSPO and mitotracker colocalisation showed TSPO mitochondrial subcellular location in porcine astrocytes:

a.



b.

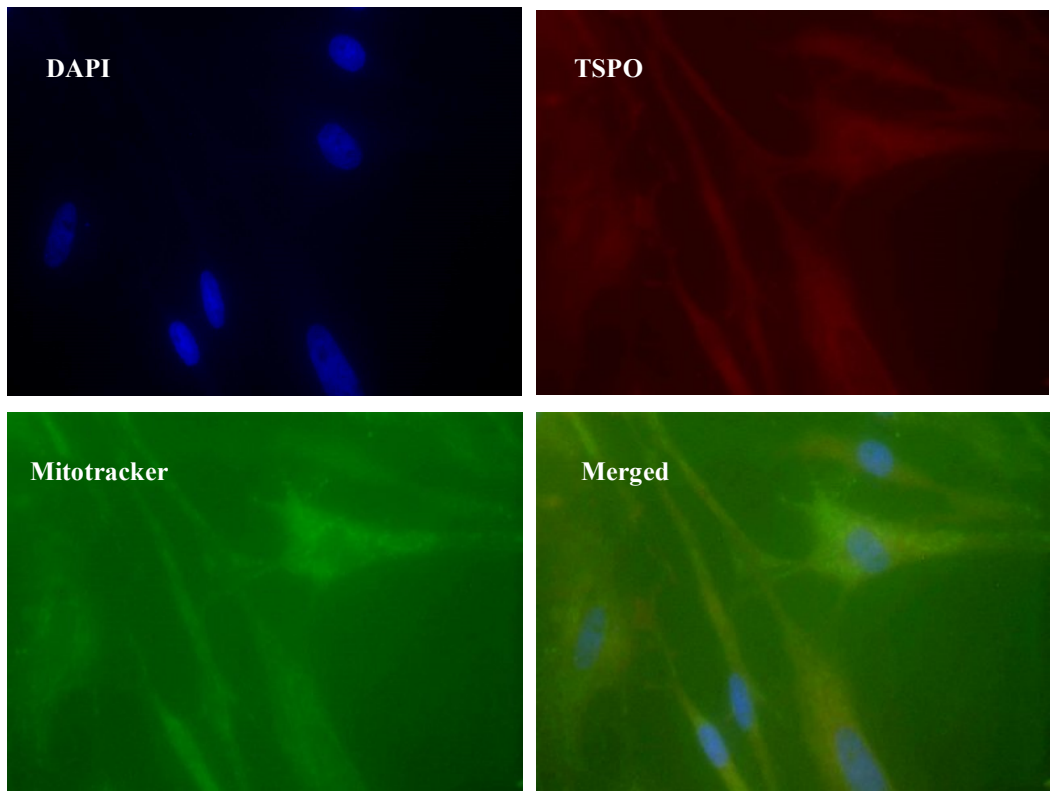


Figure 9: Representative images for TSPO/Mitotracker immunofluorescence staining showing TSPO mitochondrial subcellular location in porcine primary isolated astrocytes cells.

- a) 20x original magnification representative images for TSPO/mitotracker immunofluorescence staining showing subcellular location of TSPO in porcine primary isolated astrocytes cells.
- b) 40x original magnification representative images for TSPO/mitotracker immunofluorescence staining in porcine primary isolated astrocytes cells. MitoTracker used as a green fluorescently labelled mitochondrial-selective marker to show the TSPO location within astrocytes cells.

IV) TSPO and GFAP colocalisation in rat astrocytes:

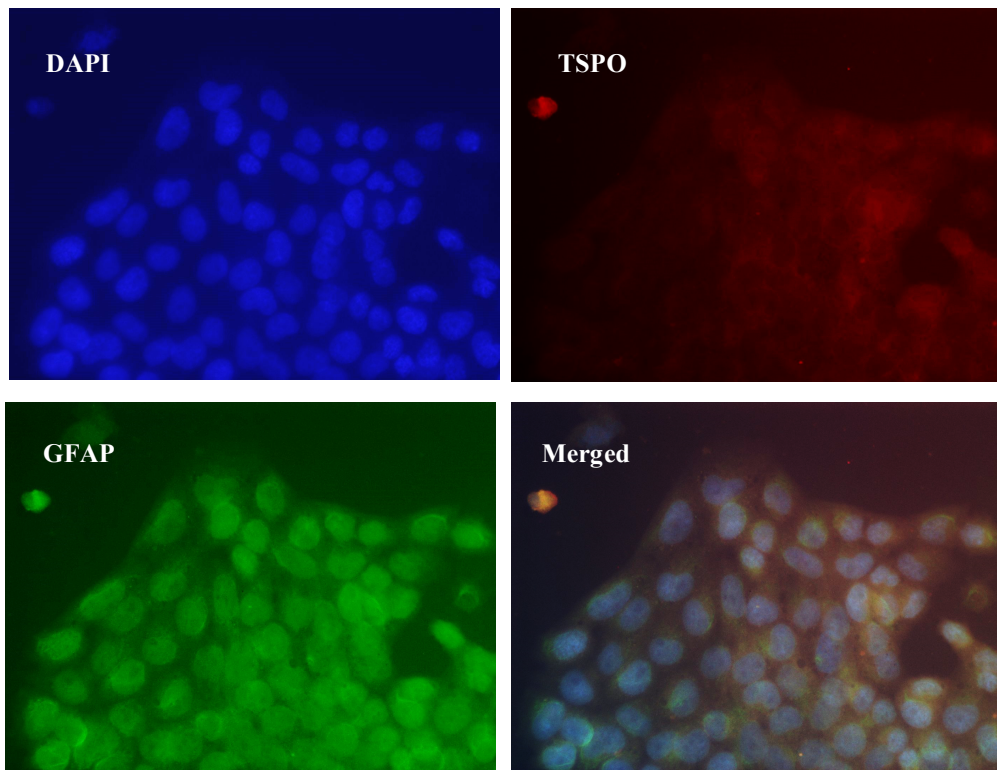


Figure 10: Representative images for TSPO/GFAP immunofluorescence staining in rat astrocytes cell line. 40x original magnification.

Rat astrocytes, was used as a positive control for the primary isolated porcine astrocytes. GFAP used as a positive marker for astrocytes cells. Rat astrocytes similarly to porcine astrocytes showed lower TSPO expression level.

V) TSPO and CD31 colocalisation in PBECs:

a.

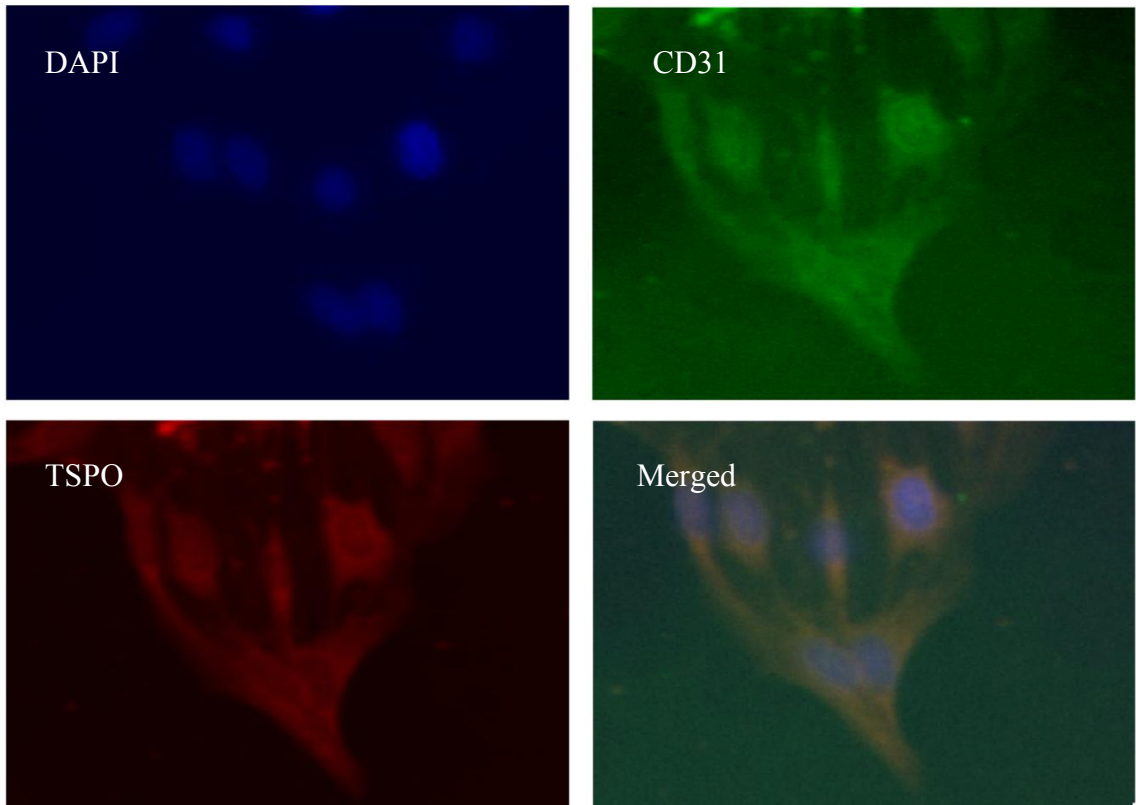


Figure 11: Representative images for TSPO/CD31 immunofluorescence staining in PBECs. 40x original magnification.

TSPO basal level in primary porcine isolated endothelial cells (PBECs) showed approximately similar TSPO level to macrophage cells and higher level than porcine astrocytes.

b. TSPO and mitotracker colocalisation showed TSPO mitochondrial subcellular location in PBECs:

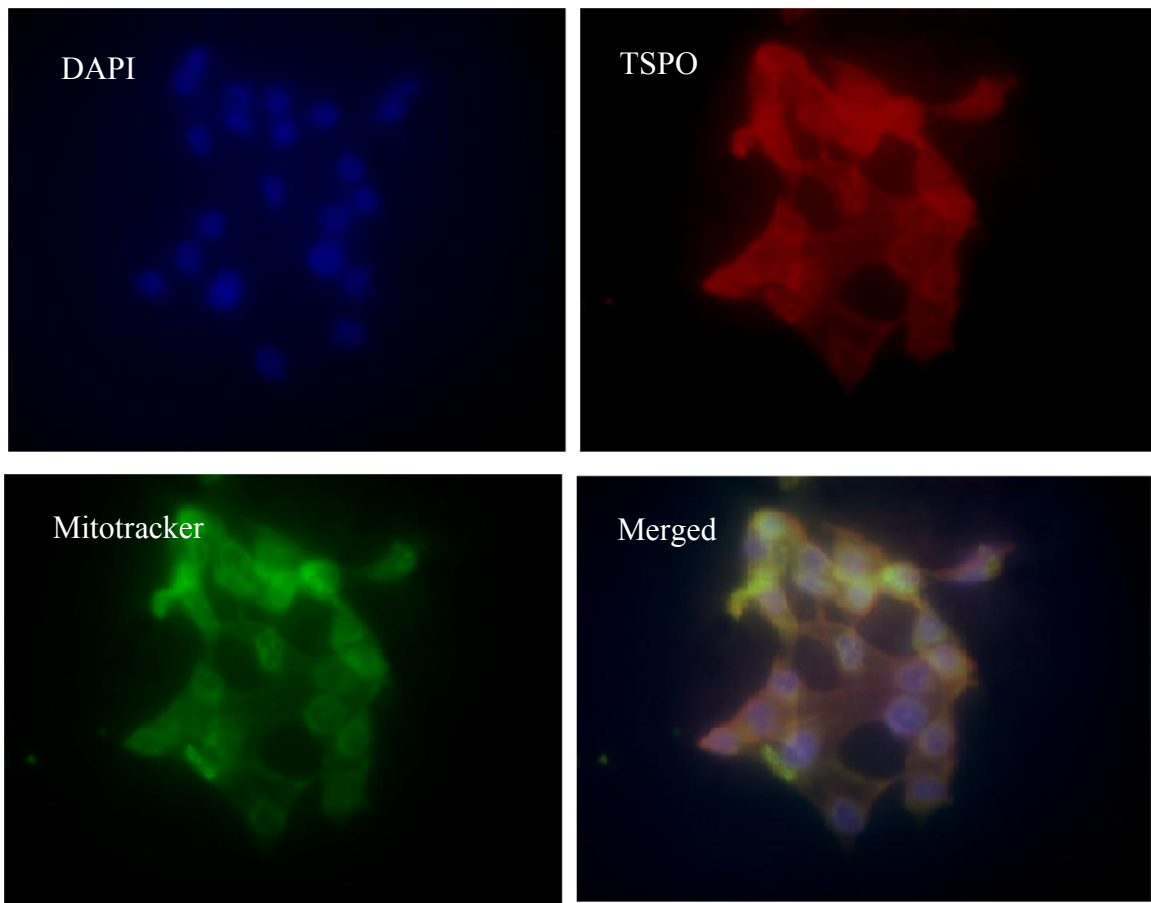


Figure 12: representative images for TSPO and Mitotracker in PBECs. 40x original magnification.

40x original magnification representative images for TSPO/mitotracker immunofluorescence staining in Porcine primary isolated endothelial (PBECs) cells. MitoTracker used as a green fluorescently labelled mitochondrial-selective marker to show the TSPO location within PBECs cells.

2.4.2. TSPO subcellular expression in porcine brain cell lines by protein extraction and western blotting:

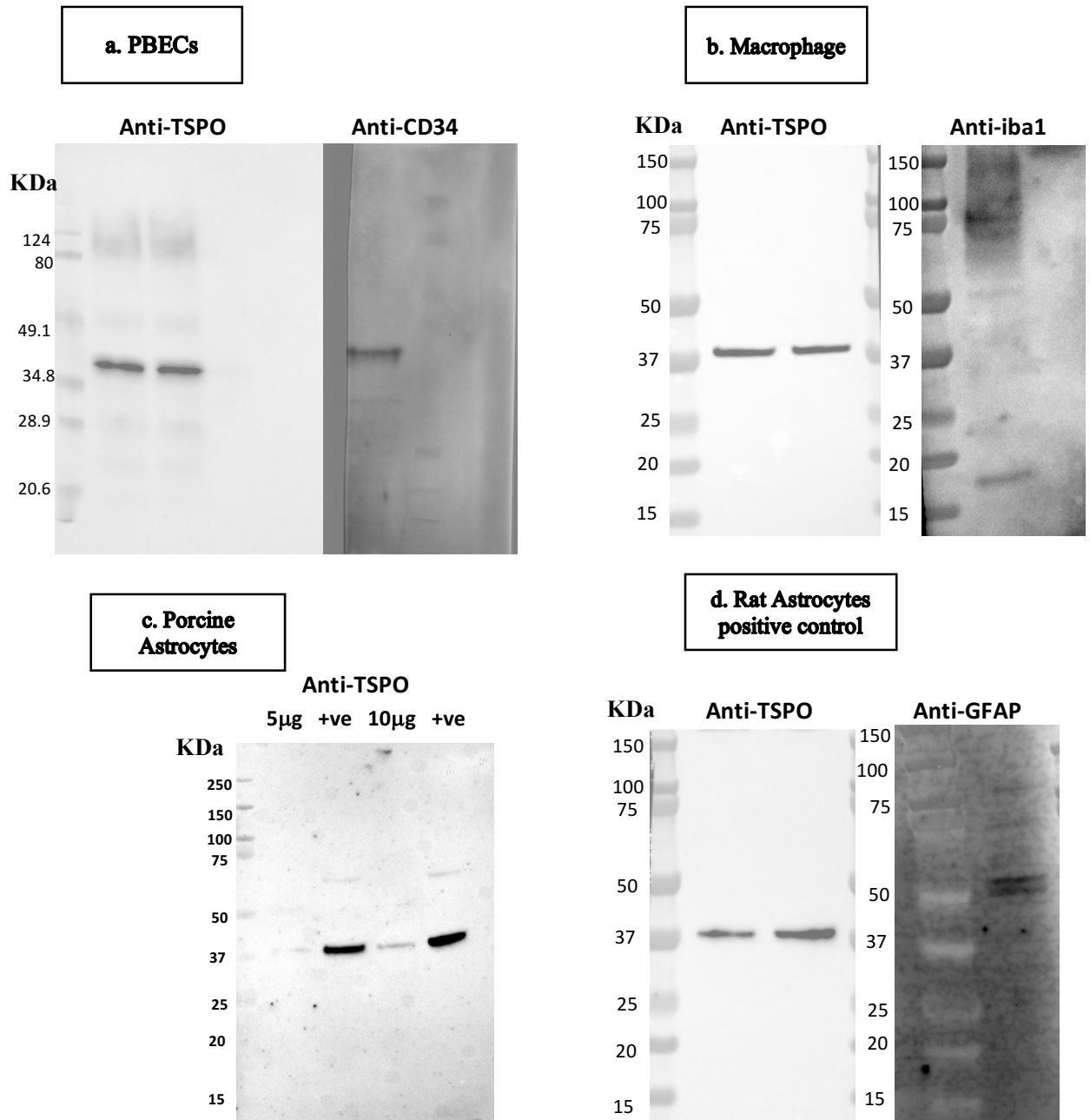


Figure 13: TSPO expression in PBECs, macrophage, and Astrocytes cell lines as assessed using Western blotting: Protein was extracted when cells exceeded 80% confluence. TSPO expression was analysed using anti-TSPO antibody. Positive control for PBECs (anti-CD34), macrophage (anti-Iba1), rat and porcine astrocytes (anti-GFAP). Rat astrocytes were used as a positive control (+ve) for the primary isolated porcine astrocytes (panel c). Porcine primary isolated endothelial cells (PBECs) and macrophage showed similar level of TSPO protein expression while porcine primary isolated astrocytes showed lower level of TSPO protein expression. The used standards for PBECs, Broad range (7.1-209 KD) Prestained SDS-PAGE Standards, broad range, 500 µl #1610318. The used standards for other cell types, dual color standard (10–250 kD) Precision Plus Protein™ Dual Color Standards, 500 µl #1610374.

2.4.3. TSPO subcellular expression in porcine astrocytes, macrophage and PBECs by RNA extraction and RTqPCR:

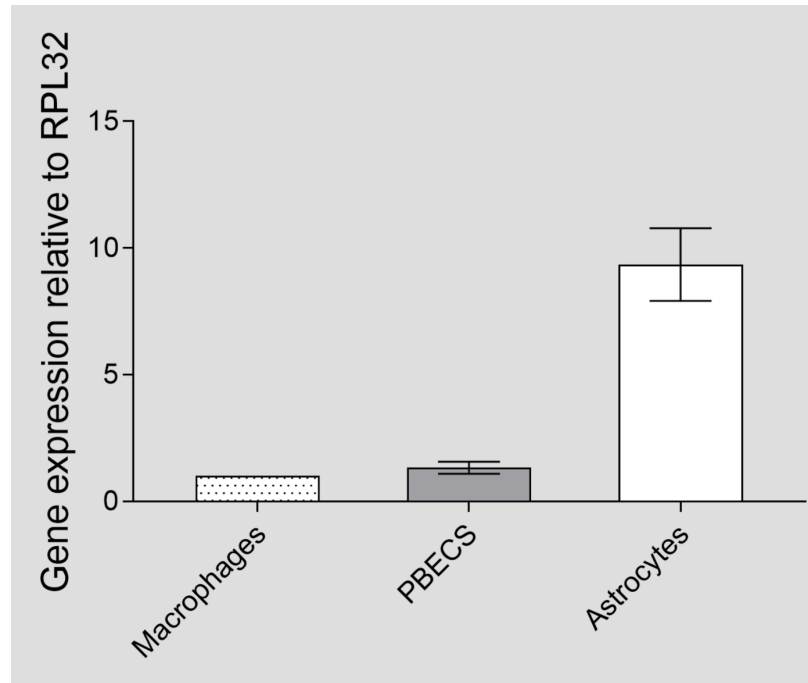


Figure 14: RT-qPCR of TSPO expression level in three different cell types, Macrophages, PBECs and Astrocytes. The normalization was done relative to the reference ribosomal protein L32 (RPL32). Porcine endothelial (PBECs) and macrophage cells showed similar level of TSPO mRNA, while astrocytes cells showed a higher TSPO mRNA level compared to macrophage and PBECs.

2.4.4. [¹⁸F]DPA-714 specific binding and affinity bindings in PBECs and macrophages:

The Scatchard assay used to measure the specific binding (B_{max}) and binding affinity (K_d) of the used radioligand [¹⁸F]DPA-714 in PET imaging. Therefore, the previously obtained TSPO expression at the cellular level could be correlated with PET imaging's ligand bindings.

TSPO ligands specific binding was calculated by subtracting the total [¹⁸F]DPA-714 radiolabeling signal from the non-specific binding. The non-specific binding was estimated by adding the unlabelled DPA-714 and PK11195 to displace the bound radiolabelled ligand. Increasing concentrations of the unlabelled DPA-714/PK11195 ligands lead to more displacement of the radiolabelled [¹⁸F]DPA-714 and less detected radiolabelled signal by using the gamma-counter. The saturation curves showed increasing radiolabelled specific bindings to the receptor until reaching the saturation level at equilibrium. The Scatchard curve showed the binding affinity of [¹⁸F]DPA-714 ligand to the TSPO receptor. High-affinity ligands showed a high saturation level at low ligand concentration and high slope value. The Scatchard assay has been done in triplicate in macrophage and four replicates in PBECs. The multiple experiments for each cell type is necessary to avoid any errors that might arise from insufficient radioligand concentration range. Moreover, estimating the typical values of B_{max}/K_d to be reasonable per milligram of membrane protein to reach equilibrium and estimating if the standard errors or confident intervals are unreasonably too high or wide [321].

B_{max} and K_d values were extracted from the saturation curve and Scatchard assay for both macrophages and PBECs. B_{max} represents the maximum specific binding and the total number of receptors at a particular tissue. B_{max} describes the maximum specific bindings in the saturation curve at Y-axis and X-axis intercept in the Scatchard plot. K_d is the dissociation constant at equilibrium, representing the needed radioligand concentration to reach 50% of the

receptor-specific bindings at a particular tissue. K_d represents the ligand concentration (X-axis), where half of the receptor sites at equilibrium were saturated (Y-axis).

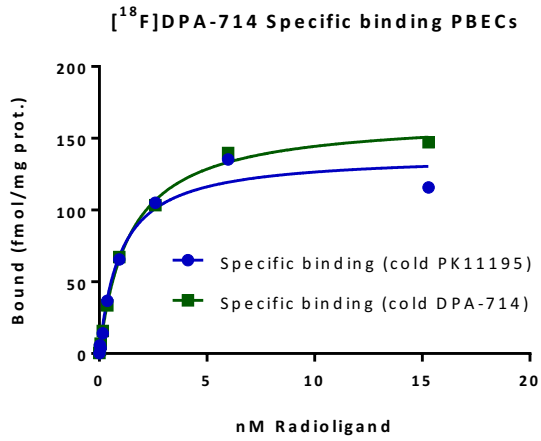
The estimated B_{max} for PBECs calculated from the four replicates independent experiments using unlabelled PK11195 were $81.7 \pm SD 5.96$, $139 \pm SD 8.46$, $98.4 \pm SD 7.81$, and $55.7 \pm SD 5.46$. The estimated K_d for the four replicates experiments were $0.47 \pm SD 0.18$, $0.97 \pm SD 0.22$, $1.62 \pm SD 0.46$, and $2.76 \pm SD 1.02$. Moreover, the B_{max} for PBECs in four replicates after using unlabelled DPA-714 to estimate the specific binding was $82.2 \pm SD 4.53$, $165 \pm SD 3.59$, $74.1 \pm SD 2.80$, and $47.8 \pm SD 5.38$. The estimated K_d for the four replicates experiments were $0.45 \pm SD 0.14$, $1.41 \pm SD 0.11$, $0.70 \pm SD 0.11$, and $1.10 \pm SD 0.54$.

The estimated B_{max} for macrophage cells calculated from the triplicate independent experiments using unlabelled PK11195 were $202 \pm SD 5.82$, $210 \pm SD 10.2$, and $238 \pm SD 19$. The estimated K_d for the triplicate experiments were $0.48 \pm SD 0.06$, $0.55 \pm SD 0.13$, $0.66 \pm SD 0.22$. Moreover, the B_{max} for macrophage cells in triplicate after using unlabelled DPA-714 to estimate the specific binding was $210 \pm SD 4.53$, $225 \pm SD 17.3$, and $217 \pm SD 19.9$. The estimated K_d for the triplicate experiments were $0.53 \pm SD 0.05$, $0.72 \pm SD 0.26$, $0.53 \pm SD 0.21$.

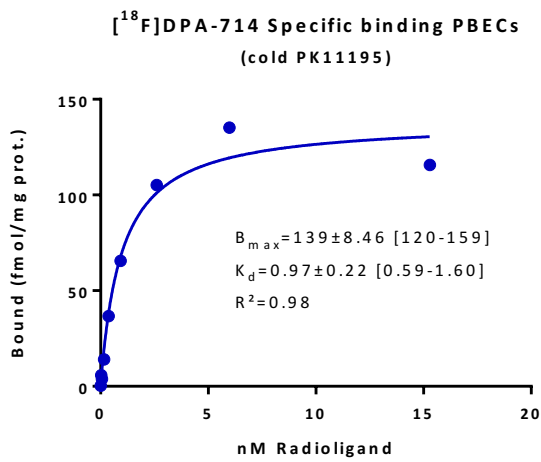
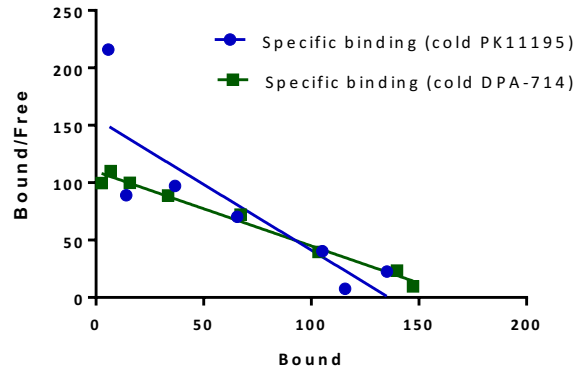
Figure 15, A, showed one of the four replicates experiments that were done for PBECs and indicated the estimated B_{max} (PK11195, $139 \pm SD 8.46$, DPA-714, $165 \pm SD 3.59$) and K_d (PK11195, $0.97 \pm SD 0.22$, DPA-714, $1.41 \pm SD 0.11$) (Figure 15, A) after using unlabelled PK11195 and unlabelled DPA-714, independently. Moreover, Figure 15, B, showed one of the triplicate experiments that were done for macrophage with B_{max} (PK11195, $202 \pm SD 5.82$, DPA-714, $210 \pm SD 4.53$) and K_d (PK11195, $0.48 \pm SD 0.06$, DPA-714, $0.53 \pm SD 0.05$) after using unlabelled PK11195 and unlabelled DPA-714, independently.

Macrophages showed significantly higher Bmax compared to PBECs (Figure 15, C). The estimated Bmax p-values after using unlabelled PK11195 from saturation and Scatchard plots were p-value 0.0022, p-value 0.0030 with Welch's t-test, respectively. Using unlabelled DPA-714, Bmax from saturation and Scatchard plots were p-value 0.0145, p-value 0.0045, using Welch's t-test. This result is indicating that macrophages express more TSPO receptors than PBECs in normal conditions. Measuring the Kd shows that the obtained outcome was not affected by ligand binding affinity. Both PK11195 and DPA-714 tracers have similar Kd and similar affinity (Figure 15, D). Non-significant difference in Kd between PBECs and macrophages, p-value 0.1689, p-value 0.9750 Welch's t-test (unlabelled PK11195 from saturation and Scatchard plots, respectively) p-value 0.2298, p-value 0.8329 Welch's t-test (unlabelled DPA-714 from saturation and Scatchard plots, respectively).

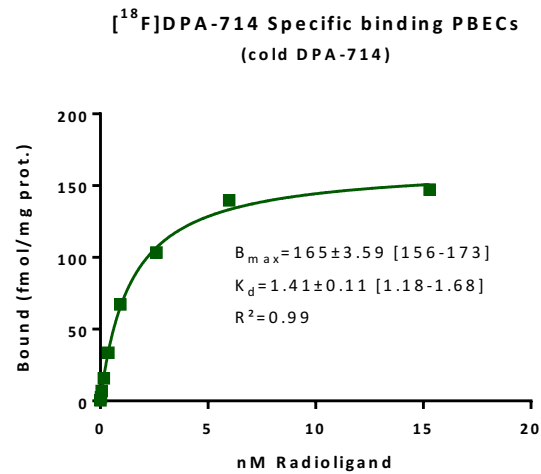
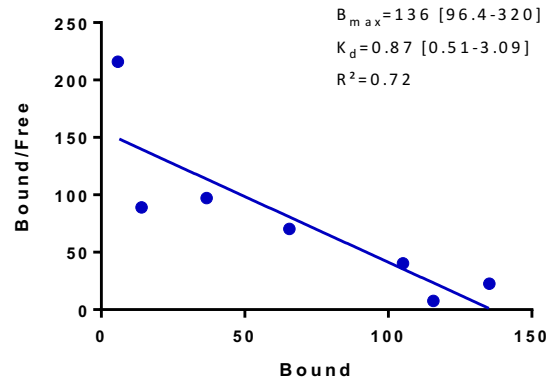
A.



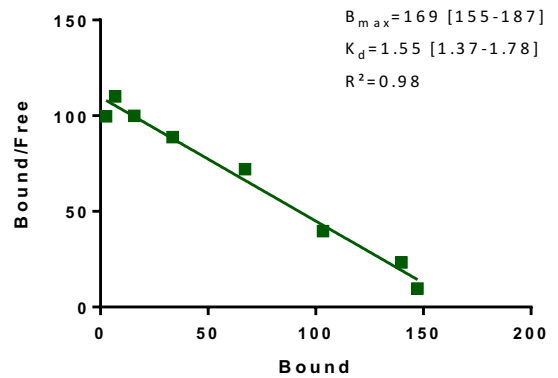
Scatchard of [¹⁸F]DPA-714 Specific binding PBECS



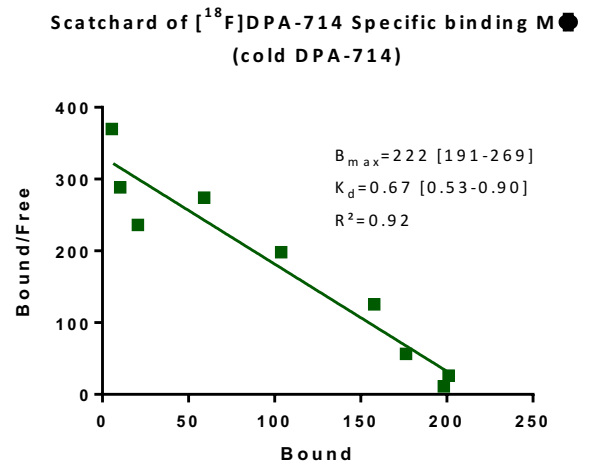
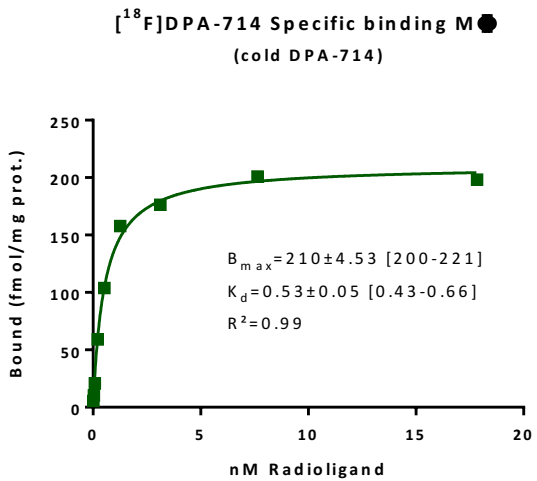
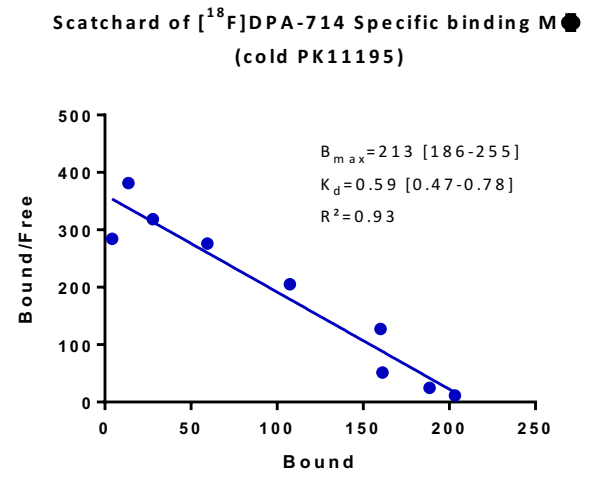
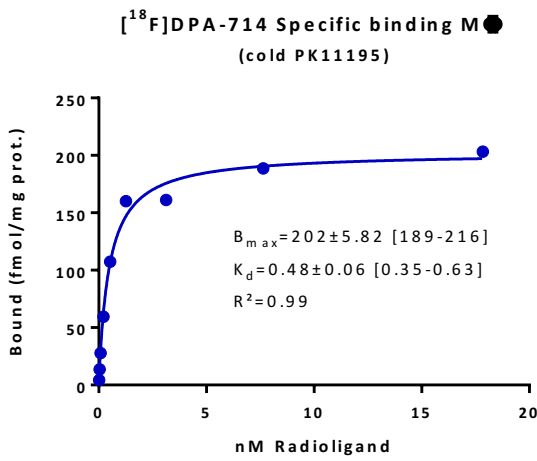
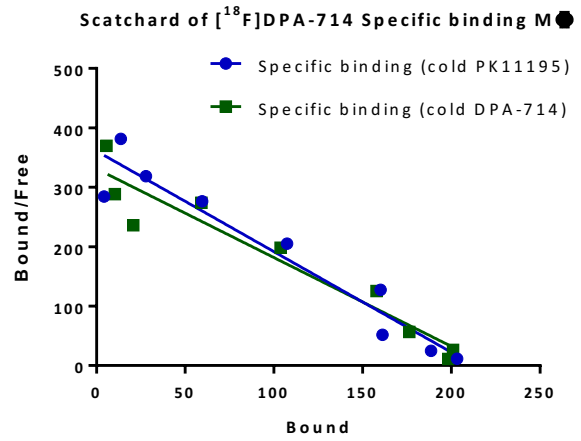
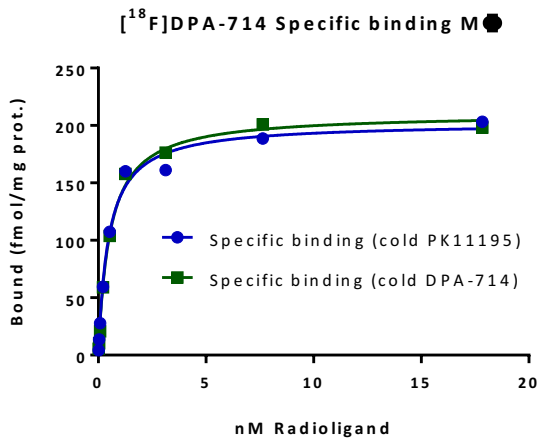
Scatchard of [¹⁸F]DPA-714 Specific binding PBECS (cold PK11195)



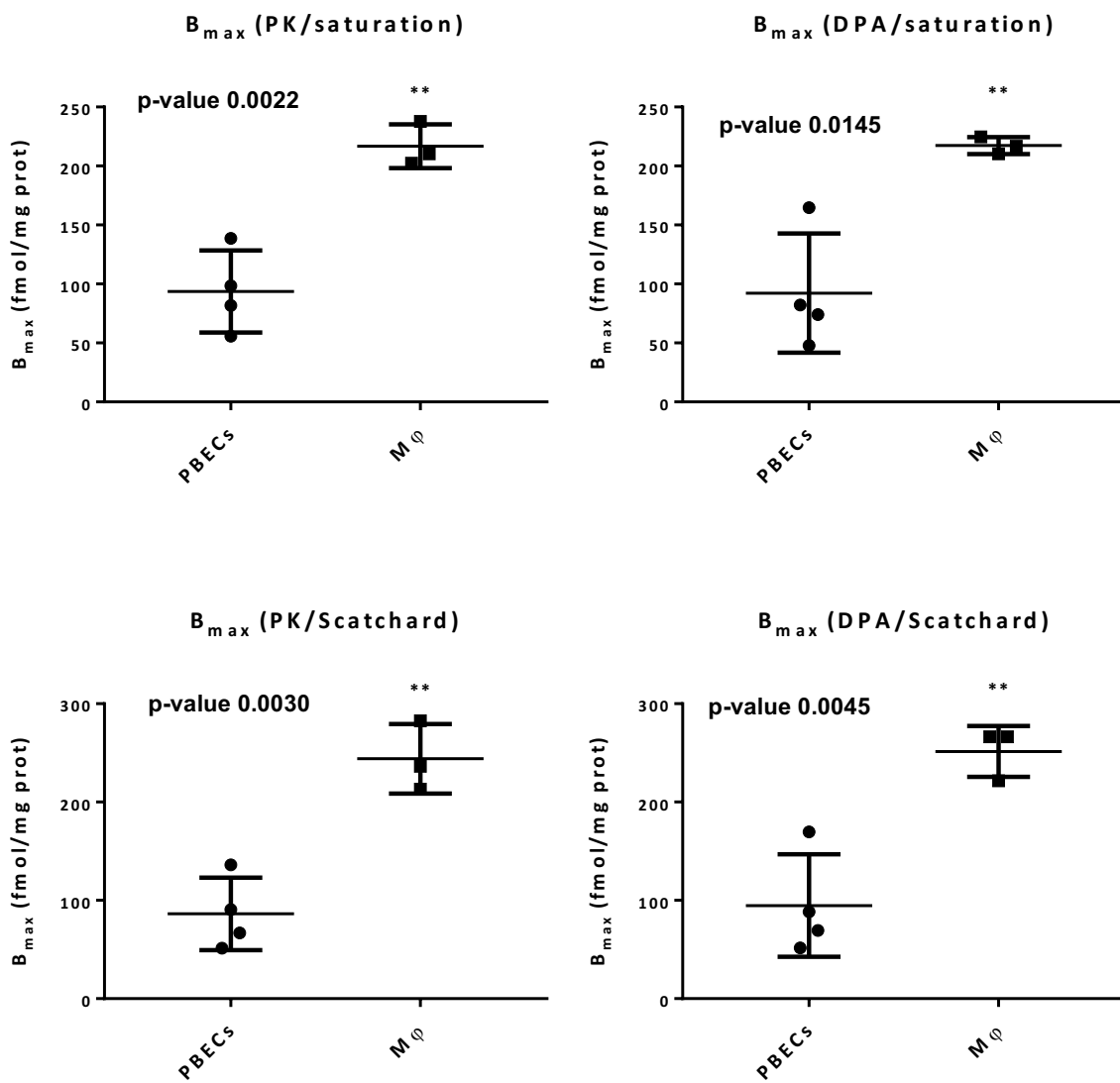
Scatchard of [¹⁸F]DPA-714 Specific binding PBECS (cold DPA-714)



B.



C. Comparisons PBECs vs M ϕ : B_{max}



Comparisons PBECs vs M ϕ : K_d

D.

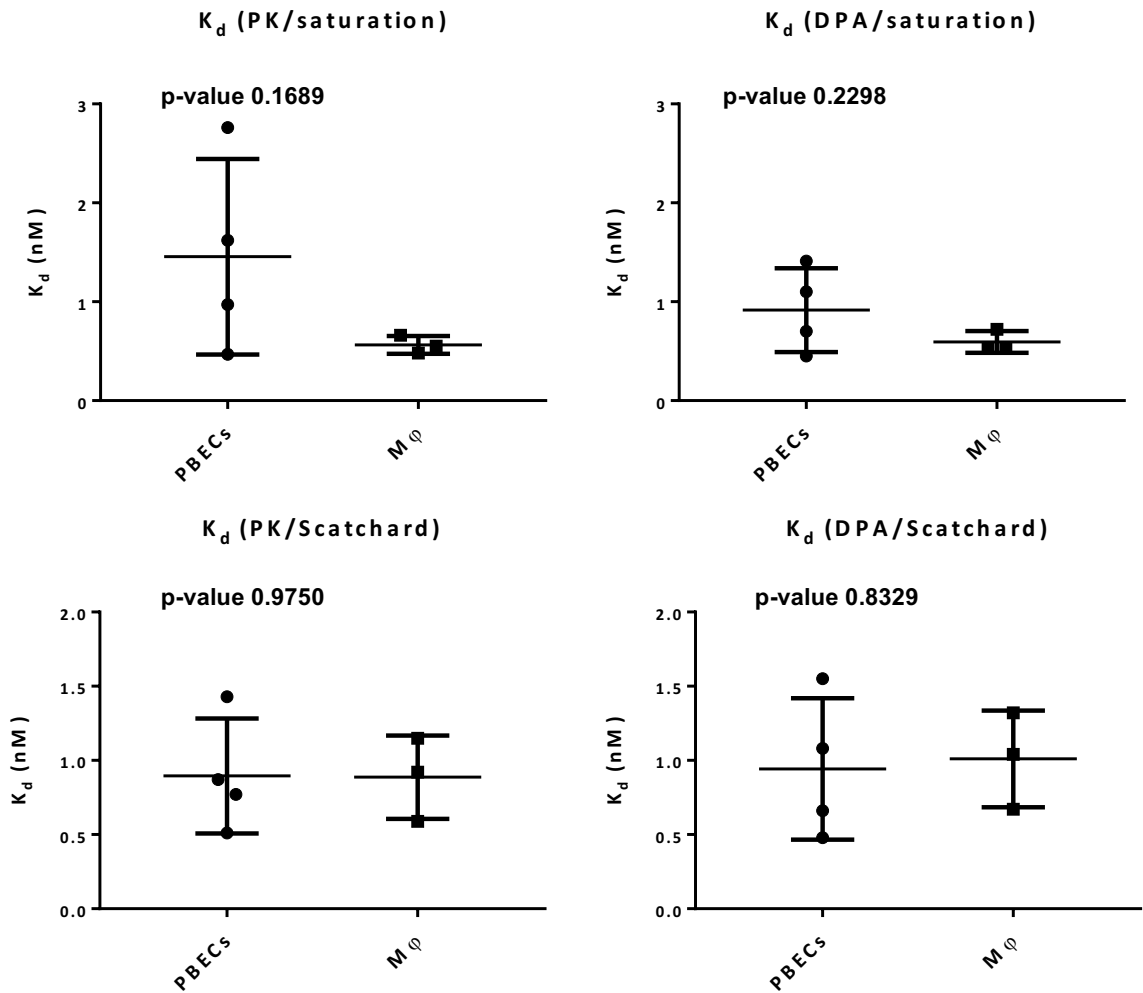


Figure 15: The Scatchard plots and saturation curves showing the estimated Bmax and Kd values for both PBECs and macrophages. (A) Scatchard plot and saturation curve for a representative experiment of the four replicates in PBECs. (B) Scatchard plot and saturation curve for a representative experiment of the three replicates experiments in macrophages. (C) Comparisons of the obtained Bmax values from four replicates for PBECs and triplicates experiments for macrophage. (D) Comparisons of the obtained Kd values between PBECs (four replicates) and macrophage (triplicates), respectively. The p-value has been estimated by Welch's t test. Macrophage Bmax was significantly higher than PBECs, while no significant difference was seen in Kd.

2.5. Discussion:

TSPO is expressed at low levels in normal brains and expressed at increased levels in activated microglia and astrocytes during inflammation [75, 277]. TSPO is used as a biomarker to detect activated microglia in many neurological disorders [277-280]. Investigating the distribution of TSPO expression level in various cellular components (such as, microglia, macrophage, and astrocytes) is still very limited in a normal brain. In the current study, TSPO expression was investigated at the NVU compartments in normal porcine brains. We found that macrophages, astrocytes and endothelial cells (PBECs) showed colocalisation with TSPO. PBECs and macrophage showed approximately similar TSPO protein expression level with ICC and western blotting (Figures 6, 7, 11, 12 and 13 a, b). However, porcine astrocytes showed a lower TSPO protein expression level with both techniques, western blotting (WB) and ICC (Figures 8, 9 and 13, c). Future further research would be interesting to check the TSPO expression level in normal porcine brain tissue sections (FFPE) astrocytes, ECs, macrophage, and microglia by immunohistochemistry (IHC) at tissue level.

Moreover, astrocytes TSPO expression was examined in another model (rat cells) to confirm these results. To confirm the ICC and WB results, we also examined the mRNA level of TSPO in all three porcine cell types by RT-qPCR, and we found approximately similar mRNA level in both PBECs and macrophage. However, astrocytes showed a higher TSPO mRNA level than macrophage and PBECs, while a lower protein level in the examined western blot was seen. To our knowledge, no previous study has investigated the TSPO expression level in different NVU cellular components of normal porcine brain. A study in normal mouse brain showed astrocytes TSPO expression basal level differ in different brain regions [257].

Astrocytes within the subependymal zone and subventricular zone showed a low TSPO expression level, while no expression was seen in astrocytes endfeet surrounding endothelial cells [257].

Moreover, some discrepancies have been found in astrocytes' contribution to TSPO expression in different neurological disorders. Reactive astrocytes showed increased TSPO expression during inflammation, indicating another cellular contribution to TSPO expression [85, 88, 322-325]. Another study in AD showed a weak or lack of TSPO expression by astrocytes [326]. Studying the basal level of astrocytes in normal brain would be beneficial to better understand its expression in different pathological conditions, including gliomas.

Regarding the ECs, Betlazar et al. found that vascular endothelial cells express TSPO in normal mouse brain within the subventricular zone, cortex, hippocampus and cerebellum. Moreover, CD31 and TSPO colocalisation was observed in all blood vessels from large arteries to capillaries and veins, indicating the basal TSPO level expressed by endothelial cells in normal mouse brain [257]. In the current study, we used a porcine model instead to study the cellular contribution to TSPO expression at the NVU. The porcine endothelial cell model of BBB was initially described by Galla et al. as a non-human source of BBB endothelial cells [327]. Many studies have described and used the primary porcine brain endothelial cells (PBECs) as *in vitro* model to study the BBB [328-333].

Moreover, using porcine brains results in high cell yields from a single isolation process compared to those obtained from rat or mouse models [329]. Additionally, PBECs can retain the BBB features for a more extended time than the other animal models [318]. The PBECs model is less expensive than the rodent model to study human disease with comparative anatomy and physiology [334]. During the primary cell isolation of PBECs, we used puromycin

treatment for purifying the isolated porcine PBECs from the contaminant cell types based on previously described protocol [333, 335-338]. The resistance of PBECs to puromycin is due to P-glycoprotein over-expression in endothelial cells, which make them more resistant to this treatment. The primary astrocytes are sensitive to puromycin; therefore, we isolated them from porcine brains by using a different novel protocol that applied different-sized filtering system (149 μm , 60 μm , 30 μm and 20 μm , respectively) and BSA gradient to better separate astrocytes from the other contaminant cells [320]. Rat astrocytes were used as a positive control for porcine astrocytes in ICC and WB. Thomsen et al. showed that within the triple culture (astrocytes, pericytes and PBECs endothelial cells), there was no significant difference in trans-endothelial electric resistance (TEER) BBB integrity between a rat or porcine astrocytes [331]. They indicated the suitability of using rat astrocytes as an alternative to porcine astrocytes in studying the in vitro BBB. Both models expressed high enough TEER values with low permeability in BBB triple culture. Another study illustrated using rat astrocytes with porcine PBECs in the BBB model [339].

Regarding macrophage contribution to TSPO expression in normal brain, a study showed that both macrophage and microglia express TSPO [88]. In the current study, macrophage showed TSPO positivity in ICC (Iba1) and detectable TSPO expression in western blot. Yaxing et al. indicated that microglia (Iba1+), astrocytes (GFAP+) and endothelial (CD31+) cells showed colocalisation with TSPO [271]. They chose specific regions in the human post-mortem brain of AD located within the cerebellum, commonly used as a reference region in TSPO PET imaging studies. They found a detectable level of TSPO mRNA in RNA-Seq dataset for ECs, astrocytes and microglia. They mentioned that mature astrocytes have higher TSPO mRNA than foetal mouse astrocytes. In the present study, we found a detectable

TSPO mRNA level in endothelial, macrophage and astrocytes of normal porcine brain cells. Macrophage and PBECs expressed similar basal TSPO level compared to astrocytes which showed a lower level of TSPO expression in western blot and ICC. Finally, the Scatchard assay showed high Bmax binding of the used TSPO ligand ($[^{18}\text{F}]\text{DPA-714}$), indicating more TSPO density in macrophage cells compared to endothelial cells (PBECs). At the same time, no significant difference was found between Kd values in these cells.

Based on the previously obtained results, considering the contribution of vascular, microglia, macrophage and astrocytes contributions to TSPO expression in normal and pathological brain conditions, including brain tumour, is essential for future research. In gliomas, TSPO expression significantly increased compared to normal brains [8, 99, 106, 254, 256, 340]. Distinct cellular components within the glioma microenvironment could contribute to the TSPO signal, including endothelial cells, microglia, and macrophages [256]. GAMMs were found to comprise 30% of cell density in biopsies taken from patients with LGG and HGG [341]. Gliomas secrete factors that recruited GAMMs within the glioma microenvironment favourable for tumour growth. Intratumoral macrophages showed significant contributions to the TSPO expression in tissues and $[^{11}\text{C}]\text{-(R)PK11195}$ PET signal in sporadic vestibular schwannoma intracranial tumours [311]. Therefore, GAMMs are reprogrammed to induce tumour growth in response to many signals, including hypoxia and gliomas chemokines [342]. Recent preliminary results in small vessels disease (SVD) showed an increase in microglial proliferation, but TSPO positive cell population was reduced. TSPO expression interpretation in microglia cells could not be translated as simple 'TSPO upregulation equals activated microglia'. During inflammation, microglia and macrophage release high levels of ROS. The TSPO expression increased during the early inflammation process to protect brain tissues from

the high generated ROS levels [308]. Later, during disease progression, the TSPO expression reduced in microglia, reflecting a chronic toxic state where the ROS generation level exceeds the protective role of TSPO as an antioxidant [140]. Moreover, in anaplastic astrocytomas, tumour infiltrating activated microglia did not show TSPO expression, indicating a possible TSPO expression suppression mechanism to support tumour progression and inhibit anti-inflammation role [230].

Moreover, vascular endothelial cells express a transient increased TSPO expression with high CD31 density in a mouse model of chronic cerebral hypoxia, resembling angiogenesis remodelling induced by hypoxia [310]. However, the high CD31 density was not accompanied with sustained increase of TSPO expression after 4 days of hypoxia. Furthermore, during tumour growth, increased mitotic activity and extensive hypoxia leading to intense neovascularisation [343-346]. In addition, the vascular compartment inclusion in PET signal quantification modelling of TSPO was encouraged by many studies [255, 258-261]. Based on the previously mentioned studies, studying different cellular contributions to TSPO expression within the gliomas microenvironment is an attractive aim that investigated and discussed in Chapter 3 of the current dissertation.

2.6. Conclusion:

Different cellular components at the NVU showed TSPO expression in the normal porcine brain, including macrophages, ECs and astrocytes. Later, these cellular TSPO expression levels were examined in gliomas for comparison with normal conditions.

CHAPTER 3

THE MITOCHONDRIAL TRANSLOCATOR PROTEIN CAN PREDICT ANAPLASTIC TRANSFORMATION OF DIFFUSE GLIOMAS

CHAPTER 3

3.1. Hypotheses:

Hypothesis 1:

TSPO can be used as a biomarker to differentiate between low-grade and transforming higher grade oligodendrogliomas. For that purpose, fifty cases were selected from Salford Royal Hospital, Salford, United Kingdom, by Prof. Federico Roncaroli. All the selected patients were diagnosed with oligodendrogliomas, including low-grade (LGO or WHO II) (n = 27) and Anaplastic oligodendrogliomas (AO or WHO III) (n = 23). They all harboured IDH1 and 1p/19q co-deletions, which have been identified as the hallmark for oligodendrogliomas. Fifty samples of formalin-fixed paraffin-embedded (FFPE) tissues were stained with TSPO immunoperoxidase antibody (IHC). Moreover, another cohort was studied by twenty-six patients with glioma (LGO, AO, LGA, and AA). For twenty-six patients with gliomas, PET imaging was done to show the binding potential BPND level within the tumour region.

Individual contributions:

IHC was performed at Salford Royal hospital, Salford, UK, with Helen Mayers help.

Individual contributions in PET imaging of the twenty-six cohort of oligodendrogliomas and astrocytomas:

PET scans were performed at the Wolfson Molecular Imaging Centre (WMIC) on a dedicated PET brain scanner: The High-Resolution Research Tomograph (HRRT, Siemens/CTI, Knoxville, TE, USA). Fourteen patients were part of a previous study cohort (TSPO imaging

in Glioma, REC reference 09/H1014/41). They were recruited from January 2010 to November 2012. The remaining twelve patients were part of the project commenced in April 2014 (TSPO imaging in Transforming Glioma, REC reference 15/NW/0071).

BPND parametric map creation was created by me with Dr Rainer Hinz guidance, and Erjon Agushi helps (Figures 27-30). Further, tumour VOI for each subject was defined and further projected onto the BPND parametric map by Erjon Agushi. Mean BPND maximum binding potential (BPNDmax) analysis was performed in R statistics (R foundation for statistical computing, Vienna, Austria). The initial steps (indicated below from Figures 21-23), including image co-registration (PET-MRI), segmentation, brain mask ROI, and BP map, were created by me with Dr Rainer Hinz supervision.

Hypothesis 2: The increased TSPO protein expression in high-grade cases on tissues (IHC) and [¹¹C]-(R)PK11195 binding in positron emission tomography (PET) imaging might be mainly contributed by neoplastic cells (IDH1). Therefore, it leads to further investigation about the other cellular sources for TSPO overall expression, GAMMs (Iba1) or vascular endothelial cells (CD31) that could contribute to the final TSPO signal?

Two approaches have been chosen. First, tissue microarray (TMA) was conducted for three patients diagnosed with anaplastic oligodendrogliomas (n = 3). The TMA tissue sections were later stained with four different markers, including Iba1 (microglia/macrophage-specific marker), CD31 (endothelial cell marker), TSPO and IDH1 (a molecular marker for gliomas). A 3D tissue map analysis of the stained tissues was created for the four different markers to quantify each cell type's contribution to the final obtained TSPO expression level. Second, to confirm the previous findings, mass cytometry analysis of four different FFPE sections for

patients diagnosed with low grade (LGO; n = 2) and anaplastic oligodendroglioma (AO; n = 2) was conducted.

Individual contributions:

TMA construction and IHC staining were conducted at the Imperial College Health Care Tissue Bank in London. Dominic Mosses and I performed 3D image reconstruction for TSPO/CD31, TSPO/Iba1, TSPO/IDH1 by using ImageJ (<https://ImageJ.nih.gov/ij>) for Mander's coefficient calculations (in duplicates) and Imaris software (for 3D visualization) (Bitplane AG Zurich, Switzerland) for visualizing the stained stacked regions in three dimensions.

Hypothesis 3: TSPO expression could be a biomarker of tumour progression and could predict patient survival. Kaplan Meier analysis was used to estimate the overall survival (OS) and progression-free survival (PFS) in fifty oligodendrogliomas patients.

Hypothesis 4: Oligodendroglioma's patients would harbour the TSPO rs6971 polymorphism. This polymorphism has been shown to affect TSPO tracers' binding affinity with PET brain imaging and may affect the final obtained signal interpretation. This polymorphism should be considered to explain better whether the low binding/signal obtained accurately reflects the TSPO expression or whether it is affected by low binding affinity to the mutated TSPO. To examine this, DNA was isolated from FFPE for fifty cases, and the polymorphism was later checked using Sanger sequencing.

Individual contributions:

I performed DNA isolation from all FFPE tissues for fifty oligodendrogliomas cases, PCR and all polymorphism analysis. Sanger sequencing was performed at Manchester Centre for Genomic Medicine, St. Mary's Hospital, with Dr Nicola Roberts.

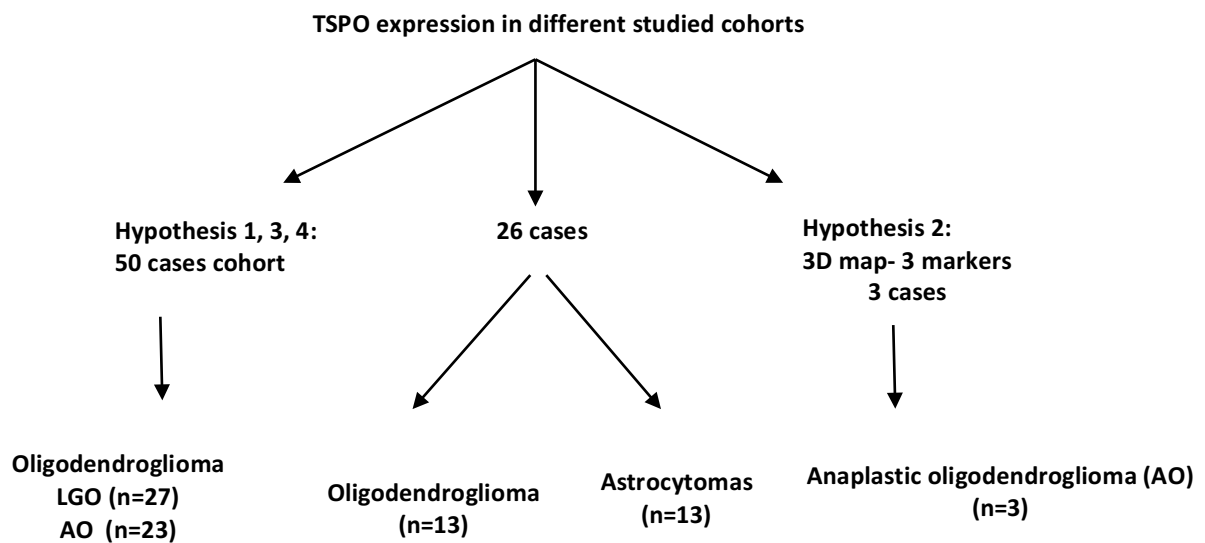


Figure 16: Flow chart summarising three different cohorts in TSPO expression study.

To examine hypothesis 1, two different cohorts with different cases were studied and illustrated below in table 3 and table 4. Later, in order to examine hypothesis 3 and 4, a cohort of fifty oligodendrogliomas cases was studied. The twenty-six cases were used to further examine hypothesis 1 in astrocytomas and later confirmed with PET imaging.

3.2. Study rational and background:

Oligodendrogliomas account for 5–20% of all gliomas, with a mean survival time of about 11.6 years for LGO and 3.5–4.5 years for AO [185, 187, 188]. The molecular genetic hallmark of this subtype is IDH1 mutation and 1p/19q co-deletion [160]. Therefore, all the selected patients were positive for both IDH1 mutation and 1p/19q co-deletion. Low-grade gliomas tend to transform into higher grades, but this occurs at an unpredicted time interval. TSPO is overexpressed in many cancers, including brain tumours [99, 104]. Therefore, it was interesting to investigate if TSPO is a predictive biomarker of anaplastic transformation and overall survival in oligodendrogliomas patients (first hypothesis and third hypothesis).

Tumour microenvironment heterogeneity in brain tumours is a prominent factor in tumour progression [292]. During tumour growth, increased mitotic activity and extensive hypoxia lead to intense neovascularisation [343, 344]. Moreover, glioma cells secrete factors to recruit microglia and macrophages within the tumour microenvironment, promoting glioma progression [307, 347-349]. Different cellular components within the tumour microenvironment could express TSPO [5, 239, 254, 257, 281]. Studying the different cellular contribution within the tumour microenvironment was not well investigated. Only few studies in the literature indicated the microglia and macrophage TSPO expression level in various diseases, including Alzheimer disease (AD), small vessel disease (SVD) and gliomas. In Alzheimer disease, a pre-clinical study in a rat model of AD (TgAPP21) indicated no TSPO expression in activated microglia within white matter and no elevated uptake of [18F]FEPPA PET was observed in the AD rat model compared with WT [309]. Moreover, the same group investigated the ET1 stroke rat model and found no significant TSPO expression increase was accompanied by increased MHCII level [309]. Reduced TSPO positive expression level with

increased density of Iba1 positive microglia was observed in SVD, suggesting a possible reduced TSPO level during a chronic state of SVD. The reduced TSPO level might resemble a mitochondrial dysfunction or altered microglia phenotype with lower TSPO expression (M2) [308]. Initial TSPO increase could be a protective approach due to the chronic state of high ROS level (an oxidative stress condition). Later during a disease progression, TSPO expression got reduced. Studying and quantifying TSPO expression in different pathological conditions, especially in gliomas, was not well studied. There is an increasing interest in the literature to develop better quantification method to quantify TSPO expression in different cells within the TME. The endothelial TSPO expression level within high grade gliomas TME was not precisely previously estimated and quantified. A preliminary study in gliomas indicated that GAMMs partially contribute to the overall TSPO expression in gliomas. In the current thesis, 3D quantification was conducted to quantify TSPO in GAMMs and endothelial cells (second hypothesis). In addition to GAMMs, TSPO expression in endothelial cells was not previously studied in gliomas. However, a pre-clinical study in SVD showed an unchanged level of TSPO in vessels. In pre-clinical research, a transient increase expression level of vascular TSPO (TSPO and CD31) during the early phase of hypoxia, but no increase was seen after four days of reduced exposed oxygen concentration level in mice housed in hypoxic chambers (during chronic state) [310]. High CD31 density was not accompanied by a sustained increase in TSPO expression [310]. Based on the previously indicated studies, TSPO expression in microglia and macrophage are more complex than the simple assumption of TSPO upregulation relates to microglia activation. Therefore, understanding the different cellular contribution (GAMMs and endothelial cells) to TSPO expression within the tumour microenvironment was an important step forward investigated in this chapter (second hypothesis).

Targeting TSPO using specific ligands with PET imaging is beneficial in assessing glioma progression in the literature [8, 227, 230, 245, 246, 350]. Some researchers have used TSPO tracers with PET imaging and shown affinity variations, specifically with second-generation ligands. The tracers' affinity variations are caused by TSPO polymorphism, which is caused by an amino acid substitution from alanine (non-polar amino acid) to threonine (polar amino acid) and a nucleotide substitution from guanosine to adenosine (G to A). This substitution reduces the TSPO binding affinity to different molecules, including cholesterol, and later reduces steroid production. One study indicated that this amino acid substitution leads to variation in the TSPO-ligand binding affinity [124, 351]. In the current study, the percentage of this polymorphism was determined among the selected oligodendroglioma cases (fourth hypothesis). Moreover, we studied if it is a survival risk factor and its effect on protein expression. TSPO polymorphism consideration could lead to a more accurate interpretation of TSPO tracer distribution in PET imaging. Clarifying whether this obtained signal is related to TSPO density differences (expression) or different binding affinities to TSPO would be beneficial. For example, the PBR28 ligand showed lower binding to the low-affinity binder (LAB) compared with high-affinity binder (HAB) cases [352]. [¹¹C]-(R)PK11195 showed exceptionally low sensitivity to the rs6971 polymorphism both *in vitro* [21] and *in vivo* [353]. Other developed ligands in the literature showed better specificity to TSPO but a high sensitivity for this polymorphism; these ligands included [¹¹C]PBR28, [¹¹C]DPA 713, [¹⁸F]PBR111, [¹⁸F]FEPPA, and [¹⁸F]FBR. Genotyping for rs6971 is required to correct this binding sensitivity. [¹⁸F]FEBMP is a newly developed radiotracer that showed high binding affinity to TSPO with less sensitivity to rs6971 and suitable lipophilicity [354].

3.3. Material and methods:

3.3.1. Immunohistochemistry of FFPE tissue sections for oligodendrogliomas:

The purpose of using immunoperoxidase staining method is to estimate the protein expression in formalin-fixed paraffin-embedded (FFPE) tissues by peroxidase-catalysed reaction. FFPE tissue sections (5µm thick) were applied for deparaffinization in Ez prep solution 70°C for 1h. Next, antigen retrieval step was proceeded by heat induced based approach using Heat Induced Epitope Retrieval (HIER) in Tris-EDTA buffer pH 7.8 at 95°C for 44 minutes (standard CC1) or Citrate based buffer (CC2) pH 6.5 at 95°C for 20 minutes. This step is to unmask the endogenous antigen and make it more accessible to the applied primary antibody by removing protein-protein formalin crosslink in the FFPE tissues. The blocking step was proceeded with Inhibitor CM for reducing the endogenous peroxidase activity, at 37°C for 4 minutes. The primary antibody was incubated for 60 minutes (anti-TSPO, goat polyclonal; Abnova, Walnut, CA USA; at dilution 1:500). One drop of OmniMap anti-goat HRP was added and incubated for 60 minutes. One drop of 3',3'-diaminobenzidine (DAB) CM and One Drop H₂O₂ CM were added and incubate for 8 minutes. One drop of Copper CM was added for signal enhancement and incubated for 5 minutes. DAB and H₂O₂ are substrates for peroxidase that would give brown product. The advantage of using the DAB precipitate is its stability over number of years which makes the samples suitable to be archived. Next, the sections were counterstained with Hematoxylin and were incubated for 8 minutes. Post counterstain, sections were incubated with Bluing Reagent for 8 minutes. The bluing process is to convert the initial soluble red color of the hematoxylin that stain the nucleus to an insoluble and more stable blue color in alkaline

solution. H&E staining is important step for histology and to clarify the nucleus location. Slides were cleaned with tap water and dehydration in increasing alcohol concentrations of 70%, 90% and 100% (1 x 3 mins) to xylene. The IHC staining process was conducted at Salford Royal Hospital with Ricky J Williams and Helen Mayers helps.

3.3.2. Evaluation of peroxidase immunohistochemistry:

TSPO immunostaining was evaluated by computer-assisted analysis with using ImageJ (<https://ImageJ.nih.gov/ij>) software. Ten representative images were captured at a magnification of 20× (Nikon Fluoroplan 0.75mm, Nikon, Ltd. Japan) using a digital camera (DS Camera Control Unit DS-L1 and DS Camera Head DS-5M, Nikon, Ltd. Japan). Images were applied to colour deconvolution (split channels) tool in order to exclude signals coming from the nucleus. The RGB image would be converted by colour deconvolution and separated into 3 channels, the red or brown channel represents the oxidized DAB brown precipitate indicating positive immunohistochemistry staining for TSPO. Later, the image was converted to binary image. Further, the threshold was adjusted to minimize background staining artifacts for each image independently. The percentage area of the positively stained signal calculated with the Analyse particles tool. The analysis process was based on counting the percentage of area that occupied by the DAB positive staining for TSPO HRP conjugated antibody that was used in the IHC protocol and conducted by two observers (Figure 17).

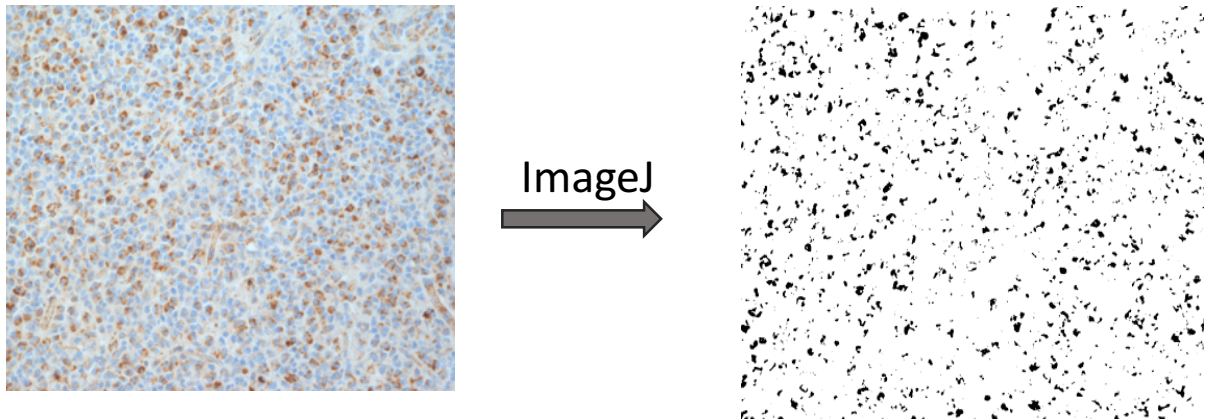


Figure 17: ImageJ thresholding to quantify the TSPO expression.

A representative raw image of one case (left) and the outcome processed image (right) after colour deconvolution to remove nucleus staining and thresholding. The RGB image was converted with colour deconvolution tool (split channels) and separated into 3 different channels, the red or brown channel represents the oxidized DAB brown precipitate indicating positive immunohistochemistry staining for TSPO. Further, threshold was applied with image apply threshold tool in order to minimize the background staining artifacts for each image. The black and white image (right) showed the TSPO positive stained area, DAB positive TSPO (black). The percentage area was calculated automatically by Imagej analyze particle tool.

3.3.2.1. Statistical analysis:

Data was analysed by using Prism Graph Pad version 8.0.2 (159) (GraphPad Software Inc., San Diego, CA). Statistical unpaired t-test, p-value <0.001, using Welch's correction (no assumption of equal SD). P-value below <0.05 was considered to be significant.

3.3.3. Tissue microarrays (TMA):

Tissue microarrays are a useful diagnostic tool and research technique in pathology for estimating protein expressions in tissues. It can contain hundreds of different tissue samples from different donors in a single slide, and therefore it allows high output analysis of multiple specimens at the same time. Thus, TMAs will reduce time and reagents. The reason here behind using this technique is that TMA cores are easier to be stacked for 3D reconstruction. TMAs are composed of small cores, usually ranging in size from 0.6 to 4 x5 mm size cylinders. TMAs are constructed by transferring about 0.6-4 mm size circular segments from formalin-fixed, paraffin-embedded (FFPE) tissue blocks (donor block) to empty prepared recipient block in specific fixed positions [355].

3.3.3.1. The TMA construction process:

First, the recipient block was prepared by melting paraffin, pouring it into a mold and covering it with a cassette until it was solidified [355]. Then, the circular segments were taken manually or by automatic tissue microarrayer with an approximate 2.5-3 mm margin and 0.8 mm space between the cores. Second, the region of interest is selected from the donor block, which has been stained previously with hematoxylin and eosin (H&E). A 0.6-4 mm diameter punch will be taken from the donor tissue block and relocated into a previously prepared recipient block.

Third, it will be incubated in the oven at 37 °C for 10-15 minutes to allow the transferred cores to merge to the wall of holes in the block. Fourth, 4- 5 µm thick sections will be cut using a conventional microtome. The section will be then transferred to a heated water bath or oven (37-39 °C) and the sections should be taken out immediately after they have been stretched to

avoid sensitive tissue spots melting. The warming time incubation period depends on the type of paraffin wax used. Fifth, the sections will be transferred to a glass slide and left overnight at room temperature. Later, the slides will be baked at 50 °C for 12-24 hours. Before peroxidase IHC staining, the slides will be deparaffinised in xylene (paraffin solvent), graded Ethanol (rehydration) and finished with distilled water. Finally, slides were stained by peroxidase immunohistochemistry (IHC) approach for each marker (e.g. TSPO, CD31, IDH1 and Iba1). TSPO (polyclonal goat anti-TSPO, dilution 1:750, GeneTex, Hamburg, Germany), IDH1R132H (Dianova, Hamburg, Germany monoclonal H09, 1:200) for IDH1 mutant tumour cells, the vascular marker CD31 (Dako Clone JC7QA Ref M0823, dilution 1:30) and macrophages / microglia (polyclonal rabbit anti-Iba1, dilution 1:500, WAKO, Neuss, Germany). Super Sensitive Polymer HRP IHC Detection System was used (BioGenex Laboratories, Inc. San Ramon, CA, USA). This process has been conducted in collaboration with staff at the Imperial College Health Care Tissue Bank in London (Figure 18).

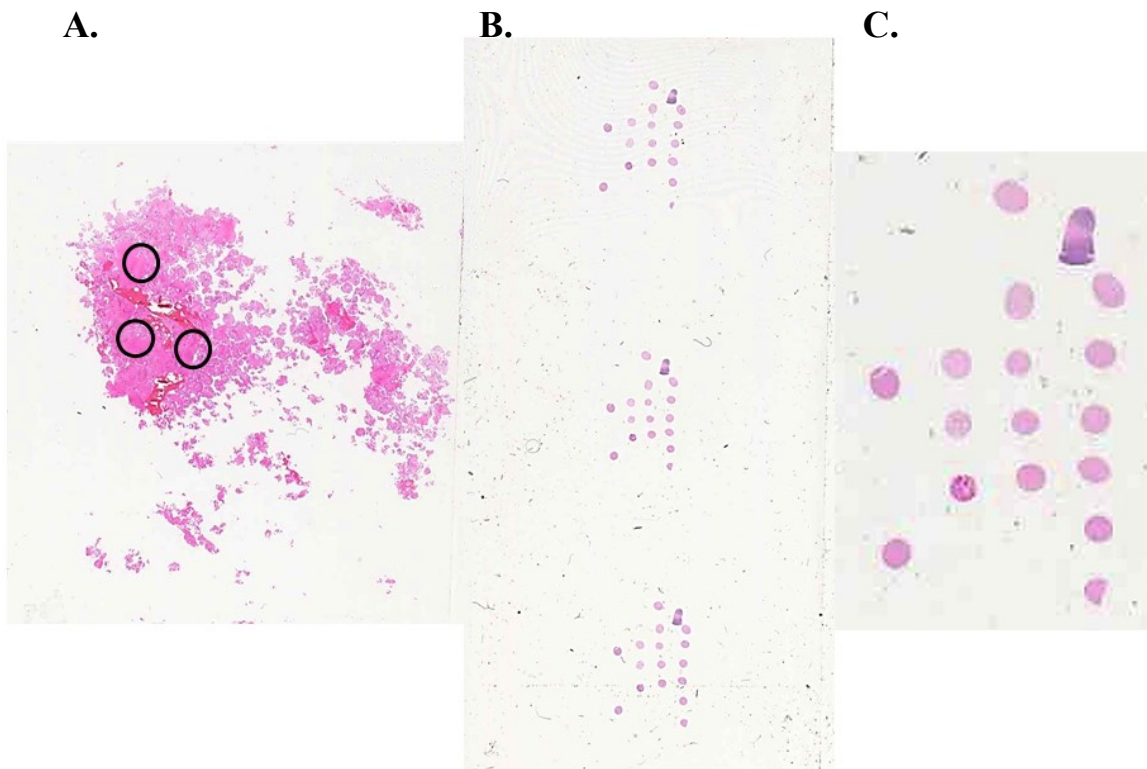


Figure 18: TMA construction and staining process:

These pictures show the process to construct tissue microarrays. A) Representative areas are selected in a case of oligodendroglioma (Haematoxylin-eosin), whole mount; the cores are transferred into a receipt block; each tumour is sampled in three different regions; cores are stained with haematoxylin-eosin (B, C); serial sections are cut from each TMA block to be used for immunostains.

3.3.3.2. TMA 3D analysis for TSPO in neoplastic, GAMMs, and endothelial cells:

This technique was used to estimate the extent of TSPO expression in microglia, neurovascular endothelial cells, and neoplastic cells. TMA slides were prepared as previously described above. TMA slides were stained individually for CD31, TSPO, IDH1, and Iba1 by using peroxidase immunohistochemistry (IHC) approach. Further, they were scanned at native resolution optical zoom 40x at the University of Manchester (UoM) Bioimaging Facility using a 3DHistech Panoramic 250 Flash slide scanner (3DHISTECH Ltd. Budapest, HUNGARY). The regions of interest (ROI) were selected and exported as tiff images by using CaseViewer at UoM Bioimaging Facility. Images uploaded into ImageJ tool (RGB). Images stained for TSPO (Channel 1) was stacked by using images to stack tool and later converted to 8-bit greyscale. The same step was repeated for the examined next channel 2 (CD31 or IDH1) by ImageJ (<https://ImageJ.nih.gov/ij>). Dimensions (x, y and z) for each stack must be identical between the two stacked channels by adjusting the canvas size under image tool. Colocalization between the two channels was estimated by Coloc2 under analyze tool. The analysis was allowed to run by Plugin tool. Imaris software (Bitplane AG Zurich, Switzerland) is used for visualizing the stained stacked regions in three dimensions (Figure 19).

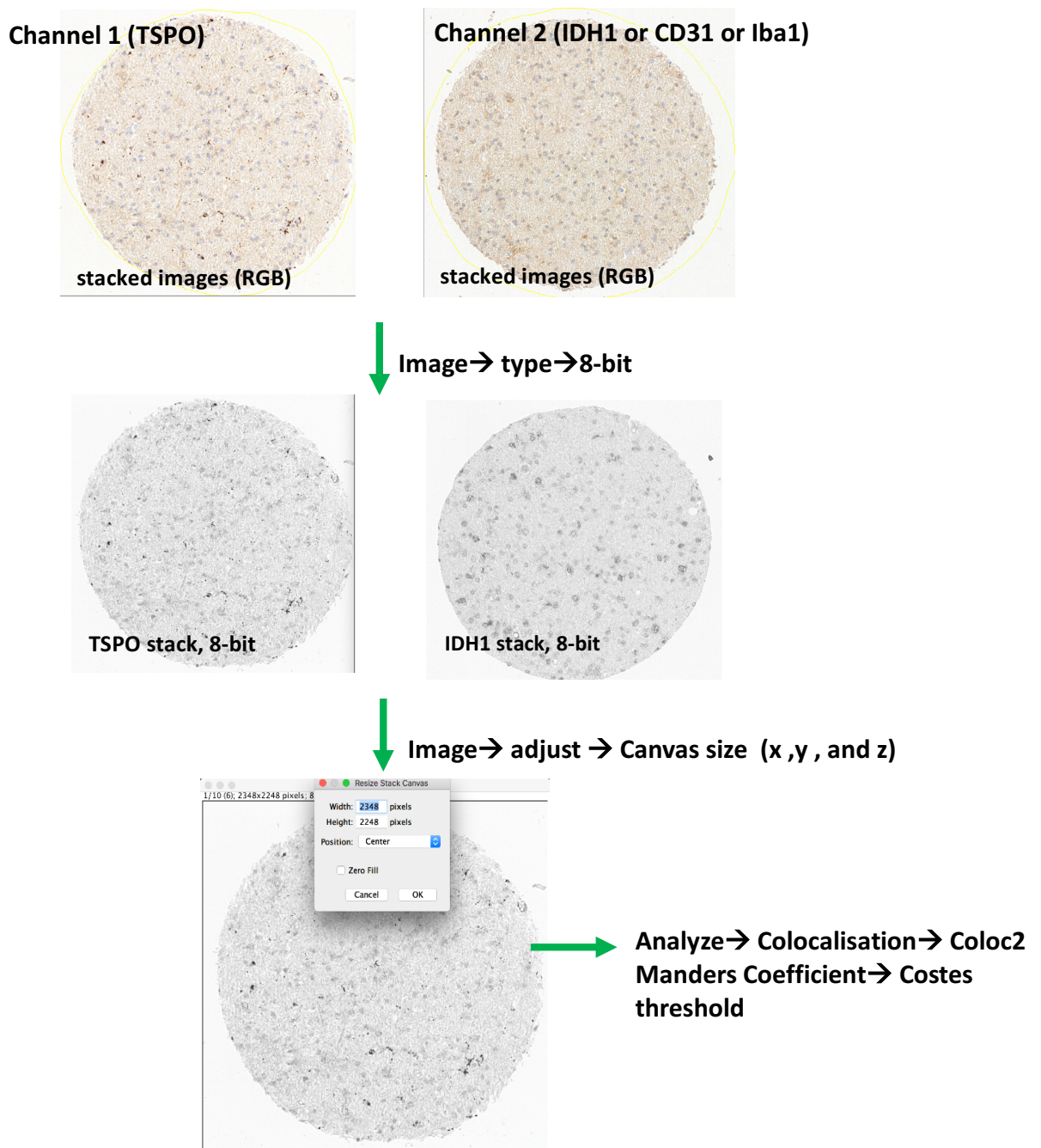


Figure 19: TSPo Colocalisation algorithm protocol for 3D quantification.

TMA stained with TSPo, CD31, Iba1 and region of interest (ROI) was estimated and saved as Tiff file. Then, in Imagej software, images were imported and saved as RGB. Later, all each case images were imported to Imagej and stacked by Image tool to be named as Channel 1 (TSPo). Next, similar to the previous step, channel 2 images (either CD31 or IDH1) were stacked and named as channel 2. RGB

stacked image was converted to 8-bit. Channel 1 and channel 2 canvas size (x, y, and z) was adjusted to be equal. Finally, the analysis was run for both channels automatically with analyze tool to measure the colocalization by using Mander's coefficient and Costes threshold.

3.3.4. Mass Cytometry Analysis:

Mass cytometry was supplied by Fluidigm (<https://www.fluidigm.com>), South San Francisco, California. The main steps for the protocol includes dewaxing, hydration, antigen retrieval (AR), blocking, primary incubation, and secondary incubation. The slides were baked in oven for 2 hours at 60 °C until all visible wax was removed. Dewaxing in xylene by soaking the holder containing slides in xylene for 20 minutes. Hydration step in descending grades of ethanol (100%, 95%, 80%, 70%) for 5 minutes at each concentration followed at final stage by washing in deionized for 5 minutes. The tissue slides were arranged side by side (back to back) in container containing 1x antigen retrieval solution (40ml) and allowed for heating at 96 °C for 30 minutes. The slides container with antigen retrieval solutions was allowed for cooling down into 70 °C for 5 minutes on the bench (by monitoring the solution temperature). The holder containing the slides was moved into water container for washing step in Coplin jar for 10 minutes. The slides were later washed in PBS for 10 minutes. Blocking step was held in 3% BSA in PBS at room temperature for 45 minutes. The Fluidigm Maxpar antibodies were diluted based on the optimized concentration in 0.5% BSA/PBS (around 500-700 µl to cover the entire tissue slide) and incubated for overnight at 4°C in hydration chamber (an empty tips box while the slides on the tip shelf and bottom was filled halfway with water). Using MaxPar metal tagged special antibodies for a fast-comprehensive profiling of tumour complexity with different cell types (different protein markers at a time) within the tissue section. Slides were washed in 0.2% Triton X-100 in PBS for 8 minutes and followed by PBS washing for 8 minutes.

The data analysis and visualization was conducted by CyTof software v7.0 and MCDTM Viewer software with Mass Cytometry imaging system for conversion of tissue scans into TIFF images displaying the expression of each protein. TSPO (Abnova, Pab7095). Iba1 (Wako, 019-19741). GFAP (Dako, M0761), TMEM119 (Abcam, ab209064). Experiment and analysis were supplied with Michael Haley helps.

3.3.5. DNA isolation for polymorphism:

DNA isolation from the FFPE tissues, QIAamp DNA FFPE tissue kit (Qiagen, Hilden, Germany) was used. The paraffin was removed from FFPE slides for 50 cases by using Xylene solvent. Each slide was soaked for 5 minutes in xylene. Next, each slide was carefully transferred to 100% ethanol and soaked for another 5 minutes. Later, the slides were allowed to dry at room temperature for 10 to 15 minutes. Slides macro-dissection was done accompanied by H&E stained corresponding slides for each case. The tissues scraped away from the slide by using sterile scalpels. Next step is to lyse the cells by adding 180 μ l ALT buffer and 20 μ l K proteinase from QIAamp DNA FFPE tissue kit (Qiagen, Hilden, Germany) in clean RNAase free screw cap tubes (STAR LAB, Hamburg, Germany). Each sample was exposed to the heating process at 56°C for 2 hours until the cells were completely lysed and later at 90°C for 1 hour to reduce the formaldehyde modification of nucleic acids. 200 μ l of AL buffer and 200 μ l 100% ethanol were added in two separated steps with vigorous vortexing after each addition. The whole lysate was later transferred to pre-labelled QIAamp MinElute column (Qiagen, Hilden, Germany) and centrifuged at 6000 xg (8000 rpm) for 1 minute. The flow-through was discarded, and 500 μ l of AW1 washing buffer (100% ethanol pre-added) was added to each QIAamp MinElute column. Each column was allowed to centrifuge at 6000 xg (8000 rpm) for

1 minute, and the collection tube containing the flow-through was discarded. 500 µl of AW2 buffer was added to each QIAamp MinElute column and allowed for centrifugation at 6000 xg (8000 rpm) for 1 minute. The collection tube containing the flow-through was discarded and replaced with a new one. To completely dry the membrane, each QIAamp MinElute column was allowed for centrifugation at full speed for 3 minutes. The QIAamp MinElute column was placed in sterile pre-labelled 1.5 ml microcentrifuge tubes. 50 µl of ATE elution buffer was added into the center of the membrane of the QIAamp MinElute column and incubated at room temperature for 5 minutes. Finally, each tube was allowed for centrifugation at full speed for 1 minute. The yield DNA sample was stored at – 20 °C until needed. The primers used for the polymorphism PCR amplification and sequencing are F- AATCTCTGCAGGCCTTGGT and R- CATGGTTGTCCCGCCATAC (Sigma, life science). GoTaq Hot Start Green Master Mix (Promega, Wisconsin, USA) was used for the PCR amplification reaction.

3.3.5.1. PCR for polymorphism:

Master Mix was prepared for 50 samples. 12.5 µl of GoTaq Hot Start Green Master Mix (Promega, Wisconsin, USA) for a final concentration of 1X. 5µl of DNA per sample was used. Primers were added at a final concentration of 0.5 µM, 1.25 µl of each primer per tube. 5 µl of nuclease-free water was added for a total volume of 25 µl per reaction. The Sanger sequencing procedure was performed at Genomic Diagnostics Laboratory, Manchester Centre for Genomic Medicine, St. Mary's Hospital, Oxford Road, Manchester with Nicola Roberts assistant (Table 2 and Figure 20).

Table 2: Primer sequences and PCR conditions

| mRNA full length | Number of cycles | Denaturation temperature and time | Annealing temperature and time | Elongation temperature and time |
|-------------------------------|------------------------------------------|------------------------------------------|---------------------------------------|----------------------------------------|
| TSPO-F | One predenaturation 35 cycles | 95 °C, 2 min 95 °C, 1 min | 62 °C, 1 min | 72 °C, 30 s |
| TSPO-R | One final elongation | | | 72 °C, 5 min |
| TSPO-F primer sequence | (5'-3') AATCTCTGCAGGCCTTGGT | | | |
| TSPO-R Primer sequence | (5'-3') CATGGTTGTCCC GCCATAC | | | |

A.

NM_000714.5

Chr 22

GTGCCTCAGGCCTCCCCATCCTCCGTCCTCCCAATCTCTGCAGGCCTTGGTGGATCTCCTGCTGGTCAGTGGGGC
 GGCGGCAGCCACTACCGTGGCCTGGTACCAGGTGAGCCCGCTGGCCGCCCGCTGCTCTACCCCTACCTGGCCT
 GGCTGGCCTTCACGACCACACTCAACTACTGCATATGGCGGGACAACCATGGCTGGCGTGGGGGACGCGGGCT
 GCCAGAGTGAGTGCCCGGCCACCAGGGACTGCAGCTGCACCAG

B.

| Primer ID | Sequence 5'-3' | Tm | GC % |
|---------------|---------------------|------|------|
| TSPO_rs6971_F | AATCTCTGCAGGCCTTGGT | 64.2 | 52.6 |
| TSPO_rs6971_R | CATGGTTGTCCCGCCATAC | 66.6 | 57.9 |

C.

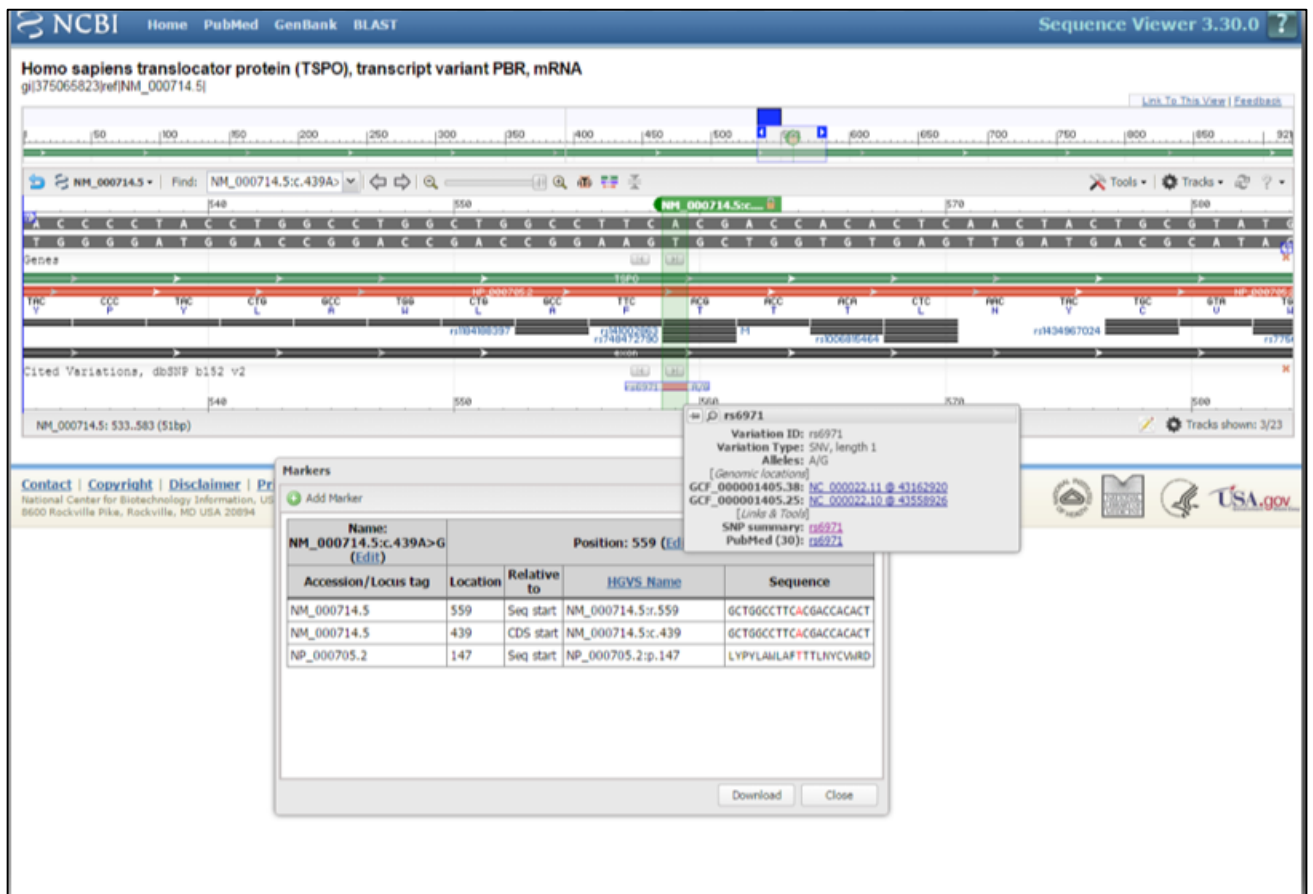


Figure 20: TSPO homo sapiens polymorphism rs6971.

A) NM_000714.5 extracted template DNA sequence to show the location of the polymorphism and the primers (forward and reverse). The yellow highlighted region is for the forward and reverse primer sequences, while letter A in red indicates the location of polymorphism.

- B) The exact sequences for the forward and reverse primers, with more details about the T_m and GC% content. C) NCBI sequence viewer 3.30.0 for the TSPO homo sapiens polymorphism rs6971 showing the polymorphism location.

3.3.5.2. Polymorphism analysis:

The Sanger sequencing has been held at Genomic Diagnostics Laboratory Manchester Centre for Genomic Medicine, St. Mary's Hospital, Manchester. Later, the analysis has been done by using Chromas version 2.6.5 www.technelysium.com.au. Clustal Omega EMBL-EBI. Conway institute, UCD and confirmed by SeqMan Pro, DNASTAR Lasergene software.

3.3.6. [¹¹C]-(R)PK11195 PET Imaging:

3.3.6.1. Patient selection:

Twenty-six patients were selected (sixteen cases diagnosed with WHO grade II, Nine cases with WHO grade III). Thirteen patients were diagnosed with astrocytoma (low and high grade), and thirteen patients were diagnosed with oligodendroglioma (low and high grade). Fourteen patients were part of a previous study cohort (TSPO imaging in Glioma, REC reference 09/H1014/41), January 2010 to November 2012 and 12 patients were from a project commenced in April 2014 (TSPO imaging in Transforming Glioma, REC reference 15/NW/0071).

[¹¹C]-(R)PK11195 PET scans were performed on High Resolution Research Tomograph (HRRT, Siemens/CTI, Knoxville, TE, US). The injected dose was 740 MBq of [¹¹C]-(R)PK11195 and the emission data acquired for 60 minutes post injection. Participants were allowed to eat and drink normally on the day of scanning but asked to stop taking benzodiazepines at least three days before the PET scanning day.

The reconstruction process was conducted with voxel size 1.22x1.22x1.22mm. Moreover, Attenuation, scatter, random coincidence, dead time corrections and normalization was processed as it was described previously [8]. To reduce image noise, 3D Gaussian filter (4mm full width at half maximum) was applied. Parametric map creation to demonstrate BPND has been done with Dr. Rainer Hinz guidance and Erjon Agushi helps. Further, tumour VOI for each subject was defined and further projected onto the BPND parametric map by Erjon Agushi. Mean BPND maximum binding potential (BPNDmax) analysis was performed in R statistics (R foundation for statistical computing, Vienna, Austria).

The initial steps (indicated below from Figure 21-23), including image co-registration (PET-MRI), segmentation, brain mask ROI, and BP map were created by me with Dr. Rainer supervision. Anatomical sequences included an axial T1 inversion recovery (TI=1150ms, pixel size(PS)=0.94x0.94mm, slice thickness (ST)=1.8mm on the 3T scanner and TI=1000ms, PS=1.19x1.19mm, ST=1.25mm on the 1.5T scanner), high resolution axial T2 (3T acquisition PS=0.26x0.26mm, ST=3.0mm and 1.5T PS=0.45x0.45mm, ST=6mm) and coronal FLAIR (3T acquisition PS=0.45x0.45mm, ST=3.0mm and 1.5T PS=1.07x1.07mm, ST=1.25mm).

3.3.6.2. PET Data analysis:

3.3.6.3. Image co-registration:

Previously reconstructed PET images for twenty-six patients in this study stored in the primary data source. The PET reconstructed images have been extracted from the Wolfson Molecular Imaging Centre (WMIC) primary database. PET and MRI were co-registered for each subject by using the summed PET image and T1- weighted MR image with FSL (FMRIB, University of Oxford, UK) toolkit or alternatively by the statistical parametric mapping (SPM) co-

registration toolkit. The purpose of co-registration was the alignment of two different modalities (MRI and PET) and the assumption of their anatomical structural similarities, although the distribution of the values in each imaging modality is different. The quality of this co-registration was visually inspected. Later, an image-derived input function was created based on the manually delineated cerebral grey matter. The first parametric binding potential map based on the previously delineated cerebellum input function was created by using RPM (receptor parametric mapping software written in Matlab).

3.3.6.4. Segmentation and normalisation:

The segmentation process is an analysis tool used in image processing to classify each pixel into classes that would represent homogenous regions. Segmentation of MRI was performed in order to compensate for the radiotracer uptake differences among the different brain tissue compartments, such as grey matter (GM), white matter (WM), and cerebrospinal fluid (CSF) (Figure 21). Statistical parametric mapping (SPM5, Functional Imaging Laboratory, Wellcome Department of Imaging Neuroscience, University College London, UK) was used for segmentation and normalisation. Spatial normalisation is a process of registering images to fit a standard template brain either by warping (non-linear registration) for small-scale anatomical differences or transformation (linear registration) for significant differences in head shape and position. The used template space is the Montreal Neurological Institute (MNI) space, and it was normalised to an individual MRI space. Each T1-weighted MRI in PET space was segmented into GM, WM, and CSF probability maps.

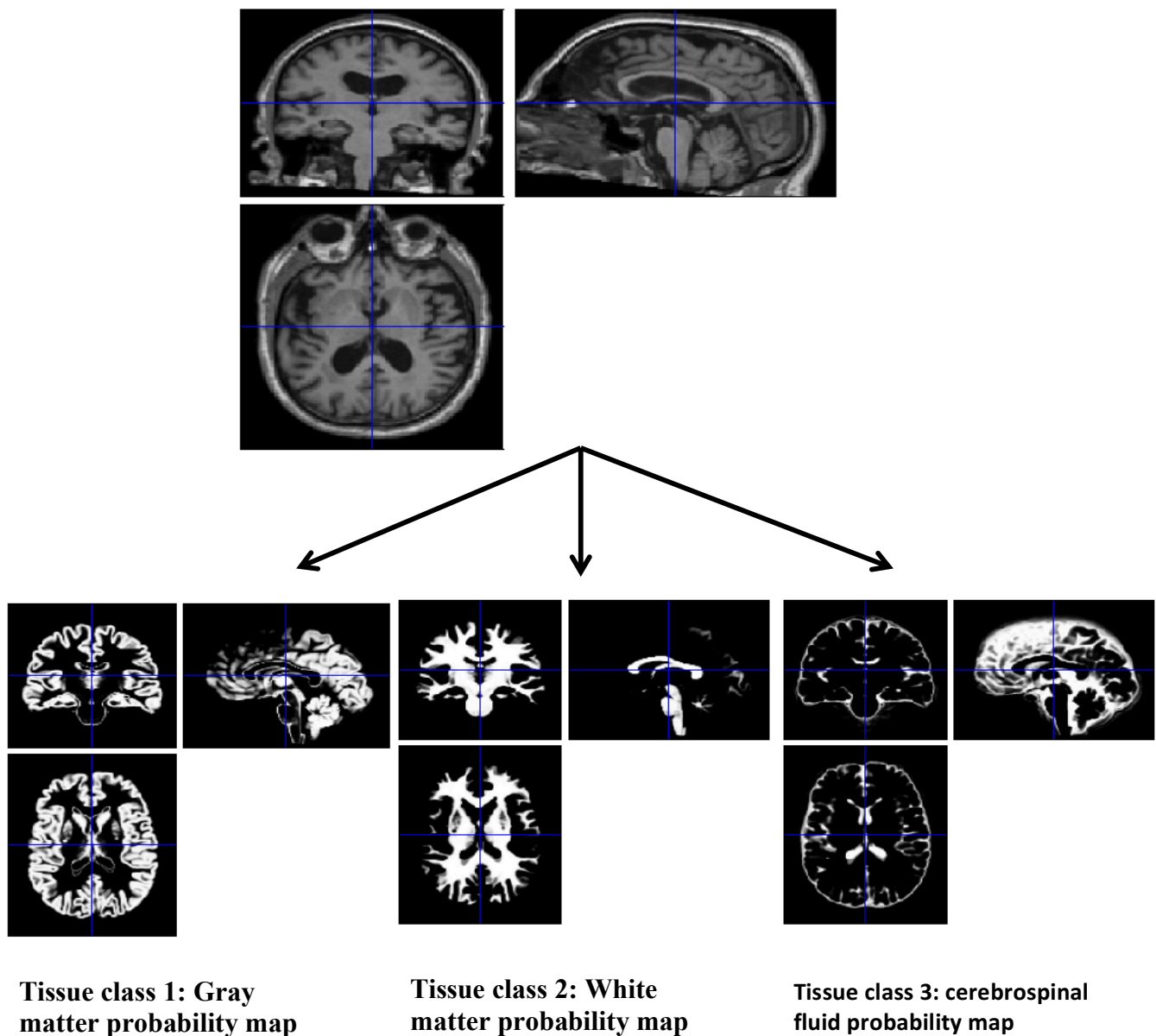


Figure 21: Segmentation process.

Segmentation process used to classify each pixel into classes; grey matter (GM), white matter (WM), and cerebrospinal fluid (CSF). T1-weighted MRI in PET space was segmented into GM and WM probability maps. The segmentation was performed in SPM5 toolkit; Statistical parametric mapping (SPM5, Functional Imaging Laboratory, Wellcome Department of Imaging Neuroscience, University College London, UK).

3.3.6.5. Parametric map creation:

The initial parametric map with the reference region input created by manual delineation of the cerebellum reference region by Analyse software (Analyse AVW, Mayo Clinic, Rochester, USA). Later, the whole brain mask was generated by using Analyze software, and a manual correction was required to adjust inaccurate brain boundaries in all three orientations (transverse, sagittal, and coronal). TSPO is expressed in the normal brain in the olfactory bulb, meninges, and pituitary gland. Therefore, hot spots in pituitary glands, scalp and other regions outside the brain were manually excluded, and internal spots in ventricles, CSF, and tumour were included (Figure 22).

The generated whole-brain mask was further applied to the probabilistic atlas for grey matter (GM) and white matter (WM). The generated individualised anatomic GM, WM were be applied to the probabilistic atlas and converted to object map. Later, individualised anatomic GM, WM and individualised three-dimensional maximum probability brain atlas object maps were used to extract tracer uptake values from PET parametric images. The final accurate parametric image for each individual was generated by using Receptor Parametric Mapping (RPM) and using cerebellar GM as a reference input function with the manually corrected whole-brain mask. A summary of the Binding potential map creation process (Figure 23).

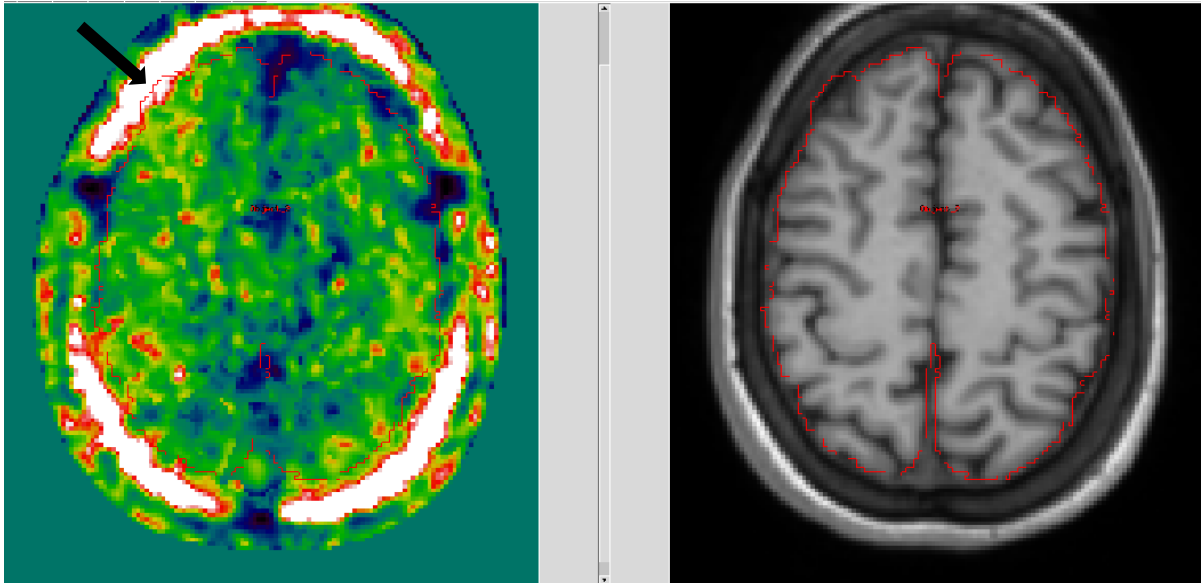


Figure 22: manual correction of the inaccurate brain boundaries by Analyze software. The arrow indicates the region where the brain mask spill-over the scalp (arrow) and it was modified manually to exclude the scalp regions in 3 orientations (transverse-sagittal-coronal). Left panel is brain mask ROI, right panel is coregistered MRI-PET for the same subject.

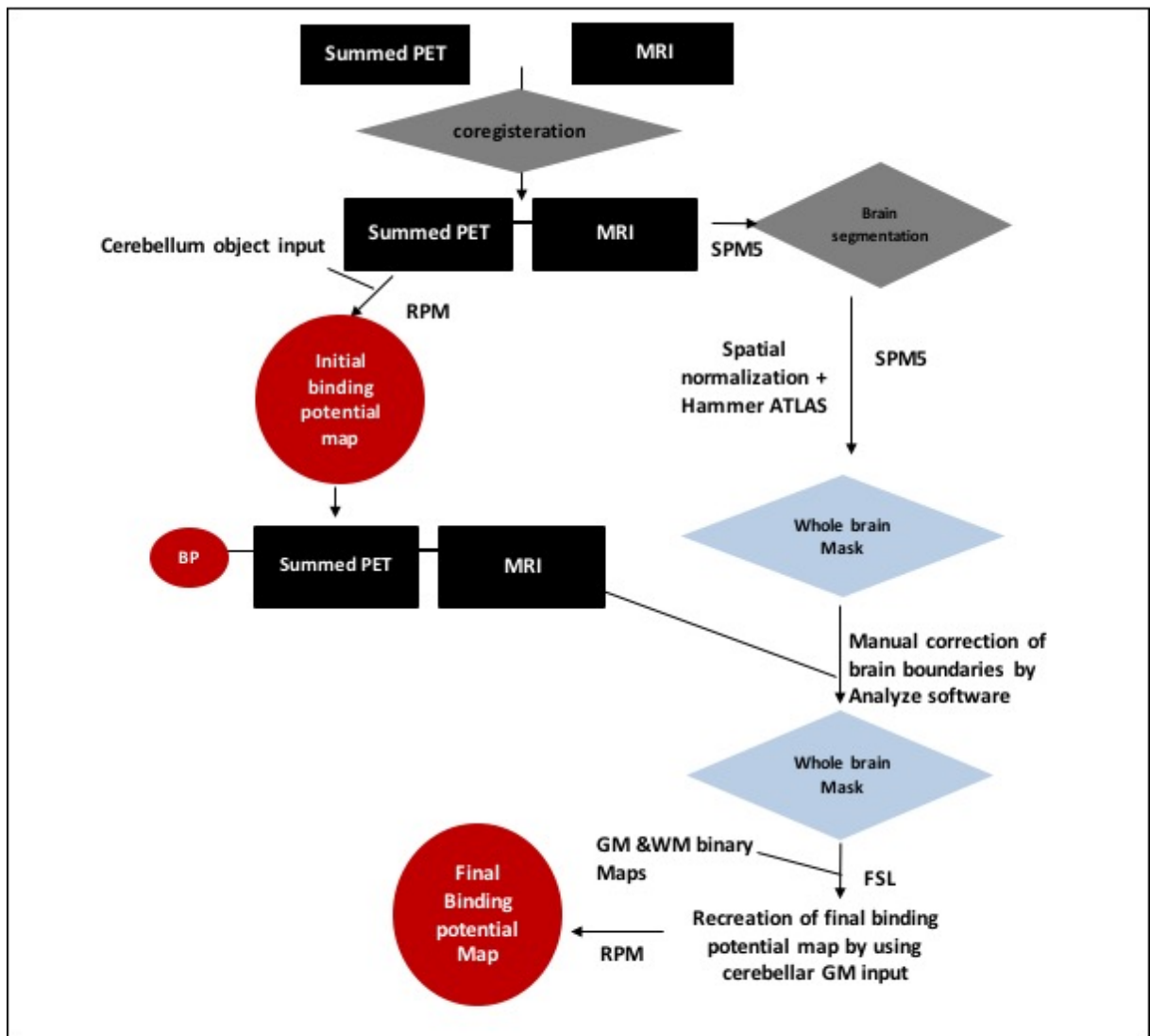


Figure 23: Steps of generating binding potential map. Creation of binding potential map includes image co-registration (PET-MRI), segmentation, brain mask ROI, manual correction of brain boundaries, creation of BP map by using GM input.

3.4. Results:

3.4.1. TSPO is a biomarker for oligodendroglioma progression.

Immunohistochemical TSPO expression on FFPE tissues (IHC):

I) Oligodendrogliomas cohort (n=50):

AO showed a significant higher TSPO expression compared to LGO (Figure 24) (unpaired t-test p-value <0.001). The Mean of TSPO expression in LGO is 1.262, and in AO is 5.955. The used oligodendrogliomas cohort in TSPO expression quantification for LGO and AO is indicated in table 3. TSPO expression (% area) level by using ImageJ and estimating the percentage of the total summed DAB stained or grey values of all pixels over the total number of pixels (white and grey) after thresholding. The obtained 3 threshold value for the % area represents the separation line between low and high grade oligodendroglioma. Figure 25, showed a visual inspection under the microscope (20x magnification) of the TSPO expression level in two representative cases of LGO (WHO II). Panels a and b showed two representative cases for LGO (WHO II). Panels c and d showed two representative cases for AO (WHO III). Panels e and f showed representative images for vascular TSPO expression on FFPE sections.

Table 3: List of oligodendrogliomas cohort used in methylation, RNA-seq, TSPO expression and survival analysis. All patients harbour IDH1 mutation and 1p/19q co-deletion.

LGO (WHO II) and AO (WHO III).

| <i>ID</i> | <i>Gender</i> | <i>Age at diagnosis</i> | <i>WHO grade</i> | <i>Progression</i> | <i>OS</i> | <i>Site</i> | <i>Follow-up months</i> |
|-----------|---------------|-------------------------|------------------|--------------------|-----------|----------------|-------------------------|
| 1 | Male | 37 | WHO III | Yes | died | Left parietal | 54 |
| 2 | Male | 41 | WHO II | Yes | died | Right temporal | 112 |
| 3 | Female | 38 | WHO II | No | alive | Left frontal | 118 |
| 4 | Male | 39 | WHO II | No | alive | Right frontal | 118 |
| 5 | Female | 57 | WHO II | No | alive | Right parietal | 116 |
| 6 | Female | 36 | WHO III | Yes | alive | Left frontal | 115 |
| 7 | Male | 31 | WHO II | Yes | alive | Left frontal | 115 |
| 8 | Female | 50 | WHO II | No | alive | Left insula | 114 |
| 9 | Female | 51 | WHO II | No | alive | Right frontal | 114 |
| 10 | Male | 40 | WHO II | No | alive | Right frontal | 111 |
| 11 | Male | 51 | WHO III | No | alive | Right frontal | 105 |
| 12 | Female | 36 | WHO III | Yes | alive | Left frontal | 102 |
| 13 | Male | 24 | WHO II | Yes | died | Right temporal | 85 |
| 14 | Male | 47 | WHO III | Yes | died | Left frontal | 86 |
| 15 | Male | 33 | WHO III | No | alive | Left temporal | 95 |
| 16 | Female | 44 | WHO III | No | alive | Right frontal | 94 |
| 17 | Male | 43 | WHO II | No | alive | Right parietal | 93 |
| 18 | Male | 52 | WHO III | Yes | alive | Left temporal | 93 |
| 19 | Male | 28 | WHO II | No | alive | Right temporal | 93 |
| 20 | Female | 48 | WHO III | Yes | died | Left frontal | 78 |
| 21 | Male | 49 | WHO II | No | alive | Left frontal | 92 |
| 22 | Male | 43 | WHO III | No | alive | Left frontal | 92 |
| 23 | Female | 53 | WHO III | Yes | died | Right frontal | 29 |
| 24 | Male | 70 | WHO II | Yes | died | Right frontal | 34 |
| 25 | Female | 44 | WHO II | Yes | alive | Left frontal | 90 |
| 26 | Male | 59 | WHO II | No | alive | Right frontal | 89 |
| 27 | Female | 53 | WHO II | No | alive | Right frontal | 90 |
| 28 | Male | 43 | WHO III | No | alive | Left frontal | 90 |
| 29 | Male | 58 | WHO II | Yes | alive | Right parietal | 89 |
| 30 | Male | 41 | WHO III | No | alive | Right frontal | 88 |
| 31 | Female | 25 | WHO II | No | alive | Right frontal | 87 |
| 32 | Female | 54 | WHO II | Yes | alive | Right frontal | 86 |
| 33 | Male | 77 | WHO III | No | died | Right frontal | 48 |
| 34 | Male | 44 | WHO II | No | alive | Right temporal | 83 |
| 35 | Female | 40 | WHO III | No | alive | Right frontal | 83 |
| 36 | Male | 45 | WHO II | No | alive | Left frontal | 83 |
| 37 | Female | 47 | WHO III | No | alive | Left frontal | 82 |
| 38 | Female | 74 | WHO III | No | died | Right frontal | 39 |
| 39 | Female | 44 | WHO II | Yes | alive | Left parietal | 79 |
| 40 | Male | 35 | WHO II | No | alive | Right frontal | 78 |
| 41 | Female | 60 | WHO II | Yes | alive | Left frontal | 77 |

| | | | | | | | |
|----|--------|----|---------|-----|-------|----------------|----|
| 42 | Female | 68 | WHO III | No | died | Right frontal | 67 |
| 43 | Male | 28 | WHO III | No | alive | Left frontal | 75 |
| 44 | Male | 42 | WHO II | No | alive | Left temporal | 75 |
| 45 | Female | 26 | WHO II | Yes | alive | Left frontal | 75 |
| 46 | Female | 70 | WHO II | Yes | alive | Left frontal | 73 |
| 47 | Female | 34 | WHO II | Yes | alive | Left frontal | 70 |
| 48 | Male | 28 | WHO II | No | alive | Left frontal | 67 |
| 49 | Male | 33 | WHO III | Yes | alive | Left occipital | 66 |
| 50 | Female | 68 | WHO III | Yes | died | Right frontal | 6 |
| 51 | Male | 35 | WHO III | No | alive | Left frontal | 65 |
| 52 | Female | 33 | WHO II | No | alive | Left frontal | 63 |
| 53 | Male | 52 | WHO III | Yes | died | Right frontal | 39 |

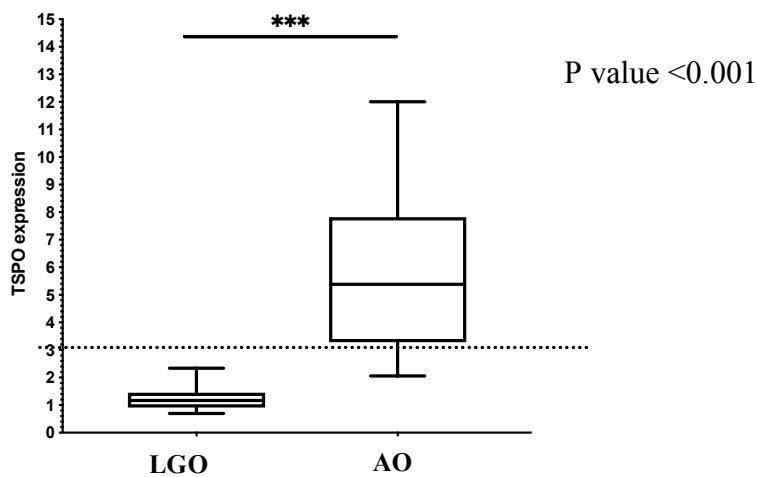


Figure 24: TSPO expression in LGO (WHO II) and AO (WHO III) by immunohistochemistry.

The quantification of TSPO expression in FFPE oligodendroglioma tissues (50 cases) was performed by ImageJ. The studied cases are LGO (WHO II) (n=27) and AO (WHO III) (n=23). TSPO expression mean in LGO is 1.262, and AO mean is 5.955. Statistical unpaired t-test, p-value <0.001, R squared 0.72, 95% CI 3.447-5.940. unpaired t-test using Welch's correction (no assumption of equal SD).

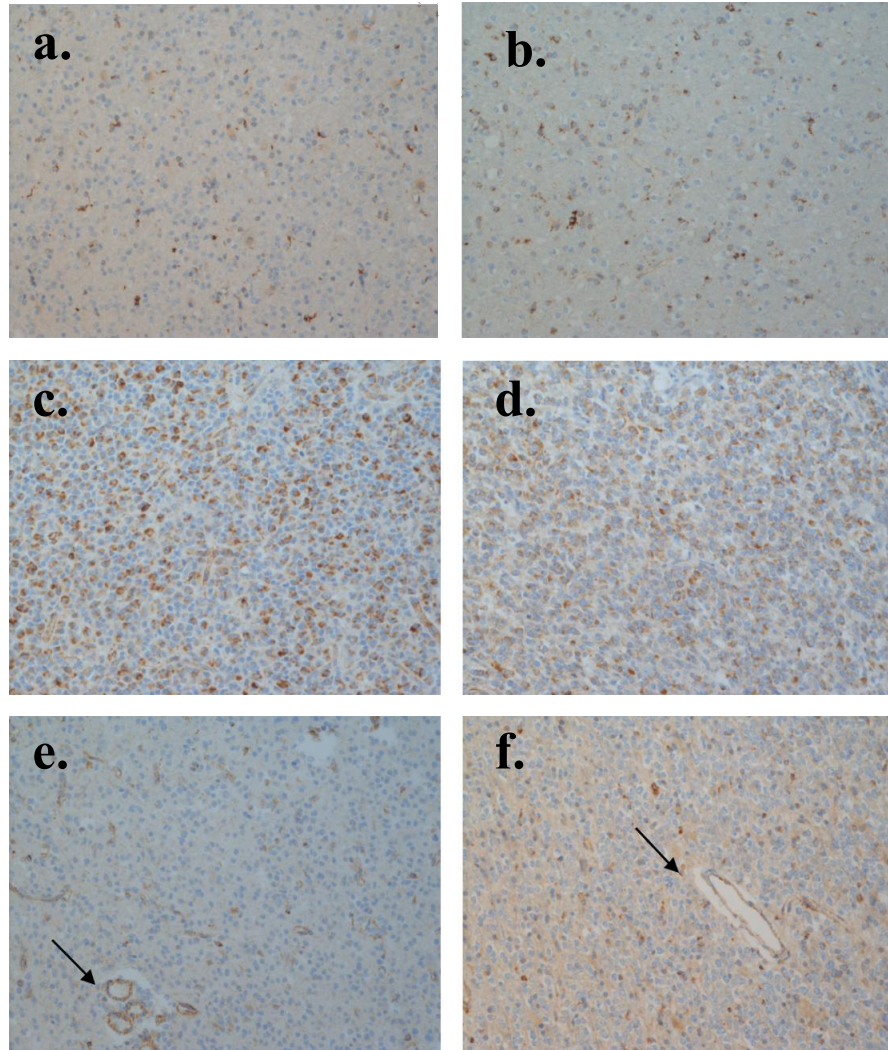


Figure 25: TSPO expression in LGO and AO by immunohistochemistry.

(Panel a and b) showed two representative images (20x magnification) for 2 cases with LGO. (Panel c and d) showed two representative images for AO. (Panel e and f) representative images for vascular TSPO expression.

II) Oligodendroglioma and Astrocytoma Cohort (n=26):

Twenty-six cases were included (sixteen cases were diagnosed as WHO grade II, nine cases were diagnosed as WHO grade III). Thirteen patients were diagnosed with astrocytoma (low and high-grade, LGA and AA), and thirteen patients were diagnosed with oligodendroglioma (low and high-grade, LGO and AO) (Table 4). Immunohistochemistry staining with TSPO was done for all cases in addition to Hematoxylin and Eosin stain to identify the histology and neoplastic cells regions. Figure 26 showed a significant higher TSPO level in AO (mean 5.55) compared with LGO (mean 0.946) ($p=0.0330$). LGA (mean 1.51) vs AA (mean 2.99) did not show a significant difference ($p=0.4760$). The statistical analysis was performed between each group's means using Welch's ANOVA test ($p=0.016$). Figures (27-30) showed co-registered FLAIR and [^{11}C]-(R)PK11195 PET images for LGO, AO, LGA and AA cases. These figures showed the [^{11}C]-(R)PK11195 uptake within the tumour.

Moreover, [^{11}C]-(R)PK11195 BPNDmax calculation was done by Erjon Agushi and concluded a significant difference between Anaplastic gliomas compared to low-grade gliomas (BPNDmax: 1.59 ± 0.63 vs 0.79 ± 0.28 , $p=0.001$). Oligodendrogliomas (LGO and AO) and astrocytomas (LGA and AA) representative cases in the cohorts were displayed with their corresponding co-registered BPND PET and FLAIR-MRI imaging in figures 27 to 30.

Table 4: List of twenty-six patients of Astrocytomas and Oligodendroglioma.

| <i>ID</i> | <i>Sex</i> | <i>Age</i> | <i>Histology</i> | <i>Location</i> |
|-----------|------------|------------|--------------------------------------|-----------------------|
| 1 | M | 41 | Oligodendroglioma WHO II | Right temporal |
| 2 | F | 25 | Astrocytoma WHO II | Right frontal |
| 3 | F | 37 | Anaplastic Astrocytoma WHO III | Right fronto-temporal |
| 4 | M | 45 | Oligodendroglioma WHO II | Right temporal |
| 5 | F | 24 | Oligodendroglioma WHO II | Right occipital |
| 6 | M | 40 | Oligodendroglioma WHO II | Right frontal |
| 7 | F | 63 | Astrocytoma WHO II | Left parietal |
| 8 | M | 33 | Astrocytoma WHO II | Right parietal |
| 9 | M | 42 | Anaplastic Astrocytoma WHO III | Left frontal |
| 10 | M | 31 | Oligodendroglioma WHO II | Right frontal |
| 11 | F | 47 | Astrocytoma WHO II | Left temporal |
| 12 | M | 47 | Anaplastic Astrocytoma WHO III | Left temporal |
| 13 | M | 22 | Anaplastic Oligodendroglioma WHO III | Right parietal |
| 14 | M | 33 | Astrocytoma WHO II | Left frontal |
| 15 | M | 42 | Astrocytoma WHO II | Left temporal |
| 16 | M | 24 | Oligodendroglioma WHO II | Right temporal |
| 17 | F | 50 | Oligodendroglioma II | Left frontal |
| 18 | M | 24 | Anaplastic Oligodendroglioma III | Left frontal |
| 19 | M | 38 | Astrocytoma II | Left frontal |
| 20 | F | 52 | Oligodendroglioma II | Right temporal |
| 21 | M | 37 | Oligodendroglioma II | Left frontal |
| 22 | F | 54 | Anaplastic Astrocytoma III | Right temporal |
| 23 | F | 48 | Oligodendroglioma II | Left parietal |
| 24 | M | 19 | Anaplastic Astrocytoma III | Right fronto-temporal |
| 25 | M | 24 | Anaplastic Oligodendroglioma III | Left frontal |
| 26 | F | 45 | Oligodendroglioma II | Right frontal |

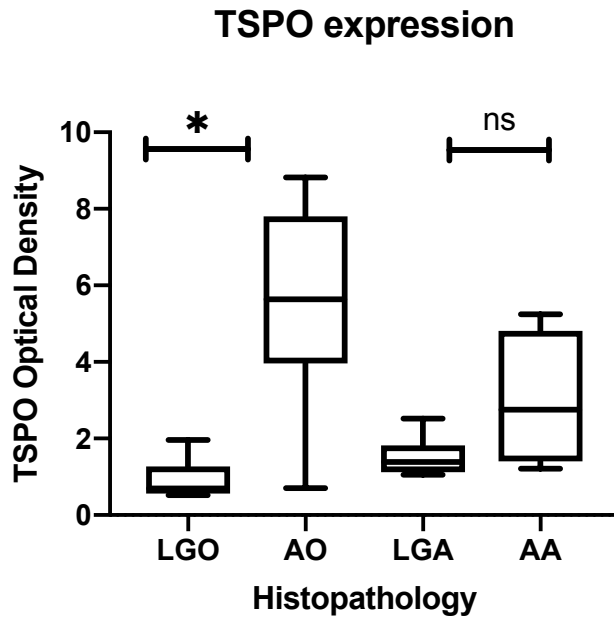


Figure 26: TSPO expression (IHC) quantification by ImageJ in Oligodendroglioma (LGO and AO) and Astrocytomas (LGA and AA).

AO showed significant higher TSPO level compared with LGO ($p=0.0330$), while LGA vs AA did not show a significant difference ($p=0.4760$).

Table 5: Statistical analysis of the TSPO expression in LGO, AO, LGA, and AA.

| GAMES-HOWELL'S MULTIPLE COMPARISON TEST | MEAN DIFF. | 95.00% CI OF DIFF. | SIGNIFICANT? | SUMMARY | ADJUSTED P-VALUE |
|-----------------------------------------|------------|--------------------|--------------|---------|------------------|
| LGO VS AO | -4.604 | -8.739 to -0.4687 | Yes | * | 0.0330 |
| LGO VS LGA | -0.5651 | -1.452 to 0.3214 | No | ns | 0.2731 |
| LGO VS AA | -2.046 | -6.184 to 2.092 | No | ns | 0.2780 |
| AO VS LGA | 4.039 | -0.09204 to 8.169 | No | ns | 0.0544 |
| AO VS AA | 2.558 | -2.048 to 7.164 | No | ns | 0.3487 |
| LGA VS AA | -1.481 | -5.594 to 2.632 | No | ns | 0.4760 |

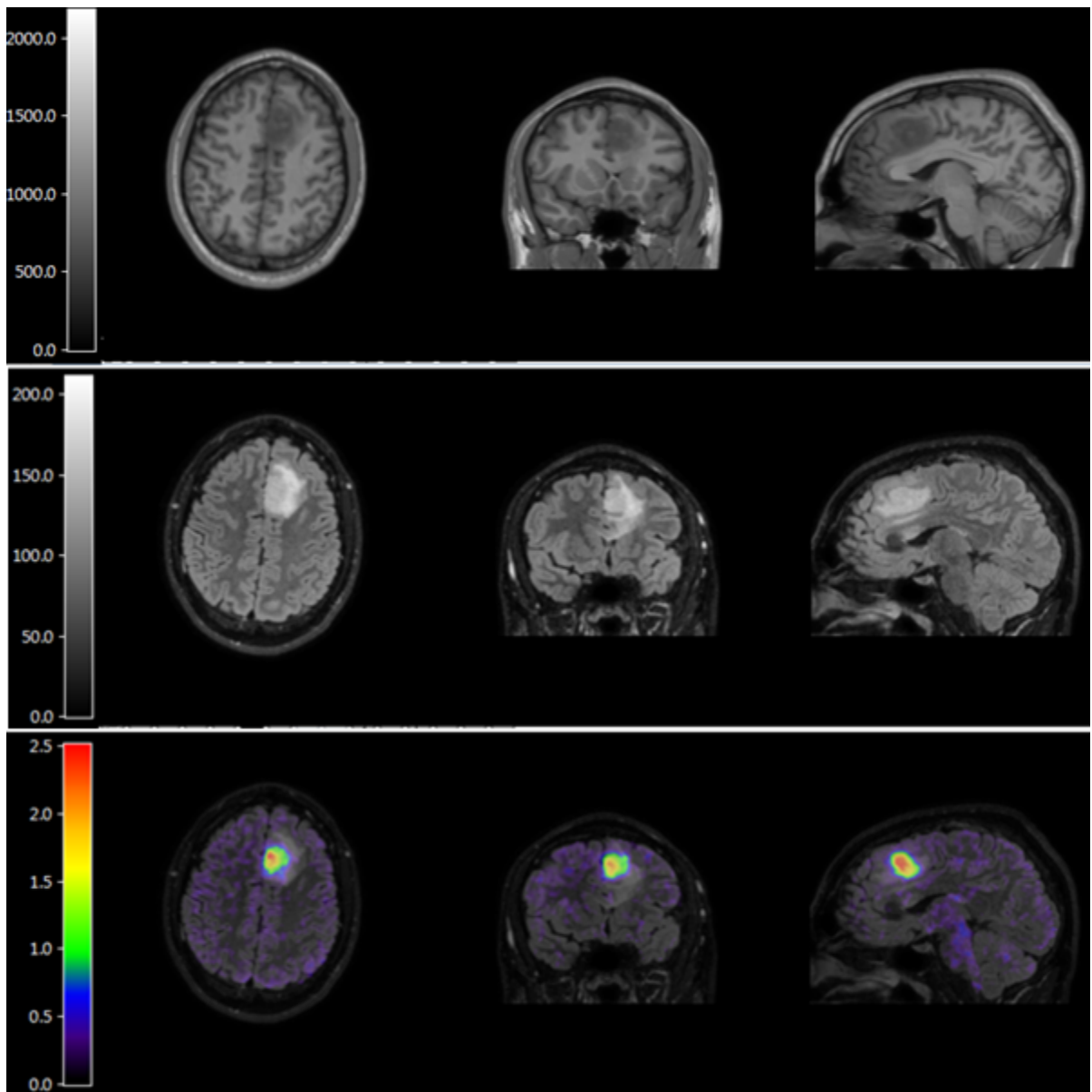


Figure 27: Anaplastic oligodendroglioma (AO) showing areas with increased $[^{11}\text{C}]$ - (R)PK11195 uptake, (transverse- coronal -sagittal).
 Upper panel: post-contrast T1-weighted MRI. Middle panel: FLAIR. Lower panel Lower panel co registered BPND PET and FLAIR-MRI. Colour bar indicating BPND.

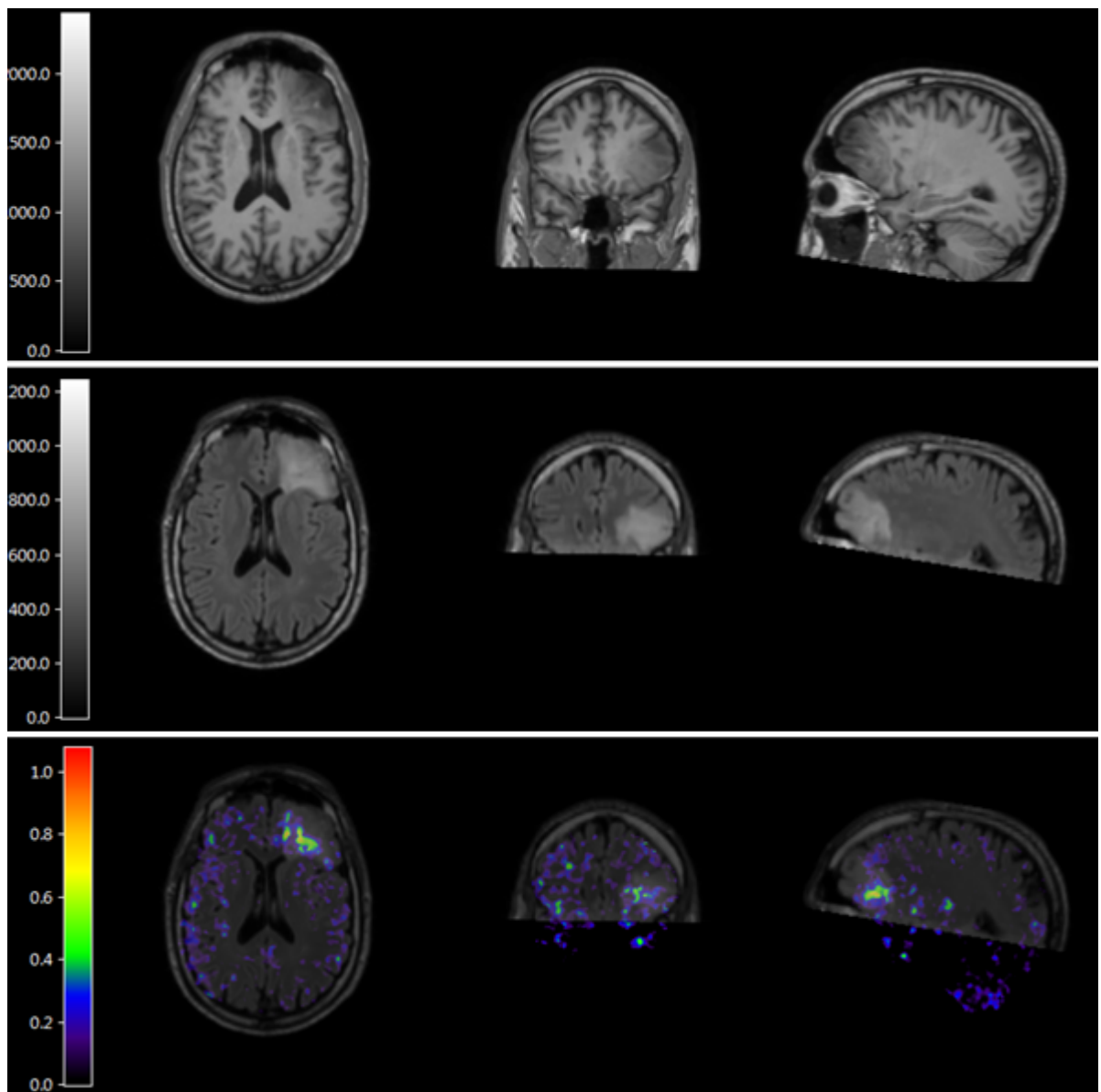


Figure 28: Low grade oligodendroglioma (LGO) showing areas with [^{11}C]- (R)PK11195 uptake, (transverse- coronal –sagittal).

Upper panel: post-contrast T1-weighted MRI. Middle panel: FLAIR. Lower panel Lower panel co-registered BPND PET and FLAIR-MRI. **Colour bar indicating BPND**

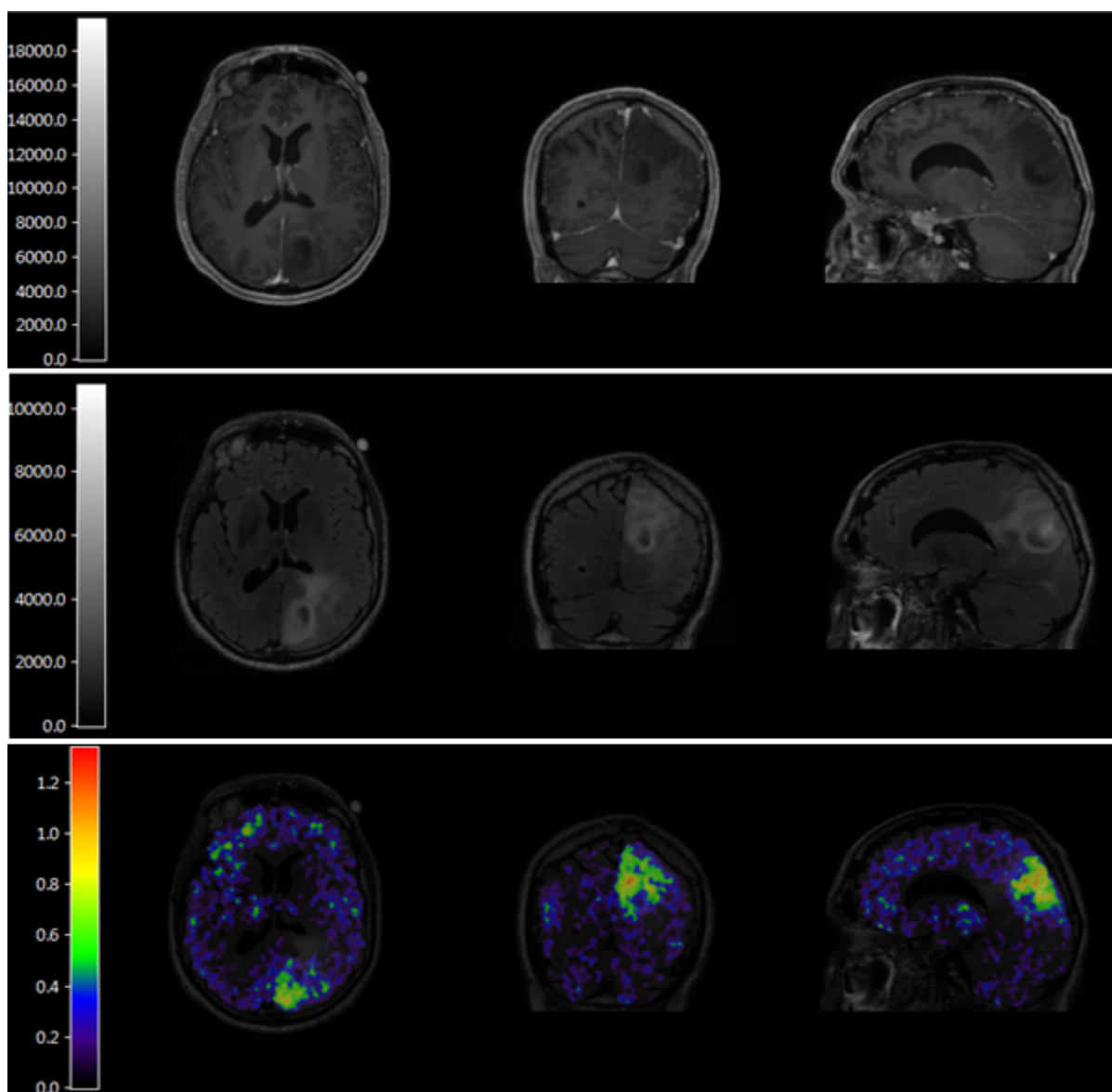


Figure 29: Anaplastic astrocytoma (AA) showing areas with increased $[^{11}\text{C}]$ -(R)PK11195 uptake, (transverse- coronal -sagittal).

Upper panel: post-contrast T1-weighted MRI. Middle panel: FLAIR. Lower panel co-registered BPND PET and FLAIR-MRI. Colour bar indicating BPND

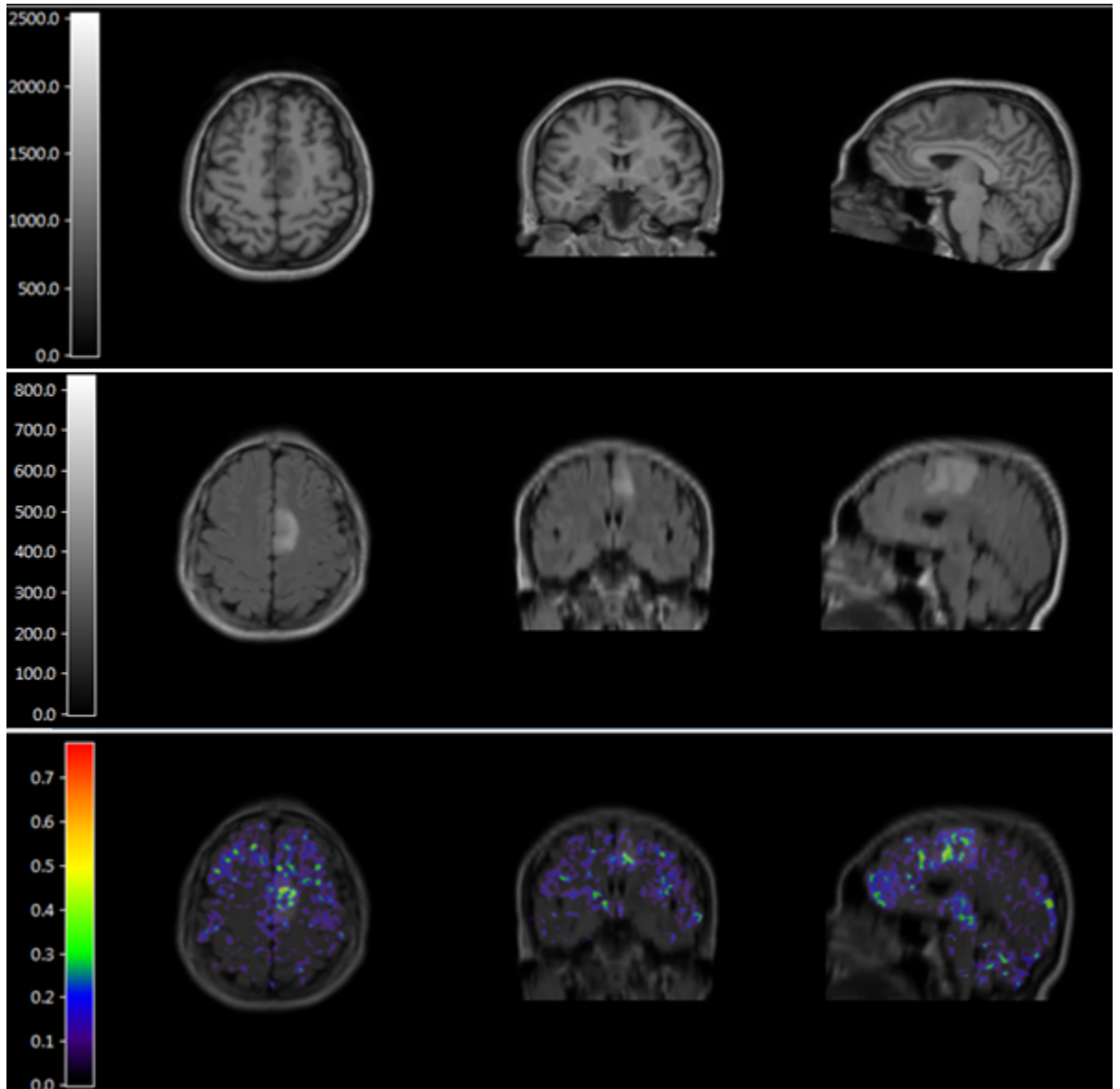


Figure 30: Low grade astrocytoma (LGA) showing areas with [^{11}C]-(R)PK11195 uptake, (transverse- coronal –sagittal).

Upper panel: post-contrast T1-weighted MRI. Middle panel: FLAIR. Lower panel co-registered BPND PET and FLAIR-MRI. Colour bar indicating BPND.

3.4.2. TSPO expression analysis in neoplastic cells, GAMMs and endothelial cells (3D tissue analysis):

TSPO expression in neoplastic cells, endothelium and GAMMs, was examined. A previous preliminary study suggested that TSPO positive GAMMs in double immunofluorescence quantification partially contribute to overall TSPO cell expression in gliomas [8]. In the current study, biopsies were taken from high binding potential (BPND_{max}) of [¹¹C]-(R)PK-11195 for three anaplastic oligodendrogliomas cases (WHO III) (Figure 31 a, b). Tissue microarray (TMA) was performed for these cases. TMA was stained with Iba1 (microglia/macrophages specific marker), CD31 (endothelial cells marker), TSPO, and IDH1 (a molecular marker for gliomas) (Figure 31, d). A 3D map was built for each case with the four markers mentioned above to quantify these markers' colocalisation with TSPO per case. Manders coefficient 1 (tM1) represents the amount of TSPO as a ratio of the total intensity value (voxels) of TSPO (channel 1), which colocalises with channel 2 (CD31, Iba1 or IDH1) (Figure 31, g).

A study indicated a practical guide for evaluating and quantifying the colocalisation between two different channels, including the Pearson correlation (PCC) coefficient and the Manders coefficient (MCC). They indicated PCC as a coefficient for measuring the signal intensity pixel by pixel by subtracting the mean intensity at a specific channel in relation to the other channel, which may generate negative values. PCC is sensitive to pixels' intensity variability and artefacts, making PCC more complicated to interpret when the two probes do not follow a simple linear correlation relationship. Spearman rank correlation value (SRCC) is another correlation coefficient to assess the relationship between two probes pursuing a monotonic relationship. However, using either of these correlations could be affected by signal artefacts and signal variability between the two channels. Therefore, they suggested to use

Mander's coefficient, which does not consider a linear relationship between both colocalised probes within the two different channels, but it still sensitive to the background signal. However, Costes et al. suggested using Coste's automatic threshold to eliminate the background signal [356, 357].

In the current result, Mander's coefficient quantifies the total intensity of TSPO colocalised pixels with either CD31 or IDH1 or Iba1 over the total intensity of all TSPO (channel 1) regardless of the fixed proportion of intensity between the two probes. In other words, it measures the quantity of one probe (Channel 1) that colocalise with the other probe (Channel 2). Moreover, MCC is sensitive to the ROI background, which can be distinguished by applying the automated thresholding method (Costes) [356]. In the current study, Costes was chosen in ImageJ quantification [358]. MCC is a range from zero (no colocalisation) to 1 (strong colocalisation). However, the three used cases cores showed moderate strength among different used cores. Although the colocalisation calculation was automatic by ImageJ, the analysis was performed in duplicate by two observers. The mean SRCC of duplicate analysis for each case were 0.529 (IDH1/TSPO), 0.512 (Iba1/TSPO), 0.480 (CD31/TSPO) for one of the cases. The second case were 0.370 (IDH1/TSPO), 0.352 (Iba1/TSPO), 0.394 (CD31/TSPO) for one of the cases. The third case SRCC were 0.457 (IDH1/TSPO), 0.439 (Iba1/TSPO), 0.430 (CD31/TSPO). The SRCC values were consistent with approximately close relative values among different markers (IDH1, CD31, Iba1) within each case. However, the correlation coefficient is still affected in terms of their values due to differences between the two channels intensity variability and the signal obtained artefacts. Costes et al. suggested Mander's coefficient to be used with applying Coste's threshold.

The dot-plot showed that the major contributions to the TSPO expression were predominantly from neoplastic (IDH1 expressing) cells (Mander coefficient's mean 0.470) compared to endothelial (CD31 expressing cells) (Mander coefficient's mean 0.336) and microglial cells (Iba1 expressing cells) (Mander coefficient's mean 0.349) (Figure 31, g). This result suggests that the noticed increase in TSPO expression during the progression and transformation to higher-grade was mainly from neoplastic cells (IDH1) and not from GAMMs (Iba1) or vascular component (CD31). This experiment was performed in collaboration with Dr David Coope and Erjon Agushi [437].

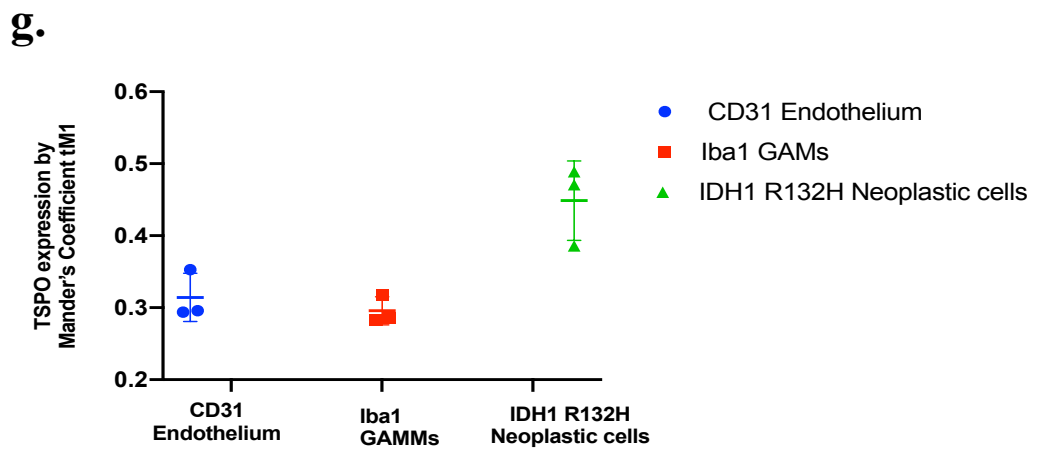
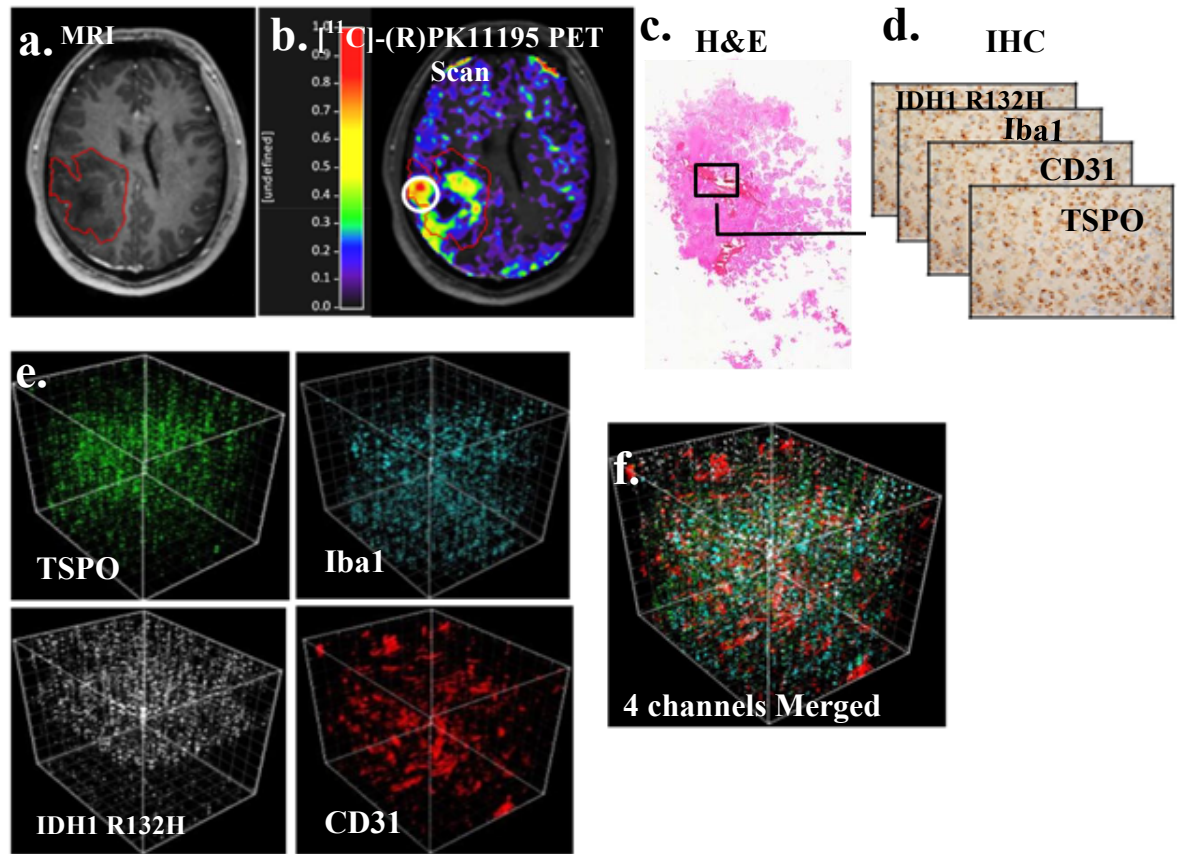


Figure 31: Quantification of TSPO expression from vascular endothelial cells, neoplastic and GAMMs in 3D constructed TMA of biopsies taken from high [¹¹C]-(R)PK11195 binding potential BPND.

a) Post-contrast axial T1 MRI scan delineated by red line. b) Coregistered fused PET and the region of biopsy defined by white circle PET scan. c) H&E for biopsied region. d) Immunoperoxidase (IHC) staining for TSPO, IDH1 R132H (tumour cells expressed mutant IDH1 protein), and Iba1 (GAMMs marker). e) 3D reconstruction image to present the TSPO signal contribution in neoplastic cells (IDH1 R132H-white), in GAMMs (Iba1-blue), in endothelium (CD31- red). f) Merged all four channels to calculate the colocalisation. g) dot-plot shows the TSPO expression level in the endothelium, GAMMs, and neoplastic cells in anaplastic gliomas cases. This result was done in collaboration with Erjon Agushi.

Table 6: Statistical analysis summary for the studied cases. Statistical Multiple ANOVA with Tukey's test for anaplastic oligodendrogliomas (AO).

| TUKEY'S MULTIPLE COMPARISONS TEST | MEAN DIFF. | 95.00% CI OF DIFF. | SIGNIFICANT? | SUMMARY | ADJUSTED P-VALUE |
|------------------------------------------------------|-----------------------|-------------------------------|---------------------|----------------|-----------------------------|
| CD31 VS IBA1 | 0.01867 | -0.07863 to 0.1160 | No | ns | 0.8311 |
| CD31 VS IDH1 | -0.1343 | -0.2316 to -0.03704 | Yes | * | 0.0129 |
| IBA1 VS IDH1 | -0.1530 | -0.2503 to -0.05570 | Yes | ** | 0.0070 |

3.4.3. TSPO can predict the overall survival of oligodendrogliomas patients but not the progression free.

The next question is if TSPO could predict the patient's survival and the progression-free time in oligodendrogliomas (n=50). Two groups of patients have been included, a group of low TSPO expression (n=32) and a group that showed high TSPO expression level in the examined FFPE tissues (n=18). Kaplan-Meier survival analysis showed that oligodendroglioma patients with high TSPO expression had significantly shorter overall survival than those with low TSPO expression (n=50, log-rank, p=0.001) (Table 7). Therefore, TSPO found to be a prognostic biomarker of overall survival but not progression-free survival. A significant difference has been found between low and high TSPO expression groups in overall survival analysis (Kaplan Meier) (Figure 32 a, b). In contrast, the difference between these two groups was non-significant to predict progression-free survival (Figure 33). Censored cases are patients who have not experienced the expected time to event of interest (death) during the follow-up time or lost their follow-up during the follow-up time.

3.4.4. TSPO polymorphism (rs6971) in oligodendrogliomas

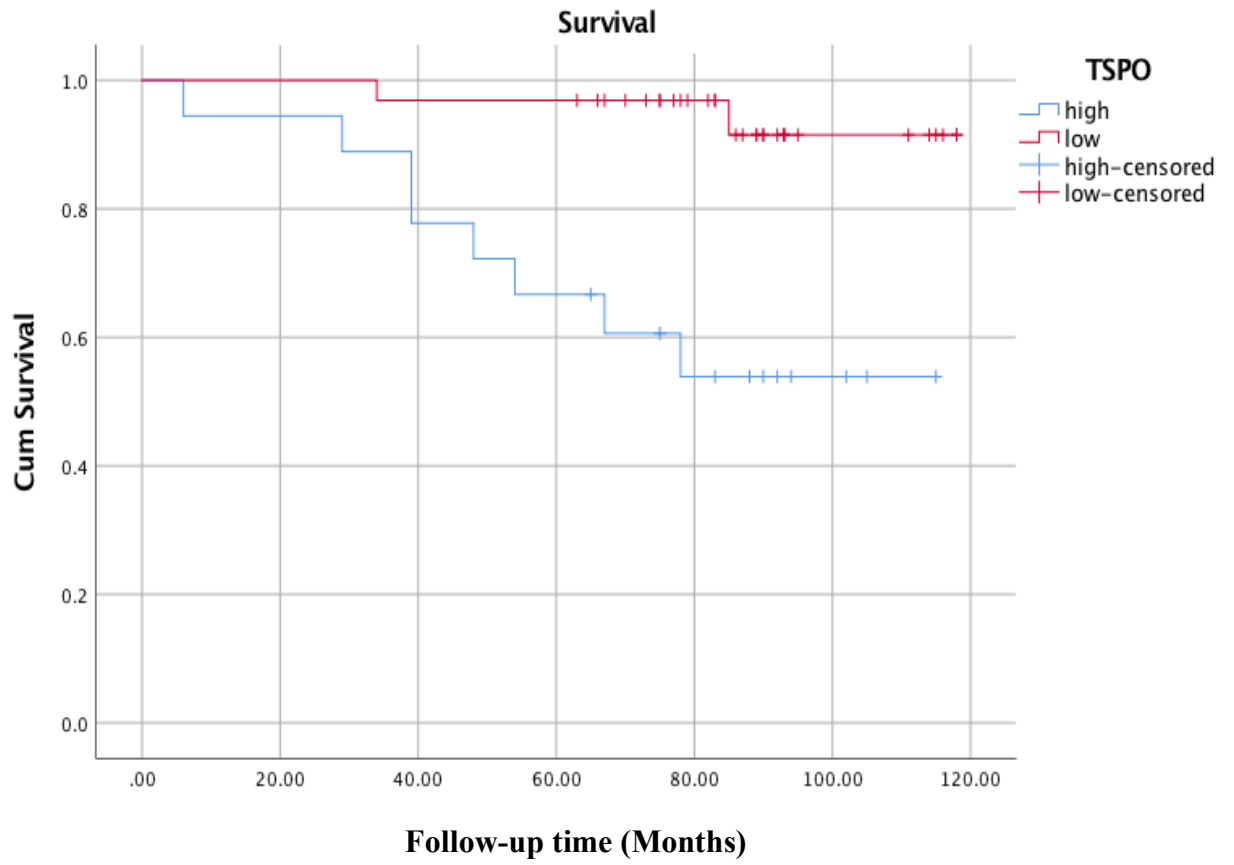
A common polymorphism SNP (rs6971) in TSPO leads to an amino-acid substitution (Ala147Thr) in the TSPO protein and further lead to binding affinity diversity [22].

In this study, the polymorphism rs6971 gene was examined for fifty DNA samples isolated from formalin-fixed paraffin-embedded tissues (FFPE) for oligodendroglioma cases. Twenty-eight (56%) of the studied patients harbour the polymorphism (rs6971), which encodes to threonine with low TSPO affinity binding. The remaining cases, twenty-two (44%), encodes to

alanine with high TSPO binding affinity. Further, no difference was found in the level of TSPO expression between the groups who harbour Ala147Thr polymorphism or native normal TSPO. TSPO Ala147Thr polymorphism did not affect the TSPO protein expression level in the studied fifty cases of oligodendrogliomas. Also, it did not show a prognostic value of patient overall survival between the two groups, (rs6971 [Ala147Thr] and Native [wild type]) TSPO protein (Figure 34). We tested if the TSPO polymorphism (A147T) could be predictive of overall survival between the two groups (A147T and normal). No significant difference between the two groups was estimated (n=50, log-rank, p-value 0.308) (Table 9).

I) Overall survival (OS):

A.



B.

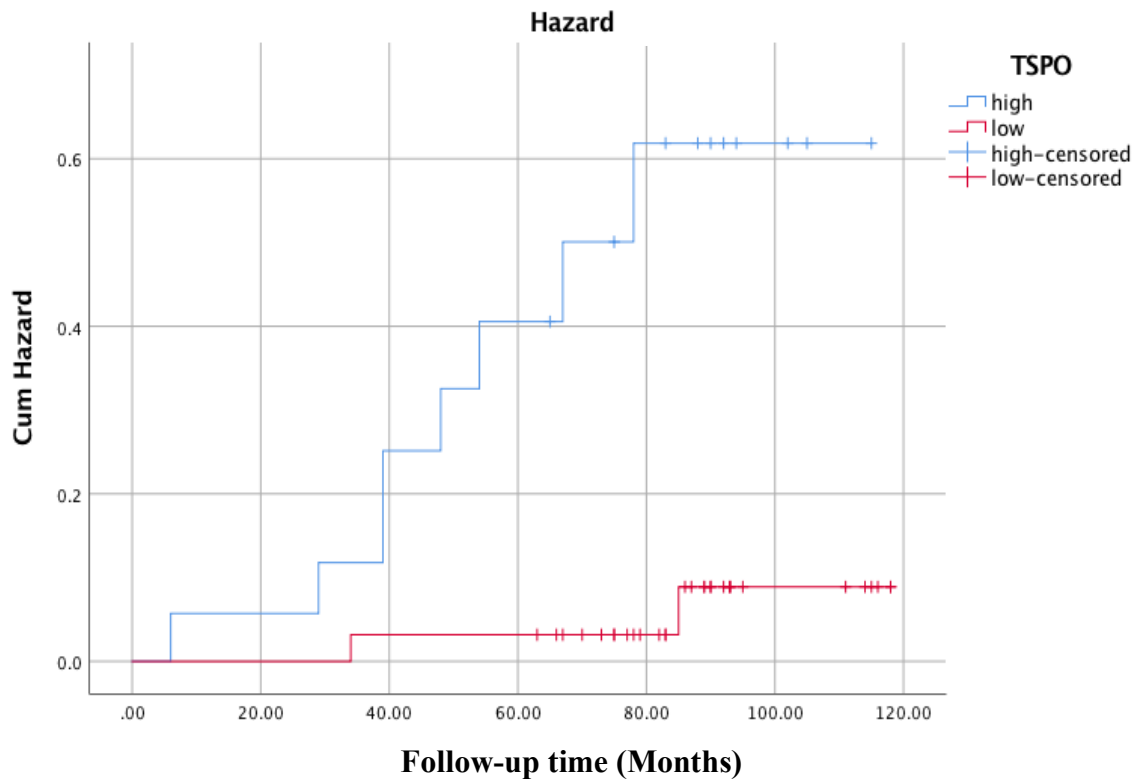


Figure 32: Kaplan-Meier survival analysis of overall survival in oligodendroglioma cases (n=50) with high and low TSPO expression level.

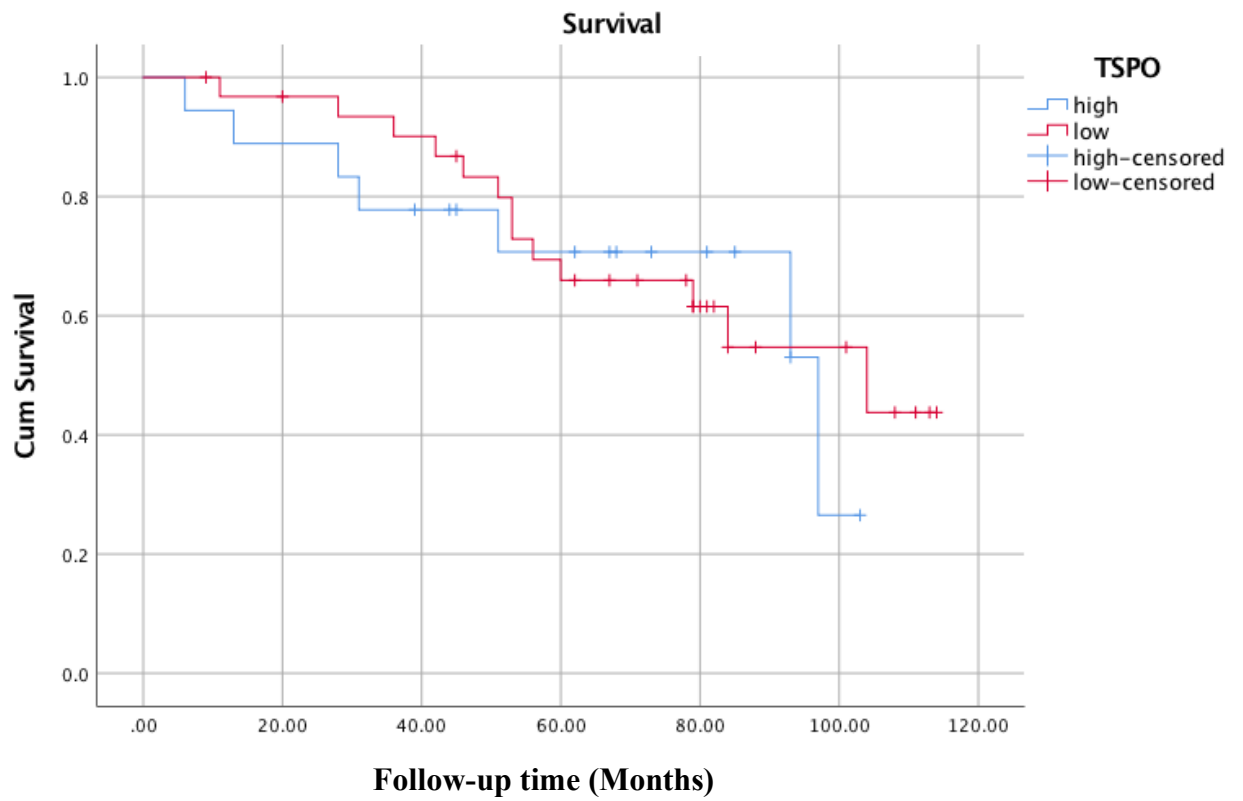
TSPO is a prognostic biomarker of survival. A) showed overall survival Kaplan Meier curve and B) showed Cum Hazard for both groups of high TSPO expression and low TSPO expression. Both showed a significant difference between low and high TSPO subgroups (p-value = 0.001). Both curves and statistical values have been created by IBM SPSS statistics version 25, 25.0.0.1 release.

Table 7: Chi-square and statistical analysis of Kaplan- Meier overall survival (OS): df is degree of freedom, sig. means significance. Chi-Square showed a significant difference between groups with high TSPO level and low TSPO level in overall survival suggesting TSPO to be a prognostic factor of survival.

| | Chi-Square | df | Sig. |
|--------------------------------|------------|----|------|
| Log Rank (Mantel-Cox) | 10.908 | 1 | .001 |
| Breslow (Generalized Wilcoxon) | 11.509 | 1 | .001 |
| Tarone-Ware | 11.367 | 1 | .001 |

II) Progression-free survival (PFS):

A.



B.

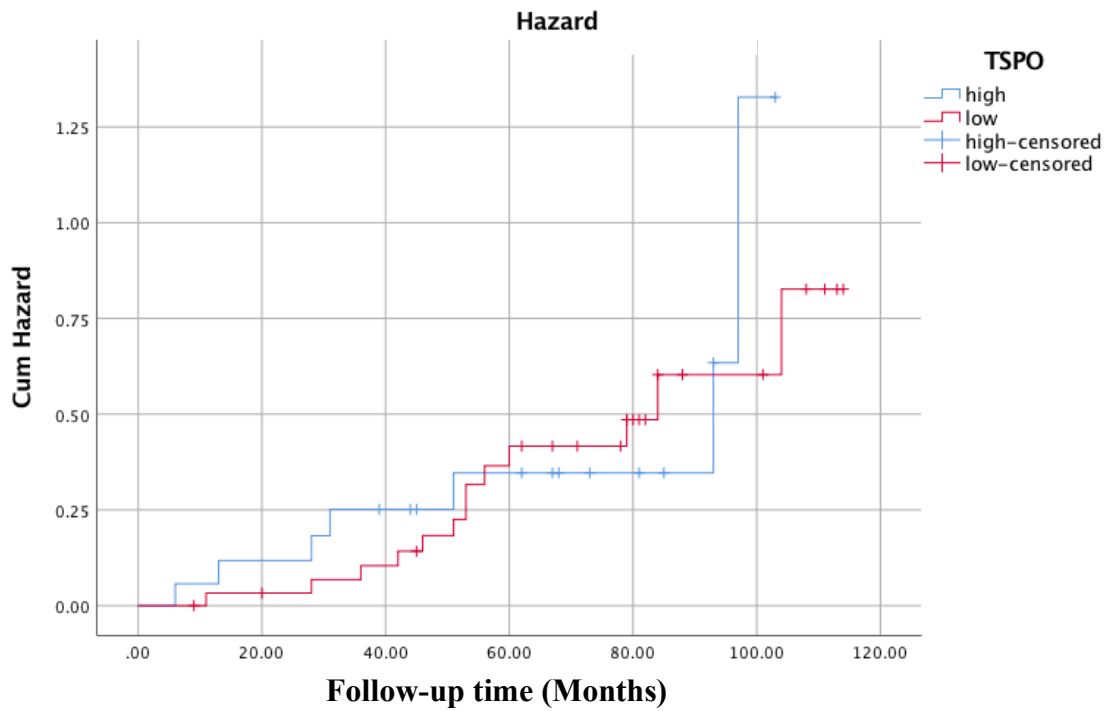


Figure 33: Kaplan-Meier survival analysis of progression-free in oligodendroglioma cases (n=50) with high and low TSPO expression level. A) showed overall survival Kaplan Meier curve and B) showed Cum Hazard for both groups of high TSPO expression and low TSPO expression. Non-significant difference between low and high TSPO subgroup (p-value=0.725). PFS has been created by IBM SPSS statistics version 25, 25.0.0.1 release.

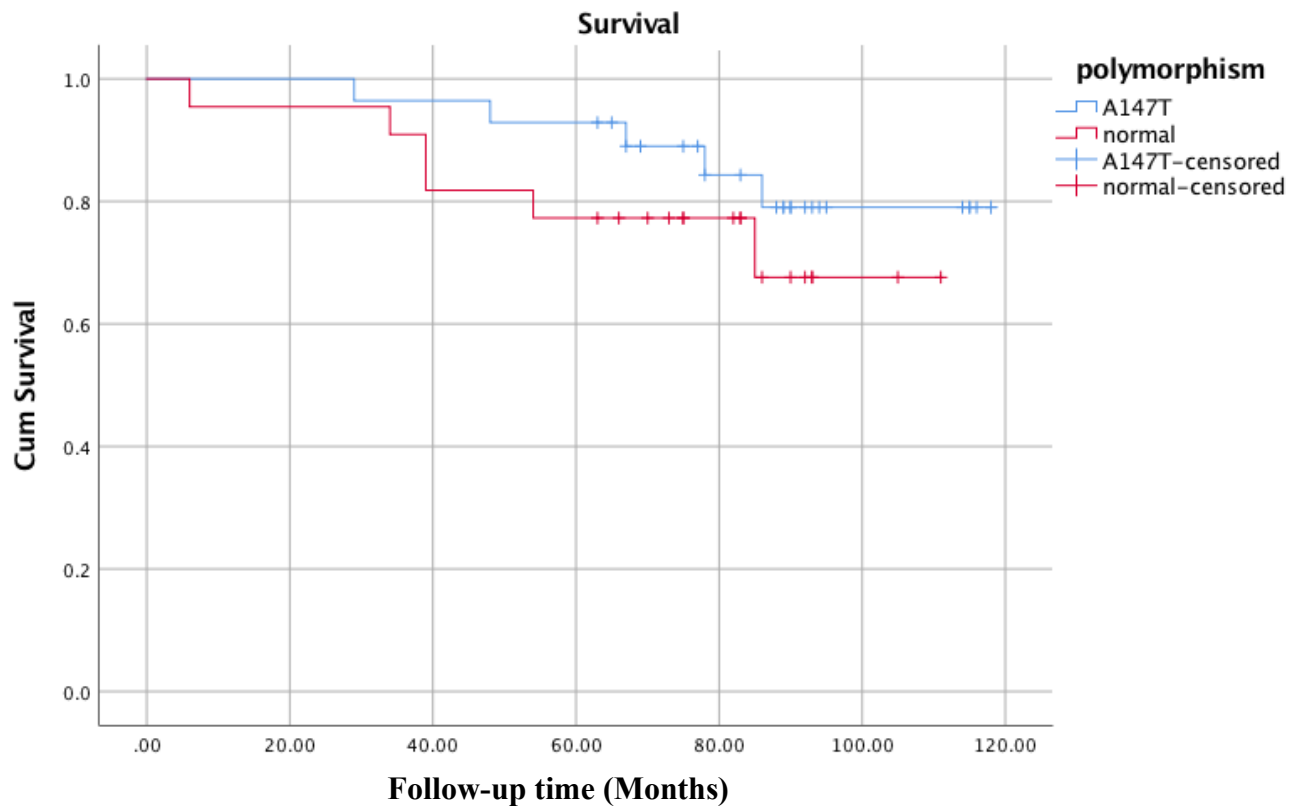
Table 8: Chi-square and statistical analysis of Kaplan- Meier Progression-Free survival analysis:

df is degree of freedom, sig. is significance. Chi-Square shows non-significant difference between groups with high TSPO level and low TSPO level.

| | Chi-Square | df | Sig. |
|--------------------------------|------------|----|------|
| Log Rank (Mantel-Cox) | .124 | 1 | .725 |
| Breslow (Generalized Wilcoxon) | .088 | 1 | .767 |
| Tarone-Ware | .067 | 1 | .796 |

III) TSPO polymorphism A147T and overall survival:

A.



B.

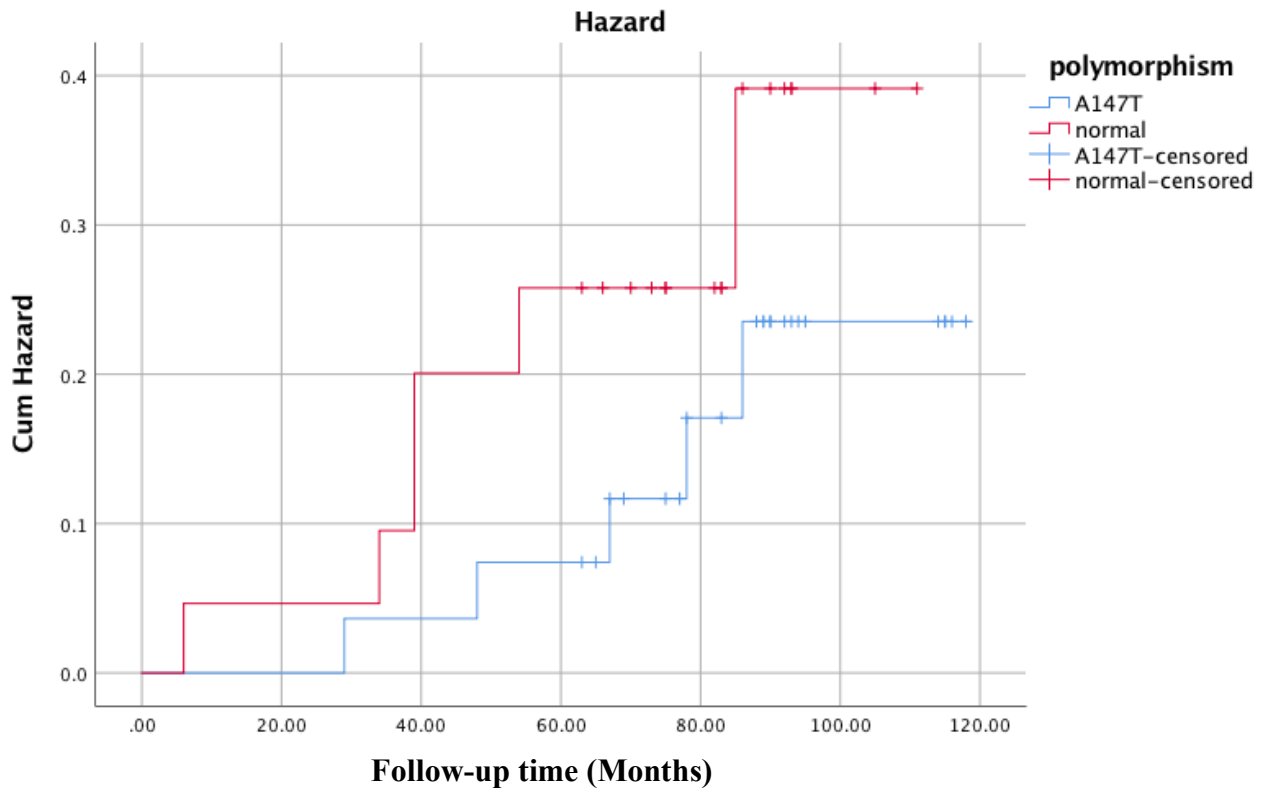


Figure 34: Kaplan-Meier overall survival in oligodendroglioma cases with A147T polymorphism (n=50). TSPO polymorphism is not a prognostic biomarker of survival. Non-Significant difference between A147T (mutated) and Normal groups (p-value 0.407). A) showed overall survival Kaplan Meier curve and B) showed Cum Hazard for both groups of TSPO (A147T) and TSPO (normal) OS curves and statistical values have been created by IBM SPSS statistics version 25, 25.0.0.1 release.

Table 9: Chi-square and statistical analysis of Kaplan- Meier overall-survival (OS) between group of A147T (mutated) TSPO and normal group: df is degree of freedom, sig. is significance. Chi-Square shows non-significant difference between groups with high TSPO level and low TSPO level.

| | Chi-Square | df | Sig. |
|--------------------------------|------------|----|------|
| Log Rank (Mantel-Cox) | 1.040 | 1 | .308 |
| Breslow (Generalized Wilcoxon) | 1.360 | 1 | .244 |
| Tarone-Ware | 1.214 | 1 | .271 |

3.5. Discussion:

IHC staining showed a significant increase in TSPO expression in anaplastic oligodendrogliomas compared with LGO. Consistent studies have shown an increase in astrocytomas' TSPO protein expression [2, 89, 94]. Moreover, a positive correlation between TSPO expression and tumour grades has been found in gliomas [94].

In a previous preliminary study, neoplastic tissues were a superior source of TSPO in gliomas than GAMMs and endothelial cells. TSPO expression in GAMMs, endothelial cells and neoplastic cells was assessed by double immunofluorescence [8]. In the current study, we performed a novel 3D construction of the double IHC sections for TSPO, CD31 (endothelium) and Iba1 (GAMMs). Our results supported the previous results, indicating that neoplastic cells are the predominant source of TSPO. In LGG (Figure 27-30), the increased signal observed with PET imaging was in the tumour margins, suggesting possible pro-inflammatory signals around the tumour margins. During the progression to a higher grade, the high TSPO expression may be mainly driven by neoplastic cells within the tumour.

A previous study indicated that, in gliomas, a large proportion of non-neoplastic tissues in the tumour microenvironment contain GAMMs [290, 359]. In astrocytomas, it was shown that GAMMs expressed TSPO in the tumour microenvironment [254]. Su et al. and Buck et al. considered partial contributions of GAMMs to TSPO expression in gliomas compared with neoplastic cells [8, 281]. No significant difference was seen with CD68+ (macrophage/microglial marker) between low-grade and high-grade gliomas. Winkeler et al. also suggested by immunofluorescence a minor contribution from the GAMMs compared with neoplastic cells and no astrocytes TSPO expression was seen within the tumour region [239]. Moreover, in vestibular schwannomas (extra-axial tumours) where no microglial cells

contribution was present, macrophage (Iba1 positive) showed to express high level of TSPO in growing tumours [311].

Microglia/macrophages may adopt one of two phenotypes during neuroinflammation, the pro-inflammatory (M1) or anti-inflammatory/neuroprotective (M2) phenotype. During the early development of glioma, microglia initiate a pro-inflammatory immune response to inhibit tumour growth. Glioma cells secrete different factors, leading to a switch from the pro-inflammatory phenotype of microglia/macrophages into an anti-inflammatory (pro-tumorigenic) phenotype that supports glioma growth and angiogenesis [307, 347-349]. In our results, we indicated a reduced level of TSPO in GAMMs compared with neoplastic cells in anaplastic oligodendrogliomas. This result may suggest a mechanism that reduces TSPO expression within these cells in response to anti-inflammatory signals; however, more studies need to be done to explore this possibility. The microglia and macrophage polarisation switch in the tumour microenvironment have become an interesting research field, but the role of TSPO in this process is not fully understood.

In previous studies, TSPO expression was increased in microglia in response to pro-inflammatory factors (e.g. TNF), while no change (no increase) in TSPO expression was noticed after anti-inflammatory stimulation by IL-4 [284, 285]. TSPO expression was found to be reduced during M2 polarisation. One possible mechanism for this is PPAR activation. A previous study found that over-expression of TSPO in microglia impaired the IL-4-induced M2-phenotype activation response via the PPAR pathway [286]. Moreover, TSPO is involved in creating a balance between the pro-inflammatory phenotype (M1) and anti-inflammatory phenotype/repair (M2) during neuroinflammation-associated disease in microglia. TSPO ligands can modulate its M1/M2 polarisation balance (PK11195, M2 promoting; or IFGIN-27,

M2 inhibiting). TSPO may be used as a therapeutic target to modulate GAMMs' polarisation [286].

GAMMs contribute to the immunosuppressive tumour microenvironment via secreting anti-inflammatory cytokines, such as IL-10 and TNF, with increased STAT3 signalling [300, 360-362]. The neoplastic cells contribute to recruiting GAMMs in the tumour microenvironment. The suspected role of infiltrating GAMMs in the glioma microenvironment was discussed in the introduction of chapter 1. Glioma cells secrete different factors that recruit microglia and macrophages to the glioma microenvironment, such as monocyte chemoattractant protein-1 (MCP-1 or CCL2), the growth factor glial cell-derived neurotrophic factor (GDNF) and hepatocyte growth factor [301]. Glioma-associated microglia and macrophages could also release factors that promote glioma growth and invasion into healthy tissue [299, 363, 364]. A recent study by Zinnhardt et al. showed that TSPO was restrictively expressed in activated GAMMs and tumour-infiltrating myeloid-derived suppressor cells (MDSC) [313]. MDSC are myeloid cells that have a role in suppressing the immune response in cancer. Therefore, TSPO could be used as a non-invasive target with PET imaging to selectively image the glioma-associated immunosuppressive tumour-associated microglia/macrophages [254, 313].

In the current study, TSPO might be increased in M1 pro-inflammatory GAMMs in low-grade glioma, which may be the source of TSPO expression signal in the margins. During this process, neoplastic cells are recruiting GAMMs to support their growth. During progression, the TSPO expression level is reduced within the recruited GAMMs. A suggested switch to M2 polarisation could be driven by signals coming from the tumour and its microenvironment to support tumour growth. In low grade, TSPO expression within a tumour

could represent a quiescent state with increased TSPO within the surrounding margin suggesting a state of neuroinflammation. TSPO expression in the tumour margins could indicate M1 polarisation phenotype within GAMMs. During tumour progression, the main TSPO signal was predominantly driven by neoplastic cells.

In addition, other studies have identified endothelial cells as another potent source of TSPO [5, 257, 262]. During glioma growth, hypoxia is one of the major causal factors for macrophage/microglial phenotype change. The increased level of growth during tumour progression leads to hypoxic regions with inadequate oxygen and nutrient supplies. Therefore, hypoxia-inducible factors may be released, leading to angiogenesis. In GBM, macrophage polarisation into the M2 phenotype correlates with the hypoxia level (HIF2 α), supporting tumour progression [365]. This observation suggests the importance of considering vascular endothelial cells' contribution to TSPO expression in the tumour microenvironment. In the current study, we found that the major source of TSPO was driven by neoplastic cells in anaplastic oligodendrogliomas.

Next, we asked whether TSPO could be a biomarker of a patient's outcome, a possibility that has been suggested previously in astrocytomas [366, 367]. Miettinen et al. investigated 86 human astrocytomas and showed a negative correlation between TSPO expression levels and patient outcomes. A similar result was shown by Vlodaysky et al. in 130 gliomas; they also negatively correlated with outcomes [94]. In this study, we found that TSPO served as a biomarker for the patient's overall survival, showing a negative correlation in which a worse outcome accompanies high TSPO expression. However, TSPO expression did not significantly differ in progression-free survival (PFS) between cases with high and low TSPO expression. It may require a longer extended follow-up time to observe a significant separation between the

two groups, especially with oligodendrogliomas. Oligodendrogliomas are known to be slow-growing tumours, and this tumour type is chemosensitive and responds well to treatment.

TSPO could counteract the oxidative stress induced by chemotherapeutics and ROS generation by inducing steroidogenesis [368]. A study indicated that TSPO ligands suppress oxidative stress and release pro-inflammatory cytokines via steroidogenesis and an up-regulated cholesterol mechanism [369]. Moreover, in response to pro-inflammatory stimuli, NADPH oxidase (NOX2) is activated, leading to oxidative stress and increased ROS generation. TSPO has a role in counteracting oxidative stress and the increased ROS level via interaction with NOX2, leading to the release and translocation of nuclear factor erythroid2 (Nfr2) to the nucleus ARE element, further inducing the anti-oxidative stress process [42, 140, 141].

Finally, we examined the TSPO polymorphism in fifty cases of oligodendrogliomas, and we found that 56% of the studied group (n=50) harboured the rs6971 polymorphism. The incidence of this polymorphism has not been previously studied in oligodendrogliomas. TSPO polymorphism leads to reduced affinity to second-generation ligands and further affects the accuracy of PET imaging interpretation. Moreover, it found that TSPO polymorphism Ala147Thr reduces TSPO cholesterol bindings and decreases steroidogenesis [370]. Furthermore, we did not find a difference between the two groups (Ala147Thr and native [WT] TSPO) effect on tissues' TSPO protein expression level. Although a study suggested that the TSPO polymorphism affected protein stability, we did not find a significant difference between the two groups [23]. TSPO polymorphism might affect the affinity of ligand binding to the TSPO structure instead of inducing protein degradation. Additionally, the high percentage of

the Ala147Thr polymorphism among the studied oligodendrogliomas patients was not found as a risk factor for worse survival.

3.6. Conclusion:

Examining TSPO expression using the IHC approach showed a significant difference between low- and high-grade oligodendrogliomas, suggesting that TSPO is a reliable biomarker for tumour progression. TSPO expression was predominantly driven by neoplastic cells within the tumour microenvironment compared with GAMMs and endothelial cells. High TSPO expression was prognostic of shorter overall patient survival in a cohort of fifty patients with oligodendrogliomas.

CHAPTER 4

TSPO EXPRESSION REGULATION IN BRAIN TUMOURS

CHAPTER 4

4.1. Hypotheses:

Although a few studies have previously investigated TSPO expression regulation in breast cancer and Leydig cells, TSPO expression regulation is still not fully understood. In this chapter, two different suggested regulatory mechanisms are introduced, including epigenetic regulation (methylation of the TSPO promoter at CpG islands) and regulatory factors. The two following hypotheses that were tested in the current chapter:

Hypothesis 1: TSPO expression is epigenetically regulated by promoter methylation.

To study the first hypothesis, we isolated DNA from 50 FFPE brain tissues for patients diagnosed with oligodendrogliomas. Further, methylation array sequencing was performed to check the CpG island methylation status level.

Hypothesis 2: Different upstream regulatory genes could regulate TSPO expression in oligodendrogliomas and astrocytomas.

A hundred cases of oligodendroglioma and a hundred cases of astrocytoma were extracted from The Cancer Genome Atlas (TCGA; <https://portal.gdc.cancer.gov>) database [371]. The entire genome transcriptome was extracted per patient for both oligodendrogliomas and astrocytomas. The correlation coefficient for each gene with the TSPO transcriptome level was calculated. Next, the enriched pathway upstream of TSPO was identified for the selected genes using the IPA knowledge base. In parallel with the TCGA database, RNA sequencing data

analysis was done for eighteen cases diagnosed with oligodendroglioma. The RNA was isolated from frozen brain tumour tissues for eighteen cases of oligodendrogliomas.

4.2. Study rationale and background:

TSPO expressed at a low level in the normal brain, while its expression increased in many diseases, including gliomas. TSPO expression was shown to increase in different cancers, including gliomas [2, 89-92, 94, 142]. TSPO expression regulation is still not well understood. In microglia, Rashid et al. suggested that the Ap1, Ets, and Sp binding site elements in the TSPO promoter region are strongly positive and essential elements for regulating TSPO expression [142]. Pu.1, Ap1, Stat3, Sp1, Sp3 and Sp4 are important factors that bind to endogenous TSPO promoter region in murine BV-2 microglia and human ARPE-19 cells epithelial cells. Further, understanding if similar factors may regulate TSPO expression in gliomas was an important aim in this chapter.

In MA-10 mouse Leydig cells and NIH/3T3 mouse embryo fibroblasts, Batarseh et al. concluded that the V-Ets erythroblastosis virus E26 oncogene homolog (Ets1, Ets2), and AP-1 are essential positive regulatory elements in the TSPO promoter [143]. Sp1, Sp3 and GA-binding protein transcription factor (GABP) are suggested to have an essential role in TSPO expression regulation. PKC is involved in enhancing TSPO expression in steroidogenic and non-steroidogenic cells [144]. It has been suggested to work upstream of c-Jun, c-Fos (AP1 family) and GABP (Ets family), leading to TSPO mRNA and protein expression increase in NIH-3T3 fibroblast cells [144]. PKC induces TSPO expression through the MAPK signal transduction pathway (Raf1-MEK1/2-ERK1/2), c-Jun and Stat3 in both TSPO-rich

steroidogenic cells (MA-10 Leydig) and TSPO-poor non-steroidogenic cells (NIH 3T3 fibroblasts) [143].

The second TSPO mechanism suggested in the literature is epigenetic regulation of TSPO expression through methylation. The term *epigenetics* relates to the heritable alteration of the genes' expression pattern without any changes in the gene sequence [146, 147]. This type of alteration includes methylation of the gene promoter region at CpG islands and further silenced gene transcription. During the DNA methylation process, a methyl group is transferred from S-adenosyl-methionine by enzyme DNA methyltransferases (DNMTs) to the cytosine's fifth cytosine base pyrimidine ring of a CpG dinucleotide that precedes the guanosine base at CpG island [148]. Many studies in different cancer types have indicated that this epigenetic CpG methylation causes gene expression silencing. For instance, the expression of DNA repair genes, such as O6-alkylguanine DNA alkyltransferase (O6-MGMT), breast cancer susceptibility gene (BRCA1) and MutL homolog (MLH1), can also be silenced by CpG island hypermethylation [152-154]. Many studies indicated that in brain tumours, promoter hypermethylation is a possible regulatory mechanism of many genes involved in tumorigenesis and tumour progression [152, 167, 170-177, 372].

4.3. Material and methods:

4.3.1. RNA isolation from frozen brain tissues of oligodendrogliomas cases:

RNA isolation from frozen tissue (n=18). The used kit was RNeasy Mini Kit (50), Qiagen, 74104. 10µl of beta-mercaptoethanol or BME was added per 1ml of the RLT. The frozen tissue was carefully placed in the pre-labelled tube (RNase free) and 600 µl of RLT was added to the frozen tissue (based on how big is the tissue sample). Next, the tissue was homogenised by Pestle Motor Mixer (Argos Technologies, UK) for 10-15 min. Later, the tube was applied to centrifugation at maximum speed for 3 min. 350 µl of 70% ethanol was added to the homogenised tissues. 700 µl of the mixture was transferred into the RNeasy Mini spin column placed in a clean 2ml collection tube. Later, the column was centrifuged for 15 seconds at 9000 rpm, and the flow-through was discarded. 700 µl of RW1 to the column and allowed later for centrifugation for 15 seconds at 9000 rpm. Next, 500 µl of RPE to the column and allowed for centrifugation for 15 seconds at 9000 rpm. The flow-through was discarded. 500 µl RPE was added again, and the column was centrifuged for 2 minutes at 9000 rpm. The column next was placed in a new clean collection tube and allowed for centrifugation at full speed for 1 minute. The column was transferred to a pre-labelled Eppendorf tube 1.5ml, and 30 µl was added to the spin membrane carefully. Finally, the tube was centrifuged for 1 minute at 9000 rpm to elute the RNA. RNA concentration measurement was done by nanodrop Thermo scientific 1000 spectrophotometer.

4.3.2. RNA sequencing: Illumina Truseq RNA libraries:

Total RNA was sent to the University of Manchester Genomic Technologies Core Facility (GTFCF). The RNA concentration and integrity were measured by 2200 TapeStation (Agilent Technologies). The starting RNA input is (0.1-4µg). Polyadenylated containing mRNA molecules were purified by using poly-T attached magnetic beads within two round of purification. Poly A purification step used to elute the only mRNA that is distinguished from the other different RNA types (ribosomal and translational RNA) by its poly-A tail. Next, the attached eluted mRNA was fragmented by divalent cations. Then, the first strand of cDNA was formed by a reverse transcriptase reaction. The second strand of cDNA will be formed by incorporating dUTP instead of dTTP during amplification to quench the template RNA and form blunt cDNA by the end. In this step, two enzymes were used, DNA polymerase for amplification and RNase to degrade the RNA template. Next, a single adenosine (A) nucleotide (A tailing mix) was added at both 3' end of the blunt cDNA before the adaptor ligation step to supply an overhang for ligating the adaptor to this fragment. Later, multiple indexing adapters were added to the ends of ds cDNA by two consecutive steps 3' ligation and 5' ligation to both ends of the cDNA. Next, these DNA fragments ligated to the adaptors were enriched by PCR amplification process around 15 cycles. Each previously ligated adaptors are constructed to be complementary to oligos on the used flow cell library. The flow cell is a thick glass slide with lanes coated with different oligonucleotides that are made to be complementary to the ligated adaptor. Cluster generation on the flow cell occurs by using a cBot instrument to generate multiplex libraries that are covalently attached to the flow cell, including the cDNA insert with the adaptors. Adaptor sequence hybridises on the flow cell-attached oligos and extended by polymerase. The resulted double-strand DNA denatured and the original template strand

washed out to leave only the newly synthesised strand attached covalently to the flow cell. This copy was amplified through a process called bridge amplification. Double strand bridges were denatured and the reversible strand cleaved and washed away, leaving only the forward strand. This strand 3' end was blocked by (dideoxynucleotide) to prevent any other adaptors annealing to the neighbour oligos. Then, the sequencing was started by using specific primers annealed to the adaptor sequence. Paired-end sequencing (76+ 76 cycles including indexes) by using HiSeq4000 instrument. The incorporated fluorescent tagged nucleotide was followed by images detected for the signal and later cleaved before the next cycle.

4.3.3. RNAseq data analysis:

The sequencing analysis has been taken by the Bioinformatics Core Facility (BCF), University of Manchester and analysed with the help and supervision of Dr. Rachel Scholey. DESeq2 Differential gene expression analysis has been used to generate the internal normalisation for each gene across all samples. Mean count, p-value, log₂ expression value, padj or false discovery rate were calculated for each gene across all samples has been calculated. Next, QIAGEN Ingenuity Pathway Analysis (IPA) has been used to identify upstream regulators of TSPO and clustered enriched pathways.

Illumina TruSeq Stranded mRNA, sequenced paired-end 76 bp on Illumina HISEQ4000 was used for RNA sequencing. The RNA-seq reads were quality assessed using FastQC (v 0.11.3), FastQ Screen (v 0.9.2). The sequencing was quality trimmed using Trimmomatic (v 0.36) (<http://www.bioinformatics.babraham.ac.uk/projects/fastqc/>). Sequence adapters were removed, and reads were quality trimmed using Trimmomatic_0.36 [373]. The RNA-seq reads were mapped against the reference human genome **Genome Reference Consortium Human**

Build 38 (GRCh38/hg38) using Spliced Transcripts Alignment to Reference (STAR) (version 2.5.3a) [374]. Then, counts per gene were calculated by STAR using annotation from GENCODE 31 (<http://www.gencodegenes.org/>) [374]. The normalisation, Principal Components Analysis, and differential expression were calculated with DESeq2_1.20.0 [375]. The estimation of fold change and dispersion for RNA-seq data were assessed with DESeq2 [375].

4.3.4. TSPO promoter methylation analysis:

4.3.4.1. Patient selection:

Thirty-eight patients diagnosed with oligodendroglioma were selected from Salford Royal Hospital, Salford, UK and Christie Hospital, Manchester, UK. All patients harbour IDH1 mutant and 1p/19q co-deletion. Tumours were graded according to the WHO into either LGO (WHO II) or AO (WHO III). Formalin-fixed Paraffin-embedded tissues samples (FFPE) for thirty-eight cases were sectioned and stained at Salford Royal Hospital.

4.3.4.2. DNA isolation for methylation analysis:

For DNA isolation from the FFPE tissues, QIAamp DNA FFPE tissue kit (Qiagen, Hilden, Germany) was used. The paraffin was removed from FFPE slides for 50 cases by using Xylene solvent. Each slide was soaked for 5 minutes in Xylene. Further, each slide was carefully transferred to 100% ethanol and soaked for another 5 minutes. Later, the slides were allowed to dry at room temperature for 10 to 15 minutes. Slides macro-dissection was done accompanied by H&E stained corresponding slides for each case. The tissues scraped away from the slide by

using sterile scalpels. Next step is to lyse the cells by adding 180 μ l ALT buffer and 20 μ l K proteinase from QIAamp DNA FFPE tissue kit (Qiagen, Hilden, Germany) in clean RNAase free screw cap tubes (STAR LAB, Hamburg, Germany). Each sample was exposed to the heating process at 56°C for 2 hours until the cells completely lysed and later at 90°C for 1 hour to reduce the formaldehyde modification of nucleic acids. 200 μ l of AL buffer and 200 μ l 100% ethanol were added in two separated steps with vigorous vortexing after each addition. The whole lysate later transferred to pre-labelled QIAamp minelute column (Qiagen, Hilden, Germany) and centrifuged at 6000 xg (8000 rpm) for 1 minute. The flow-through was discarded, and 500 μ l of AW1 washing buffer (100% ethanol pre-added) was added to each QIAamp minelute column. Each column was allowed to centrifuge at 6000 xg (8000 rpm) for 1 minute, and the collection tube containing the flow-through was discarded. 500 μ l of AW2 buffer was added to each QIAamp minelute column and allowed for centrifugation at 6000 xg (8000 rpm) for 1 minute. The collection tube containing the flow-through was discarded and replaced with a new one. To completely dry the membrane, each QIAamp minelute column was allowed for centrifugation at full speed for 3 minutes. The QIAamp minelute column was placed in sterile pre-labelled 1.5 ml microcentrifuge tubes. 50 μ l of ATE elution buffer was added into the center of the membrane of the QIAamp minelute column and incubated at room temperature for 5 minutes. Finally, each tube was allowed for centrifugation at full speed for 1 minute. The yield DNA sample was stored at – 20 °C until needed. The DNA concentration was measured thermoscientific Nanodrop 1000 spectrophotometer (DNA input 800 ng).

4.3.4.3. Infinium methylation EPIC beadChip/Infinium human methylation 450 bead chip:

This experiment was conducted at St. Mary's Hospital, Department of Genomic Medicine in collaboration with Dr James O'Sullivan.

Infinium human methylation 450 bead chip (HM450) has been first validated by Juan et al. in colorectal cancer and confirmed its reliability in DNA methylation analysis [376]. It has also been used in studying the G-CIMP status in GBM [377]. Infinium methylation EPIC bead chip showed improvement coverage over the HM450 including coverage of 850,000 CpG sites (>90 % of the CpGs that covered by HM450) and regulatory regions (enhancers) that were not covered by HM450. In this study, the Infinium methylation EPIC beadChip has been used.

It is a multi-step automated protocol for methylation array including, DNA quantification, Bisulfite conversion, amplification of bisulfite converted DNA (BCD), fragmentation of DNA, DNA precipitation, hybridisation to bead chip, extension, and image bead chip. All these previous steps are summarised in the flow chart below (Figure 35).

First, Illumina Infinium HD FFPE QC assay (Illumina, San Diego, CA, WG-901-2004) was applied based on the Illumina protocol instructions, for the DNA isolated from FFPE to restore DNA that might be degraded due to formalin fixation process [378]. **Pre restore (PRS) plate** first will be used and 4-8 µl of DNA will be transferred to the plate. 4µl of 0.1N NaOH, 34 µl Primer Pre Restore reagent (PPR) reagent, and 38 µl AMR reagent were added respectively to each well in the plate. The plate was sealed by cap mat to invert for mixing ten times and later centrifuged at 280 xg for 1 min. The plate was incubated at 37°C on a heat plate for one hour and later centrifuged at 280 xg for 1 min. New **Zymo-spin I-96 plate** (binding plate) placed on a collection plate was used for DNA binding step. 560 µl of the specific Zymo binding buffer

was added to the previous PRS DNA containing plate, and the mixture was mixed by pipetting to transfer it to the new Zymo-spin I-96 plate for DNA binding process. The Zymo-spin I-96 plate was centrifuged at 2250xg for 2 min, and the flow through to collection tube was discarded. 600µl (Zymo washing buffer with ethanol) was added to each well, and further was centrifuged at 2250xg for 2 min and the flow through to collection tube was discarded. New plate called **RST plate** (elution plate) next was used for the elution step. The Zymo-spin I-96 plate was placed on the RST plate and 13 µl of ERB buffer was added to the column matrix in each well. Later, it was centrifuged at 2250xg for 1 min to elute the DNA. The RST plate was sealed with foil adhesive seal to incubate it at 95 °C for 2 min on the heat block and later immediately was transferred on ice for 5 min. 10 µl of Convert Master Mix (CMM) reagent was added to each well and later was mixed by vortexing at 1600rpm for 1 min. After centrifugation for 1 min at 280xg, the plate was incubated at 37 °C for 1h and further allowed for another centrifugation at 280xg for 1 min.

New Zymo-spin I-96 plate was used for the DNA binding step. 140 µl of Zymo DNA binding buffer (7 volumes of the DNA) was added to each well of the **RST plate** that contains the eluted DNA from the previous step and later the mixtures were mixed by pipetting to transfer it to the Zymo-spin I-96 plate. The Zymo plate was centrifuged at 2250xg for 2 min, and the flow-through was discarded. Later, the Zymo plate was transferred to a new **MSA5 plate** for the DNA elution step. 10µl of dH₂O was added directly to the column matrix and incubated at room temperature for 5 min. Finally, the Plate was centrifuged at 2250xg for 1 min to elute the final restored DNA to be used for the DNA methylation analysis.

Step 2, Zymo Ez DNA methylation kit was used (cat, D5001) with DNA input 1000 ng gDNA.

This kit has been used due to its high efficiency in the bisulfite conversion of non-methylated cytosine that reached 99% efficiency, more compatible for Infinium methylation array, it designed to have a reduced possibilities of template degradation and DNA loss by using specific column. It is mainly composed of three main steps including, DNA denaturation, bisulfite conversion, and elution. DNA First day step included DNA denaturation step and bisulfite conversion. Bisulfite conversion sequencing is currently still the gold standard to test the methylation status of CpG sites [379].

Bisulfite-converted DNA (BCD) plate was prepared where cytosine and 5-methylcytosine to deamination by bisulfite and under acidic solution unmethylated cytosine only will be converted to uracil and further to T after extension. While on the other hand, methylated cytosine will remain by the end as cytosine and after extension C. First, in day 1, the instructions in the Zymo EZ DNA Methylation Kit to denature the genomic DNA because the conversion will work on single DNA strand. Following the denaturation, the bisulfite conversion was done. The thermal cycler was adjusted for 95°C for 30 min and 50°C for 1h for 16 cycles, hold step at 4 °C for 10 min. Binding and washing step was followed on Zymo-spin column or filter plate by using M washing buffer to be added to each sample followed by centrifugation at full speed for 30 seconds. Further, the plate washed by M washing buffer followed with centrifugation step at full speed for 30 seconds. Desulfonation buffer was later added to the column/plate and incubated for 15 min at room temperature followed by washing step and centrifugation as it was illustrated in the previous step. M-elution buffer was used to elute the converted DNA

followed by centrifugation at full speed for 5 min. The bisulfite converted DNA was transferred to a **BCD labelled plate** for the next amplification step.

On day 2, the amplification process contains four different reagents in order to prepare (**MSA4 plate**) including, MA1 (Multi-Sample Amplification Mix1), 0.1NaoH (to denature DNA), RPM (random primer mix), and MSM (Multi-Sample Amplification Master Mix) master mix respectively. DNA was transferred from the BCD plate to MSA4 plate and then was incubated at 37 °C for hybridisation for 20-24h in the hybridisation oven.

Next step in day 3 was fragmentation, FMS (Fragmentation solution reagent) was used, and fragmentation was held at 37 °C for 1h. Next, precipitation was held by using PM1 (Precipitation solution reagent) and 2-propanol 100% followed by vortexing at 1600rpm, incubation at 37 °C for 5 min and centrifugation at 280xg. The MSA4 plate was placed back to the machine for another incubation at 4°C for 30 min. The supernatant was decanted and the plate inverted on the adsorbent pad to dry for one h at room temperature. Later, RA1 reagent (Resuspension, hybridization, and wash Solution) used for resuspension followed by incubation at 48 °C for 1h, vortexing at 1800 rpm for 1 min, and centrifugation at 280xg, respectively. The MSA7 plate was placed on the heat block at 95 °C for 20 minutes to denature the DNA followed by centrifugation at 280xg. For the hybridization step, Hyb chamber was filled with PB2 reagent (Reagent used to prepare BeadChips for hybridization buffer) and later the lid was closed. The DNA was loaded on bead chips and further placed in the Hyb chamber for hybridisation in illumine hybridisation oven for 24 h, at 48°C overnight.

On day 4, the bead chips were washed with PB1 washing buffer in multi-sample bead chip alignment fixture to wash away unhybridised DNA and excess reagents. For Beadchip extend and stain step, the following reagents were used, RA1 (to wash way the unhybridised DNA),

XC1 (XStain BeadChip solution 1), XC2 (extension reaction reagents), TEM (Two-Color Extension Master Mix, single-base extension of primers and labelled nucleotide to be incorporated into the extended primers), 95% Formamide / 1mM EDTA (neutralisation), PB1 (washing), XC4 (coating). Total estimated time for this step is 2h and 10 min with 55 min drying. Finally, after the run was completed, bead chips imaged by using illumina system beads based on high-resolution laser images for two channels (red and green). The iscan software determines the value for each signal and creates data files (.bpm) [438].

Infinium HD Methylation Assay, Manual Protocol

Experienced User Card

For Research Use Only. Not for use in diagnostic procedures.

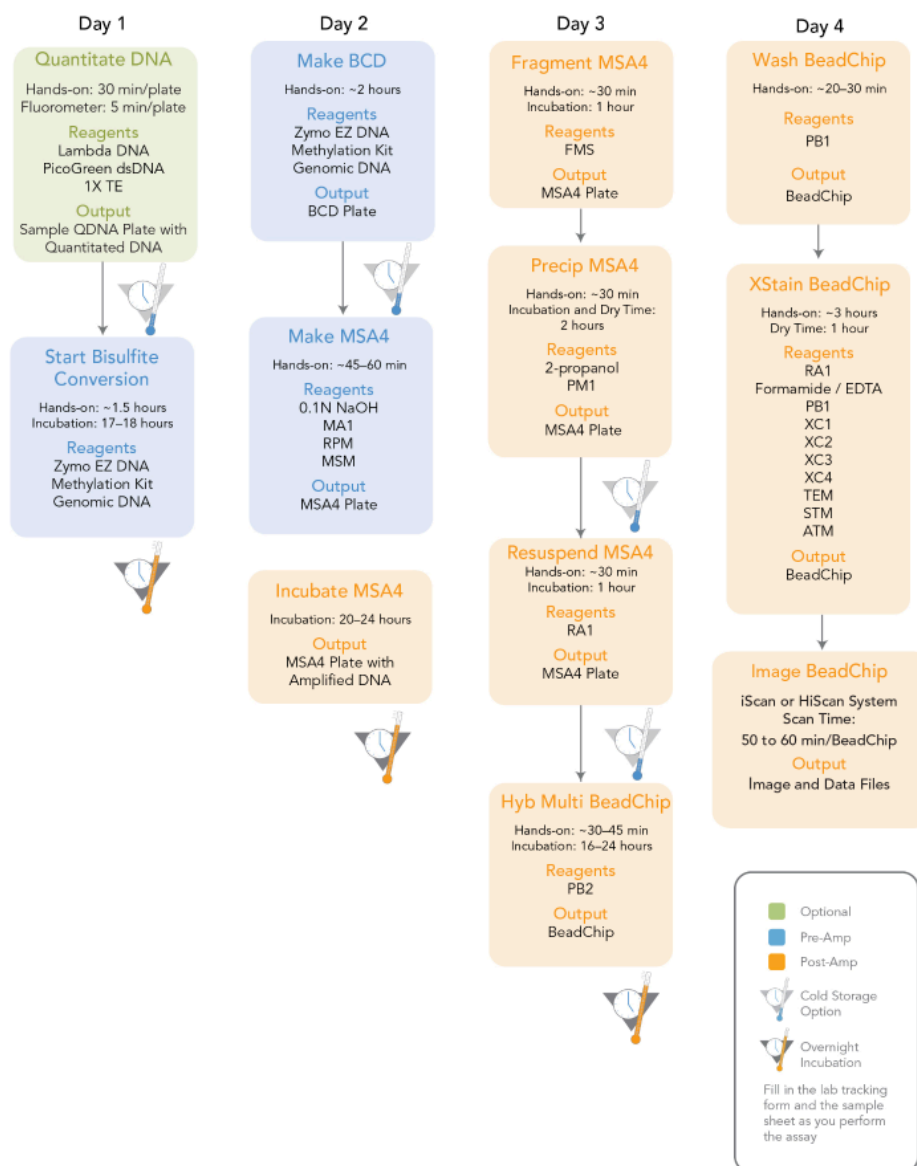


Figure 35: Infinium HD methylation protocol workflow [438]

The workflow represents the main steps identified by days (4 days steps). First day, the bisulfite conversion of the previously pre-restored DNA. Second day includes defulfonation, and DNA amplification. Third day includes DNA hybridization on beadchip in Hyb chamber. Fourth day includes washing unhybridised DNA, single base labelled extension (different Xstain reagents), washing, drying and imaging.

4.3.4.4. Methylation array analysis:

Methylation analysis was conducted in collaboration with the Bioinformatics Core Facility (BCF), University of Manchester, by Dr. Donaldson. Cross-package Bioconductor workflow package was used for analysing methylation array. Version 3. F1000Res. 2016 Jun 8 [380]. <https://www.bioconductor.org/packages/release/workflows/html/methylationArrayAnalysis.html>.

4.3.5. In-silico candidate genes expression analysis from The Cancer Genome

Atlas Programme database:

The Cancer Genome Atlas (TCGA) is a publicly available database project which provide comprehensive genomic profiles for cancer causing genomic alteration and transcriptomic expression changes. TCGA is based on cooperative comprehensive project for research developing that involves different cooperating centers for sample collection (tissue source site [TSSs]), samples processing, RNA isolation and DNA isolation (Biospecimen Core Resources [BCR]), high-throughput sequencing (Genome Sequencing Centers [GSCs]). The available provided data types and platforms are including, RNA sequencing (RNAseq), MicroRNA sequencing (miRNAseq), DNA sequencing (DNAseq), SNP-based platforms, and DNA methylation sequencing [371]. A hundred cases of oligodendrogliomas and a hundred cases of astrocytomas were randomly selected from The Cancer Genome Atlas database. The TSPO transcriptome level (FPKM file) was extracted for each patient one by one, and further 25th percentile and 75th percentile was calculated for oligodendroglioma (25th 6.734 n=25, 75th 21.145, n=24) and Astrocytoma (25th 19.132 n=23 and 75th 41.533 n=26). Below 25th percentile

was considered to be the cases that exhibited low TSPO level and above 75th percentile was considered to represent the cases with high TSPO level (Figure 39).

Further, the transcriptome expression level of the entire genome was extracted for each case. The mRNA level (transcriptome FPKM) that strongly correlated with TSPO was calculated (Correlation coefficient > 0.6).

Later, the selected genes candidates that strongly correlated with TSPO expression were uploaded into the QIAGEN Ingenuity Pathway Analysis (IPA) software. Further, the common upstream pathway of TSPO were selected by using analyse tool. Next, the upstream regulators of TSPO were selected among the candidate genes by IPA. IPA knowledge base overlaid the uploaded genes (either from TCGA or RNA sequencing) based on the previously known enriched pathways and interactions in the specified field. In this study, the field of interest was filtered to both cancer and central nervous system (CNS) field. Moreover, the same candidates were overlaid on the IPA knowledge base in cancer field only. Then, comparison have been made between the two-different analysis.

4.4. Results:

4.4.1. RNA sequencing (RNA-seq) data selection:

RNA was extracted from eighteen samples of frozen brain tumour tissues for oligodendrogliomas cases (n=18) and analysed by RNA sequencing. 25th Percentile (226.2796) and 75th percentile (568.1188) have been identified. Normalised mRNA counts below 25th percentile (226.2796) (n=5 samples) and above 75th percentile (568.1188) (n=5 samples) were used to represent cases with low TSPO and high TSPO mRNA levels, respectively (Figure 36). Furthermore, the candidate genes list in high versus low TSPO transcriptome expression profiles were compared. The identified genes were aligned to the IPA database to show their corresponding interactive pathways, which may be involved in TSPO expression regulation. The IPA knowledge base was filtered by selecting the field of interest 'in cancer' and 'CNS'. Moreover, the same candidates were overlaid by the IPA knowledge base in the cancer field only. Then, the two obtained profiles in low versus high TSPO transcriptome level was compared.

| | |
|-----------------------------|------------|
| 25 th Percentile | 226.2796 |
| median | 376.323315 |
| 75 th percentile | 568.118898 |

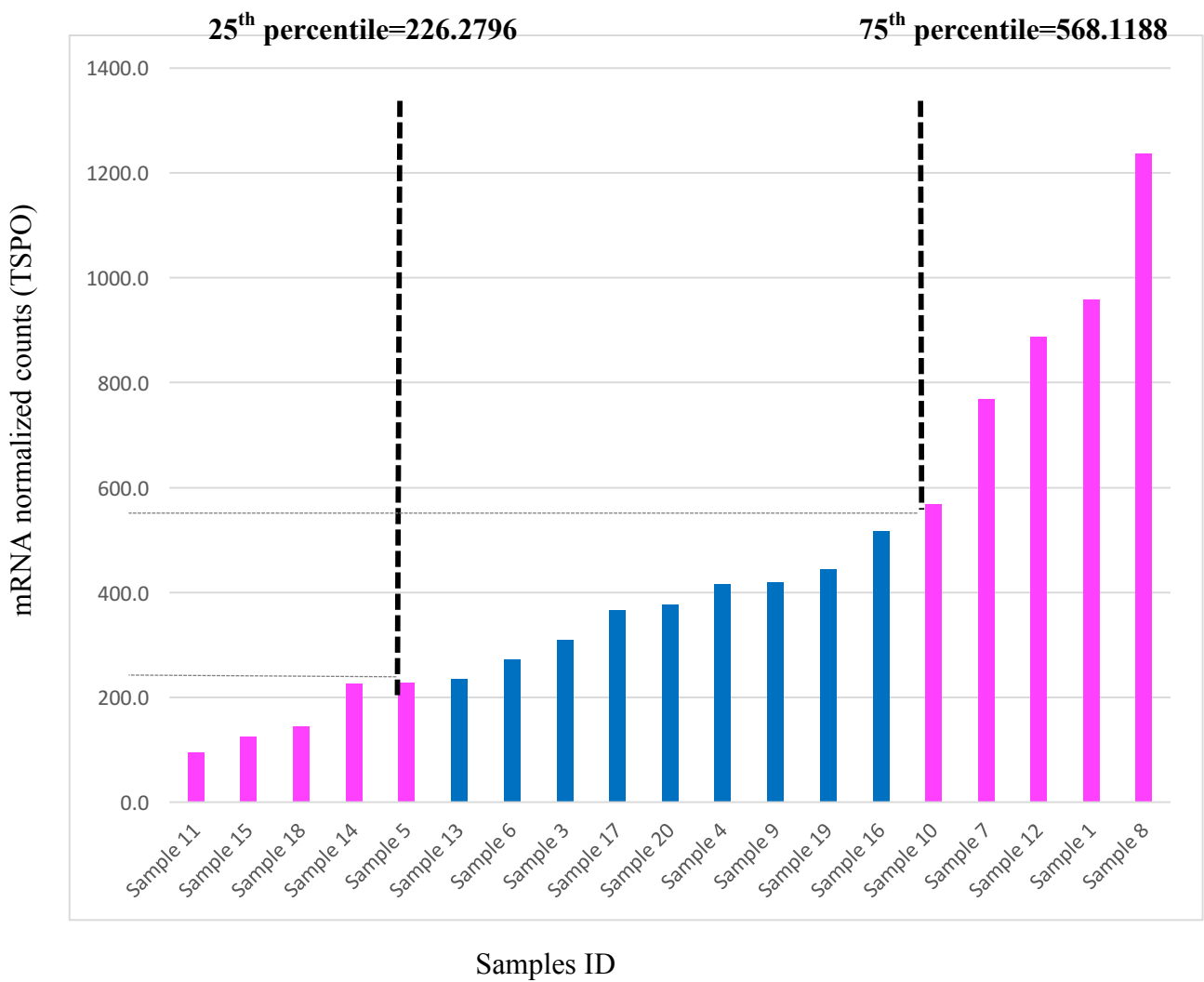


Figure 36: mRNA normalized counts generated from RNA-seq. Values below 25th percentile considered as low TSPO and values above 75th percentile considered as high TSPO (red highlighted).

4.4.2. RNA sequencing (RNA-seq) analysis:

Figure 37 created by using IPA for the selected genes from the RNA seq dataset that might directly (it is estimated in figures by solid lines) or indirectly (it is estimated in figures by dotted or broken lines) regulate TSPO expression. Candidate genes overlaid with the IPA Ingenuity Knowledge base to find the enriched corresponding common pathways. The RNA-seq candidate genes were applied for IPA filtering based on finding upstream TSPO effectors. The candidate genes were also filtered based on the knowledge base in both CNS and cancer. The candidate genes in all presented figures are filtered genes based on CNS and cancer. The candidate genes are summarised in table 10. The main common TSPO upstream regulators through the analysis were estimated in table 10 include, Toll-like receptor-4 (TLR4), Zinc finger protein 106 (ZNF106), SP1 and huntingtin (HTT). Toll-like receptor-4 (TLR4) is a transmembrane receptor, the activity of which shows a positive correlation with TSPO expression in rats [381]. TLR4 was shown to be an upstream regulator of Nuclear factor-kappa B (NFkB), which is a positive regulator of Tumour Necrosis Factor-alpha (TNF). Tumour protein 53 (TP53) and SP1 (transcription regulator) indirectly control TSPO expression through HTT. TP53 was found to positively regulate HTT expression [382]. Furthermore, SP1 and HTT showed protein-protein interaction [383]. HTT might, therefore, indirectly regulate TSPO expression.

SP1 transcription factor (SP1) is a nuclear protein. When SP1 expression was silenced, a study showed a reduction in TSPO expression in breast cancer (positive correlation) [157]. TSPO has binding sites to both SP1 and SP3 [157]. ESR1/2 is involved in the TSPO expression

regulation via inducing the activation of PKA and PKC kinases [384]. Peroxisome proliferator-activated receptor alpha (PPARA) null mutant (preventative of protein production) increases TSPO protein expression, indicating that it's a negative regulator of TSPO expression [385]. Proto-oncogen bHLH (MYC) (a proto-oncogene) is involved in TSPO expression regulation at the TSPO transcription level. FOXO1 is a transcription factor involved in insulin signalling and pancreatic beta-cell maturation. FOXO1 mutation decreases TSPO mRNA expression in pancreatic cells [386]. Leptin is a growth factor that negatively regulates TSPO expression in the adrenal gland [387]. Leptin inhibited ACTH-induced secretion of corticosteroid through reduced TSPO expression. ASAH1 shRNA silencing increases TSPO transcription [388].

Moreover, CDC Like Kinase 3 (CLK3) and Elastase; Neutrophil Expressed (ELANE), are involved in protein-protein interaction with distinct molecules, which might lead to the regulation of TSPO function. Forkhead box L2 (FOXL2) has been previously shown to have protein-protein interaction with ESR1/ESR2 [389]. FOXL2 may indirectly regulate TSPO expression via ESR1/2. RNF4 is a RING finger motif and acts as a transcription regulator. RNF4 is also involved in protein-protein interaction with oncoprotein MYC and SP1 [390, 391]. Therefore, RNF4 may further indirectly affect TSPO expression in oligodendrogliomas, especially that SP1 was shown previously as a positive regulator of TSPO expression. Solute Carrier Family 2 Member 12 (SLC2A12), Solute Carrier Family 5 Member 8 (SLC5A8), transmembrane P24 Trafficking Protein 10 (TMED10) (transporters), and VDAC1 (ion channel) are involved either indirectly or directly in TSPO protein-protein interaction. VDAC is a positive regulator of TSPO expression in GBM [38]. In table 10, all the previously suggested candidate regulatory genes were listed in both cancer and CNS fields.

Next, table 11 and figure 37 showed the candidate genes from the RNA-seq dataset filtered based on the IPA knowledge base disease in both cancer and CNS, with p-value <0.05, Fold-change >1. Moreover, the same genes but the p-value was corrected by FDR<0.05, in both CNS and cancer. In figure 37, all the obtained candidate genes were highlighted in grey.

The candidate genes were selected based on their mRNA expression fold change $\log_2 >1$ and p-value <0.05 (Table 11). All the obtained candidates are clustered upstream of TSPO through HTT and TLR4.

Pro-inflammatory cytokine IL-15 is upstream of HTT through Interferon gamma (IFNG) and insulin growth factor 1 (IGF1) (Figure 37) [392]. Suppression of IL-15 activity inhibited the production of IFNG. Figure 37, showed indirect interaction with different factors upstream of IFNG (broken lines). IGF1 is involved (indirect, referred as broken lines) in the phosphorylation of HTT and in cell survival (neuroprotection) [393]. TATA-binding protein-associated factor 4 (TAF4) is upstream of HTT and through SP1 (Figure 37). SP1 showed in figure 37 a direct interaction with HTT (solid line), and HTT further indirectly regulate TSPO (broken line). TAF4 directly interact with SP1 (solid line). Ribosomal protein S7 (RPS7) exhibits RNA-protein interaction with fragile X mental retardation protein (FMR1) (direct effect indicated with solid line), which is also upstream of HTT [394, 395]. Protein Phosphatase 1 Catalytic Subunit Alpha (PPP1CA) is upstream of HTT through Inositol 1,4,5-Trisphosphate Receptor Type 1 (ITPR1). PPP1CA directly interact with ITPR1 which is upstream of HTT. P38 mitogen-activated protein kinases (P38 MAPK) is upstream of HTT indirectly (broken lines) through 4 factors including, TP53, nerve growth factor (NGF), Peroxisome proliferator-activated receptor gamma (PPRAG) and SP1. IL-12 and Intraflagellar Transport 57 (IFT57) are both indirectly

(broken lines) upstream of HTT through caspase-3. IFNG is upstream of HTT through five factors: NGF, IGF1, vitamin D receptor (VDR), glial cell-derived neurotrophic factor (GDNF), and caspase 3. VDR directly interact upstream of HTT (solid line), while GDNF showed indirect effect upstream of HTT (broken lines). E1A binding protein p300 (EP300) is upstream of HTT through direct effect with SP1 [396]. Cytochrome B 245 beta chain activation (CYBB) is upstream HTT through direct (solid line) effect on glutamate ionotropic receptor NMDA type subunit 1 (GRIN1)[397]. C-C motif chemokine ligand2 (CCL2) is an indirect (broken line) upstream regulator through glutamate ionotropic receptor NMDA type subunit 2A (GRIN2A) and Disc large MAGUK scaffold protein 4 (DLG4). C-X-C motif chemokine receptor 3 (CXCR3) is an indirect (broken line) upstream regulator through IFNG [398]. Brain-derived neurotrophic factor (BDNF) is indirectly (broken lines) upstream of HTT through ten factors including, caspase 3, GRIN2B, snap25, mTOR, SYN1, GRIN2A, DLG4 (or PSD-95), GRIN1, eukaryotic translation elongation factor 1 delta (EEF1D), and thyroid hormone receptor alpha (THRA) as indicated in figure 37. The IPA knowledge base was also filtered to a broader and less restricted field range (cancer field only). Overlaying the obtained gene candidates of RNA-seq to the cancer field will cover other regulatory genes previously studied in different cancer cell types and, therefore, might have a prominent role in gliomas. A summary of these obtained genes is shown in table 11. In conclusion, all these genes are mainly upstream of TSPO through HTT, TP53, SP1, SP3, TLR4, FOXO1, FOXL2, MYC, VEGFA, and ESR1.

Next, the RNA-seq candidate genes were filtered based on false discovery rate value (FDR <0.05) and corrected p-value equal to and less than 0.05. Furthermore, the obtained candidates were separated based on the Log2 fold change (Table 12, Figure 38).

The obtained candidate genes are BCL2 family apoptosis regulator receptor (BOK), Androgen receptor (AR), 2',3'-cyclic nucleotide 3' phosphodiesterase (CNP), presenilin enhancer, gamma-secretase subunit (PSENEN), nuclear factor of activated T cells, cytoplasmic, calcineurin dependent 1 (NFATC1) and interferon regulatory factor 3 (IRF3). All these candidates are interacting with different factors upstream of TSPO through HTT and TLR4. IRF3 (indirect effect) and NFATC1 (direct effect) affect the expression of IFNG, which is upstream of HTT through VDR and CAV1. PSENEN is upstream of HTT through APOE4 (protein-protein interaction) and caspase 3 (activation). CNP is upstream of HTT indirectly through GRIN2A and DLG4, which were previously described. AR is an upstream regulator through insulin-like growth factor 1 (IGF1), POU class 4 homobox 1 (POU4F1), nuclear receptor subfamily 3 group C member 1 (NR3C1), and SP1. PSENEN is upstream of HTT through presenilin 1 (PSEN1), PPARG, mTOR, TP53, and P21 activated (RAC1) activated kinase 1 (PAK1). The white highlighted genes are candidates extracted from the IPA knowledge base, which indirectly interact with the selected RNA-seq gene candidates leading to TSPO expression modulation. Based on filtering the IPA knowledge base for the cancer field only, table 12 showed the candidate genes that interact with TLR4, HTT, SP1, TP53 leading to TSPO expression modulation. These shared genes are HTT, TP53, SP1, SP3, TLR4, VDAC1, MYC, LEP, and ESR1.

Table 12 summarised the outcome candidate genes with false discovery rate value (FDR <0.05) and corrected p-value equal to and less than 0.05. In summary, they include in the cancer field, Bcl-2-Associated Transcription Factor 1 (BCLAF1), BTK tyrosine kinase, CCAAT Enhancer Binding Protein Alpha (CEBPA), CUL4A (ubiquitin ligase component), UV-Damaged DNA-Binding Protein 2 (DDB2), Actin-Depolymerizing Factor (GSN), Heme Oxygenase 1

(HMOX1), Iron Responsive Element Binding Protein 2 (IREB2), Integrin Subunit Beta 4 (ITGB4), Nuclear Factor Of Activated T Cells 1 (NFATC1), Phosphoinositide-3-Kinase Regulatory Subunit 1 (PIK3R1), Protein Phosphatase 1 Regulatory Inhibitor Subunit 1B (PPP1R1B), Platelet Activating Factor Receptor (PTAFR), Ribosomal Protein S6 Kinase A1 (RPS6KA1), and SPI-1 Proto-Oncogene (SPI1).

The common genes (hub genes) that interacts with different chosen candidates and lead to TSPO expression regulation, including HTT, TLR-4, SP1, and TP53. Further, the red highlighted genes are selected common (similar) obtained genes based on comparing RNA-seq with TCGA analysis. These red highlighted genes are the final suggested candidate for further future studies *in vitro* si RNA analysis to confirm their role in TSPO expression regulation.

4.4.3. RNA-seq analysis for oligodendroglioma cases with high vs low TSPO transcriptome expression level (Frozen tissue samples):

Table 10: Genes from RNA-seq dataset and their corresponding interactive pathways are extracted from IPA Ingenuity Knowledge base and have been filtered based on the knowledge base disease in both cancer only field. Moreover, the same candidates were overlaid on the IPA knowledge base in cancer and central nervous system fields.

All the listed genes in the table were applied to the cutoff threshold $p\text{-value} < 0.05$, \log_2 ratios > 1 .

**Cancer
and CNS**

Cancer

| Gene symbol | Gene name | function | Gene symbol | Gene name | function |
|-------------|--------------------------|------------------------|-------------|--------------------------------------------------|--------------------------------------------------------------------------------------------------------------------------------------------------------------------------------------------------------------------------------------------------------------------------------------------------------------|
| HTT | huntingtin | | ASAH1 | N-acylsphingosine amidohydroxylase1 | Innate immune system Sphigolipid metabolism |
| SP1 | SP1 transcription factor | Transcription factor | ESR1 | Estrogen receptor1 | Nuclear hormone receptor that is involved in estrogen and steroid hormone transcription regulation and reproductive function |
| TLR4 | Toll like receptor-4 | Transmembrane receptor | ESR2 | Estrogen receptor 2 | Similar to ESR1 |
| TP53 | Tumor protein 53 | Transcription factor | FOXO1 | Forkhead boxO1 | Transcription factor (TF) Associated with ERK signaling, insulin signaling and metabolic homeostasis regulation in response to oxidative stress. |
| ZNF106 | Zinc finger protein 106 | | LEP | leptin | Growth factor upstream of different target genes involved in cell cycle regulation such as CCND1, via JAK2-STAT3 pathway, or VEGFA, via MAPK1/3 and PI3K-AKT1 pathways Regulation of energy homeostasis. In hypothalmas, regulation of appetite, pro-angiogenic in endothelila cells, innate immunity. |
| | | | MYC | Proto-oncogen bHLH | Transcription factor (TF) Involved in proliferation, angiogenesis, cancer progression |
| | | | PPARA | Peroxisome proliferator activated receptor alpha | Affect target genes expression that are involved in proliferation, cell differentiation and inflammation responses |
| | | | SP1 | SP1 transcription factor | Zink finger transcription factor binds to DNA rich CG content and regulate gene expression involved in cell differentiation, growth, apoptosis. |
| | | | SP3 | SP3 transcription factor | TF cell cycle regulation |

| | | |
|-------------|-----------------------------------------------------|----------------------------------------------------------------------------------------------------------------------------------------------------------------------------------------------------------------|
| TLR4 | Toll like receptor-4 | Transmembrane receptor Pathogen recognition and innate immunity activation. TLR4 form heterodimer and activates NF-kappa-B-dependent production of CXCL1, CXCL2 and CCL9 cytokines, MYD88 signaling |
| ZNF106 | Zinc finger protein 106 | Required for normal expression of essential genes involved in motor neuron and skeletal muscles function |
| CLK3 | CDC Like Kinase 3 | Serine/threonine type protein kinase family |
| ELANE | Elastase, Neutrophil Expressed | Innate immune system |
| FOXL2 | Forkhead box L2 | TF contains DNA binding domain involved in ovary differentiation and maintenance |
| HTT | huntingtin | Related to p53 and AKT pathways |
| RBCK1 | RANBP2-Type and C3HC4-Type Zinc Finger Containing 1 | ubiquitination |
| RNF4 | Ring Finger Protein 4 | Ubiquitination |
| SLC2A12 | SOLUTE CARRIER FAMILY 2 | Glucose carrier and transporter |
| SLC5A8 | Solute Carrier Family 5 Member 8 | Sodium transporter Mediates short fatty acid (lactate) and ketone bodies transport involved in neuron function and energy maintenance. |
| TMED10 | transmembrane P24 Trafficking Protein 10 | Plasma membrane protein involved in vesicular protein trafficking |
| TP53 | Tumor protein 53 | Tumour suppressor induces tumour growth arrest or apoptosis |
| VDAC1 | Voltage Dependent Anion Channel 1 | Gating for metabolites and ions |
| VEGFA | Vascular Endothelial Growth Factor A | Growth factor induces vascular endothelial proliferation and migration. Upregulated in cancer and induce angiogenesis, tumour growth |

4.4.3.1. IPA adjusted to p-value <0.05, Fold-change >1, CNS and cancer

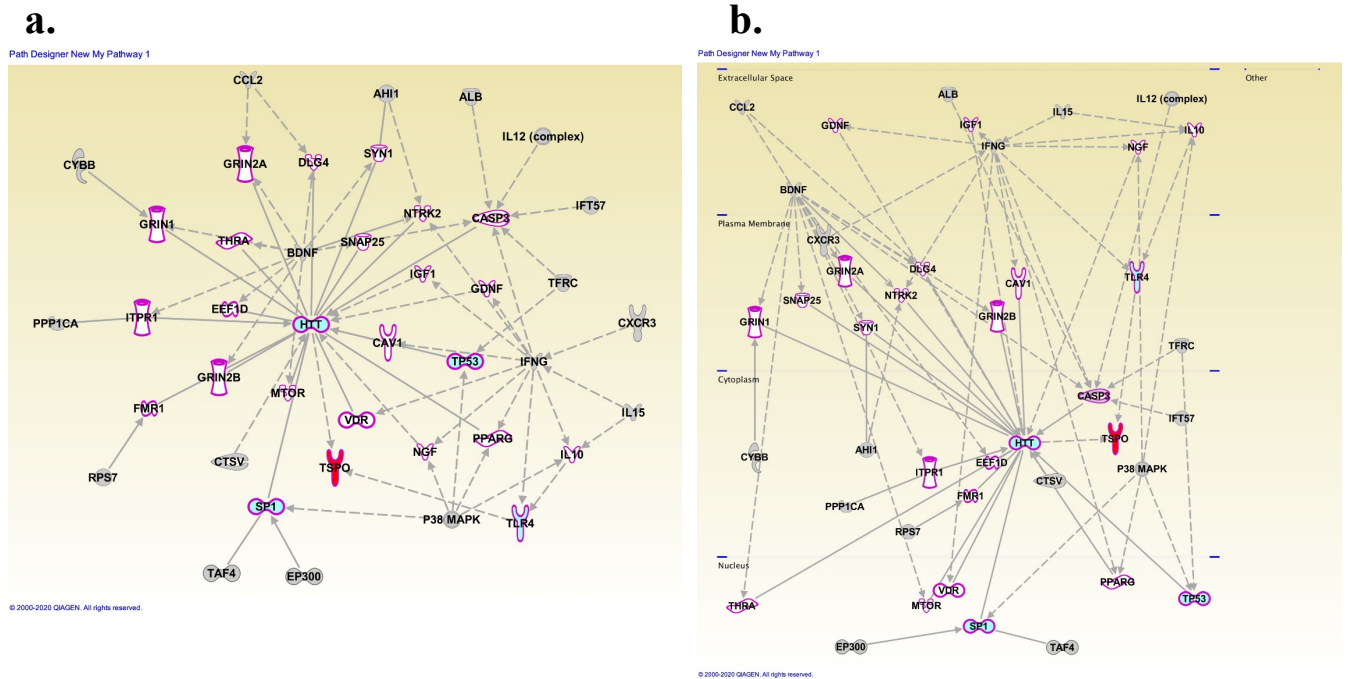


Figure 37: Candidate genes from RNA-seq with IPA adjusted to p-value <0.05, Fold-change >1, CNS and cancer.

Genes from RNA-seq dataset and their interactive pathways upstream of TSPO are extracted from IPA Ingenuity Knowledge base and have been filtered based on the knowledge base disease in cancer and central nervous system fields. All the listed genes in the table were applied to the cutoff threshold p-value <0.05, log 2 ratios >1. Solid line represents the genes that have direct effect on the downstream pathways such as (AHI1 (upstream SYN1), HTT, SP1, TAF4 (upstream of SP1), EP300 (upstream of SP1), RPS7, PPP1CA, CYBB), broken lines represent the indirect downstream effect such as (ALB, IL12, IFT57, TFRC, CXCR3, IL15, TLR4, p38MAPK, CTSV, BDNF, IFNG, IL12 (complex), CCL2).

a. Candidate genes list and their interactive pathways upstream of TSPO.

b. Subcellular location of the selected candidate genes in cancer and CNS fields.

Table 11: Summary of the candidate genes from RNA-seq Dataset that have been filtered based on the IPA knowledge base in both cancer and central nervous system fields, p-value<0.05, log 2 ratios >1

All the listed genes in the table were applied to the cutoff threshold p-value<0.05, log 2 ratios >1. The red highlighted genes are the common selected genes between RNA-seq and TCGA analysis which were indicated below in the synopsis figure 46. These genes were later selected for the final candidate genes list in figure 46.

| Cancer and CNS | Cancer | | | |
|-----------------------|---------------|----------------|----------|---------|
| AHI1 | ABCB7 | GABPB1 | NCOA4 | TRADD |
| ALB | ADAR | GADD45GIP1 | NFE2 | USF1 |
| BDNF | ALB | HBEGF | NFE2L2 | USP14 |
| P38 MAPK | APLN | HDAC9 | NR2C2 | VDAC1 |
| PPP1CA | BDNF | HIPK2 | ONECUT2 | VEGFA |
| CCL2 | BRD2 | HMOX1 | P38 MAPK | ZKSCAN3 |
| CTSV | CBFA2T3 | HNRNPK | PADI4 | ZNF143 |
| CXCR3 | CDK19 | HP | PES1 | ESR1 |
| CYBB | CEBPA | HTT | PIK3R1 | LEP |
| SP1 | CHD8 | IFN alpha/beta | PPP1CA | TAF1 |
| EEF1D | CTSV | IFNG | RBCK1 | |
| EP300 | CUX1 | IL15 | RBMY1A1 | |
| HTT | CXCL8 | IL32 | RPS7 | |
| IFT57 | CYBB | IL12 | SOX9 | |
| IGF1 | DLST | JUNB | SP1 | |
| IL12 | DNAJB12 | JUND | SP3 | |
| RPS7 | EGLN | KDM3A | SPI1 | |
| TAF4 | FOXL2 | LDB1 | TCF7 | |
| TFRC | FOXO1 | MBP | TFRC | |
| TLR4 | FTH1 | MRAP2 | TLR4 | |
| TP53 | GABPA | MYC | TP53 | |
| | TAF4 | NCOA3 | ESR2 | |

4.4.3.2. IPA adjusted to p-value <0.05, Fold-change >1, FDR<0.05, CNS and cancer

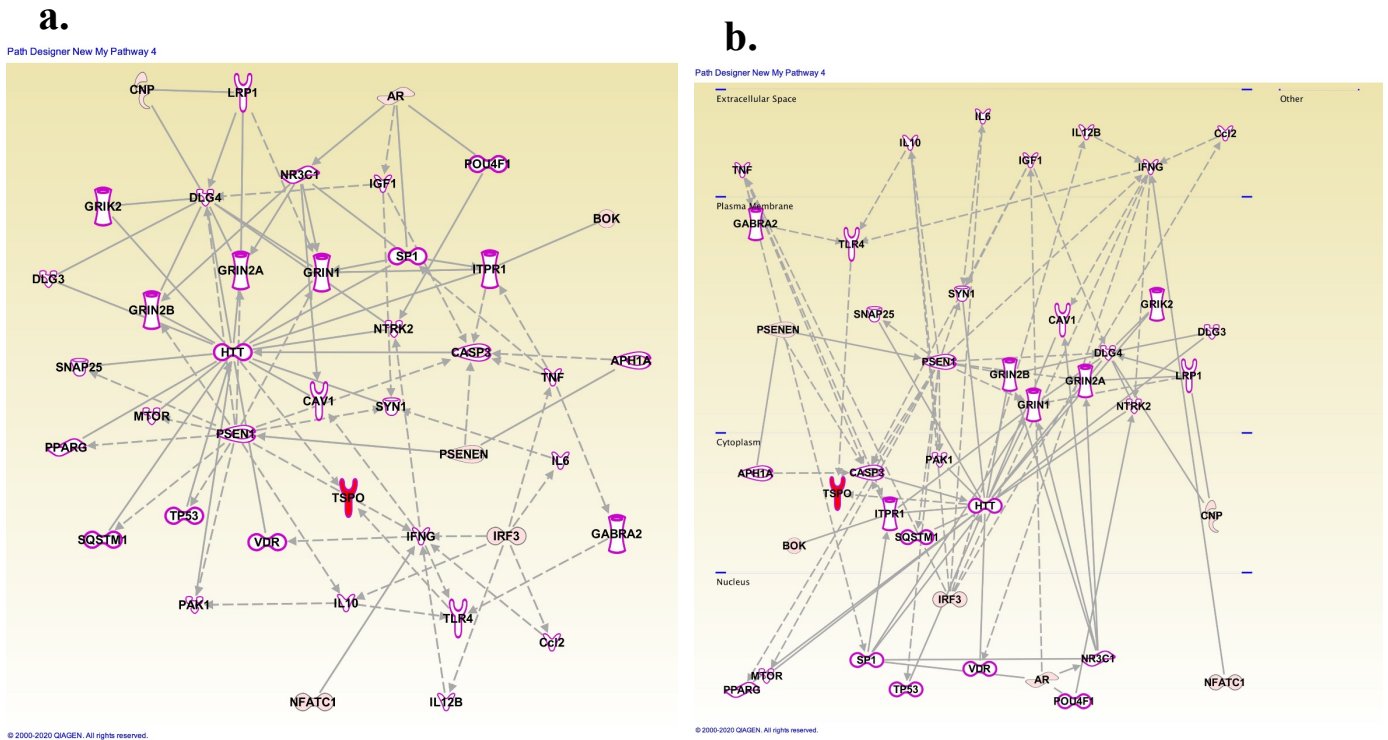


Figure 38: Candidate genes from RNA-seq with IPA adjusted to p-value <0.05, Fold-change >1, FDR<0.05, CNS and cancer. Candidate genes from RNA seq dataset extracted from IPA Ingenuity Knowledge base and have been filtered based on the knowledge base disease in cancer and central nervous system (CNS) fields. All the listed genes in the table were applied to the cutoff threshold p-value<0.05, FDR <0.05, log 2 ratios >1. Solid line represents the genes that have direct effect on the downstream pathways, such as (BOK, NFATC1, CNP, AR, PSENEN, TP53), broken lines represent the indirect downstream effect such as (IRF3, IL-6, IGF1, IFNG, TLR4).

a. Candidate genes list and their interactive pathways upstream of TSPO.

b. Subcellular location of the selected candidate genes in cancer and CNS fields.

Table 12: Summary of candidate genes from RNA seq dataset that have been filtered based on the IPA knowledge base in both cancer and central nervous system (CNS) fields, p-value<0.05, FDR <0.05, log 2 ratios >1. All the listed genes in the table were applied to the cutoff threshold p-value<0.05, FDR <0.05, log 2 ratios >1. The red highlighted genes are the common selected genes between RNA-seq and TCGA analysis which were indicated below in the synopsis figure 46. These genes were later selected for the final candidate genes list in figure 46.

| CANCER AND CNS | CANCER |
|-----------------------|---------------|
| AR | AR |
| BOK | BCLAF1 |
| CCL2 | BTK |
| CNP | CEBPA |
| HTT | CUL4A |
| IFNG | DDB2 |
| IGF1 | GSN |
| IRF3 | HMOX1 |
| NFATC1 | HTT |
| PSENN | IREB2 |
| SP1 | ITGB4 |
| TLR4 | LEP |
| TP53 | MYC |
| | NFATC1 |
| | NPY |
| | PIK3R1 |
| | PPP1R1B |
| | PSENN |
| | PTAFR |
| | PYCARD |
| | RPS6KA1 |
| | SP1 |
| | SPI1 |
| | TLR4 |
| | TP53 |
| | VDAC1 |
| | IL-6 |

4.4.4. The Cancer Genome Atlas program online database (TCGA):

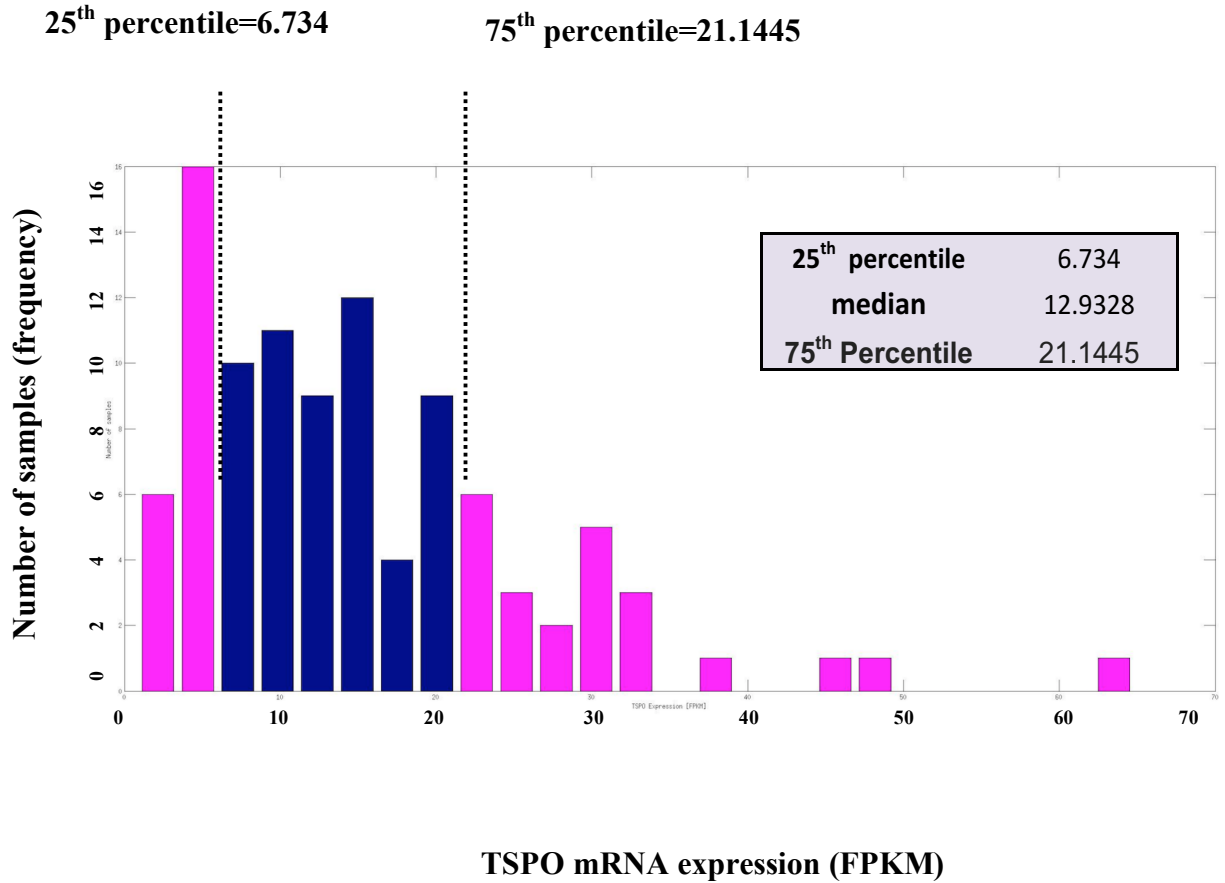


Figure 39: FPKM values were extracted from TCGA database. Values below 25th percentile considered as low TSP0 and values above 75th percentile considered high TSP0. FPKM is Fragments Per Kilobase of transcript per Million mapped reads.

4.4.4.1. Oligodendroglioma cases with high TSPO transcriptome expression level (n=25):

Figure 39 shows the applied threshold to the selected cases from the TCGA database. The red highlighted oligodendroglioma cases (n=25) are the extracted cases from TCGA that showed a high TSPO transcriptome expression, more than the 75th percentile (indicated to the right side of Figure 39). All genes were extracted from TCGA for each case one by one. Later, the selected candidate genes for each patient were correlated with TSPO expression level with a correlation coefficient (>0.6) (Figure 40, a and b). All TCGA candidates were further analysed using IPA Ingenuity Knowledge base and filtered back based on the literature background in the CNS and cancer fields. IPA adjusted the selected candidate genes analysis to be upstream of the TSPO target. The grey highlighted genes are candidates from the TCGA database. In contrast, the white highlighted genes are candidates from the IPA knowledge base that might indirectly work upstream within the same enriched pathway of TLR4, TP53, HTT (blue highlighted) and TSPO (red highlighted) (Figure 40, a and b). TLR4, TP53 and HTT (blue highlighted) are candidate genes that have been identified as common (shared) upstream regulators of TSPO expression in the previously discussed RNAseq analysis.

The main regulators in high TSPO expression cases were HTT and TLR4. All the remaining below discussed candidate genes were involved within this enriched pathway through these two genes.

Arachidonate-5-lipoxygenase (ALOX5) participated indirectly (broken line) in the activation of PPARG, and knocking out its expression reduced the PPARG protein level [399]. PPARG has been shown before to have direct (solid line) protein-protein interaction with HTT (indicated in solid line) [383]. AVL9 cell migration associated protein (AVL9) directly (solid

line) interacts with Gamma-Aminobutyric Acid Type A Receptor Subunit Alpha2 (GABRA2) (solid line indicates a direct protein-protein interaction) which is upstream of TLR-4 and HTT. Casein Kinase 1 gamma 2 (CSNK1G2) is upstream of TSPO through FMR1(FMRP translation regulator 1) and HTT. C-X-C motif chemokine ligand 9 (CXCL9) (indirectly), C-X-C motif chemokine receptor 3 (CXCR3) (indirectly), Signal Transducer And Activator Of Transcription 2 (STAT2)(directly), and DEF6 Guanine Nucleotide Exchange Factor (DEF6)(indirectly) are all upstream regulators of Interferon-gamma (IFN- γ or IFNG) that affect HTT expression [400-404]. Defects in DEF6 leads to defects in TLR4 signalling [408]. Moreover, pro-inflammatory cytokine (IL-15) is involved indirectly with IFNG within the same pathway during the innate immune response. Innate immune signal transduction adaptor (MYD88) showed protein-protein interaction with TLR4 [405]. TLR4, in response to stimuli, is known to induce downstream signalling including, MYD88, NFkB, TNF, CCL2 and others pro-inflammatory cytokines [406]. Protein C (PROC), Oncostatin M receptor (OSMR), and POU class 5 homebox 1 (POU5F1) are all related to the caspase 3 apoptotic process [407]. Matrix metalloprotease 7 (MMP7) is involved directly (solid line) in NGF cleavage (Pro-NGF cleavage) [408]. NGF is a factor involved in neuronal growth, survival and development. Paired box2 (PAX2), ISL LIM home box1 (ISL1), and polypyrimidine tract binding protein 1 (PTBP1) are all indirectly involved through intermediate molecules in regulating HTT function. Lin-7 homolog A (LIN7A) has been previously shown to have direct (solid line) protein-protein interaction with glutamate ionotropic receptor NMDA type subunit 2B (GRIN2B), DLG4, and gamma-aminobutyric acid type A receptor subunit alpha2 (GABRA2) upstream of HTT. Synovial Apoptosis Inhibitor 1 (SYVN1) and VDR are also direct (solid lines) regulators upstream HTT.

In the cancer field, a more extensive range of genes were obtained. Still, similar common genes with RNA seq analysis were noticed to be indirectly involved in the TSPO regulation in oligodendroglioma cases with high TSPO expression, including TLR4, TP53, HTT, LEP, VEGFA, SP1, ELANE, PAPRA, ESR1/ESR2, VDAC1, MYC, TEMED19, RNF4, RBCK1, and CLK2.

A summary of all previously identified genes was introduced in Table 13 listed. Tammy et al. and Lorena et al. indicated MYD88, TLR4, and CCL2 to be involved within the same pathways leading to induce TSPO [315, 406].

4.4.4.2. Oligodendroglioma cases with low TSPO transcriptome expression level (n=24):

Figure 39 shows the applied threshold to the selected cases from the TCGA database. The red highlighted oligodendroglioma cases (n=24) are the extracted cases from TCGA that showed a low TSPO transcriptome expression, less than the 25th percentile (indicated to the left side of Figure 39). All genes were extracted from TCGA for each case one by one. Later, the selected candidate genes for each patient were correlated with TSPO expression level with a correlation coefficient (>0.6) (Figures 41 and 42). All TCGA candidates were further analysed using IPA Ingenuity Knowledge base and filtered back based on the literature background in the CNS and cancer fields. The selected candidate genes analysis was adjusted by IPA to be upstream of the TSPO target. In oligodendroglioma cases (n=24), TLR4, TP53, HTT, FOXO1 and SP1 (all blue highlighted) were indirectly involved in the TSPO regulation was consistent with the RNA-seq gene candidates profiling analysis. Table 13 listed the gene candidates that positively and negatively correlate with TSPO expression with a coefficient correlation higher

than 0.6 and might have a role in TSPO regulation. In cancer and CNS fields, nineteen genes were selected from the TCGA dataset and highlighted with grey in Figure 41 and 42.

Most of the selected genes act upstream of the common gene HTT. ABL proto-oncogen 2 (ABL2), a non-receptor tyrosine kinase upstream of HTT through Integrin Subunit Beta 1 (ITGB1) via direct (solid line) interaction to activate Able family kinases. ABL2 is involved in many biological functions, including cancer cell invasiveness through β 1 integrins/Abl2 signalling [409]. Vesicle associated membrane protein 7 (VAMP7), a member of the SNARE family, is involved in neuronal differentiation in eukaryotes. VAMP7 forms complexes with SNAP25 (direct), which is upstream of HTT [410]. Phosphodiester 6B (PDE6B) works indirectly (broken line) upstream of proto-oncogene c-FOS and indirectly affects its expression. CRK proto-oncogene works directly (solid line) upstream of MAPK8 (JNK1) through protein-protein interaction and further downstream to HTT and caspase 3. X-linked inhibitor of apoptosis (XIAP) works directly upstream of caspase 3 by inhibiting its function [411]. Glutamine-fructose-6-phosphate transaminase1 (GFPT1) is known to be involved in glucose flux in the hexosamine pathway and during the glycosylation of many proteins. IPA knowledge base showed GFPT1 to work directly upstream of gamma-aminobutyric acid type A receptor alpha2 (GABRA2). Rho family GTPase 3 (RND3) knockdown induced the expression of Notch1 protein in the mouse brain [412]. Exocyst complex component 4 is involved in cdc42 signalling (EXOC4) upstream of GABRA2 and participates in many functional pathways, including Golgi transport to membrane, oligodendrocyte differentiation, and exocytosis. GABRA2 is indirectly linked downstream to TLR4 and has previously been mentioned as affecting TSPO expression. Choline-phosphate cytidylytransferase (PCYT1A) is involved in the lipid metabolic process and phospholipid biosynthesis. PCYT1A is indirectly upstream of

TLR4 through controlling the expression of CCL2 (chemokine C-C motif ligand 2), while it is indirectly upstream HTT through fibroblast growth factor receptor 1 (FGFR1). Kinesin family member 2A (KIF2A) is indirectly (broken line) upstream of Insulin-like growth factor 1 receptor (IGF1R) and IGF-1 factors found to stimulate the axonal assembly in a KIF2A dependent manner through IGF1R [413]. Both SKI like proto-oncogene (SKIL) and Serine/threonine kinase 4 (STK4) are upstream of FOXO1. SKIL mediates FOXO1 function via protein-protein interaction, while STK4/MST1 mediates the FOXO1 translocation into the nucleus and its functional activation. Macrophage Stimulating 1 (MST1) deficiency is associated with induced T-cell apoptosis and reduced FOXO1 expression [414]. ATRX chromatin remodeler that is indirectly upstream of glutamate ionotropic receptor NMDA type subunit 2B (GRIN2B) through Kalirin RhoGEF Kinase (KALRN), Discs Large MAGUK Scaffold Protein 3 (DLG3), and glutamate ionotropic receptor NMDA type subunit 2A (GRIN2A). ATP binding cassette subfamily A member 1 (ABCA1) is indirectly (broken line) upstream of apolipoprotein E (APOE) and GRIN2B. ABCA1 is involved in many functions including, cholesterol homeostasis, efflux and transport. Complex of inhibitor of nuclear factor-kappa B kinase (CHUK) phosphorylation is necessary for GRIN2B protein function, which is known to be upstream of HTT.

In the cancer field, TLR4, TP53, HTT, LEP, VEGFA, SP1, ELANE, PAPRA, ESR1/ESR2, VDAC1, MYC, TEMED19, RNF4, and RBCK1 (blue highlighted) are found to be common regulators genes upstream of TSPO. TLR4, TP53, HTT, LEP, VEGFA, SP1, ESR1/ESR2, VDAC1, MYC are common genes in the RNAseq and TCGA candidate genes upstream of TSPO. Table 14 lists all the extracted TCGA gene candidates that are positively or

negatively correlated with TSPO expression and might have a role in TSPO expression regulation.

4.4.4.3. Astrocytomas cases with high TSPO expression (n=26):

A similar strategy was followed with the astrocytomas cases. In cancer and CNS fields analysis, astrocytomas cases (n=26) with higher TSPO transcriptome level than the 75th percentile suggested TLR4, TP5 and HTT to interact with distinct regulatory genes upstream of TSPO. These genes including, Actin Related Protein 2/3 Complex Subunit 4 (ARPC4), ATP Synthase Peripheral Stalk Subunit (ATP5PO), BCL2 Associated Agonist Of Cell Death (BAD), BCL2 Associated X, Apoptosis Regulator (BAX), Enoyl-CoA Delta Isomerase 1 (ECI1), Glutathione Peroxidase 4 (GPX4), HECT And RLD Domain Containing E3 Ubiquitin Protein Ligase 2 (HERC2), Myosin VI (MYO6), Profilin 1 member family of small actin-binding proteins (PFN1), Prohibitin tumour suppressor (PHB), Protein Phosphatase 1 Catalytic Subunit Alpha (PPP1CA), Solute Carrier Family 25 Member 11 (SLC25A11), TSC Complex tumour suppressor Subunit 1 (TSC1), Hydroxysteroid 17-Beta Dehydrogenase 8 (HSD17B8) Interferon Regulatory Factor 3 (IRF3), and Macrophage Migration Inhibitory Factor (MIF) (Figure 43). The previously mentioned genes are highlighted in grey in figure 43. The different enriched pathways and functions among the mentioned genes include apoptosis, tumour growth suppression, inflammation regulation, actin filaments polymerization, estrogen and steroid biosynthesis. The suggested genes might, therefore, be involved in TSPO expression modulation through these different pathways.

4.4.4.4. Astrocytomas cases with low TSPO expression (n=23):

In astrocytomas cases (n=23) with lower TSPO expression than the 25th percentile, a distinct range of candidate genes that might be involved in TSPO expression regulation is summarised in table 15. The candidate genes generated by IPA in astrocytoma cases were different than those observed in oligodendroglioma cases. Still, they interacted with many common (shared) genes including, HTT, FOXO1, FOXL2, VEGFA, SP1/SP3, TLR4, VDAC1, MYC, and ESR1/2.

These genes might be involved in many intrinsic different pathways, including ATP synthesis (ATP Synthase F1 Subunit Beta [ATP5F1B]), chromatin remodeling (ATRX Chromatin Remodeler [ATRX]), methylation/inactivation of neurotransmitter (Catecholamine-O-methyltransferase [COMT]), and apoptosis inhibition (Fas Apoptotic Inhibitory Molecule [FAIM]), and DNA repair (Tumor Protein P53 Binding Protein 1 [TP53BP1]) (Figure 44). Moreover, Heat Shock Protein Family A (Hsp70) Member 9 (HSPA9) is involved in stress response and mitochondria maintenance. L1 Cell Adhesion Molecule (L1CAM) and NCK Associated Protein 1 (NCKAP1) is involved in nervous system development and actin remodeling, respectively. Nuclear Factor I A (NFIA) is a highly expressed transcription factor in astrocytomas that regulate gliosis, promote astrocyte differentiation and correlate with astrocytomas progression [415]. Sec23 Homolog A COPII Coat Complex Component (SEC23A) and Tryptophan Hydroxylase 2 (TPH2) are involved in the endoplasmic reticulum/Golgi trafficking and serotonin biosynthesis, respectively. These previously mentioned genes are highlighted by grey in figure 44.

Oligodendrogloma cases with high TSPO transcriptome expression level (n=25):

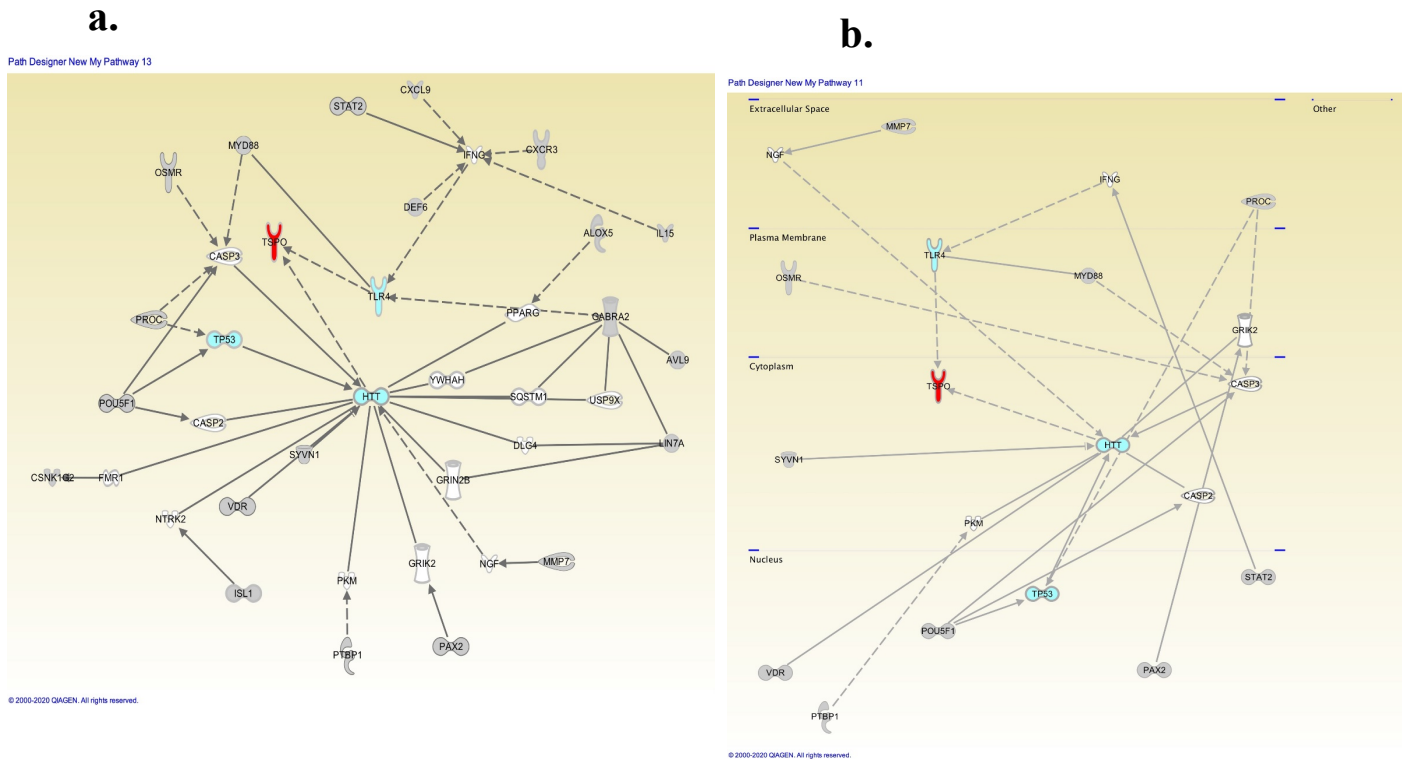


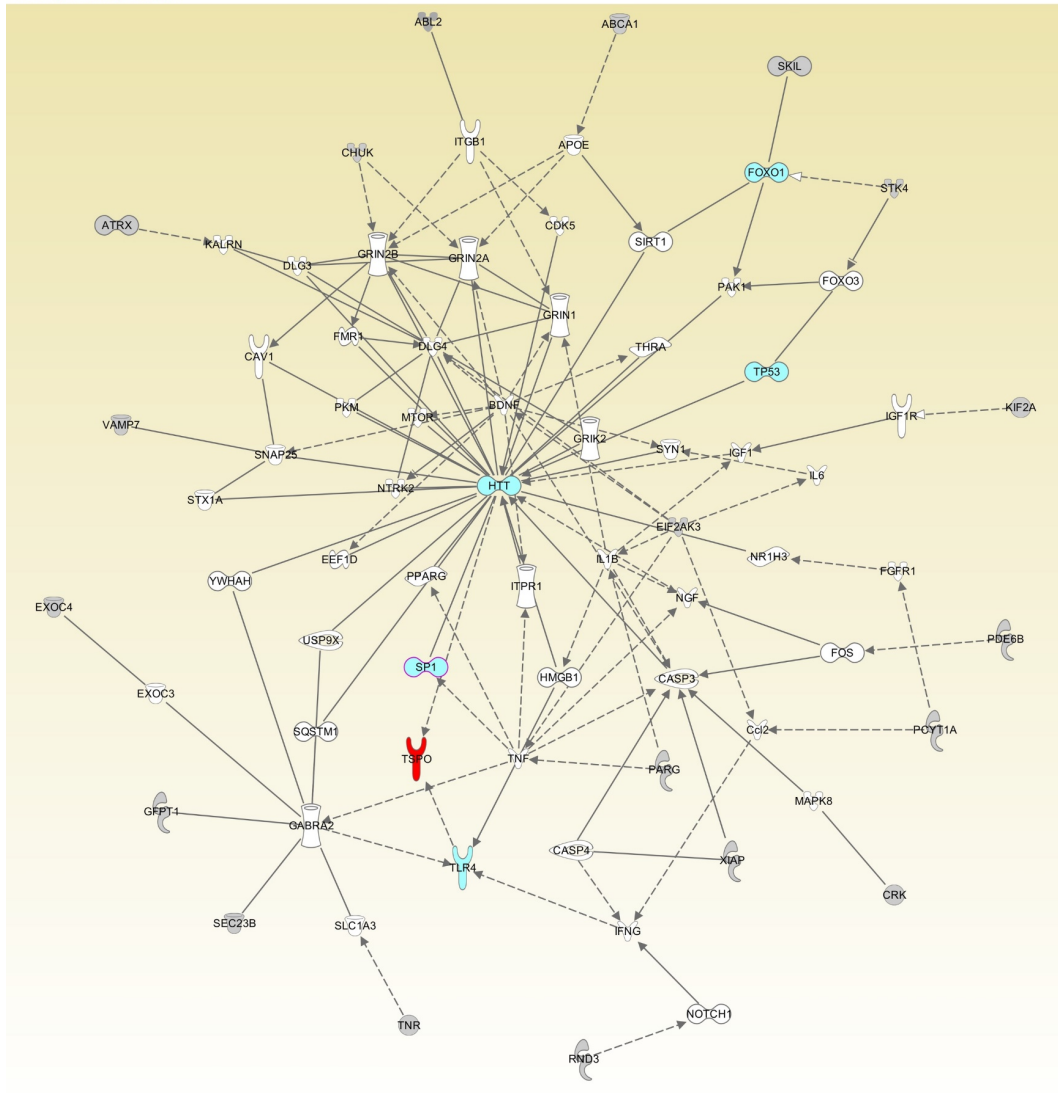
Figure 40: Candidate genes for oligodendrogloma cases (n=25) extracted from TCGA that has high level of TSPO expression more than the 75th percentiles in cancer and CNS. The grey highlighted genes are candidates from the TCGA database, white highlighted genes are candidates from the IPA knowledge base that have been shown in the literature to work upstream of TLR4, TP53, HTT (blue highlighted) and TSPO (red highlighted). TLR4, TP53, and HTT were blue highlighted as common genes with the RNAseq candidate gene analysis. The IPA database was filtered to CNS and cancer field knowledge base. Solid line represents the genes that have direct effect on the downstream pathways such as [STAT2 (upstream of IFNG), AVL9 (upstream of GABRA2), MYD88 (upstream of TLR4), POU5F2 (upstream of HTT), VDR (upstream of SVN1 and HTT)], broken lines represent the indirect downstream effect such as [CXCR3 (upstream of IFNG), IL15 (upstream of TLR4), ALOX5 (upstream of PPARG and HTT), HTT (upstream of TSPO), TLR4 (upstream of TSPO), PPARG (upstream TLR4)].

a. Candidate genes list and their interactive pathways upstream of TSPO.

b. Subcellular location of the selected candidate genes in cancer and CNS fields.

Oligodendrogloma cases with low transcriptome TSPO expression (n=24):

Path Designer New My Pathway 11



© 2000-2020 QIAGEN. All rights reserved.

Figure 41: Candidate genes for oligodendrogloma cases (n=24) extracted from TCGA that has low level of TSPO expression less than the 25th percentile. The grey highlighted genes are candidates from the TCGA database, white highlighted genes are candidates from the IPA knowledge base that have been shown in the literature to work indirectly upstream TLR4, TP53, HTT, FOXO1, SP1 (all blue highlighted) and TSPO (red highlighted). The IPA database was filtered to cancer and CNS field knowledge base. TLR4, TP53, HTT, FOXO1, SP1 (all blue highlighted) are common genes with the gene candidates illustrated above in the RNA seq analysis. Solid line represents the genes that have direct effect on the downstream pathways such as [ABL2 (upstream of ITGB1), SKIL (upstream of FOXO1 leading downstream to HTT), VAMP7 (upstream of SNAP25 and HTT), GFPT1 and SEC23B

(upstream of GABRA2 and TLR4), XIAP (upstream of caspase3), TP53 (upstream of HTT), SP1 (upstream of HTT)], broken lines represent the indirect downstream effect such as [TNF (upstream of SP1), HTT (upstream of TSPO), TLR4 (upstream of TSPO), CCL2 (upstream IFNG and TLR4), PDE6B (upstream Fos)].

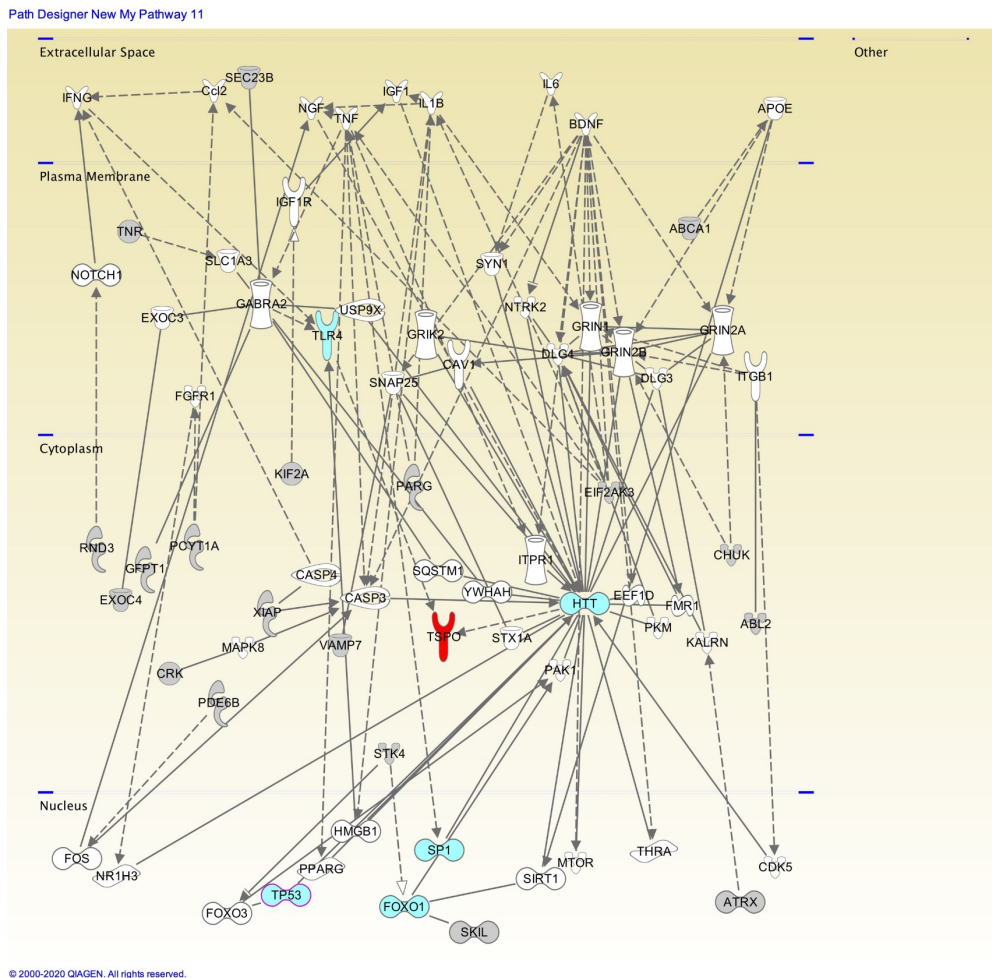


Figure 42: Candidate genes for oligodendroglioma cases (n=24) subcellular compartment view of the gene candidate's subcellular distribution in cancer and CNS field. The grey highlighted genes are candidates from the TCGA database, white highlighted genes are candidates from the IPA knowledge base that have been shown in the literature to work indirectly upstream TLR4, TP53, HTT, FOXO1, SP1 (all blue highlighted) and TSPO (red highlighted). The IPA database was filtered to cancer and CNS field knowledge base. TLR4, TP53, HTT, FOXO1, and SP1 (all blue highlighted) are common genes with the gene candidates illustrated above in the RNA seq analysis.

Table 13: Summary of candidate genes in oligodendrogloma cases with low and high TSPO transcriptome expression level in CNS and cancer. The red highlighted genes are the common selected genes between RNA-seq and TCGA analysis which were indicated below in the synopsis figure 46. These genes were later selected for the final candidate genes list in figure 46.

| Oligodendroglomas | |
|--------------------------|------------------|
| CNS and cancer | |
| Low TSPO | High TSPO |
| ABCA1 | ALOX5 |
| ABL2 | AVL9 |
| ATRX | CSNK1G2 |
| BDNF | CXCL9 |
| CASP3 | CXCR3 |
| CASP4 | DEF6 |
| CAV1 | GABRA2 |
| Ccl2 | HTT |
| CHUK | IL15 |
| CRK | ISL1 |
| EIF2AK3 | LIN7A |
| FOXO1 | MMP7 |
| GFPT1 | MYD88 |
| HTT | OSMR |
| IL6 | PAX2 |
| KIF2A | POU5F1 |
| PARG | PROC |
| PCYT1A | PTBP1 |
| PDE6B | STAT2 |
| PPARG | SYVN1 |
| RND3 | TLR4 |
| SEC23B | TP53 |
| SKIL | VDR |
| SP1 | |
| STK4 | |
| TNR | |
| TP53 | |
| VAMP7 | |
| XIAP | |

Table 14: Summary of candidate genes from TCGA dataset in oligodendroglioma cases with low TSPO expression and high TSPO expression in cancer field. The red highlighted genes are the common selected genes between RNA-seq and TCGA analysis which were indicated below in the synopsis figure 46. These genes were later selected for the final candidate genes list in figure 46. **A)** A summary of candidate genes in oligodendroglioma cases with low TSPO transcriptome level after filtering back the obtained data to cancer field. **B)** A summary of candidate genes in oligodendroglioma cases with high TSPO transcriptome level after filtering back the obtained data to cancer field.

A)

| Oligodendrogliomas | | |
|---------------------------|---------|---------|
| Low TSPO | | |
| Cancer | | |
| ABCA1 | HTT | SP1 |
| AGFG1 | IDE | SPRTN |
| ALCAM | JMY | STAM2 |
| ASXL2 | KIF2A | STK4 |
| ATG12 | KIFBP | TEAD2 |
| ATP2C1 | LCLAT1 | TERF2 |
| ATP7A | LEMD3 | TLR4 |
| ATRX | LEP | TMEM131 |
| BRCC3 | MIA3 | TNKS |
| CHUK | MKLN1 | TNPO1 |
| CNOT1 | MMGT1 | TNR |
| COPB2 | MYC | TP53 |
| CRK | NBAS | TRIP12 |
| CSNK1G3 | NBR1 | VAMP7 |
| CSTF2 | NT5E | VDAC1 |
| CUL4B | PRKAB2 | VEGFA |
| DDX52 | PSMD2 | VTI1A |
| DNAJC13 | PSMD11 | WAC |
| EFEMP2 | PSME3 | XIAP |
| EIF2AK3 | PTGDS | XPO7 |
| ENTPD7 | RAB21 | YAF2 |
| ERCC4 | RAD50 | ZFP64 |
| ESR1 | RBBP5 | ZFP90 |
| ESR2 | RND3 | ZMIZ1 |
| EXOC4 | RPRD2 | |
| FOXL2 | SEC23B | |
| FOXO1 | SKIL | |
| GFPT1 | SLC30A6 | |
| GOLPH3L | SLU7 | |
| HNRNPH2 | SMG7 | |

B)

| Oligodendrogliomas | | | | | |
|---------------------------|---------|---------------|----------|----------|-------------|
| High TSPO | | | | | |
| Cancer | | | | | |
| ABCB8 | CREB5 | GOLPH3L | MED10 | POU5F1 | SPI1 |
| ADAR | CREB3L1 | GPR65 | MFAP4 | PPARA | TARS2 |
| ADM2 | CSF2 | GPR89A/GPR89B | MINDY4 | PYHIN1 | TCF7 |
| AMIGO2 | EBF2 | HS2ST1 | MMP7 | RAB18 | TEC |
| ANAPC7 | ELANE | HSD11B1 | MRPS17 | RAC2 | TLN1 |
| AP3B1 | EOMES | HTR4 | MSTO1 | RARRES2 | TLR4 |
| ARHGEF1 | EPRS1 | HTT | MX1 | REEP4 | TMCO1 |
| ARL1 | EPSTI1 | IL7 | MYC | RGS19 | TMED2 |
| ASS1 | ESR1 | IL15 | MYD88 | RNF4 | TMED10 |
| ATP2B1 | ESR2 | IL27 | MYO19 | RP9 | TMEM33 |
| AVL9 | FAM71F1 | IL13RA2 | MYO1G | RPS6KA4 | TMEM214 |
| BLZF1 | FCGR2B | IL2RB | NBPF1 | RUNX2 | TMTC3 |
| C1orf226 | FGF21 | IL2RG | NIPSNAP2 | S100A4 | TOR1AIP2 |
| CAPN15 | FLG2 | INTS3 | NME7 | SEC61G | TOR4A |
| CC2D1A | FLII | IQGAP2 | NOD2 | SEMA3C | TP53 |
| CCN4 | FMNL1 | IRF7 | NOP2 | SEPTIN7 | TPBG |
| CCT6A | FOXL2 | ISL1 | NPY2R | SERPINA1 | TPM3 |
| CD109 | FOXO1 | KANSL3 | NSMCE3 | SERPINA3 | TRIL |
| CFAP54 | G0S2 | KLHL12 | NSUN2 | SERPINC1 | TRIM69 |
| CGB3 | GABRA2 | L3MBTL2 | OAS2 | SLC1A5 | TRIOBP |
| CHCHD2 | GALNT3 | LAP3 | OAS3 | SLC2A12 | UNC45A |
| CLEC7A | GARS1 | LEP | OASL | SLC30A5 | UNC93B1 |
| CLK3 | GATM | LMF2 | ODF2 | SLC35E1 | UTP15 |
| CLN6 | GGCT | LNPEP | OSMR | SLC5A8 | VDAC1 |
| CLPTM1L | GGCX | LPIN3 | PARP12 | SLFN11 | VDR |
| CNOT11 | GLI3 | LTB4R | PGK2 | SMG7 | VEGFA |
| CNR1 | GMPPB | LYST | PITX2 | SP1 | VGLL2 |
| COPA | GNPAT | LYZ | PLEKHA7 | SP3 | ZCCHC9 |
| CORO1A | GNRH2 | MAPK15 | PLXNB2 | SP110 | ZDHHC23 |
| | GOLGA2 | MARS1 | PML | SPECC1L | |

Astrocytomas cases with high TSPO transcriptome expression level:

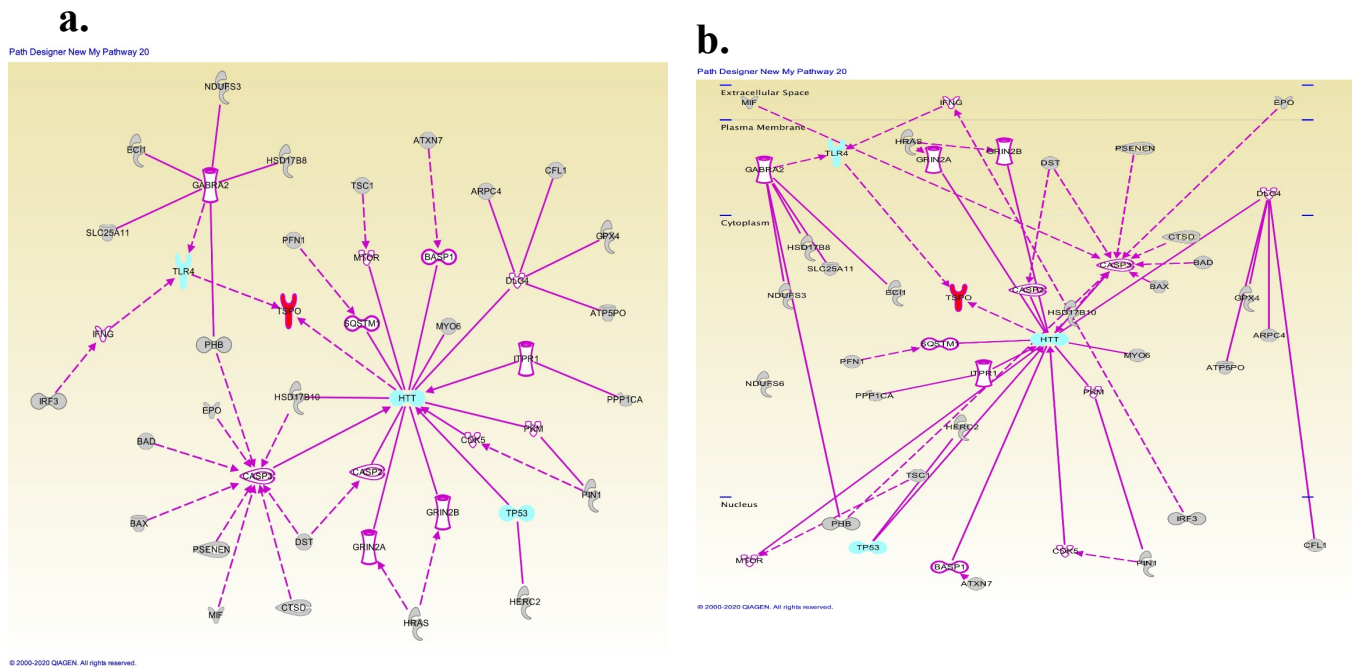


Figure 43: Candidate genes for astrocytomas cases (n=26) extracted from TCGA that has high level of TSPO expression more than the 75th percentiles. The grey highlighted genes are candidates from the TCGA database. The white highlighted genes are candidates from the IPA knowledge base that have been shown in the literature to work indirectly upstream of TLR4, TP53, HTT and TSPO (red highlighted). TLR4, TP53, HTT (blue highlighted are common genes with the RNAseq dataset gene candidates). The IPA database was filtered to CNS and cancer field knowledge base. Solid line represents the genes that have direct effect on the downstream pathways such as [HERC2 (upstream of TP53), PIN1 (upstream of HTT), PPP1CA (upstream of ITPR1 and HTT)]. Broken lines represent the indirect downstream effect such as [CXCR3 (upstream of IFNG), IL15 (upstream of TLR4), ALOX5 (upstream of PPARG and HTT), HTT (upstream of TSPO), TLR4 (upstream of TSPO), BAD, BAX (upstream caspase 3), IRF3 (upstream of TLR4)].

a. Candidate genes list.

b. Subcellular functional location of the selected candidate genes in cancer and CNS fields.

Astrocytomas cases with low TSPO transcriptome expression level:

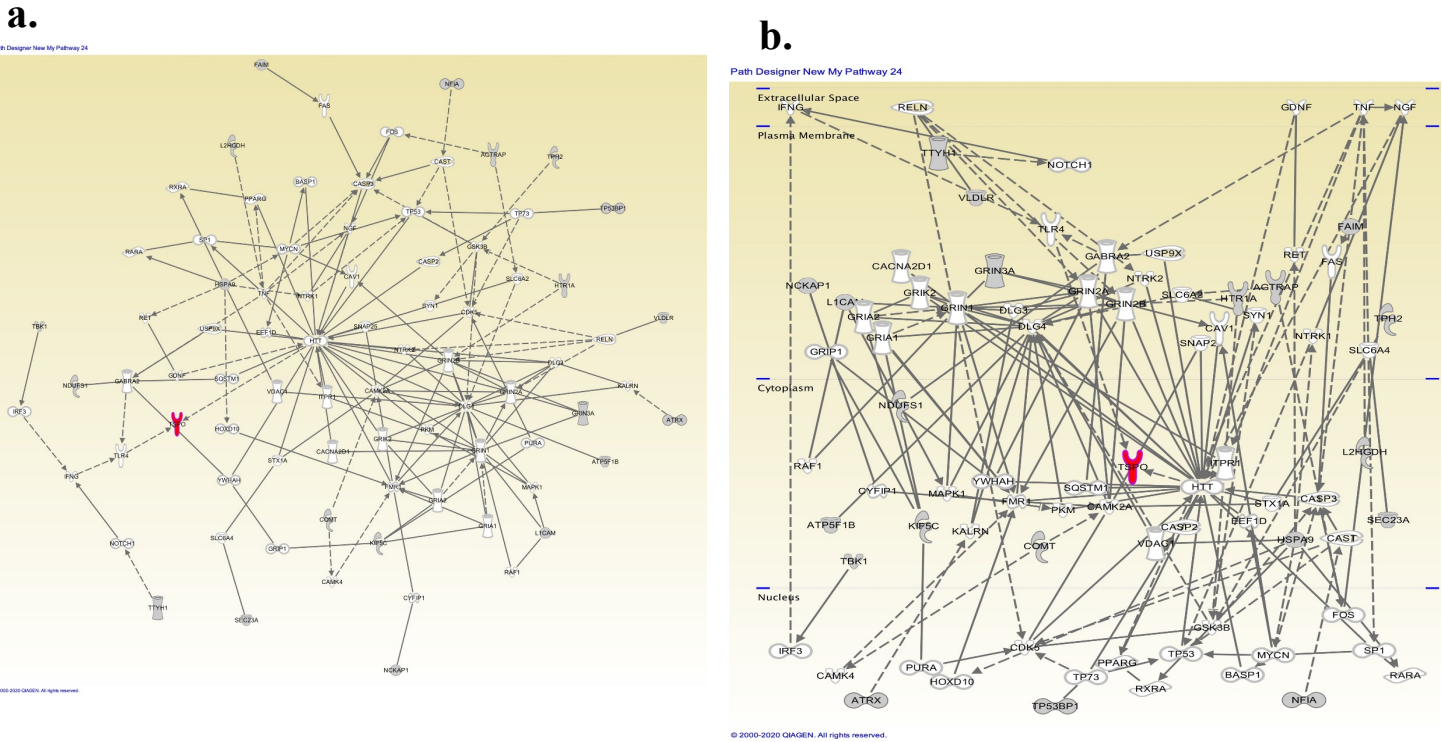


Figure 44: Candidate genes for astrocytomas cases (n=23) extracted from TCGA that has low level of TSPO expression less than the 25th percentile. The grey highlighted genes are candidates from the TCGA database. The white highlighted genes are candidates from the IPA knowledge base that have been shown in the literature to work indirectly upstream of TSPO (red highlighted). The IPA database was filtered to cancer and CNS fields knowledge base. Solid line represents the genes that have direct effect on the downstream pathways such as [SEC23A (upstream of HTT through different downstream genes), TBK1 (upstream of IRF3 and TLR4 leading to TSPO), FAIM (upstream of FAS leading to HTT downstream), ATP5F1B (upstream of DLG4 leading downstream to HTT)]. Broken lines represent the indirect downstream effect such as [NFIA (upstream of CAST leading downstream to HTT), HTT (upstream of TSPO), TLR4 (upstream of TSPO), TPH2 (upstream SYN1 and HTT)].

- Candidate genes list.
- Subcellular functional location of the selected candidate genes in cancer and CNS fields.

Table 15: Summary of candidate genes from TCGA dataset in astrocytomas with low and high TSPO expression in cancer and CNS. The candidate genes are extracted from the TCGA dataset for cases that showed low TSPO expression (below 25th percentile) and high TSPO expression (above 75th percentile). The IPA knowledge base was filtered based on cancer and CNS. The obtained candidate genes might directly or indirectly regulate TSPO expression.

| Cancer and CNS | |
|-----------------------|-------------|
| Low | High |
| AGTRAP | ARPC4 |
| ATP5F1B | ATP5PO |
| ATRX | ATXN7 |
| COMT | BAD |
| FAIM | BAX |
| GRIN3A | CFL1 |
| HSPA9 | CTSD |
| HTR1A | DST |
| KIF5C | EC11 |
| L1CAM | EPO |
| L2HGDH | GPX4 |
| NCKAP1 | HERC2 |
| NDUFS1 | HRAS |
| NFIA | HSD17B8 |
| SEC23A | HSD17B10 |
| TBK1 | IRF3 |
| TP53BP1 | MIF |
| TPH2 | MYO6 |
| TTYH1 | NDUFS3 |
| VLDLR | PFN1 |
| | PHB |
| | PIN1 |
| | PPP1CA |
| | SLC25A11 |
| | TSC1 |

4.4.4.5. Synopsis of the results:

The primarily selected candidate genes based on comparing TCGA with RNA-seq data analysis include SPI1, CAV1, CCL2, IL-15, IL-6, CXCR3, ADAR, TLR4, HTT, SP1, SP3, TP53, and FOXO1 (Figure 45, red box) in oligodendrogliomas. SP1 and SP3 regulators were consistent with the Batarseh et al. study in breast cancer cells. Batarseh et al. showed binding sites for SP1 and SP3 within the TSPO promoter region, which involved in inducing TSPO expression in this cell type. We suggested these factors to be involved in regulating TSPO expression in oligodendrogliomas cases. Further *in vitro* (si RNA) study is required to investigate SP1 and SP3 effect on TSPO expression in oligodendrogliomas cases. In figure 45, Batarseh et al. finding suggested PKC as an upstream regulator of TSPO through the MAPK pathway (RAS/Raf1/MEK1/2/ERK1/2). In our analysis, these regulators were not found in the studied oligodendrogliomas cases. Further *in vitro* study is warranted to investigate their possible role in oligodendrogliomas. Sequence alignment (proximal region CpG island within TSPO promoter) between mouse and human showed 70% homology in Batarseh et al. study [157]. This homology indicates the possibility of finding common TSPO regulatory factors in human. SPI1 encodes to Pu.1, which is a transcription regulator of TSPO expression in microglia cells. Pu.1 was identified by Rashid et al. to have a corresponding binding site within the proximal region of the TSPO promoter, which increased TSPO expression in microglia [142]. TLR4 is an upstream regulator of TNF and TSPO through MYD88 and NFkB in microglia [315]. In the current study, TLR4 /MYD88 was one of the suggest regulators in oligodendrogliomas. This preliminary result requires further investigation *in vitro* (si RNA) in gliomas. To our knowledge, the role of CAV1, CCL2, IL-15, CXCR3, ADAR, TP53, and HTT candidate's genes on TSPO expression was not previously identified.

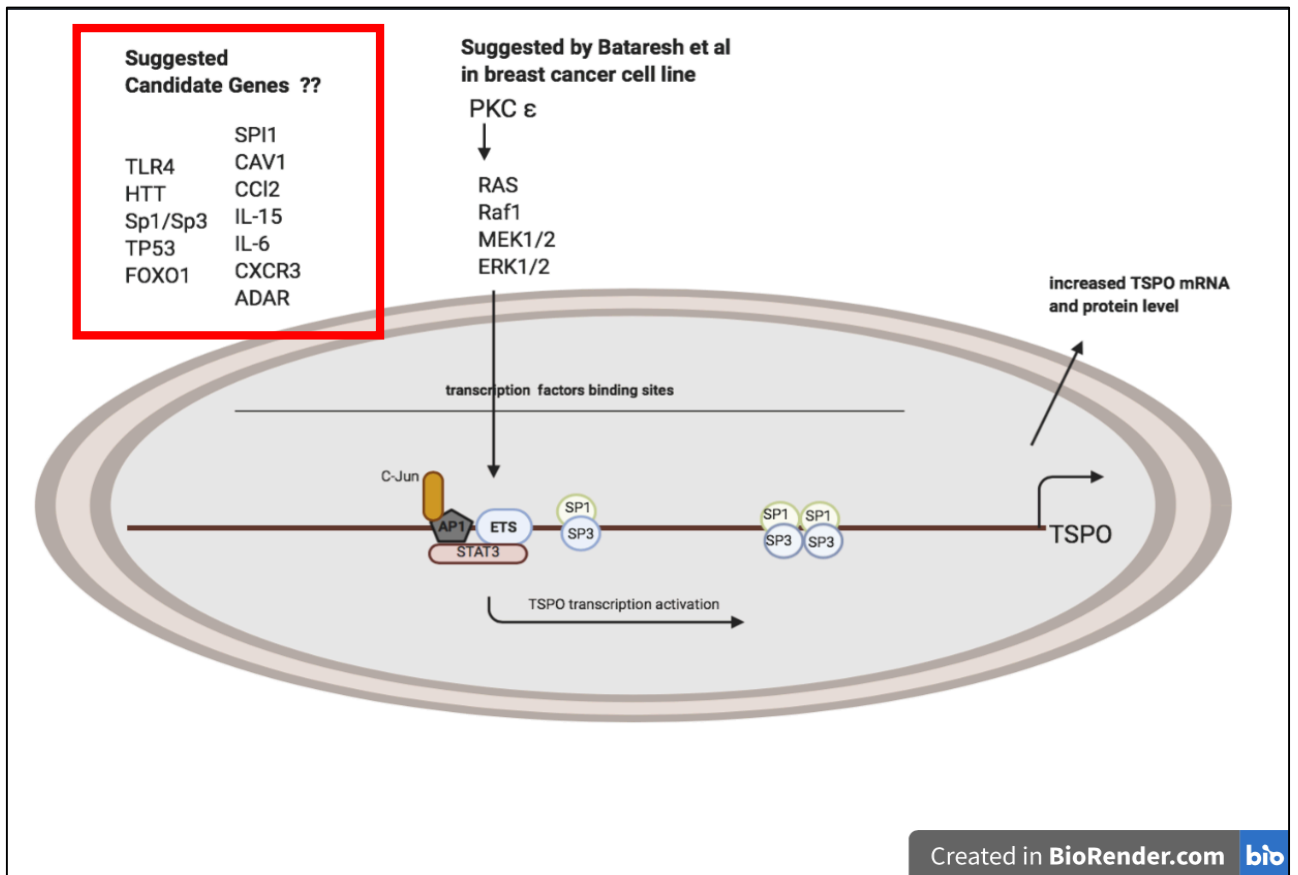
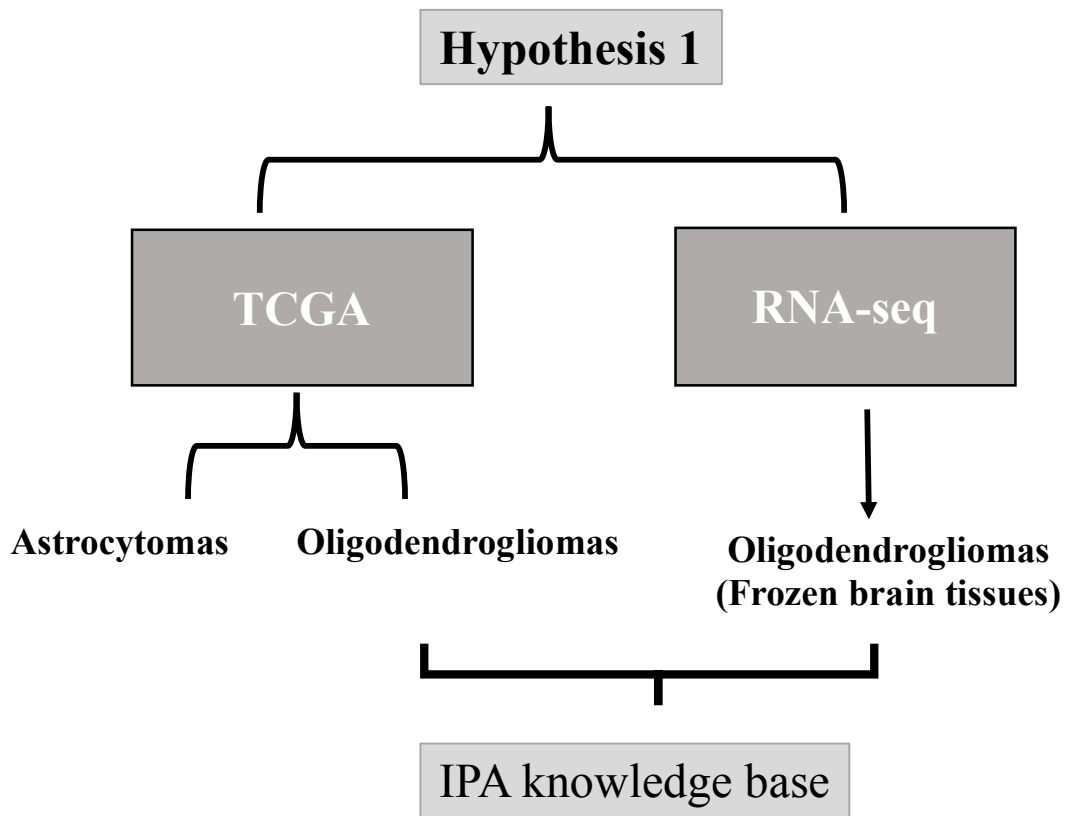


Figure 45: Synopsis of the previously suggested candidate genes in the literature and candidate genes from current study. The candidate genes introduced in this dissertation are SPI1, CAV1, CCL2, IL-15, IL-6, CXCR3, ADAR, TLR4, HTT, SP1, SP3, TP53, and FOXO1 (Red box). SP1 and SP3 were consistent to Bataresh et al. findings that indicate both factors to be involved in TSP0 expression regulation [143]. SPI1 encodes to Pu.1 (transcription factor that has binding site to the TSP0 promoter region and regulate TSP0 expression as it was indicated by Rashid et al. [142]. TLR4 and CCL2 are involved within the same pathway leading downstream to TSP0 expression regulation. IL-6 was suggested in GBM to be upstream PPARG in inducing tumour growth [312]. The remaining candidates were first introduced in TSP0 expression regulation in oligodendrogliomas including, CAV1, IL-15, TP53, FOXO1, CXCR3, and ADAR. Created with BioRender.com



Common genes between TCGA and RNA-seq analysis:

| | |
|-------|-------|
| SP1 | SPI1 |
| TLR4 | CAV1 |
| HTT | CC12 |
| TP53 | IL-15 |
| FOXO1 | IL-6 |
| | CXCR3 |
| | ADAR |

Figure 46: Synopsis of the main candidate genes after comparing TCGA and RNA-seq data analysis. The selected candidate genes are common genes between RNA-seq and TCGA for oligodendrogliomas. In astrocytomas cases, TCGA analysis was the only performed analysis because their frozen tissues samples were not available. The obtained candidate genes for the studied oligodendroglioma cases are SPI1, CAV1, CCL2, IL-15, IL-6, CXCR3, ADAR, TLR4, HTT, SP1, SP3, TP53, and FOXO1 (List below). The applied threshold was consistent among the entire cohorts in IPA.

4.4.5. Methylation analysis results:

The TSPO promoter sequence was extracted from the UCSC genome browser on human (GRCh37/hg19) assembly, with the Genehancer and CpG island options visible in the regulation section. The promoter is located at chr22:43150780-43154156.

The EPIC array has CpG probes in the promoter region, 5' of the gene, and across the gene's body. The different probe IDs were pulled from the Array Manifest available from the Illumina website https://emea.support.illumina.com/array/array_kits/infinium-methylationepic-beadchip-kit/downloads.html.

In the current study, no difference in the promoter methylation pattern at the CpG sites was detected in oligodendrogliomas cases with high and low TSPO protein expression. Methylated TSPO promoter leads to silencing TSPO transcription and further the protein expression (low TSPO), while unmethylated TSPO promoter would reflect high subsequent TSPO expression. The methylation level for each group was estimated by calculating the beta value (Figure 47, 48). The beta value is the methylated probe intensity ratio divided by the total intensity of both methylated and unmethylated probe intensities [416, 417]. This value is ranged from 0 to 1, being unmethylated at zero while fully methylated at 1.

Methylation across TSPO CPG island

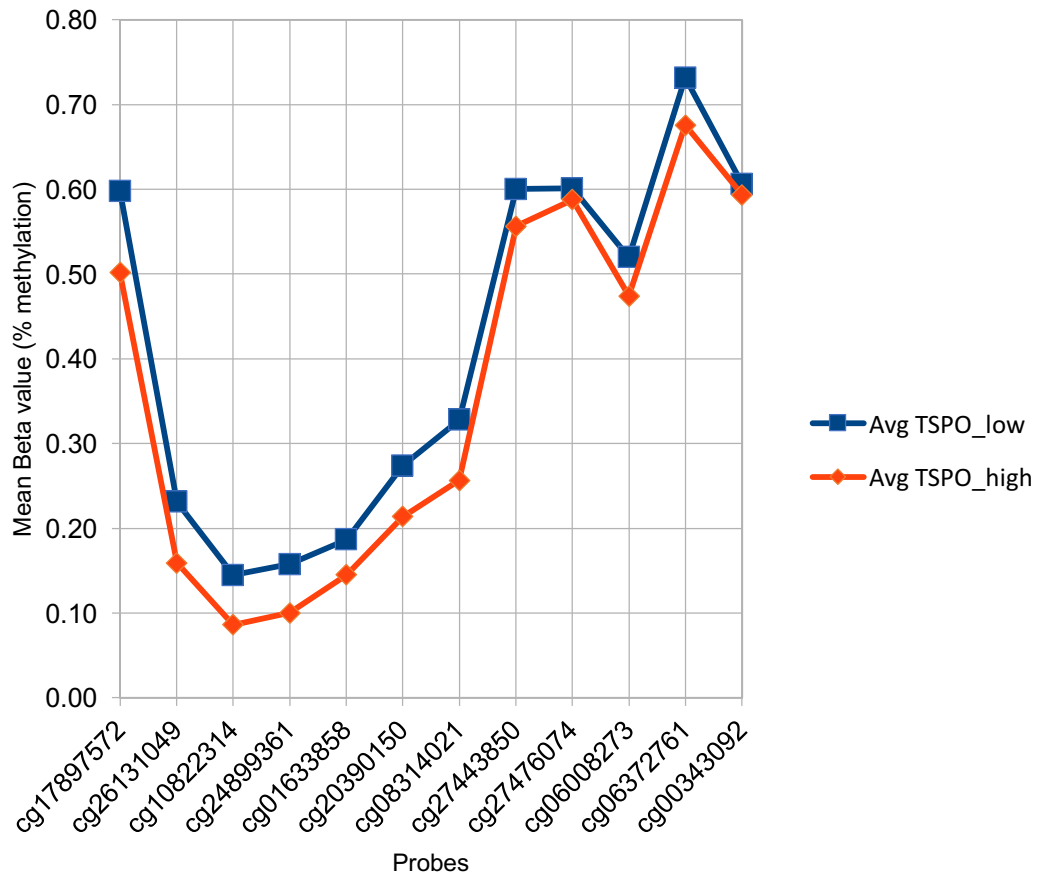


Figure 47: The average mean beta pattern difference between two groups (TSPO low and high protein expression level) along the CpG island. The average of beta value of all cases was calculated at each CpG probe for both groups (High and low TSPO protein expression). No significant difference was seen between the two groups, suggesting another possible or alternative mechanism that could regulate TSPO expression in oligodendroglioma cases. Probes (cg17897572 - cg00343092) are twelve different IDs for the probes that have been pulled from the Array Manifest available from the Illumina website https://emea.support.illumina.com/array/array_kits/infinium-methylationepic-beadchip-kit/downloads.html. These probes cover the CpG regions within the TSPO promoter.

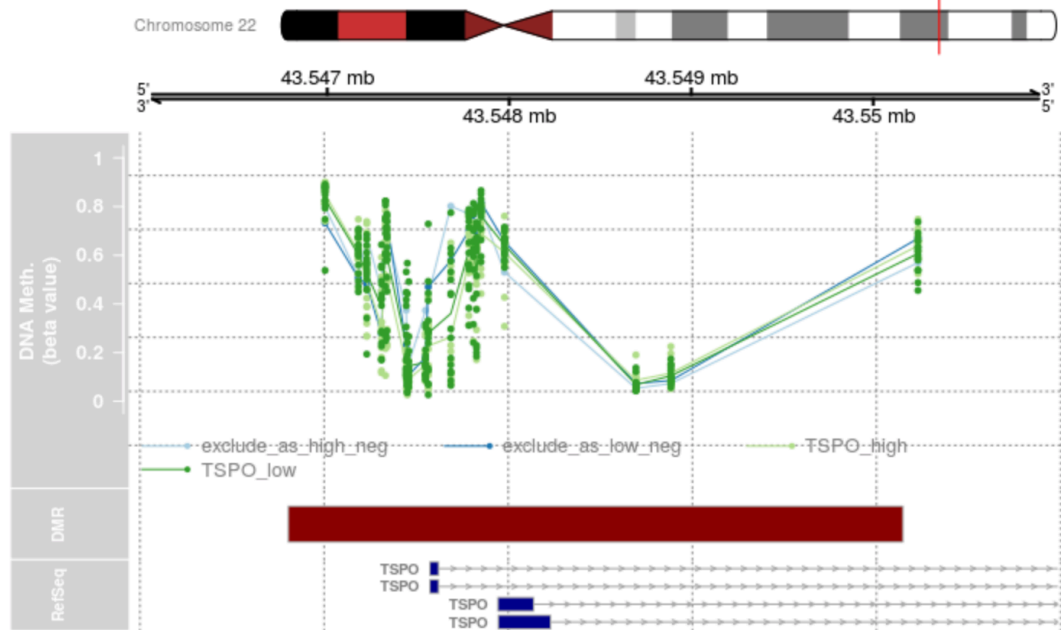


Figure 48: DNA methylation (beta value) across the TSPO CpG sequence BLAT matched to hg19 = chr22:43,547,320-43,548,169. The oligodendroglioma cases with high TSPO expression (light green) and low TSPO expression (dark green) were displayed as beta values for the methylation level across the CpG sequence along the promoter and TSPO gene. No significant difference was found between the two groups. All the studied cases harboured IDH1 mutation and 1p/19q codeletion. The excluded cases (two cases) were found to be IDH1 WT (negative) and identified separately in the figure.

4.5. Discussion:

The work presented in this chapter describes the possible mechanisms that regulate TSPO expression in oligodendrogliomas. The TSPO expression regulation mechanisms proposed in the literature knowledge suggested epigenetic methylation at the promoter CpG islands region of TSPO to be one of the possible mechanism that regulates TSPO expression in breast cancer and Leukemia [156, 157]. Batarseh et al. treated MCF-7 breast cancer cell line with 5-aza-2'-deoxycytidine (5-aza-dC), known to inactivate DNA methyltransferase activity and caused demethylation of CpG sites. They showed a threefold increase in TSPO expression in 5-aza-dC breast cancer cells suggesting epigenetic regulation of TSPO in this cell type [157].

Middleton et al. showed that treating T cell leukemia cell line with a DNA methyltransferase inhibitor (5-aza-dC) reduced TSPO promoter methylation with a corresponding increase in TSPO mRNA levels [156]. The same group examined the 5-aza-dC drug effect on TSPO expression level in GBM (U87-MG) cells, and they did not find a significant impact. Therefore, a question raised about the epigenetic regulation impacts TSPO expression in different diseases such as oligodendrogliomas and astrocytomas. No previous studies in the literature examined the epigenetic regulation effect on TSPO expression in oligodendrogliomas or astrocytomas.

Moreover, different regulatory genes were suggested to regulate TSPO expression, including SP1, SP3, c-Jun, STAT3, and PKC in breast cancer, murine BV-2 microglia, MA-10 mouse tumour Leydig cells, non-steroidogenic NIH-3T3 mouse fibroblasts, and human ARPE-19 epithelial cells [142, 157].

TSPO expression regulation in brain tumour, especially oligodendroglioma and astrocytoma, have not been studied before. In the current study, our analysis showed that TSPO expression is not regulated by epigenetic methylation of the CpG islands within the TSPO promoter region. This current result indicated a lack of TSPO promoter methylation within the CpG island region of the TSPO gene in oligodendrogliomas. A possible explanation for this is that TSPO expression a cell type-specific protein, and its regulation mechanism is orchestrated based on its distinct corresponding functions in different cell types. The enormous suggested functions for TSPO in the literature indicated that this gene regulation might differ based on its related functions in different cell types.

Furthermore, we examined other alternative mechanisms that might regulate TSPO in oligodendrogliomas and astrocytomas. TCGA analysis and RNA-seq were conducted to compare TSPO transcriptomic expression profiles between two groups of low and high TSPO transcriptome expression levels. For that purpose, RNA was isolated from frozen brain tissues of cases diagnosed with oligodendrogliomas (LGO and AO) and followed with RNA-seq analysis. The selected candidate genes were applied to the cut-off threshold $p\text{-value} < 0.05$, with \log_2 ratios > 1 -fold change with the $p\text{-value}$ corrected $FDR < 0.05$, to avoid any false estimation of the $p\text{-value}$. The selected genes were then applied to the IPA database to find the possible upstream regulators of TSPO in cancer and CNS fields. Similarly, the exact threshold was applied to the TCGA database cases for oligodendrogliomas and astrocytomas. The obtained gene lists from both analyses (TCGA and RNA-seq) were compared, and the common candidate genes between them were further selected.

In conclusion, the commonly found genes between the two studies (TCGA and RNA-seq) were ADAR, CAV1, CCI2, CXCR3, IL-6, SPI1, IL15, TLR4, HTT, TP53, FOXO1, SP1 and SP3. As discussed in details in the introduction (Chapter 1), many genes have been suggested to positively regulate TSPO expression in microglia and MA-10 cells, including Pu.1, SP1, SP3, Sp4, c-Jun, c-Fos and Stat3 [142, 143]. They have specific binding sites at the proximal region within the TSPO promoter, such as Ap1, Ets and Sp [3, 142, 143, 157]. They suggested Ap1, Ets and Sp as binding sites for many transcription factors that have been shown to regulate TSPO in microglia and steroidogenic cells. SP1, SP3 and GABP are suggested to have a regulatory effect on TSPO expression through these binding sites. Consistent with Batarseh et al.'s study, our RNA-seq analysis identified SP1 and SP3 as suggested candidates that may regulate TSPO expression in oligodendrogliomas.

Moreover, IL-6 was previously found to be involved in glioma development with STAT3 signalling [418]. Batarseh et al. found that STAT3 is involved in increasing TSPO expression in Leydig cells and breast cancer, suggesting a possible role in gliomas as well [143]. Based on these studies, future investigation to examine the roles of both IL-6 and STAT3 in TSPO expression regulation in gliomas would be interesting.

CCI2 is an essential chemokine released from the glioma microenvironment to recruit regulatory T cells and MDSCs in GBM, supporting immunosuppression and tumour growth [419]. A recent study showed that TSPO was restrictively expressed in activated GAMMs and tumour-infiltrating MDSCs [313]. Therefore, a possible role for TSPO in the immunosuppressive tumour microenvironment; this possibility needs further investigation. Moreover, another study in GBM suggested a cross-talk between glioma and microglia through

CCL2/CCR2/IL-6 that enhanced tumour invasiveness [361]. CCL2 (secreted from GBM) stimulated microglia to produce IL-6, promoting glioma cells' invasiveness [361].

An interesting study conducted in 2017 showed that cytokine IL-15 signalling is essential for T cell proliferation and persistence activity in the tumour microenvironment, which induces an anti-tumour effect [420]. ADAR gene is an Adenosine Deaminase RNA specific gene involved in the site-specific deamination process of adenosine to inosine [421]. This RNA editing affects many thousands of genes across the genome, and it has been found to have a role in cancer development [421]. A study in GBM (U87 cells) found that this gene's over-expression led to decreased tumour proliferation [422]. CXCR3 is a member of the CXC chemokine receptor subfamily; while it is expressed by human glioma cells and activated T cells, it has also been found to have a role in tumour progression [402, 404]. SPI1 is a proto-oncogene encoding for the transcription factor Pu.1, which has been shown to have a role in glioma progression [423].

Rashid et al. suggested that the Pu.1 transcription factor binds to the TSPO promoter and further enhances TSPO transcription in microglia [142]. It would be interesting to investigate whether Pu.1 has a similar role in oligodendroglioma. Moreover, TP53 mutation is associated with increased tumour progression and worse patient's survival [424]. It will be interesting to check if there is an indirect effect for TP53 on regulating TSPO expression and further affect tumour progression. TP53 positively regulate HTT expression [382]. The role of toll-like receptors (TLRs) in terms of tumour progression is controversial. One study indicated an anti-tumour effect in gliomas but a tumour growth supportive role in hepatocellular carcinoma [425, 426]. LPS induced MYD88, NFkB and TNF via TLR4, leading to induced

TSPO expression in microglial cells [142, 315, 406]. Moreover, TLR4/MYD88/STAT3 pathway was suggested to have a role in inducing the malignancy of hepatocellular carcinoma (HCC) [426]. Further investigation is recommended to check this pathway role in regulating TSPO expression in gliomas.

FOXO1 protein is a negative regulator of glioma cell invasion and growth [427]. FOXO1 suppresses glioma cell migration and may induce cell death under oxidative stress condition [427, 428]. CAV1 is plasma membrane subdomains that participate in many biological functions, including T-cell proliferation, NFkB activation, AKT signalling, and cell proliferation. It got overexpressed in GBM and promoted invasiveness [429].

For all the genes mentioned above, their roles in TSPO expression regulation are still not well understood, and further *in vitro* investigation is warranted.

4.6. Conclusion:

In the current study, many candidate genes were suggested to regulate TSPO expression in oligodendrogliomas, including ADAR, CAV1, CCL2, CXCR3, IL-6, SPI1 and IL-15. The common genes that may regulate TSPO expression were TLR4, HTT, TP53, FOXO1, SP1 and SP3. Epigenetic regulation of TSPO expression by promoter methylation was not a reliable mechanism in oligodendrogliomas. No significant difference was identified in the methylation level at different CpG islands along the TSPO promoter region between patients with low and high TSPO expression levels.

CHAPTER 5

GENERAL DISCUSSION

Chapter 5

5.1. General discussion

TSPO expressed at a low level in the normal brain while up-regulated in neurodegenerative disorder diseases and brain tumours [5-7, 9, 10]. In the first chapter of this dissertation, we examined the different cellular components of NVU that could express TSPO. We concluded that vascular endothelial cells, macrophages and astrocytes express TSPO at the NVU. This study was conducted by using porcine macrophage, astrocytes and endothelial cells. The TSPO expressions were examined by IHC, DIF, and Scatchard assay with [^{18}F]DPA-714 and [^{11}C]-(R)PK11195 tracers. The porcine model was used for several reasons, including its high cell yield from a single pig brain, more extended time of sustaining the BBB features than other models and lower cost with comparative anatomy and physiology to humans [318, 334]. Our results were consistent with many studies in normal mouse brain, AD and tumour diseases [256, 271, 272, 430, 431]. Studying GAMMs and vascular TSPO expression level within the tumour microenvironment, specifically in oligodendrogliomas, was an interesting new field that was discussed in Chapter 3.

There is a positive correlation between TSPO and tumour proliferation, progression and aggressiveness [2, 89, 96]. A positive correlation has been found in brain tumours between high TSPO expression and increased proliferation, tumorigenicity, and invasion. Therefore, TSPO was suggested as a promising target for use in glioma PET imaging. In the current study, we examined TSPO expression in FFPE tissues for fifty oligodendroglioma cases. We found a

significant difference between low-grade and anaplastic oligodendrogliomas, indicating the possibility of using TSPO as a biomarker of oligodendroglioma progression. Moreover, we found that TSPO is a prognostic biomarker of overall survival in patients with oligodendrogliomas. Interestingly, patients with high TSPO expression level were associated with worse overall survival compared with the low TSPO expression group (p value 0.01). It was the first study that introduced TSPO expression level as a biomarker of tumour progression and patient overall survival in oligodendrogliomas.

Consistent results in astrocytomas showed a positive correlation between TSPO expression and grade of malignancy [94]. Consistent results in different cancers showed increased TSPO protein expression in various cancer tissues, leading to induced proliferation and tumour progression [2, 89, 94]. Preliminary data found that the TSPO expression level from IHC correlated significantly with the obtained [¹¹C]-(R)PK11195 BPNDmax (Pearson $r = 0.73$, $p < 0.001$). Moreover, another result demonstrated a cut-off of 1.4 for the [¹¹C]-(R)PK11195 BPNDmax to differentiate between low- and high-grade oligodendrogliomas, while an overlap was seen in the rCBV values. The increased [¹¹C]-(R)PK11195 signal represented increased cellularity in high-grade oligodendroglioma instead of high vascularity during progression.

The heterogeneity of the tumour microenvironment led to examining the other cellular contribution to TSPO expression in oligodendrogliomas. We found that neoplastic cells predominantly expressed TSPO during tumour progression, while GAMMs and endothelial cells partially contributed to the overall TSPO expression obtained. Other preliminary results have shown that intratumoral macrophages/microglia GAMMs have a partial contribution to the overall TSPO expression and [¹¹C]-(R)PK11195 PET signal in the tumour microenvironment [8]. Findings consistent with our results have shown TSPO within the

tumour microenvironment was predominantly expressed by neoplastic cells, supporting our results [281]. A preliminary study by Takaya et al. exhibited TSPO expression in the microglia infiltrating glioma cells [230]. In anaplastic astrocytomas, a possible mechanism could inhibit the inflammatory response and TSPO expression in microglia during tumour progression. The exact mechanism for this is still not understood. A future investigation regarding the TSPO role in supporting tumour growth via suppressing anti-inflammatory mechanisms is an essential field of interest.

Finally, we asked about the mechanism that could regulate TSPO expression in oligodendrogliomas. The regulation of TSPO is still not fully understood. The present thesis suggested two possible mechanisms promoter methylation and upstream gene regulators that may be involved in TSPO expression regulation. TSPO expression's epigenetic regulation has been studied in different glioma subtypes but not in oligodendrogliomas [432-436]. A larger sample (n = 38) was examined in the current thesis to assess the TSPO expression's epigenetic regulation, which has not been previously studied. Our results indicated no differences in the methylation status within the TSPO promoter region's CpG sites between low- and high-TSPO cases; this suggests that another possible mechanism may regulate TSPO expression. Next, we referred to many candidate genes that might directly or indirectly contribute to TSPO expression regulation in gliomas. Based on the two conducted studies (TCGA and RNA-seq), we found the following candidate genes that could regulate TSPO expression in oligodendrogliomas: ADAR, CAV1, CCL2, CXCR3, IL6, SPI1 and IL15. The common genes were TLR4, HTT, TP53, FOXO1, SP1 and SP3.

It was interesting to find that one of our suggested candidates (CCL2) is a factor previously suggested to be released by glioma cells to support tumour growth and

immunosuppression [419]. An important future direction involves checking whether CCL2 can regulate TSPO expression and support tumour growth. A cross-talk between the factors released from glioma cells and GAMMs could be suggested, leading to tumour progression. Another interesting candidate was IL-6, which was previously found to be involved in glioma development with STAT3 signalling. Batarseh et al. suggested that STAT3 induces TSPO expression in Leydig and breast cancer cells [143]. Studying the down-regulation (si-RNA) of IL-6 and STAT3 in glioma cell lines would be an essential approach to check their direct downstream effect on TSPO expression level.

Moreover, SPI1 encodes for the transcription factor PU.1, which has been shown to play a role in glioma progression [423]. Furthermore, Rashid et al. suggested that PU.1 transcription factor binds to the TSPO promoter and further enhances TSPO transcription in microglia [142]. Studying the effect of SPI1 on TSPO expression in gliomas is a fascinating future field that could connect TSPO expression regulation with tumour growth. Using the si-RNA approach to down-regulate SPI1 and check its regulatory effect on TSPO expression would be an essential next step. Finally, a summary of the main findings in each chapter was presented in figure 49.

5.2. General conclusion

5.2.1. Synopsis of the main findings

This dissertation showed that TSPO is a biomarker of oligodendroglioma progression and patient survival. We concluded that a high expression of TSPO could indicate high-grade oligodendroglioma progression with poor clinical outcomes. The role of TSPO in enhancing tumour growth has not specifically been studied in oligodendrogliomas before. This thesis's findings will have implications for using TSPO as a biomarker of tumour progression in this subtype. Current findings also identified a high percentage (56%) of the studied oligodendrogliomas cases (50 cases) harboured rs6971 TSPO polymorphism for the first time. Although we did not find an effect of this polymorphism on protein expression or the patient's overall survival, it will be important to be considered in oligodendrogliomas PET imaging, especially after using sensitive tracers to this polymorphism.

TSPO expression regulation is still poorly understood; the present thesis discussed the mechanisms that could control TSPO expression in oligodendrogliomas. In the current study, the epigenetic regulation of TSPO expression was examined by estimating the methylation level within the TSPO promoter region. In oligodendrogliomas, the TSPO promoter methylation status (beta value) did not exhibit distinct methylation patterns across the CpG islands between low and high TSPO expression cases. As an alternative suggested regulatory mechanism, a list of candidate genes was proposed to directly or indirectly regulate TSPO expression based on both *in silico* TCGA and RNA-seq analysis.

5.2.2 Further Direction

It would be interesting to examine the introduced candidate genes in cell culture (*in vitro*). Genetic manipulation of gene expression (si-RNA) could be used to check its downstream effect on TSPO expression *in vitro*. Moreover, a microarray expression analysis could be performed after knocking down each gene candidate to check the corresponding downstream effect on TSPO expression. Down-regulation of the candidate genes expression would validate their downstream effect in regulating TSPO expression *in vitro*.

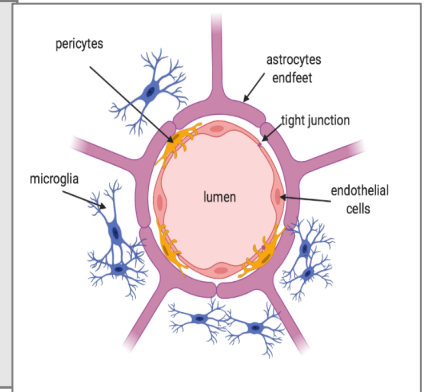
Furthermore, the mass cytometry approach could be used to check the expression of multiple and wider range of different cellular markers with better resolution and less overlap. This method was planned to be used as a confirmation technique for the 3D TMA tissue analysis but was not completed due to COVID-19. A comparison could be carried out between LGO and AO to indicate the TSPO expression levels for neoplastic cells (IDH1), microglia (TMEM119/Iba1), astrocytes (GFAP), pericytes (PDGFR), smooth muscles (SMA) and endothelial cells (CD31) in different FFPE tissue samples. It will estimate the TSPO expression level in glial cells and endothelial cells in oligodendrogliomas which were not previously examined. Moreover, to confirm our immunofluorescence staining at cellular level in astrocytes, endothelial and macrophages cells, double immunostaining on FFPE tissue sections for porcine normal brains could be done.

Chapter 2: TSPO and NVU

Main findings:

Different alternative methods were used to examine TSPO expression at the NVU.

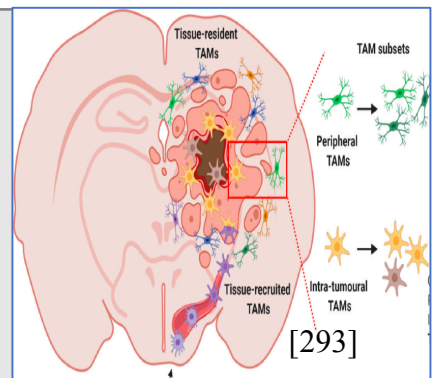
Macrophage and endothelial cells in normal porcine brain showed higher expression than astrocytes in western blot and ICC. Scatchard assay showed higher Bmax in macrophage compared to endothelial cells. RT-qPCR showed similar TSPO mRNA level for macrophage and endothelial cells. However, astrocytes showed higher TSPO mRNA level



Chapter 3: TSPO in Oligodendrogliomas

Main findings:

- TSPO predicts tumour progression in oligodendroglioma cases.
- GAMMs (Iba1) and endothelial cells (CD31) contribute partially to TSPO expression compared to neoplastic cells (IDH1) in anaplastic oligodendrogliomas.
- Neoplastic cells are the main contributor to TSPO expression in anaplastic oligodendrogliomas



Chapter 4: TSPO expression regulation

Main findings:

- TSPO expression is not epigenetically regulated in oligodendrogliomas
- The main candidate genes from RNA-seq and TCGA analysis are TLR4, HTT, SP1, SP3, TP53, FOXO1, SPI1, CCL2, IL-15, IL-6, CXCR3, CAV-1 and ADAR.

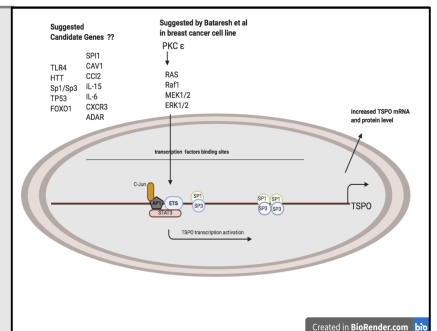


Figure 49: Summary for the main findings in the thesis. Understanding the different cellular contributions to TSPO expression at cellular levels in NVU (chapter 2) and oligodendrogliomas (chapter 3). The mechanism of TSPO expression regulation in oligodendrogliomas (chapter 4).

References

1. Braestrup, C. and R.F. Squires, *Specific benzodiazepine receptors in rat brain characterized by high-affinity (3H)diazepam binding*. Proc Natl Acad Sci U S A, 1977. **74**(9): p. 3805-9.
2. Hardwick, M., et al., *Peripheral-type benzodiazepine receptor (PBR) in human breast cancer: correlation of breast cancer cell aggressive phenotype with PBR expression, nuclear localization, and PBR-mediated cell proliferation and nuclear transport of cholesterol*. Cancer Res, 1999. **59**(4): p. 831-42.
3. Batarseh, A. and V. Papadopoulos, *Regulation of translocator protein 18 kDa (TSPO) expression in health and disease states*. Mol Cell Endocrinol, 2010. **327**(1-2): p. 1-12.
4. Miettinen, H., et al., *Expression of peripheral-type benzodiazepine receptor and diazepam binding inhibitor in human astrocytomas: relationship to cell proliferation*. Cancer Res, 1995. **55**(12): p. 2691-5.
5. Cosenza-Nashat, M., et al., *Expression of the translocator protein of 18 kDa by microglia, macrophages and astrocytes based on immunohistochemical localization in abnormal human brain*. Neuropathology and applied neurobiology, 2009. **35**(3): p. 306-328.
6. Yasuno, F., et al., *Increased binding of peripheral benzodiazepine receptor in Alzheimer's disease measured by positron emission tomography with [¹¹C]DAA1106*. Biol Psychiatry, 2008. **64**(10): p. 835-41.
7. Werry, E.L., et al., *Recent Developments in TSPO PET Imaging as A Biomarker of Neuroinflammation in Neurodegenerative Disorders*. Int J Mol Sci, 2019. **20**(13).
8. Su, Z., et al., *The 18-kDa mitochondrial translocator protein in human gliomas: an ¹¹C-(R)PK11195 PET imaging and neuropathology study*. J Nucl Med, 2015. **56**(4): p. 512-7.
9. Dupont, A.-C., et al., *Translocator Protein-18 kDa (TSPO) Positron Emission Tomography (PET) Imaging and Its Clinical Impact in Neurodegenerative Diseases*. International journal of molecular sciences, 2017. **18**(4): p. 785.
10. Vowinckel, E., et al., *PK11195 binding to the peripheral benzodiazepine receptor as a marker of microglia activation in multiple sclerosis and experimental autoimmune encephalomyelitis*. J Neurosci Res, 1997. **50**(2): p. 345-53.
11. Chang, Y.J., et al., *The human "peripheral-type" benzodiazepine receptor: regional mapping of the gene and characterization of the receptor expressed from cDNA*. DNA Cell Biol, 1992. **11**(6): p. 471-80.
12. Riond, J., et al., *Molecular cloning and chromosomal localization of a human peripheral-type benzodiazepine receptor*. Eur J Biochem, 1991. **195**(2): p. 305-11.
13. Lin, D., et al., *The human peripheral benzodiazepine receptor gene: cloning and characterization of alternative splicing in normal tissues and in a patient with congenital lipoid adrenal hyperplasia*. Genomics, 1993. **18**(3): p. 643-50.

14. Giatzakis, C. and V. Papadopoulos, *Differential utilization of the promoter of peripheral-type benzodiazepine receptor by steroidogenic versus nonsteroidogenic cell lines and the role of Sp1 and Sp3 in the regulation of basal activity*. *Endocrinology*, 2004. **145**(3): p. 1113-23.
15. *proteinatlas.org*.
16. Bernassau, J.M., et al., *A 3D model of the peripheral benzodiazepine receptor and its implication in intra mitochondrial cholesterol transport*. *Journal of Molecular Graphics*, 1993. **11**(4): p. 236-244.
17. Riond, J., et al., *Expression and pharmacological characterization of the human peripheral-type benzodiazepine receptor in yeast*. *Eur J Pharmacol*, 1991. **208**(4): p. 307-12.
18. Fan, J., et al., *Structural and functional evolution of the translocator protein (18 kDa)*. *Curr Mol Med*, 2012. **12**(4): p. 369-86.
19. Selvaraj, V. and D.M. Stocco, *The changing landscape in translocator protein (TSPO) function*. *Trends Endocrinol Metab*, 2015. **26**(7): p. 341-8.
20. Ginter, C., I. Kiburu, and O. Boudker, *Chemical Catalysis by the Translocator Protein (18 kDa)*. *Biochemistry*, 2013. **52**(21): p. 3609-3611.
21. Owen, D.R., et al., *Mixed-affinity binding in humans with 18-kDa translocator protein ligands*. *J Nucl Med*, 2011. **52**(1): p. 24-32.
22. Owen, D.R., et al., *An 18-kDa translocator protein (TSPO) polymorphism explains differences in binding affinity of the PET radioligand PBR28*. *J Cereb Blood Flow Metab*, 2012. **32**(1): p. 1-5.
23. Milenkovic, V.M., et al., *Effects of genetic variants in the TSPO gene on protein structure and stability*. *PloS one*, 2018. **13**(4): p. e0195627-e0195627.
24. Kunduzova, O.R., et al., *Involvement of peripheral benzodiazepine receptor in the oxidative stress, death-signaling pathways, and renal injury induced by ischemia-reperfusion*. *J Am Soc Nephrol*, 2004. **15**(8): p. 2152-60.
25. Jordà, E.G., et al., *Evidence in favour of a role for peripheral-type benzodiazepine receptor ligands in amplification of neuronal apoptosis*. *Apoptosis*, 2005. **10**(1): p. 91-104.
26. Selvaraj, V., D.M. Stocco, and L.N. Tu, *Minireview: translocator protein (TSPO) and steroidogenesis: a reappraisal*. *Mol Endocrinol*, 2015. **29**(4): p. 490-501.
27. Budelier, M.M., et al., *Photoaffinity labeling with cholesterol analogues precisely maps a cholesterol-binding site in voltage-dependent anion channel-1*. *J Biol Chem*, 2017. **292**(22): p. 9294-9304.
28. Bogan, R.L., T.L. Davis, and G.D. Niswender, *Peripheral-type benzodiazepine receptor (PBR) aggregation and absence of steroidogenic acute regulatory protein (StAR)/PBR association in the mitochondrial membrane as determined by bioluminescence resonance energy transfer (BRET)*. *J Steroid Biochem Mol Biol*, 2007. **104**(1-2): p. 61-7.
29. Fan, J., et al., *Conditional steroidogenic cell-targeted deletion of TSPO unveils a crucial role in viability and hormone-dependent steroid formation*. *Proc Natl Acad Sci U S A*, 2015. **112**(23): p. 7261-6.
30. Rone, M.B., et al., *Identification of a dynamic mitochondrial protein complex driving cholesterol import, trafficking, and metabolism to steroid hormones*. *Mol Endocrinol*, 2012. **26**(11): p. 1868-82.

31. Selvaraj, V., D.M. Stocco, and B.J. Clark, *Current knowledge on the acute regulation of steroidogenesis*. Biology of Reproduction, 2018. **99**(1): p. 13-26.
32. Zirkin, B.R. and V. Papadopoulos, *Leydig cells: formation, function, and regulation*. Biology of Reproduction, 2018. **99**(1): p. 101-111.
33. Shoshan-Barmatz, V., E.N. Maldonado, and Y. Krelin, *VDAC1 at the crossroads of cell metabolism, apoptosis and cell stress*. Cell Stress, 2017. **1**(1): p. 11-36.
34. Baines, C.P., et al., *Voltage-dependent anion channels are dispensable for mitochondrial-dependent cell death*. Nat Cell Biol, 2007. **9**(5): p. 550-5.
35. Kokoszka, J.E., et al., *The ADP/ATP translocator is not essential for the mitochondrial permeability transition pore*. Nature, 2004. **427**(6973): p. 461-5.
36. Madesh, M. and G. Hajnóczky, *VDAC-dependent permeabilization of the outer mitochondrial membrane by superoxide induces rapid and massive cytochrome c release*. J Cell Biol, 2001. **155**(6): p. 1003-15.
37. Arif, T., et al., *Rewiring of Cancer Cell Metabolism by Mitochondrial VDAC1 Depletion Results in Time-Dependent Tumor Reprogramming: Glioblastoma as a Proof of Concept*. Cells, 2019. **8**(11): p. 1330.
38. Shoshan-Barmatz, V., S. Pittala, and D. Mizrahi, *VDAC1 and the TSPO: Expression, Interactions, and Associated Functions in Health and Disease States*. Int J Mol Sci, 2019. **20**(13).
39. Aghazadeh, Y., et al., *Induction of androgen formation in the male by a TAT-VDAC1 fusion peptide blocking 14-3-3 ϵ protein adaptor and mitochondrial VDAC1 interactions*. Mol Ther, 2014. **22**(10): p. 1779-91.
40. Gatliff, J., et al., *TSPO interacts with VDAC1 and triggers a ROS-mediated inhibition of mitochondrial quality control*. Autophagy, 2014. **10**(12): p. 2279-96.
41. Veenman, L., Y. Shandalov, and M. Gavish, *VDAC activation by the 18 kDa translocator protein (TSPO), implications for apoptosis*. Journal of Bioenergetics and Biomembranes, 2008. **40**(3): p. 199-205.
42. Loth, M.K., et al., *A Novel Interaction of Translocator Protein 18 kDa (TSPO) with NADPH Oxidase in Microglia*. Molecular Neurobiology, 2020.
43. Delavoie, F., et al., *In vivo and in vitro peripheral-type benzodiazepine receptor polymerization: functional significance in drug ligand and cholesterol binding*. Biochemistry, 2003. **42**(15): p. 4506-19.
44. Jaremko, L., et al., *Structure of the mitochondrial translocator protein in complex with a diagnostic ligand*. Science, 2014. **343**(6177): p. 1363-6.
45. Fantini, J. and F.J. Barrantes, *How cholesterol interacts with membrane proteins: an exploration of cholesterol-binding sites including CRAC, CARC, and tilted domains*. Front Physiol, 2013. **4**: p. 31.
46. Korkhov, V.M., et al., *Three-dimensional structure of TspO by electron cryomicroscopy of helical crystals*. Structure, 2010. **18**(6): p. 677-87.
47. Yeliseev, A.A. and S. Kaplan, *TspO of rhodobacter sphaeroides. A structural and functional model for the mammalian peripheral benzodiazepine receptor*. J Biol Chem, 2000. **275**(8): p. 5657-67.
48. Li, F., et al., *Protein structure. Crystal structures of translocator protein (TSPO) and mutant mimic of a human polymorphism*. Science (New York, N.Y.), 2015. **347**(6221): p. 555-558.

49. Guo, Y., et al., *Structure and activity of tryptophan-rich TSPO proteins*. Science, 2015. **347**(6221): p. 551.
50. Guo, Y., *Be Cautious with Crystal Structures of Membrane Proteins or Complexes Prepared in Detergents*. Crystals, 2020. **10**(2): p. 86.
51. Papadopoulos, V., et al., *Translocator protein (18kDa): new nomenclature for the peripheral-type benzodiazepine receptor based on its structure and molecular function*. Trends Pharmacol Sci, 2006. **27**(8): p. 402-9.
52. Gavish, M., et al., *Enigma of the peripheral benzodiazepine receptor*. Pharmacol Rev, 1999. **51**(4): p. 629-50.
53. A Verma, a. and S.H. Snyder, *Peripheral Type Benzodiazepine Receptors*. Annual Review of Pharmacology and Toxicology, 1989. **29**(1): p. 307-322.
54. Papadopoulos, V., et al., *Peripheral-type benzodiazepine receptor in neurosteroid biosynthesis, neuropathology and neurological disorders*. Neuroscience, 2006. **138**(3): p. 749-56.
55. Benavides, J., et al., *"Peripheral type" benzodiazepine binding sites in rat adrenals: binding studies with [3H]PK 11195 and autoradiographic localization*. Arch Int Pharmacodyn Ther, 1983. **266**(1): p. 38-49.
56. Le Fur, G., et al., *Differentiation between two ligands for peripheral benzodiazepine binding sites, [3H]R05-4864 and [3H]PK 11195, by thermodynamic studies*. Life Sciences, 1983. **33**(5): p. 449-457.
57. Benavides, J., et al., *In vivo labelling in several rat tissues of 'peripheral type' benzodiazepine binding sites*. Eur J Pharmacol, 1984. **99**(1): p. 1-7.
58. Wang, J.K., T. Taniguchi, and S. Spector, *Properties of [3H]diazepam binding sites on rat blood platelets*. Life Sci, 1980. **27**(20): p. 1881-8.
59. Schoemaker, H., et al., *Specific high-affinity binding sites for [3H]Ro 5-4864 in rat brain and kidney*. J Pharmacol Exp Ther, 1983. **225**(1): p. 61-9.
60. Zeno, S., et al., *The 18 kDa mitochondrial translocator protein (TSPO) prevents accumulation of protoporphyrin IX. Involvement of reactive oxygen species (ROS)*. Curr Mol Med, 2012. **12**(4): p. 494-501.
61. Veenman, L., et al., *Tetrapyrroles as Endogenous TSPO Ligands in Eukaryotes and Prokaryotes: Comparisons with Synthetic Ligands*. Int J Mol Sci, 2016. **17**(6).
62. Wu, Y., et al., *Rasagiline and selegiline suppress calcium efflux from mitochondria by PK11195-induced opening of mitochondrial permeability transition pore: a novel anti-apoptotic function for neuroprotection*. Journal of neural transmission (Vienna, Austria : 1996), 2015. **122**(10): p. 1399-1407.
63. Azarashvili, T., et al., *The peripheral-type benzodiazepine receptor is involved in control of Ca²⁺-induced permeability transition pore opening in rat brain mitochondria*. Cell Calcium, 2007. **42**(1): p. 27-39.
64. Kugler, W., et al., *Ligands of the mitochondrial 18 kDa translocator protein attenuate apoptosis of human glioblastoma cells exposed to erucylphosphocholine*. Cell Oncol, 2008. **30**(5): p. 435-50.
65. Rosenberg, N., et al., *In vitro effect of FGIN-1-27, a ligand to 18 kDa mitochondrial translocator protein, in human osteoblast-like cells*. J Bioenerg Biomembr, 2014. **46**(3): p. 197-204.
66. Pellow, S. and S.E. File, *Behavioural actions of Ro 5-4864: a peripheral-type benzodiazepine?* Life Sci, 1984. **35**(3): p. 229-40.

67. Lee, D.H., et al., *Effects of peripheral benzodiazepine receptor ligands on proliferation and differentiation of human mesenchymal stem cells*. J Cell Physiol, 2004. **198**(1): p. 91-9.
68. Kuhlmann, A.C. and T.R. Guilarte, *Regional and temporal expression of the peripheral benzodiazepine receptor in MPTP neurotoxicity*. Toxicol Sci, 1999. **48**(1): p. 107-16.
69. Chen, M.K., et al., *Peripheral benzodiazepine receptor imaging in CNS demyelination: functional implications of anatomical and cellular localization*. Brain, 2004. **127**(Pt 6): p. 1379-92.
70. Veenman, L. and M. Gavish, *The peripheral-type benzodiazepine receptor and the cardiovascular system. Implications for drug development*. Pharmacol Ther, 2006. **110**(3): p. 503-24.
71. Doorduyn, J., et al., *PET imaging of the peripheral benzodiazepine receptor: monitoring disease progression and therapy response in neurodegenerative disorders*. Curr Pharm Des, 2008. **14**(31): p. 3297-315.
72. Fujimura, Y., et al., *Increased peripheral benzodiazepine receptors in arterial plaque of patients with atherosclerosis: an autoradiographic study with [(3)H]PK 11195*. Atherosclerosis, 2008. **201**(1): p. 108-11.
73. Laitinen, I., et al., *Uptake of inflammatory cell marker [11C]PK11195 into mouse atherosclerotic plaques*. Eur J Nucl Med Mol Imaging, 2009. **36**(1): p. 73-80.
74. Scarf, A.M. and M. Kassiou, *The translocator protein*. J Nucl Med, 2011. **52**(5): p. 677-80.
75. Liu, G.-J., et al., *The 18 kDa Translocator Protein, Microglia and Neuroinflammation*. Brain Pathology, 2014. **24**.
76. Surinkaew, S., S. Chattipakorn, and N. Chattipakorn, *Roles of mitochondrial benzodiazepine receptor in the heart*. Can J Cardiol, 2011. **27**(2): p. 262.e3 -13.
77. Benavides, J., et al., *Labelling of "Peripheral-Type" Benzodiazepine Binding Sites in the Rat Brain By Using [3 H]PK 11195, an Isoquinoline Carboxamide Derivative: Kinetic Studies and Autoradiographic Localization*. Journal of neurochemistry, 1984. **41**: p. 1744-50.
78. Gehlert, D.R., H.I. Yamamura, and J.K. Wamsley, *Autoradiographic localization of 'peripheral' benzodiazepine binding sites in the rat brain and kidney using [3H]RO5-4864*. Eur J Pharmacol, 1983. **95**(3-4): p. 329-30.
79. Anholt, R.R., et al., *Peripheral-type benzodiazepine receptors in the central nervous system: localization to olfactory nerves*. J Neurosci, 1984. **4**(2): p. 593-603.
80. Veenman, L. and M. Gavish, *Peripheral-type benzodiazepine receptors: Their implication in brain disease*. Drug Development Research, 2000. **50**(3-4): p. 355-370.
81. Chen, M.-K. and T.R. Guilarte, *Translocator protein 18 kDa (TSPO): Molecular sensor of brain injury and repair*. Pharmacology & Therapeutics, 2008. **118**(1): p. 1-17.
82. Papadopoulos, V. and L. Lecanu, *Translocator protein (18 kDa) TSPO: an emerging therapeutic target in neurotrauma*. Exp Neurol, 2009. **219**(1): p. 53-7.
83. Rupprecht, R., et al., *Translocator protein (18 kDa) (TSPO) as a therapeutic target for neurological and psychiatric disorders*. Nat Rev Drug Discov, 2010. **9**(12): p. 971-88.

84. Werry, E.L., et al., *Recent Developments in TSPO PET Imaging as A Biomarker of Neuroinflammation in Neurodegenerative Disorders*. International journal of molecular sciences, 2019. **20**(13): p. 3161.
85. Maeda, J., et al., *Phase-dependent roles of reactive microglia and astrocytes in nervous system injury as delineated by imaging of peripheral benzodiazepine receptor*. Brain Research, 2007. **1157**: p. 100-111.
86. Trapani, A., et al., *Targeting of the Translocator Protein 18 kDa (TSPO): A Valuable Approach for Nuclear and Optical Imaging of Activated Microglia*. Bioconjugate Chemistry, 2013. **24**(9): p. 1415-1428.
87. Lee, Y., et al., *Translocator protein (TSPO): the new story of the old protein in neuroinflammation*. BMB Rep, 2020. **53**(1): p. 20-27.
88. Cosenza-Nashat, M., et al., *Expression of the translocator protein of 18 kDa by microglia, macrophages and astrocytes based on immunohistochemical localization in abnormal human brain*. Neuropathology and Applied Neurobiology, 2009. **35**(3): p. 306-328.
89. Han, Z., et al., *Expression of peripheral benzodiazepine receptor (PBR) in human tumors: relationship to breast, colorectal, and prostate tumor progression*. J Recept Signal Transduct Res, 2003. **23**(2-3): p. 225-38.
90. Katz, Y., et al., *Dramatic increase in peripheral benzodiazepine binding sites in human colonic adenocarcinoma as compared to normal colon*. Eur J Pharmacol, 1988. **148**(3): p. 483-4.
91. Katz, Y., et al., *Increased density of peripheral benzodiazepine-binding sites in ovarian carcinomas as compared with benign ovarian tumours and normal ovaries*. Clin Sci (Lond), 1990. **78**(2): p. 155-8.
92. Venturini, I., et al., *Up-regulation of peripheral benzodiazepine receptor system in hepatocellular carcinoma*. Life Sci, 1998. **63**(14): p. 1269-80.
93. Beinlich, A., et al., *Relation of cell proliferation to expression of peripheral benzodiazepine receptors in human breast cancer cell lines*. Biochem Pharmacol, 2000. **60**(3): p. 397-402.
94. Vlodaysky, E. and J.F. Soustiel, *Immunohistochemical expression of peripheral benzodiazepine receptors in human astrocytomas and its correlation with grade of malignancy, proliferation, apoptosis and survival*. J Neurooncol, 2007. **81**(1): p. 1-7.
95. Hardwick, M., et al., *Peripheral-type benzodiazepine receptor (PBR) gene amplification in MDA-MB-231 aggressive breast cancer cells*. Cancer Genet Cytogenet, 2002. **139**(1): p. 48-51.
96. Papadopoulos, V., et al., *Drug-induced inhibition of the peripheral-type benzodiazepine receptor expression and cell proliferation in human breast cancer cells*. Anticancer Res, 2000. **20**(5a): p. 2835-47.
97. Hardwick, M., et al., *Peripheral-type benzodiazepine receptor levels correlate with the ability of human breast cancer MDA-MB-231 cell line to grow in SCID mice*. Int J Cancer, 2001. **94**(3): p. 322-7.
98. Bhoola, N.H., et al., *Translocator Protein (TSPO) as a Potential Biomarker in Human Cancers*. Int J Mol Sci, 2018. **19**(8).
99. Starosta-Rubinstein, S., et al., *Imaging of a glioma using peripheral benzodiazepine receptor ligands*. Proc Natl Acad Sci U S A, 1987. **84**(3): p. 891-5.

100. Syapin, P.J. and P. Skolnick, *CHARACTERIZATION OF BENZODIAZEPINE BINDING SITES IN CULTURED CELLS OF NEURAL ORIGIN*. Journal of Neurochemistry, 1979. **32**(3): p. 1047-1051.
101. Anholt, R.R., et al., *Peripheral-type benzodiazepine receptors: autoradiographic localization in whole-body sections of neonatal rats*. J Pharmacol Exp Ther, 1985. **233**(2): p. 517-26.
102. Black, K.L., et al., *Specific high-affinity binding of peripheral benzodiazepine receptor ligands to brain tumors in rat and man*. Cancer, 1990. **65**(1): p. 93-7.
103. Miyazawa, N., E. Hamel, and M. Diksic, *Assessment of the peripheral benzodiazepine receptors in human gliomas by two methods*. J Neurooncol, 1998. **38**(1): p. 19-26.
104. Veenman, L., et al., *Peripheral-type benzodiazepine receptor density and in vitro tumorigenicity of glioma cell lines*. Biochem Pharmacol, 2004. **68**(4): p. 689-98.
105. Rechichi, M., et al., *TSPO over-expression increases motility, transmigration and proliferation properties of C6 rat glioma cells*. Biochim Biophys Acta, 2008. **1782**(2): p. 118-25.
106. Cornu, P., et al., *Increase in omega 3 (peripheral-type benzodiazepine) binding site densities in different types of human brain tumours. A quantitative autoradiography study*. Acta Neurochir (Wien), 1992. **119**(1-4): p. 146-52.
107. Woods, M.J., D.M. Zisterer, and D.C. Williams, *Two cellular and subcellular locations for the peripheral-type benzodiazepine receptor in rat liver*. Biochem Pharmacol, 1996. **51**(10): p. 1283-92.
108. Olson, J.M., et al., *Presence of peripheral-type benzodiazepine binding sites on human erythrocyte membranes*. Eur J Pharmacol, 1988. **152**(1-2): p. 47-53.
109. Brown, R.C., et al., *Location-dependent role of the human glioma cell peripheral-type benzodiazepine receptor in proliferation and steroid biosynthesis*. Cancer Lett, 2000. **156**(2): p. 125-32.
110. Banati, R.B., et al., *Positron emission tomography and functional characterization of a complete PBR/TSPO knockout*. Nat Commun, 2014. **5**: p. 5452.
111. Fu, Y., et al., *TSPO deficiency induces mitochondrial dysfunction, leading to hypoxia, angiogenesis, and a growth-promoting metabolic shift toward glycolysis in glioblastoma*. Neuro Oncol, 2020. **22**(2): p. 240-252.
112. Verma, A., J.S. Nye, and S.H. Snyder, *Porphyrins are endogenous ligands for the mitochondrial (peripheral-type) benzodiazepine receptor*. Proc Natl Acad Sci U S A, 1987. **84**(8): p. 2256-60.
113. Campanella, M., G. Szabadkai, and R. Rizzuto, *Modulation of intracellular Ca²⁺ signalling in HeLa cells by the apoptotic cell death enhancer PK11195*. Biochem Pharmacol, 2008. **76**(11): p. 1628-36.
114. Veenman, L., et al., *Potential involvement of F0F1-ATP(synth)ase and reactive oxygen species in apoptosis induction by the antineoplastic agent erucylphosphohomocholine in glioblastoma cell lines : a mechanism for induction of apoptosis via the 18 kDa mitochondrial translocator protein*. Apoptosis, 2010. **15**(7): p. 753-68.
115. Caballero, B., L. Veenman, and M. Gavish, *Role of Mitochondrial Translocator Protein (18 kDa) on Mitochondrial- Related Cell Death Processes*. Recent patents on endocrine, metabolic & immune drug discovery, 2013. **7**.

116. Veenman, L., M. Gavish, and W. Kugler, *Apoptosis induction by erucylphosphocholine via the 18 kDa mitochondrial translocator protein: implications for cancer treatment*. *Anticancer Agents Med Chem*, 2014. **14**(4): p. 559-77.
117. Chelli, B., et al., *Peripheral-type benzodiazepine receptor ligands: mitochondrial permeability transition induction in rat cardiac tissue*. *Biochem Pharmacol*, 2001. **61**(6): p. 695-705.
118. Li, J., J. Wang, and Y. Zeng, *Peripheral benzodiazepine receptor ligand, PK11195 induces mitochondria cytochrome c release and dissipation of mitochondria potential via induction of mitochondria permeability transition*. *Eur J Pharmacol*, 2007. **560**(2-3): p. 117-22.
119. Weisinger, G., et al., *Peripheral benzodiazepine receptor antisense knockout increases tumorigenicity of MA-10 Leydig cells in vivo and in vitro*. *Biochemistry*, 2004. **43**(38): p. 12315-21.
120. Liu, J., M. Rone, and V. Papadopoulos, *Protein-Protein Interactions Mediate Mitochondrial Cholesterol Transport and Steroid Biosynthesis*. *The Journal of biological chemistry*, 2007. **281**: p. 38879-93.
121. Lacapère, J.J. and V. Papadopoulos, *Peripheral-type benzodiazepine receptor: structure and function of a cholesterol-binding protein in steroid and bile acid biosynthesis*. *Steroids*, 2003. **68**(7-8): p. 569-85.
122. Kelly-HersHKovitz, E., et al., *Effects of peripheral-type benzodiazepine receptor antisense knockout on MA-10 Leydig cell proliferation and steroidogenesis*. *J Biol Chem*, 1998. **273**(10): p. 5478-83.
123. Hauet, T., et al., *Peripheral-type benzodiazepine receptor-mediated action of steroidogenic acute regulatory protein on cholesterol entry into leydig cell mitochondria*. *Mol Endocrinol*, 2005. **19**(2): p. 540-54.
124. Owen, D.R., et al., *TSPO mutations in rats and a human polymorphism impair the rate of steroid synthesis*. *Biochem J*, 2017. **474**(23): p. 3985-3999.
125. Barron, A.M., et al., *Steroidogenic abnormalities in translocator protein knockout mice and significance in the aging male*. *Biochem J*, 2018. **475**(1): p. 75-85.
126. Morohaku, K., et al., *Translocator protein/peripheral benzodiazepine receptor is not required for steroid hormone biosynthesis*. *Endocrinology*, 2014. **155**(1): p. 89-97.
127. Tu, L.N., et al., *Peripheral benzodiazepine receptor/translocator protein global knock-out mice are viable with no effects on steroid hormone biosynthesis*. *J Biol Chem*, 2014. **289**(40): p. 27444-54.
128. Šileikytė, J., et al., *Regulation of the mitochondrial permeability transition pore by the outer membrane does not involve the peripheral benzodiazepine receptor (Translocator Protein of 18 kDa (TSPO))*. *J Biol Chem*, 2014. **289**(20): p. 13769-81.
129. Wang, H., et al., *Global Deletion of TSPO Does Not Affect the Viability and Gene Expression Profile*. *PLoS One*, 2016. **11**(12): p. e0167307.
130. Beinlich, A., et al., *Specific binding of benzodiazepines to human breast cancer cell lines*. *Life Sci*, 1999. **65**(20): p. 2099-108.
131. Sanger, N., et al., *Cell cycle-related expression and ligand binding of peripheral benzodiazepine receptor in human breast cancer cell lines*. *Eur J Cancer*, 2000. **36**(16): p. 2157-63.

132. Carmel, I., et al., *Peripheral-type benzodiazepine receptors in the regulation of proliferation of MCF-7 human breast carcinoma cell line*. *Biochem Pharmacol*, 1999. **58**(2): p. 273-8.
133. Li, W., et al., *Peripheral-type benzodiazepine receptor overexpression and knockdown in human breast cancer cells indicate its prominent role in tumor cell proliferation*. *Biochem Pharmacol*, 2007. **73**(4): p. 491-503.
134. Ikezaki, K. and K.L. Black, *Stimulation of cell growth and DNA synthesis by peripheral benzodiazepine*. *Cancer Lett*, 1990. **49**(2): p. 115-20.
135. Garnier, M., et al., *Diazepam binding inhibitor is a paracrine/autocrine regulator of Leydig cell proliferation and steroidogenesis: action via peripheral-type benzodiazepine receptor and independent mechanisms*. *Endocrinology*, 1993. **132**(1): p. 444-58.
136. Bode, J., et al., *The 18 kDa translocator protein influences angiogenesis, as well as aggressiveness, adhesion, migration, and proliferation of glioblastoma cells*. *Pharmacogenet Genomics*, 2012. **22**(7): p. 538-50.
137. Levin, E., et al., *The Peripheral-Type Benzodiazepine Receptor and Tumorigenicity: Isoquinoline Binding Protein (IBP) Antisense Knockdown in the C6 Glioma Cell Line*. *Biochemistry*, 2005. **44**(29): p. 9924-9935.
138. Carayon, P., et al., *Involvement of peripheral benzodiazepine receptors in the protection of hematopoietic cells against oxygen radical damage*. *Blood*, 1996. **87**(8): p. 3170-8.
139. Stoebner, P.E., et al., *Transient protection by peripheral benzodiazepine receptors during the early events of ultraviolet light-induced apoptosis*. *Cell Death Differ*, 2001. **8**(7): p. 747-53.
140. Guilarte, T.R., M.K. Loth, and S.R. Guariglia, *TSPO Finds NOX2 in Microglia for Redox Homeostasis*. *Trends in pharmacological sciences*, 2016. **37**(5): p. 334-343.
141. Simpson, D.S.A. and P.L. Oliver, *ROS Generation in Microglia: Understanding Oxidative Stress and Inflammation in Neurodegenerative Disease*. *Antioxidants (Basel, Switzerland)*, 2020. **9**(8): p. 743.
142. Rashid, K., et al., *Transcriptional regulation of Translocator protein (18 kDa) (TSPO) in microglia requires Pu.1, Ap1 and Sp factors*. *Biochim Biophys Acta Gene Regul Mech*, 2018. **1861**(12): p. 1119-1133.
143. Batarseh, A., J. Li, and V. Papadopoulos, *Protein Kinase Cε Regulation of Translocator Protein (18 kDa) Tspo Gene Expression Is Mediated through a MAPK Pathway Targeting STAT3 and c-Jun Transcription Factors*. *Biochemistry*, 2010. **49**: p. 4766-78.
144. Batarseh, A., C. Giatzakis, and V. Papadopoulos, *Phorbol-12-myristate 13-acetate acting through protein kinase Cε induces translocator protein (18-kDa) TSPO gene expression*. *Biochemistry*, 2008. **47**(48): p. 12886-99.
145. Garczarczyk, D., et al., *Signal transduction of constitutively active protein kinase C ε*. *Cell Signal*, 2009. **21**(5): p. 745-52.
146. Bird, A., *DNA methylation patterns and epigenetic memory*. *Genes Dev*, 2002. **16**(1): p. 6-21.
147. Jones, P.A. and P.W. Laird, *Cancer epigenetics comes of age*. *Nat Genet*, 1999. **21**(2): p. 163-7.

148. Moore, L., T. Le, and G. Fan, *DNA Methylation and Its Basic Function*. Neuropsychopharmacology : official publication of the American College of Neuropsychopharmacology, 2012. **38**.
149. Takai, D. and P.A. Jones, *Comprehensive analysis of CpG islands in human chromosomes 21 and 22*. Proc Natl Acad Sci U S A, 2002. **99**(6): p. 3740-5.
150. Egger, G., et al., *Epigenetics in human disease and prospects for epigenetic therapy*. Nature, 2004. **429**(6990): p. 457-63.
151. Toyota, M., et al., *CpG island methylator phenotype in colorectal cancer*. Proc Natl Acad Sci U S A, 1999. **96**(15): p. 8681-6.
152. Rivera, A., et al., *MGMT promoter methylation is predictive of response to radiotherapy and prognostic in the absence of adjuvant alkylating chemotherapy for glioblastoma*. Neuro-oncology, 2010. **12**: p. 116-21.
153. Esteller, M., et al., *Promoter hypermethylation and BRCA1 inactivation in sporadic breast and ovarian tumors*. J Natl Cancer Inst, 2000. **92**(7): p. 564-9.
154. Shigeyasu, K., et al., *Clinical Significance of MLH1 Methylation and CpG Island Methylator Phenotype as Prognostic Markers in Patients with Gastric Cancer*. PLoS One, 2015. **10**(6): p. e0130409.
155. Lind, G.E., et al., *A CpG island hypermethylation profile of primary colorectal carcinomas and colon cancer cell lines*. Molecular Cancer, 2004. **3**(1): p. 28.
156. Middleton, R.J., et al., *Epigenetic Silencing of the Human 18 kDa Translocator Protein in a T Cell Leukemia Cell Line*. DNA Cell Biol, 2017. **36**(2): p. 103-108.
157. Batarseh, A., et al., *Functional characterization of the human translocator protein (18kDa) gene promoter in human breast cancer cell lines*. Biochim Biophys Acta, 2012. **1819**(1): p. 38-56.
158. Zhu, Y. and L.F. Parada, *The molecular and genetic basis of neurological tumours*. Nat Rev Cancer, 2002. **2**(8): p. 616-26.
159. Ostrom, Q.T., et al., *CBTRUS Statistical Report: Primary Brain and Central Nervous System Tumors Diagnosed in the United States in 2007–2011*. Neuro-Oncology, 2014. **16**(suppl_4): p. iv1-iv63.
160. Louis, D.N., et al., *The 2016 World Health Organization Classification of Tumors of the Central Nervous System: a summary*. Acta Neuropathol, 2016. **131**(6): p. 803-20.
161. Cohen, A.L., S.L. Holmen, and H. Colman, *IDH1 and IDH2 mutations in gliomas*. Current neurology and neuroscience reports, 2013. **13**(5): p. 345-345.
162. Yan, H., et al., *IDH1 and IDH2 mutations in gliomas*. N Engl J Med, 2009. **360**(8): p. 765-73.
163. Koschmann, C., et al., *ATRX Loss Promotes Tumor Growth and Impairs Non-Homologous End Joining DNA Repair in Glioma*. Science translational medicine, 2016. **8**: p. 328ra28-328ra28.
164. Komori, T., *The 2016 WHO Classification of Tumours of the Central Nervous System: The Major Points of Revision*. Neurologia medico-chirurgica, 2017. **57**(7): p. 301-311.
165. Malzkorn, B., et al., *Unraveling the glioma epigenome: from molecular mechanisms to novel biomarkers and therapeutic targets*. Brain Pathol, 2011. **21**(6): p. 619-32.
166. Fueyo, J., et al., *Hypermethylation of the CpG island of p16/CDKN2 correlates with gene inactivation in gliomas*. Oncogene, 1996. **13**(8): p. 1615-9.
167. Park, S.H., et al., *5' CpG island methylation of p16 is associated with absence of p16 expression in glioblastomas*. J Korean Med Sci, 2000. **15**(5): p. 555-9.

168. Jesionek-Kupnicka, D., et al., *TP53 promoter methylation in primary glioblastoma: relationship with TP53 mRNA and protein expression and mutation status*. DNA Cell Biol, 2014. **33**(4): p. 217-26.
169. Costello, J.F., et al., *Silencing of p16/CDKN2 expression in human gliomas by methylation and chromatin condensation*. Cancer Res, 1996. **56**(10): p. 2405-10.
170. Esteller, M., et al., *Inactivation of the DNA-repair gene MGMT and the clinical response of gliomas to alkylating agents*. N Engl J Med, 2000. **343**(19): p. 1350-4.
171. Dong, S.M., et al., *Concurrent hypermethylation of multiple genes is associated with grade of oligodendroglial tumors*. J Neuropathol Exp Neurol, 2001. **60**(8): p. 808-16.
172. Capper, D., et al., *DNA methylation-based classification of central nervous system tumours*. Nature, 2018. **555**(7697): p. 469-474.
173. Christensen, B.C., et al., *DNA methylation, isocitrate dehydrogenase mutation, and survival in glioma*. J Natl Cancer Inst, 2011. **103**(2): p. 143-53.
174. de Souza, C.F., et al., *A Distinct DNA Methylation Shift in a Subset of Glioma CpG Island Methylator Phenotypes during Tumor Recurrence*. Cell Rep, 2018. **23**(2): p. 637-651.
175. Laffaire, J., et al., *Methylation profiling identifies 2 groups of gliomas according to their tumorigenesis*. Neuro Oncol, 2011. **13**(1): p. 84-98.
176. Noushmehr, H., et al., *Identification of a CpG island methylator phenotype that defines a distinct subgroup of glioma*. Cancer Cell, 2010. **17**(5): p. 510-22.
177. Sturm, D., et al., *Hotspot mutations in H3F3A and IDH1 define distinct epigenetic and biological subgroups of glioblastoma*. Cancer Cell, 2012. **22**(4): p. 425-37.
178. Laffaire, J., et al., *Methylation profiling identifies 2 groups of gliomas according to their tumorigenesis*. Neuro-oncology, 2011. **13**(1): p. 84-98.
179. Turcan, S., et al., *IDH1 mutation is sufficient to establish the glioma hypermethylator phenotype*. Nature, 2012. **483**(7390): p. 479-83.
180. Xu, W., et al., *Oncometabolite 2-hydroxyglutarate is a competitive inhibitor of α -ketoglutarate-dependent dioxygenases*. Cancer Cell, 2011. **19**(1): p. 17-30.
181. Dang, L., et al., *Cancer-associated IDH1 mutations produce 2-hydroxyglutarate*. Nature, 2009. **462**(7274): p. 739-44.
182. Reifenberger, G., et al., *Molecular characterization of long-term survivors of glioblastoma using genome- and transcriptome-wide profiling*. Int J Cancer, 2014. **135**(8): p. 1822-31.
183. Ceccarelli, M., et al., *Molecular Profiling Reveals Biologically Discrete Subsets and Pathways of Progression in Diffuse Glioma*. Cell, 2016. **164**(3): p. 550-63.
184. Watanabe, T., et al., *Promoter hypermethylation and homozygous deletion of the p14ARF and p16INK4a genes in oligodendrogliomas*. Acta Neuropathol, 2001. **101**(3): p. 185-9.
185. Velnar, T., et al., *Genetic markers in oligodendroglial tumours*. Radiol Oncol, 2010. **44**(1): p. 13-8.
186. Ahmed, R., et al., *Malignant gliomas: current perspectives in diagnosis, treatment, and early response assessment using advanced quantitative imaging methods*. Cancer Manag Res, 2014. **6**: p. 149-70.
187. Van Den Bent, M.J., J.E.C. Bromberg, and J. Buckner, *Chapter 22 - Low-grade and anaplastic oligodendroglioma*, in *Handbook of Clinical Neurology*, M.S. Berger and M. Weller, Editors. 2016, Elsevier. p. 361-380.

188. Simonetti, G., et al., *Clinical management of grade III oligodendroglioma*. *Cancer Manag Res*, 2015. **7**: p. 213-23.
189. Cairncross, J.G., et al., *Benefit from procarbazine, lomustine, and vincristine in oligodendroglial tumors is associated with mutation of IDH*. *J Clin Oncol*, 2014. **32**(8): p. 783-90.
190. Brat, D., et al., *Comprehensive, Integrative Genomic Analysis of Diffuse Lower-Grade Gliomas*. *New England Journal of Medicine*, 2015. **372**: p. 2481-2498.
191. Law, M., et al., *Glioma Grading: Sensitivity, Specificity, and Predictive Values of Perfusion MR Imaging and Proton MR Spectroscopic Imaging Compared with Conventional MR Imaging*. *AJNR*. *American journal of neuroradiology*, 2003. **24**: p. 1989-98.
192. Xu, M., et al., *Comparison of magnetic resonance spectroscopy and perfusion-weighted imaging in presurgical grading of oligodendroglial tumors*. *Neurosurgery*, 2005. **56**(5): p. 919-26; discussion 919-26.
193. Lev, M.H., et al., *Glial tumor grading and outcome prediction using dynamic spin-echo MR susceptibility mapping compared with conventional contrast-enhanced MR: confounding effect of elevated rCBV of oligodendrogliomas [corrected]*. *AJNR Am J Neuroradiol*, 2004. **25**(2): p. 214-21.
194. Kros, J.M., et al., *Panel review of anaplastic oligodendroglioma from European Organization For Research and Treatment of Cancer Trial 26951: assessment of consensus in diagnosis, influence of 1p/19q loss, and correlations with outcome*. *J Neuropathol Exp Neurol*, 2007. **66**(6): p. 545-51.
195. Brown, D.C. and K.C. Gatter, *Ki67 protein: the immaculate deception?* *Histopathology*, 2002. **40**(1): p. 2-11.
196. Newlands, E.S., et al., *Temozolomide: a review of its discovery, chemical properties, pre-clinical development and clinical trials*. *Cancer Treat Rev*, 1997. **23**(1): p. 35-61.
197. Avgeropoulos, N.G. and H.B. Newton, *Clinical Pharmacology of Brain Tumor Chemotherapy*. 2018. p. 21-44.
198. Buckner, J.C., et al., *Radiation plus Procarbazine, CCNU, and Vincristine in Low-Grade Glioma*. *New England Journal of Medicine*, 2016. **374**(14): p. 1344-1355.
199. van den Bent, M.J., et al., *IDH1 and IDH2 mutations are prognostic but not predictive for outcome in anaplastic oligodendroglial tumors: a report of the European Organization for Research and Treatment of Cancer Brain Tumor Group*. *Clin Cancer Res*, 2010. **16**(5): p. 1597-604.
200. van den Bent, M.J., et al., *Adjuvant procarbazine, lomustine, and vincristine improves progression-free survival but not overall survival in newly diagnosed anaplastic oligodendrogliomas and oligoastrocytomas: a randomized European Organisation for Research and Treatment of Cancer phase III trial*. *J Clin Oncol*, 2006. **24**(18): p. 2715-22.
201. Cairncross, G., et al., *Phase III trial of chemoradiotherapy for anaplastic oligodendroglioma: long-term results of RTOG 9402*. *J Clin Oncol*, 2013. **31**(3): p. 337-43.
202. Sabha, N., et al., *Analysis of IDH mutation, 1p/19q deletion, and PTEN loss delineates prognosis in clinical low-grade diffuse gliomas*. *Neuro Oncol*, 2014. **16**(7): p. 914-23.
203. Hayashi, S., et al., *Molecular-genetic and clinicopathological prognostic factors in patients with gliomas showing total 1p19q loss: gain of chromosome 19p and*

- histological grade III negatively correlate with patient's prognosis. J Neurooncol, 2017. 132(1): p. 119-126.*
204. Fisher, B.J., et al., *Phase 2 study of temozolomide-based chemoradiation therapy for high-risk low-grade gliomas: preliminary results of Radiation Therapy Oncology Group 0424. Int J Radiat Oncol Biol Phys, 2015. 91(3): p. 497-504.*
 205. van den Bent, M.J., et al., *Long-term efficacy of early versus delayed radiotherapy for low-grade astrocytoma and oligodendroglioma in adults: the EORTC 22845 randomised trial. Lancet, 2005. 366(9490): p. 985-90.*
 206. Keles, G.E., K.R. Lamborn, and M.S. Berger, *Low-grade hemispheric gliomas in adults: a critical review of extent of resection as a factor influencing outcome. J Neurosurg, 2001. 95(5): p. 735-45.*
 207. Wessels, P.H., et al., *Supratentorial grade II astrocytoma: biological features and clinical course. Lancet Neurol, 2003. 2(7): p. 395-403.*
 208. Venneti, S., B.J. Lopresti, and C.A. Wiley, *Molecular imaging of microglia/macrophages in the brain. Glia, 2013. 61(1): p. 10-23.*
 209. Van Bree, J.B.M.M., et al., *Drug transport across the blood-brain barrier.*
 210. Pike, V.W., *PET radiotracers: crossing the blood-brain barrier and surviving metabolism. Trends Pharmacol Sci, 2009. 30(8): p. 431-40.*
 211. Santra, A., et al., *F-18 FDG PET-CT for predicting survival in patients with recurrent glioma: a prospective study. Neuroradiology, 2011. 53(12): p. 1017-24.*
 212. la Fougère, C., et al., *Molecular imaging of gliomas with PET: opportunities and limitations. Neuro Oncol, 2011. 13(8): p. 806-19.*
 213. Quartuccio, N., et al., *The Additional Value of (18)F-FDG PET and MRI in Patients with Glioma: A Review of the Literature from 2015 to 2020. Diagnostics (Basel, Switzerland), 2020. 10(6): p. 357.*
 214. Basu, S. and A. Alavi, *Molecular imaging (PET) of brain tumors. Neuroimaging Clin N Am, 2009. 19(4): p. 625-46.*
 215. Herholz, K., et al., *11C-methionine PET for differential diagnosis of low-grade gliomas. Neurology, 1998. 50(5): p. 1316-22.*
 216. Kido, Y., et al., *Molecular and functional identification of large neutral amino acid transporters LAT1 and LAT2 and their pharmacological relevance at the blood-brain barrier. J Pharm Pharmacol, 2001. 53(4): p. 497-503.*
 217. Shinozaki, N., et al., *Discrimination between low-grade oligodendrogliomas and diffuse astrocytoma with the aid of 11C-methionine positron emission tomography. J Neurosurg, 2011. 114(6): p. 1640-7.*
 218. Yamaguchi, S., et al., *Detection of histological anaplasia in gliomas with oligodendroglial components using positron emission tomography with (18)F-FDG and (11)C-methionine: report of two cases. J Neurooncol, 2011. 101(2): p. 335-41.*
 219. Singhal, T., et al., *11C-L-methionine positron emission tomography in the clinical management of cerebral gliomas. Mol Imaging Biol, 2008. 10(1): p. 1-18.*
 220. Kracht, L.W., et al., *Methyl-[11C]- l-methionine uptake as measured by positron emission tomography correlates to microvessel density in patients with glioma. Eur J Nucl Med Mol Imaging, 2003. 30(6): p. 868-73.*
 221. Saito, T., et al., *11C-methionine uptake correlates with combined 1p and 19q loss of heterozygosity in oligodendroglial tumors. AJNR Am J Neuroradiol, 2013. 34(1): p. 85-91.*

222. Chung, J.K., et al., *Usefulness of 11C-methionine PET in the evaluation of brain lesions that are hypo- or isometabolic on 18F-FDG PET*. Eur J Nucl Med Mol Imaging, 2002. **29**(2): p. 176-82.
223. Evangelista, L., et al., *Comparison Between 18F-Dopa and 18F-Fet PET/CT in Patients with Suspicious Recurrent High Grade Glioma: A Literature Review and Our Experience*. Curr Radiopharm, 2019. **12**(3): p. 220-228.
224. Zaragori, T., et al., *Use of static and dynamic [(18)F]-F-DOPA PET parameters for detecting patients with glioma recurrence or progression*. EJNMMI research, 2020. **10**(1): p. 56-56.
225. Youland, R.S., et al., *Prospective trial evaluating the sensitivity and specificity of 3,4-dihydroxy-6-[18F]-fluoro-L-phenylalanine (18F-DOPA) PET and MRI in patients with recurrent gliomas*. J Neurooncol, 2018. **137**(3): p. 583-591.
226. Venneti, S., B.J. Lopresti, and C.A. Wiley, *The peripheral benzodiazepine receptor (Translocator protein 18kDa) in microglia: from pathology to imaging*. Prog Neurobiol, 2006. **80**(6): p. 308-22.
227. Buck, J.R., et al., *Quantitative, preclinical PET of translocator protein expression in glioma using 18F-N-fluoroacetyl-N-(2,5-dimethoxybenzyl)-2-phenoxyaniline*. J Nucl Med, 2011. **52**(1): p. 107-14.
228. Venneti, S., et al., *PK11195 labels activated microglia in Alzheimer's disease and in vivo in a mouse model using PET*. Neurobiol Aging, 2009. **30**(8): p. 1217-26.
229. Pappata, S., et al., *PET study of carbon-11-PK 11195 binding to peripheral type benzodiazepine sites in glioblastoma: a case report*. J Nucl Med, 1991. **32**(8): p. 1608-10.
230. Takaya, S., et al., *The lack of expression of the peripheral benzodiazepine receptor characterises microglial response in anaplastic astrocytomas*. J Neurooncol, 2007. **85**(1): p. 95-103.
231. Boutin, H., et al., *In vivo imaging of brain lesions with [(11)C]CLINME, a new PET radioligand of peripheral benzodiazepine receptors*. Glia, 2007. **55**(14): p. 1459-68.
232. Vivash, L. and T.J. O'Brien, *Imaging Microglial Activation with TSPO PET: Lighting Up Neurologic Diseases?* J Nucl Med, 2016. **57**(2): p. 165-8.
233. Chauveau, F., et al., *Nuclear imaging of neuroinflammation: a comprehensive review of [11C]PK11195 challengers*. Eur J Nucl Med Mol Imaging, 2008. **35**(12): p. 2304-19.
234. Venneti, S., et al., *A comparison of the high-affinity peripheral benzodiazepine receptor ligands DAA1106 and (R)-PK11195 in rat models of neuroinflammation: implications for PET imaging of microglial activation*. J Neurochem, 2007. **102**(6): p. 2118-2131.
235. Fujimura, Y., et al., *Quantification of translocator protein (18 kDa) in the human brain with PET and a novel radioligand, (18)F-PBR06*. J Nucl Med, 2009. **50**(7): p. 1047-53.
236. Imaizumi, M., et al., *Brain and whole-body imaging in nonhuman primates of [11C]PBR28, a promising PET radioligand for peripheral benzodiazepine receptors*. Neuroimage, 2008. **39**(3): p. 1289-98.
237. James, M.L., et al., *DPA-714, a new translocator protein-specific ligand: synthesis, radiofluorination, and pharmacologic characterization*. J Nucl Med, 2008. **49**(5): p. 814-22.

238. Chauveau, F., et al., *Comparative evaluation of the translocator protein radioligands 11C-DPA-713, 18F-DPA-714, and 11C-PK11195 in a rat model of acute neuroinflammation*. J Nucl Med, 2009. **50**(3): p. 468-76.
239. Winkeler, A., et al., *The translocator protein ligand [¹⁸F]DPA-714 images glioma and activated microglia in vivo*. Eur J Nucl Med Mol Imaging, 2012. **39**(5): p. 811-23.
240. Awde, A.R., et al., *The translocator protein radioligand 18F-DPA-714 monitors antitumor effect of erufosine in a rat 9L intracranial glioma model*. J Nucl Med, 2013. **54**(12): p. 2125-31.
241. Stoll, H.P., et al., *Advantages of short-lived positron-emitting radioisotopes for intracoronary radiation therapy with liquid-filled balloons to prevent restenosis*. J Nucl Med, 2001. **42**(9): p. 1375-83.
242. Knezevic, D. and R. Mizrahi, *Molecular imaging of neuroinflammation in Alzheimer's disease and mild cognitive impairment*. Prog Neuropsychopharmacol Biol Psychiatry, 2018. **80**(Pt B): p. 123-131.
243. Zinnhardt, B., et al., *Combined PET Imaging of the Inflammatory Tumor Microenvironment Identifies Margins of Unique Radiotracer Uptake*. Cancer Res, 2017. **77**(8): p. 1831-1841.
244. Pigeon, H., et al., *TSPO-PET and diffusion-weighted MRI for imaging a mouse model of infiltrative human glioma*. Neuro Oncol, 2019. **21**(6): p. 755-764.
245. Zanotti-Fregonara, P., et al., *Head-to-Head Comparison of (11)C-PBR28 and (18)F-GE180 for Quantification of the Translocator Protein in the Human Brain*. J Nucl Med, 2018. **59**(8): p. 1260-1266.
246. Zanotti-Fregonara, P., et al., *Head-to-head comparison of (11)C-PBR28 and (11)C-ER176 for quantification of the translocator protein in the human brain*. Eur J Nucl Med Mol Imaging, 2019. **46**(9): p. 1822-1829.
247. Albert, N.L., et al., *In response to: The validity of 18F-GE180 as a TSPO imaging agent*. European Journal of Nuclear Medicine and Molecular Imaging, 2019. **46**(6): p. 1208-1211.
248. Unterrainer, M., et al., *TSPO PET, tumour grading and molecular genetics in histologically verified glioma: a correlative (18)F-GE-180 PET study*. Eur J Nucl Med Mol Imaging, 2020. **47**(6): p. 1368-1380.
249. Zanotti-Fregonara, P., et al., *The validity of 18F-GE180 as a TSPO imaging agent*. European Journal of Nuclear Medicine and Molecular Imaging, 2019. **46**(6): p. 1205-1207.
250. Zanotti-Fregonara, P., et al., *Anatomy of 18F-GE180, a failed radioligand for the TSPO protein*. European Journal of Nuclear Medicine and Molecular Imaging, 2020. **47**(10): p. 2233-2236.
251. Albert, N.L., et al., *In response to: Anatomy of 18F-GE180, a failed radioligand for the TSPO protein*. European Journal of Nuclear Medicine and Molecular Imaging, 2020. **47**(10): p. 2237-2241.
252. Ikawa, M., et al., *11C-ER176, a Radioligand for 18-kDa Translocator Protein, Has Adequate Sensitivity to Robustly Image All Three Affinity Genotypes in Human Brain*. J Nucl Med, 2017. **58**(2): p. 320-325.
253. Wimberley, C., et al., *Impact of endothelial TSPO on the quantification of 18 F-DPA-714*. Journal of Nuclear Medicine, 2017. **59**: p. jnumed.117.195396.

254. Roncaroli, F., et al., *TSPO expression in brain tumours: is TSPO a target for brain tumour imaging?* Clin Transl Imaging, 2016. **4**: p. 145-156.
255. Veronese, M., et al., *Kinetic modelling of [(11)C]PBR28 for 18 kDa translocator protein PET data: A validation study of vascular modelling in the brain using XBDD173 and tissue analysis.* J Cereb Blood Flow Metab, 2018. **38**(7): p. 1227-1242.
256. Cai, L., et al., *Glioblastoma Exhibits Inter-Individual Heterogeneity of TSPO and LAT1 Expression in Neoplastic and Parenchymal Cells.* International journal of molecular sciences, 2020. **21**(2): p. 612.
257. Betlazar, C., et al., *Cellular Sources and Regional Variations in the Expression of the Neuroinflammatory Marker Translocator Protein (TSPO) in the Normal Brain.* Int J Mol Sci, 2018. **19**(9).
258. Rizzo, G., et al., *Generalization of endothelial modelling of TSPO PET imaging: Considerations on tracer affinities.* J Cereb Blood Flow Metab, 2019. **39**(5): p. 874-885.
259. Wimberley, C., et al., *Impact of Endothelial 18-kDa Translocator Protein on the Quantification of (18)F-DPA-714.* J Nucl Med, 2018. **59**(2): p. 307-314.
260. Rizzo, G., et al., *Kinetic modeling without accounting for the vascular component impairs the quantification of [(11)C]PBR28 brain PET data.* J Cereb Blood Flow Metab, 2014. **34**(6): p. 1060-9.
261. Tomasi, G., et al., *Novel reference region model reveals increased microglial and reduced vascular binding of 11C-(R)-PK11195 in patients with Alzheimer's disease.* J Nucl Med, 2008. **49**(8): p. 1249-56.
262. Turkheimer, F.E., et al., *Reference and target region modeling of [11C]-(R)-PK11195 brain studies.* J Nucl Med, 2007. **48**(1): p. 158-67.
263. Filosa, J.A., et al., *Beyond neurovascular coupling, role of astrocytes in the regulation of vascular tone.* Neuroscience, 2016. **323**: p. 96-109.
264. Iliff, J.J., et al., *A paravascular pathway facilitates CSF flow through the brain parenchyma and the clearance of interstitial solutes, including amyloid β .* Sci Transl Med, 2012. **4**(147): p. 147ra111.
265. Araya, R., et al., *BMP signaling through BMPRIA in astrocytes is essential for proper cerebral angiogenesis and formation of the blood-brain-barrier.* Mol Cell Neurosci, 2008. **38**(3): p. 417-30.
266. Sofroniew, M.V. and H.V. Vinters, *Astrocytes: biology and pathology.* Acta Neuropathol, 2010. **119**(1): p. 7-35.
267. Da Pozzo, E., et al., *Targeting the 18-kDa translocator protein: recent perspectives for neuroprotection.* Biochem Soc Trans, 2015. **43**(4): p. 559-65.
268. Chechneva, O.V. and W. Deng, *Mitochondrial translocator protein (TSPO), astrocytes and neuroinflammation.* Neural regeneration research, 2016. **11**(7): p. 1056-1057.
269. Notter, T., et al., *Reconceptualization of translocator protein as a biomarker of neuroinflammation in psychiatry.* Molecular Psychiatry, 2018. **23**(1): p. 36-47.
270. Lavisse, S., et al., *Reactive astrocytes overexpress TSPO and are detected by TSPO positron emission tomography imaging.* J Neurosci, 2012. **32**(32): p. 10809-18.
271. Gui, Y., et al., *Characterization of the 18 kDa translocator protein (TSPO) expression in post-mortem normal and Alzheimer's disease brains.* Brain Pathology, 2020. **30**(1): p. 151-164.

272. Betlazar, C., et al., *Cellular Sources and Regional Variations in the Expression of the Neuroinflammatory Marker Translocator Protein (TSPO) in the Normal Brain*. International journal of molecular sciences, 2018. **19**(9): p. 2707.
273. Liddelow, S.A., et al., *Neurotoxic reactive astrocytes are induced by activated microglia*. Nature, 2017. **541**(7638): p. 481-487.
274. Henrik Heiland, D., et al., *Tumor-associated reactive astrocytes aid the evolution of immunosuppressive environment in glioblastoma*. Nature Communications, 2019. **10**(1): p. 2541.
275. Sweeney, M.D., S. Ayyadurai, and B.V. Zlokovic, *Pericytes of the neurovascular unit: key functions and signaling pathways*. Nature neuroscience, 2016. **19**(6): p. 771-783.
276. Shen, J., et al., *PDGFR- β restores blood-brain barrier functions in a mouse model of focal cerebral ischemia*. Journal of Cerebral Blood Flow & Metabolism, 2018. **39**(8): p. 1501-1515.
277. Banati, R.B., *Visualising microglial activation in vivo*. Glia, 2002. **40**(2): p. 206-17.
278. Gargiulo, S., et al., *Imaging of brain TSPO expression in a mouse model of amyotrophic lateral sclerosis with (18)F-DPA-714 and micro-PET/CT*. Eur J Nucl Med Mol Imaging, 2016. **43**(7): p. 1348-59.
279. Ji, B., et al., *Imaging of peripheral benzodiazepine receptor expression as biomarkers of detrimental versus beneficial glial responses in mouse models of Alzheimer's and other CNS pathologies*. J Neurosci, 2008. **28**(47): p. 12255-67.
280. Mirzaei, N., et al., *In vivo imaging of microglial activation by positron emission tomography with [(11)C]PBR28 in the 5XFAD model of Alzheimer's disease*. Glia, 2016. **64**(6): p. 993-1006.
281. Buck, J.R., et al., *Preclinical TSPO Ligand PET to Visualize Human Glioma Xenotransplants: A Preliminary Study*. PloS one, 2015. **10**(10): p. e0141659-e0141659.
282. Faraco, G., et al., *Brain perivascular macrophages: characterization and functional roles in health and disease*. Journal of molecular medicine (Berlin, Germany), 2017. **95**(11): p. 1143-1152.
283. Owen, D.R., et al., *Pro-inflammatory activation of primary microglia and macrophages increases 18 kDa translocator protein expression in rodents but not humans*. J Cereb Blood Flow Metab, 2017. **37**(8): p. 2679-2690.
284. Pannell, M., et al., *Imaging of translocator protein upregulation is selective for pro-inflammatory polarized astrocytes and microglia*. Glia, 2020. **68**(2): p. 280-297.
285. Beckers, L., et al., *Increased Expression of Translocator Protein (TSPO) Marks Pro-inflammatory Microglia but Does Not Predict Neurodegeneration*. Molecular Imaging and Biology, 2018. **20**(1): p. 94-102.
286. Zhou, D., L. Ji, and Y. Chen, *TSPO Modulates IL-4-Induced Microglia/Macrophage M2 Polarization via PPAR- γ Pathway*. J Mol Neurosci, 2020. **70**(4): p. 542-549.
287. Mantovani, A., et al., *The chemokine system in diverse forms of macrophage activation and polarization*. Trends Immunol, 2004. **25**(12): p. 677-86.
288. Lisi, L., et al., *Proinflammatory-activated glioma cells induce a switch in microglial polarization and activation status, from a predominant M2b phenotype to a mixture of M1 and M2a/B polarized cells*. ASN Neuro, 2014. **6**(3): p. 171-83.

289. Hambardzumyan, D., D.H. Gutmann, and H. Kettenmann, *The role of microglia and macrophages in glioma maintenance and progression*. Nat Neurosci, 2016. **19**(1): p. 20-7.
290. Hussain, S.F., et al., *The role of human glioma-infiltrating microglia/macrophages in mediating antitumor immune responses*. Neuro Oncol, 2006. **8**(3): p. 261-79.
291. Quail, D.F. and J.A. Joyce, *The Microenvironmental Landscape of Brain Tumors*. Cancer cell, 2017. **31**(3): p. 326-341.
292. Perus, L.J.M. and L.A. Walsh, *Microenvironmental Heterogeneity in Brain Malignancies*. Front Immunol, 2019. **10**: p. 2294.
293. Pires-Afonso, Y., S.P. Niclou, and A. Michelucci, *Revealing and Harnessing Tumour-Associated Microglia/Macrophage Heterogeneity in Glioblastoma*. International Journal of Molecular Sciences, 2020. **21**(3).
294. Hewedi, I.H., et al., *Perspectives on the immunologic microenvironment of astrocytomas*. Cancer Manag Res, 2013. **5**: p. 293-9.
295. Yang, I., et al., *Immune cell infiltrate differences in pilocytic astrocytoma and glioblastoma: evidence of distinct immunological microenvironments that reflect tumor biology*. J Neurosurg, 2011. **115**(3): p. 505-11.
296. Yi, L., et al., *Glioma-initiating cells: a predominant role in microglia/macrophages tropism to glioma*. J Neuroimmunol, 2011. **232**(1-2): p. 75-82.
297. Platten, M., et al., *Monocyte chemoattractant protein-1 increases microglial infiltration and aggressiveness of gliomas*. Ann Neurol, 2003. **54**(3): p. 388-92.
298. Ku, M.C., et al., *GDNF mediates glioblastoma-induced microglia attraction but not astrogliosis*. Acta Neuropathol, 2013. **125**(4): p. 609-20.
299. Coniglio, S.J., et al., *Microglial stimulation of glioblastoma invasion involves epidermal growth factor receptor (EGFR) and colony stimulating factor 1 receptor (CSF-1R) signaling*. Mol Med, 2012. **18**(1): p. 519-27.
300. Roesch, S., et al., *When Immune Cells Turn Bad-Tumor-Associated Microglia/Macrophages in Glioma*. Int J Mol Sci, 2018. **19**(2).
301. Hambardzumyan, D., D.H. Gutmann, and H. Kettenmann, *The role of microglia and macrophages in glioma maintenance and progression*. Nature neuroscience, 2016. **19**(1): p. 20-27.
302. Watters, J.J., J.M. Schartner, and B. Badie, *Microglia function in brain tumors*. J Neurosci Res, 2005. **81**(3): p. 447-55.
303. Zhai, H., F.L. Heppner, and S.E. Tsirka, *Microglia/macrophages promote glioma progression*. Glia, 2011. **59**(3): p. 472-85.
304. Allavena, P., et al., *The Yin-Yang of tumor-associated macrophages in neoplastic progression and immune surveillance*. Immunol Rev, 2008. **222**: p. 155-61.
305. Galani, I.E., et al., *Regulatory T cells control macrophage accumulation and activation in lymphoma*. Int J Cancer, 2010. **127**(5): p. 1131-40.
306. Solinas, G., et al., *Tumor-associated macrophages (TAM) as major players of the cancer-related inflammation*. J Leukoc Biol, 2009. **86**(5): p. 1065-73.
307. Guadagno, E., et al., *Role of Macrophages in Brain Tumor Growth and Progression*. International journal of molecular sciences, 2018. **19**(4): p. 1005.
308. Wright, P., et al., *Patterns of Mitochondrial TSPO Binding in Cerebral Small Vessel Disease: An in vivo PET Study With Neuropathological Comparison*. Front Neurol, 2020. **11**: p. 541377.

309. Al-Khishman, N.U., et al., *TSPO PET detects acute neuroinflammation but not diffuse chronically activated MHCII microglia in the rat*. *EJNMMI Res*, 2020. **10**(1): p. 113.
310. Kanno, I., et al., *Positron emission tomography of cerebral angiogenesis and TSPO expression in a mouse model of chronic hypoxia*. *J Cereb Blood Flow Metab*, 2018. **38**(4): p. 687-696.
311. Lewis, D., et al., *Inflammation and vascular permeability correlate with growth in sporadic vestibular schwannoma*. *Neuro Oncol*, 2019. **21**(3): p. 314-325.
312. Wang, Q., et al., *Vascular niche IL-6 induces alternative macrophage activation in glioblastoma through HIF-2 α* . *Nature Communications*, 2018. **9**(1): p. 559.
313. Zinnhardt, B., et al., *TSPO imaging-guided characterization of the immunosuppressive myeloid tumor microenvironment in patients with malignant glioma*. *Neuro Oncol*, 2020. **22**(7): p. 1030-1043.
314. Betlazar, C., et al., *The Translocator Protein (TSPO) in Mitochondrial Bioenergetics and Immune Processes*. *Cells*, 2020. **9**(2).
315. Pantaleão, L., et al., *Connections of annexin A1 and translocator protein-18 kDa on toll like receptor stimulated BV-2 cells*. *Experimental Cell Research*, 2018. **367**(2): p. 282-290.
316. Santoro, A., et al., *TSPO-ligands prevent oxidative damage and inflammatory response in C6 glioma cells by neurosteroid synthesis*. *Eur J Pharm Sci*, 2016. **88**: p. 124-31.
317. Rizzo, G., et al., *Kinetic modeling without accounting for the vascular component impairs the quantification of [11C]PBR28 brain PET data*. *Journal of cerebral blood flow and metabolism : official journal of the International Society of Cerebral Blood Flow and Metabolism*, 2014. **34**: p. 1060-1069.
318. Deli, M.A., et al., *Permeability studies on in vitro blood-brain barrier models: physiology, pathology, and pharmacology*. *Cell Mol Neurobiol*, 2005. **25**(1): p. 59-127.
319. Harhausen, D., et al., *Specific imaging of inflammation with the 18 kDa translocator protein ligand DPA-714 in animal models of epilepsy and stroke*. *PLoS One*, 2013. **8**(8): p. e69529.
320. Bobilya, D.J., *Isolation and cultivation of porcine astrocytes*. *Methods Mol Biol*, 2012. **814**: p. 127-35.
321. Motulsky, H.J. and R.R. Neubig, *Analyzing binding data*. *Curr Protoc Neurosci*, 2010. **Chapter 7**: p. Unit 7.5.
322. Daugherty, D.J., et al., *A TSPO ligand is protective in a mouse model of multiple sclerosis*. *EMBO molecular medicine*, 2013. **5**(6): p. 891-903.
323. Kuhlmann, A.C. and T.R. Guilarte, *Cellular and subcellular localization of peripheral benzodiazepine receptors after trimethyltin neurotoxicity*. *J Neurochem*, 2000. **74**(4): p. 1694-704.
324. Dickens, A.M., et al., *Detection of microglial activation in an acute model of neuroinflammation using PET and radiotracers 11C-(R)-PK11195 and 18F-GE-180*. *J Nucl Med*, 2014. **55**(3): p. 466-72.
325. Tournier, B.B., et al., *In Vivo TSPO Signal and Neuroinflammation in Alzheimer's Disease*. *Cells*, 2020. **9**(9).

326. Mirzaei, N., et al., *In vivo imaging of microglial activation by positron emission tomography with [11C]PBR28 in the 5XFAD model of Alzheimer's disease*. *Glia*, 2016. **64**(6): p. 993-1006.
327. Mischeck, U., J. Meyer, and H.-J. Galla, *Characterization of γ -glutamyl transpeptidase activity of cultured endothelial cells from porcine brain capillaries*. *Cell and Tissue Research*, 1989. **256**(1): p. 221-226.
328. Cantrill, C.A., et al., *An immortalised astrocyte cell line maintains the in vivo phenotype of a primary porcine in vitro blood–brain barrier model*. *Brain Research*, 2012. **1479**: p. 17-30.
329. Patabendige, A., et al., *A detailed method for preparation of a functional and flexible blood–brain barrier model using porcine brain endothelial cells*. *Brain Research*, 2013. **1521**: p. 16-30.
330. Nielsen, S.S.E., et al., *Improved Method for the Establishment of an In Vitro Blood-Brain Barrier Model Based on Porcine Brain Endothelial Cells*. *J Vis Exp*, 2017(127).
331. Thomsen, L.B., A. Burkhart, and T. Moos, *A Triple Culture Model of the Blood-Brain Barrier Using Porcine Brain Endothelial cells, Astrocytes and Pericytes*. *PLoS One*, 2015. **10**(8): p. e0134765.
332. Shubbar, M.H. and J.I. Penny, *Effect of amyloid beta on ATP-binding cassette transporter expression and activity in porcine brain microvascular endothelial cells*. *Biochim Biophys Acta Gen Subj*, 2018. **1862**(10): p. 2314-2322.
333. Skinner, R.A., et al., *Transport of interleukin-1 across cerebrovascular endothelial cells*. *Br J Pharmacol*, 2009. **156**(7): p. 1115-23.
334. Patabendige, A., et al., *A detailed method for preparation of a functional and flexible blood-brain barrier model using porcine brain endothelial cells*. *Brain Res*, 2013. **1521**: p. 16-30.
335. Rubin, L.L., et al., *A cell culture model of the blood-brain barrier*. *Journal of Cell Biology*, 1991. **115**(6): p. 1725-1735.
336. Bernard-Patrzynski, F., et al., *Isolation of endothelial cells, pericytes and astrocytes from mouse brain*. *PLOS ONE*, 2019. **14**(12): p. e0226302.
337. Perrière, N., et al., *Puromycin-based purification of rat brain capillary endothelial cell cultures. Effect on the expression of blood–brain barrier-specific properties*. *Journal of Neurochemistry*, 2005. **93**(2): p. 279-289.
338. Calabria, A.R., et al., *Puromycin-purified rat brain microvascular endothelial cell cultures exhibit improved barrier properties in response to glucocorticoid induction*. *Journal of Neurochemistry*, 2006. **97**(4): p. 922-933.
339. Kido, Y., et al., *Evaluation of Blood-brain Barrier Transporters by Co-culture of Brain Capillary Endothelial Cells with Astrocytes*. *Drug Metabolism and Pharmacokinetics*, 2002. **17**(1): p. 34-41.
340. Junck, L., et al., *PET imaging of human gliomas with ligands for the peripheral benzodiazepine binding site*. *Ann Neurol*, 1989. **26**(6): p. 752-8.
341. Miyauchi, J.T., et al., *Ablation of Neuropilin 1 from glioma-associated microglia and macrophages slows tumor progression*. *Oncotarget*, 2016. **7**(9): p. 9801-14.
342. Gutmann, D.H. and H. Kettenmann, *Microglia/Brain Macrophages as Central Drivers of Brain Tumor Pathobiology*. *Neuron*, 2019. **104**(3): p. 442-449.
343. Brem, S., *The role of vascular proliferation in the growth of brain tumors*. *Clin Neurosurg*, 1976. **23**: p. 440-53.

344. Zhang, L., et al., *IDH mutation status is associated with distinct vascular gene expression signatures in lower-grade gliomas*. *Neuro Oncol*, 2018. **20**(11): p. 1505-1516.
345. Kaur, B., et al., *Hypoxia and the hypoxia-inducible-factor pathway in glioma growth and angiogenesis*. *Neuro-oncology*, 2005. **7**(2): p. 134-153.
346. Monteiro, A.R., et al., *The Role of Hypoxia in Glioblastoma Invasion*. *Cells*, 2017. **6**(4): p. 45.
347. Lepore, F., et al., *CXCL16/CXCR6 Axis Drives Microglia/Macrophages Phenotype in Physiological Conditions and Plays a Crucial Role in Glioma*. *Frontiers in Immunology*, 2018. **9**(2750).
348. Gabrusiewicz, K., et al., *Characteristics of the alternative phenotype of microglia/macrophages and its modulation in experimental gliomas*. *PLoS One*, 2011. **6**(8): p. e23902.
349. Pollard, J.W., *Tumour-educated macrophages promote tumour progression and metastasis*, in *Nat Rev Cancer*. 2004: England. p. 71-8.
350. Tang, D., et al., *Quantitative preclinical imaging of TSPO expression in glioma using N,N-diethyl-2-(2-(4-(2-¹⁸F-fluoroethoxy)phenyl)-5,7-dimethylpyrazolo[1,5-a]pyrimidin-3-yl)acetamide*. *J Nucl Med*, 2012. **53**(2): p. 287-94.
351. Owen, D.R., et al., *Variation in binding affinity of the novel anxiolytic XBD173 for the 18 kDa translocator protein in human brain*. *Synapse*, 2011. **65**(3): p. 257-9.
352. Owen, D.R., et al., *Two binding sites for [³H]PBR28 in human brain: implications for TSPO PET imaging of neuroinflammation*. *J Cereb Blood Flow Metab*, 2010. **30**(9): p. 1608-18.
353. Kreisl, W.C., et al., *Comparison of [(11)C]-(R)-PK 11195 and [(11)C]PBR28, two radioligands for translocator protein (18 kDa) in human and monkey: Implications for positron emission tomographic imaging of this inflammation biomarker*. *Neuroimage*, 2010. **49**(4): p. 2924-32.
354. Tiwari, A.K., et al., *[¹⁸F]FEBMP: Positron Emission Tomography Imaging of TSPO in a Model of Neuroinflammation in Rats, and in vitro Autoradiograms of the Human Brain*. *Theranostics*, 2015. **5**(9): p. 961-9.
355. Kampf, C., et al., *Production of tissue microarrays, immunohistochemistry staining and digitalization within the human protein atlas*. *Journal of visualized experiments : JoVE*, 2012(63): p. 3620.
356. Dunn, K.W., M.M. Kamocka, and J.H. McDonald, *A practical guide to evaluating colocalization in biological microscopy*. *American journal of physiology. Cell physiology*, 2011. **300**(4): p. C723-C742.
357. Costes, S.V., et al., *Automatic and quantitative measurement of protein-protein colocalization in live cells*. *Biophys J*, 2004. **86**(6): p. 3993-4003.
358. Manders, E.M.M., F.J. Verbeek, and J.A. Aten, *Measurement of co-localization of objects in dual-colour confocal images*. *Journal of Microscopy*, 1993. **169**(3): p. 375-382.
359. Geranmayeh, F., et al., *Microglia in gemistocytic astrocytomas*. *Neurosurgery*, 2007. **60**(1): p. 159-66; discussion 166.
360. Kostianovsky, A.M., et al., *Astrocytic regulation of human monocytic/microglial activation*. *J Immunol*, 2008. **181**(8): p. 5425-32.

361. Zhang, J., et al., *A dialog between glioma and microglia that promotes tumor invasiveness through the CCL2/CCR2/interleukin-6 axis*. *Carcinogenesis*, 2012. **33**(2): p. 312-9.
362. Paulus, W., et al., *Effects of transforming growth factor-beta 1 on collagen synthesis, integrin expression, adhesion and invasion of glioma cells*. *J Neuropathol Exp Neurol*, 1995. **54**(2): p. 236-44.
363. Carvalho da Fonseca, A.C., et al., *Increased expression of stress inducible protein 1 in glioma-associated microglia/macrophages*. *Journal of neuroimmunology*, 2014. **274**(1-2): p. 71-77.
364. Wick, W., M. Platten, and M. Weller, *Glioma cell invasion: regulation of metalloproteinase activity by TGF-beta*. *J Neurooncol*, 2001. **53**(2): p. 177-85.
365. Imtiyaz, H.Z., et al., *Hypoxia-inducible factor 2alpha regulates macrophage function in mouse models of acute and tumor inflammation*. *J Clin Invest*, 2010. **120**(8): p. 2699-714.
366. Piroth, M.D., et al., *Prognostic impact of postoperative, pre-irradiation (18)F-fluoroethyl-l-tyrosine uptake in glioblastoma patients treated with radiochemotherapy*. *Radiother Oncol*, 2011. **99**(2): p. 218-24.
367. Kläsner, B., et al., *Early [18F]FET-PET in Gliomas after Surgical Resection: Comparison with MRI and Histopathology*. *PLoS One*, 2015. **10**(10): p. e0141153.
368. Pitter, K.L., et al., *Corticosteroids compromise survival in glioblastoma*. *Brain : a journal of neurology*, 2016. **139**(Pt 5): p. 1458-1471.
369. Biswas, L., et al., *TSPO Ligands Promote Cholesterol Efflux and Suppress Oxidative Stress and Inflammation in Choroidal Endothelial Cells*. *International journal of molecular sciences*, 2018. **19**(12): p. 3740.
370. Owen, D.R., et al., *TSPO mutations in rats and a human polymorphism impair the rate of steroid synthesis*. *Biochemical Journal*, 2017. **474**(23): p. 3985-3999.
371. Tomczak, K., P. Czerwińska, and M. Wiznerowicz, *The Cancer Genome Atlas (TCGA): an immeasurable source of knowledge*. *Contemporary oncology (Poznan, Poland)*, 2015. **19**(1A): p. A68-A77.
372. Li, Q., et al., *Methylation and silencing of the Thrombospondin-1 promoter in human cancer*. *Oncogene*, 1999. **18**(21): p. 3284-9.
373. Bolger, A.M., M. Lohse, and B. Usadel, *Trimmomatic: a flexible trimmer for Illumina sequence data*. *Bioinformatics*, 2014. **30**(15): p. 2114-20.
374. Dobin, A., et al., *STAR: ultrafast universal RNA-seq aligner*. *Bioinformatics*, 2013. **29**(1): p. 15-21.
375. Love, M.I., W. Huber, and S. Anders, *Moderated estimation of fold change and dispersion for RNA-seq data with DESeq2*. *Genome Biol*, 2014. **15**(12): p. 550.
376. Sandoval, J., et al., *Validation of a DNA methylation microarray for 450,000 CpG sites in the human genome*. *Epigenetics*, 2011. **6**(6): p. 692-702.
377. Baysan, M., et al., *G-cimp status prediction of glioblastoma samples using mRNA expression data*. *PLoS One*, 2012. **7**(11): p. e47839.
378. Siegel, E.M., et al., *Expanding epigenomics to archived FFPE tissues: an evaluation of DNA repair methodologies*. *Cancer epidemiology, biomarkers & prevention : a publication of the American Association for Cancer Research, cosponsored by the American Society of Preventive Oncology*, 2014. **23**(12): p. 2622-2631.

379. Frommer, M., et al., *A genomic sequencing protocol that yields a positive display of 5-methylcytosine residues in individual DNA strands*. Proc Natl Acad Sci U S A, 1992. **89**(5): p. 1827-31.
380. Maksimovic, J., B. Phipson, and A. Oshlack, *A cross-package Bioconductor workflow for analysing methylation array data*. F1000Res, 2016. **5**: p. 1281.
381. Wei, X.H., et al., *The upregulation of translocator protein (18 kDa) promotes recovery from neuropathic pain in rats*. J Neurosci, 2013. **33**(4): p. 1540-51.
382. Feng, Z., et al., *p53 tumor suppressor protein regulates the levels of huntingtin gene expression*. Oncogene, 2006. **25**(1): p. 1-7.
383. Cornett, J., et al., *Context-dependent dysregulation of transcription by mutant huntingtin*. J Biol Chem, 2006. **281**(47): p. 36198-204.
384. Chen, C., et al., *Estradiol modulates translocator protein (TSPO) and steroid acute regulatory protein (StAR) via protein kinase A (PKA) signaling in hypothalamic astrocytes*. Endocrinology, 2014. **155**(8): p. 2976-85.
385. Gazouli, M., et al., *Effect of Peroxisome Proliferators on Leydig Cell Peripheral-Type Benzodiazepine Receptor Gene Expression, Hormone-Stimulated Cholesterol Transport, and Steroidogenesis: Role of the Peroxisome Proliferator-Activator Receptor α* . Endocrinology, 2002. **143**: p. 2571-2583.
386. Kim-Muller, J.Y., et al., *FoxO1 Deacetylation Decreases Fatty Acid Oxidation in β -Cells and Sustains Insulin Secretion in Diabetes*. The Journal of biological chemistry, 2016. **291**(19): p. 10162-10172.
387. Salzmann, C., et al., *Inhibition of Steroidogenic Response to Adrenocorticotropin by Leptin: Implications for the Adrenal Response to Maternal Separation in Neonatal Rats*. Endocrinology, 2004. **145**(4): p. 1810-1822.
388. Lucki, N.C., et al., *Acid ceramidase (ASAHI) is a global regulator of steroidogenic capacity and adrenocortical gene expression*. Mol Endocrinol, 2012. **26**(2): p. 228-43.
389. Uhlenhaut, N.H., et al., *Somatic sex reprogramming of adult ovaries to testes by FOXL2 ablation*. Cell, 2009. **139**(6): p. 1130-42.
390. Wang, Y.T., et al., *Interplay of posttranslational modifications in Sp1 mediates Sp1 stability during cell cycle progression*. J Mol Biol, 2011. **414**(1): p. 1-14.
391. Thomas, J.J., et al., *RNF4-Dependent Oncogene Activation by Protein Stabilization*. Cell reports, 2016. **16**(12): p. 3388-3400.
392. Gomez-Nicola, D., B. Valle-Argos, and M. Nieto-Sampedro, *Blockade of IL-15 activity inhibits microglial activation through the NF κ B, p38, and ERK1/2 pathways, reducing cytokine and chemokine release*. Glia, 2010. **58**(3): p. 264-276.
393. Humbert, S., et al., *The IGF-1/Akt pathway is neuroprotective in Huntington's disease and involves Huntingtin phosphorylation by Akt*. Dev Cell, 2002. **2**(6): p. 831-7.
394. Culver, B.P., et al., *Proteomic analysis of wild-type and mutant huntingtin-associated proteins in mouse brains identifies unique interactions and involvement in protein synthesis*. J Biol Chem, 2012. **287**(26): p. 21599-614.
395. Brown, V., et al., *Microarray identification of FMRP-associated brain mRNAs and altered mRNA translational profiles in fragile X syndrome*. Cell, 2001. **107**(4): p. 477-87.
396. Jin, H., et al., *Histone hyperacetylation up-regulates protein kinase C δ in dopaminergic neurons to induce cell death: relevance to epigenetic mechanisms of neurodegeneration in Parkinson disease*. J Biol Chem, 2014. **289**(50): p. 34743-67.

397. De Pasquale, R., et al., *LTP and LTD in the visual cortex require the activation of NOX2*. J Neurosci, 2014. **34**(38): p. 12778-87.
398. Liu, L., et al., *Severe disease, unaltered leukocyte migration, and reduced IFN-gamma production in CXCR3^{-/-} mice with experimental autoimmune encephalomyelitis*. J Immunol, 2006. **176**(7): p. 4399-409.
399. Sobrado, M., et al., *Synthesis of lipoxin A4 by 5-lipoxygenase mediates PPARgamma-dependent, neuroprotective effects of rosiglitazone in experimental stroke*. J Neurosci, 2009. **29**(12): p. 3875-84.
400. Yoon, K.-C., et al., *Expression of CXCL9, -10, -11, and CXCR3 in the tear film and ocular surface of patients with dry eye syndrome*. Investigative ophthalmology & visual science, 2010. **51**(2): p. 643-650.
401. Steen, H.C. and A.M. Gamero, *The role of signal transducer and activator of transcription-2 in the interferon response*. J Interferon Cytokine Res, 2012. **32**(3): p. 103-10.
402. Balestrieri, M.L., et al., *Understanding the immunoangiostatic CXC chemokine network*. Cardiovascular Research, 2008. **78**(2): p. 250-256.
403. Chen, Q., S. Gupta, and A.B. Pernis, *Regulation of TLR4-mediated signaling by IBP/Def6, a novel activator of Rho GTPases*. J Leukoc Biol, 2009. **85**(3): p. 539-43.
404. Liu, C., et al., *Chemokine receptor CXCR3 promotes growth of glioma*. Carcinogenesis, 2011. **32**(2): p. 129-137.
405. Laird, M.H.W., et al., *TLR4/MyD88/PI3K interactions regulate TLR4 signaling*. Journal of Leukocyte Biology, 2009. **85**(6): p. 966-977.
406. Kielian, T., *Toll-like receptors in central nervous system glial inflammation and homeostasis*. J Neurosci Res, 2006. **83**(5): p. 711-30.
407. Auernhammer, C.J., et al., *The oncostatin M receptor/gp130 ligand murine oncostatin M induces apoptosis in adrenocortical Y-1 tumor cells*. J Endocrinol, 2004. **180**(3): p. 479-86.
408. Le, A.P. and W.J. Friedman, *Matrix metalloproteinase-7 regulates cleavage of pro-nerve growth factor and is neuroprotective following kainic acid-induced seizures*. J Neurosci, 2012. **32**(2): p. 703-12.
409. Simpson, M.A., et al., *Direct interactions with the integrin β 1 cytoplasmic tail activate the Abl2/Arg kinase*. J Biol Chem, 2015. **290**(13): p. 8360-72.
410. Hasan, N., D. Corbin, and C. Hu, *Fusogenic pairings of vesicle-associated membrane proteins (VAMPs) and plasma membrane t-SNAREs--VAMP5 as the exception*. PloS one, 2010. **5**(12): p. e14238-e14238.
411. Gibon, J., et al., *The X-linked inhibitor of apoptosis regulates long-term depression and learning rate*. The FASEB Journal, 2016. **30**(9): p. 3083-3090.
412. Lin, X., et al., *Genetic deletion of Rnd3 results in aqueductal stenosis leading to hydrocephalus through up-regulation of Notch signaling*. Proc Natl Acad Sci U S A, 2013. **110**(20): p. 8236-41.
413. Pfenninger, K., et al., *Regulation of membrane expansion at the nerve growth cone*. Journal of cell science, 2003. **116**: p. 1209-17.
414. Nehme, N.T., et al., *MST1 mutations in autosomal recessive primary immunodeficiency characterized by defective naive T-cell survival*. Blood, 2012. **119**(15): p. 3458-3468.

415. Song, H.-R., et al., *Nuclear factor IA is expressed in astrocytomas and is associated with improved survival*. Neuro-oncology, 2010. **12**(2): p. 122-132.
416. Du, P., et al., *Comparison of Beta-value and M-value methods for quantifying methylation levels by microarray analysis*. BMC Bioinformatics, 2010. **11**(1): p. 587.
417. Pidsley, R., et al., *Critical evaluation of the Illumina MethylationEPIC BeadChip microarray for whole-genome DNA methylation profiling*. Genome Biology, 2016. **17**(1): p. 208.
418. Wang, H., et al., *Targeting interleukin 6 signaling suppresses glioma stem cell survival and tumor growth*. Stem cells (Dayton, Ohio), 2009. **27**(10): p. 2393-2404.
419. Chang, A.L., et al., *CCL2 Produced by the Glioma Microenvironment Is Essential for the Recruitment of Regulatory T Cells and Myeloid-Derived Suppressor Cells*. Cancer Research, 2016. **76**(19): p. 5671.
420. Krenciute, G., et al., *Transgenic Expression of IL15 Improves Antiglioma Activity of IL13Rα2-CAR T Cells but Results in Antigen Loss Variants*. Cancer Immunology Research, 2017. **5**(7): p. 571.
421. Tomaselli, S., F. Locatelli, and A. Gallo, *The RNA editing enzymes ADARs: mechanism of action and human disease*. Cell and Tissue Research, 2014. **356**(3): p. 527-532.
422. Paz, N., et al., *Altered adenosine-to-inosine RNA editing in human cancer*. Genome Res, 2007. **17**(11): p. 1586-95.
423. Xu, Y., et al., *Transcription factor PU.1 is involved in the progression of glioma*. Oncol Lett, 2018. **15**(3): p. 3753-3759.
424. Pollack, I.F., et al., *The Relationship between *TP53* Mutations and Overexpression of p53 and Prognosis in Malignant Gliomas of Childhood*. Cancer Research, 1997. **57**(2): p. 304.
425. Han, S., et al., *LPS alters the immuno-phenotype of glioma and glioma stem-like cells and induces in vivo antitumor immunity via TLR4*. J Exp Clin Cancer Res, 2017. **36**(1): p. 83.
426. Yao, R.R., et al., *M2-polarized tumor-associated macrophages facilitated migration and epithelial-mesenchymal transition of HCC cells via the TLR4/STAT3 signaling pathway*. World J Surg Oncol, 2018. **16**(1): p. 9.
427. Chen, C., et al., *FOXO1 associated with sensitivity to chemotherapy drugs and glial-mesenchymal transition in glioma*. J Cell Biochem, 2019. **120**(1): p. 882-893.
428. Yuan, Z., et al., *Regulation of neuronal cell death by MST1-FOXO1 signaling*. The Journal of biological chemistry, 2009. **284**(17): p. 11285-11292.
429. Pu, W., et al., *Correlation of the invasive potential of glioblastoma and expression of caveola-forming proteins caveolin-1 and CAVINI*. Journal of Neuro-Oncology, 2019. **143**(2): p. 207-220.
430. Zhang, Y., et al., *An RNA-sequencing transcriptome and splicing database of glia, neurons, and vascular cells of the cerebral cortex*. J Neurosci, 2014. **34**(36): p. 11929-47.
431. Banati, R.B., R. Myers, and G.W. Kreutzberg, *PK ('peripheral benzodiazepine')--binding sites in the CNS indicate early and discrete brain lesions: microautoradiographic detection of [3H]PK11195 binding to activated microglia*. J Neurocytol, 1997. **26**(2): p. 77-82.

432. Freije, W.A., et al., *Gene expression profiling of gliomas strongly predicts survival*. Cancer Res, 2004. **64**(18): p. 6503-10.
433. Gladson, C.L., R.A. Prayson, and W.M. Liu, *The pathobiology of glioma tumors*. Annu Rev Pathol, 2010. **5**: p. 33-50.
434. Martinez, R., et al., *A microarray-based DNA methylation study of glioblastoma multiforme*. Epigenetics, 2009. **4**(4): p. 255-64.
435. Phillips, H.S., et al., *Molecular subclasses of high-grade glioma predict prognosis, delineate a pattern of disease progression, and resemble stages in neurogenesis*. Cancer Cell, 2006. **9**(3): p. 157-73.
436. Verhaak, R.G., et al., *Integrated genomic analysis identifies clinically relevant subtypes of glioblastoma characterized by abnormalities in PDGFRA, IDH1, EGFR, and NF1*. Cancer Cell, 2010. **17**(1): p. 98-110.

437. Agushi, E. *Translocator Protein and Methionine PET Imaging in Glioma* (Unpublished doctoral dissertation) University of Manchester, Manchester, UK., 2019.

438. *Infinium HD Methylation Assay Protocol Guide*. support.illumina.com/sds.html.

Appendix

a) Overall Survival Table

| TSPO | Time | Status | Cumulative Proportion Surviving at the Time | | N of Cumulative Events | N of Remaining Cases | |
|------|------|---------|---------------------------------------------|------------|------------------------|----------------------|----|
| | | | Estimate | Std. Error | | | |
| high | 1 | 6.000 | event | .944 | .054 | 1 | 17 |
| | 2 | 29.000 | event | .889 | .074 | 2 | 16 |
| | 3 | 39.000 | event | . | . | 3 | 15 |
| | 4 | 39.000 | event | .778 | .098 | 4 | 14 |
| | 5 | 48.000 | event | .722 | .106 | 5 | 13 |
| | 6 | 54.000 | event | .667 | .111 | 6 | 12 |
| | 7 | 65.000 | alive | . | . | 6 | 11 |
| | 8 | 67.000 | event | .606 | .116 | 7 | 10 |
| | 9 | 75.000 | alive | . | . | 7 | 9 |
| | 10 | 78.000 | event | .539 | .121 | 8 | 8 |
| | 11 | 83.000 | alive | . | . | 8 | 7 |
| | 12 | 88.000 | alive | . | . | 8 | 6 |
| | 13 | 90.000 | alive | . | . | 8 | 5 |
| | 14 | 92.000 | alive | . | . | 8 | 4 |
| | 15 | 94.000 | alive | . | . | 8 | 3 |
| | 16 | 102.000 | alive | . | . | 8 | 2 |
| | 17 | 105.000 | alive | . | . | 8 | 1 |
| | 18 | 115.000 | alive | . | . | 8 | 0 |
| low | 1 | 34.000 | event | .969 | .031 | 1 | 31 |
| | 2 | 63.000 | alive | . | . | 1 | 30 |
| | 3 | 66.000 | alive | . | . | 1 | 29 |
| | 4 | 67.000 | alive | . | . | 1 | 28 |
| | 5 | 70.000 | alive | . | . | 1 | 27 |
| | 6 | 73.000 | alive | . | . | 1 | 26 |
| | 7 | 75.000 | alive | . | . | 1 | 25 |
| | 8 | 75.000 | alive | . | . | 1 | 24 |
| | 9 | 77.000 | alive | . | . | 1 | 23 |
| | 10 | 78.000 | alive | . | . | 1 | 22 |
| | 11 | 79.000 | alive | . | . | 1 | 21 |
| | 12 | 82.000 | alive | . | . | 1 | 20 |
| | 13 | 83.000 | alive | . | . | 1 | 19 |

| | | | | | | |
|----|---------|-------|------|------|---|----|
| 14 | 83.000 | alive | . | . | 1 | 18 |
| 15 | 85.000 | event | .915 | .060 | 2 | 17 |
| 16 | 86.000 | alive | . | . | 2 | 16 |
| 17 | 87.000 | alive | . | . | 2 | 15 |
| 18 | 89.000 | alive | . | . | 2 | 14 |
| 19 | 89.000 | alive | . | . | 2 | 13 |
| 20 | 90.000 | alive | . | . | 2 | 12 |
| 21 | 90.000 | alive | . | . | 2 | 11 |
| 22 | 92.000 | alive | . | . | 2 | 10 |
| 23 | 93.000 | alive | . | . | 2 | 9 |
| 24 | 93.000 | alive | . | . | 2 | 8 |
| 25 | 93.000 | alive | . | . | 2 | 7 |
| 26 | 95.000 | alive | . | . | 2 | 6 |
| 27 | 111.000 | alive | . | . | 2 | 5 |
| 28 | 114.000 | alive | . | . | 2 | 4 |
| 29 | 115.000 | alive | . | . | 2 | 3 |
| 30 | 116.000 | alive | . | . | 2 | 2 |
| 31 | 118.000 | alive | . | . | 2 | 1 |
| 32 | 118.000 | alive | . | . | 2 | 0 |

b) Progression free Survival Table

| TSPO | Time | Status | Cumulative Proportion Surviving at the Time | | N of Cumulative Events | N of Remaining Cases | |
|------|------|---------|---------------------------------------------|------------|------------------------|----------------------|----|
| | | | Estimate | Std. Error | | | |
| high | 1 | 6.000 | event | .944 | .054 | 1 | 17 |
| | 2 | 13.000 | event | .889 | .074 | 2 | 16 |
| | 3 | 28.000 | event | .833 | .088 | 3 | 15 |
| | 4 | 31.000 | event | .778 | .098 | 4 | 14 |
| | 5 | 39.000 | alive | . | . | 4 | 13 |
| | 6 | 44.000 | alive | . | . | 4 | 12 |
| | 7 | 45.000 | alive | . | . | 4 | 11 |
| | 8 | 51.000 | event | .707 | .112 | 5 | 10 |
| | 9 | 62.000 | alive | . | . | 5 | 9 |
| | 10 | 67.000 | alive | . | . | 5 | 8 |
| | 11 | 68.000 | alive | . | . | 5 | 7 |
| | 12 | 73.000 | alive | . | . | 5 | 6 |
| | 13 | 81.000 | alive | . | . | 5 | 5 |
| | 14 | 85.000 | alive | . | . | 5 | 4 |
| | 15 | 93.000 | event | .530 | .175 | 6 | 3 |
| | 16 | 93.000 | alive | . | . | 6 | 2 |
| | 17 | 97.000 | event | .265 | .207 | 7 | 1 |
| | 18 | 103.000 | alive | . | . | 7 | 0 |
| low | 1 | 9.000 | alive | . | . | 0 | 31 |
| | 2 | 11.000 | event | .968 | .032 | 1 | 30 |
| | 3 | 20.000 | alive | . | . | 1 | 29 |
| | 4 | 28.000 | event | .934 | .045 | 2 | 28 |
| | 5 | 36.000 | event | .901 | .054 | 3 | 27 |
| | 6 | 42.000 | event | .868 | .062 | 4 | 26 |
| | 7 | 45.000 | alive | . | . | 4 | 25 |
| | 8 | 46.000 | event | .833 | .068 | 5 | 24 |
| | 9 | 51.000 | event | .798 | .074 | 6 | 23 |
| | 10 | 53.000 | event | . | . | 7 | 22 |
| | 11 | 53.000 | event | .729 | .082 | 8 | 21 |

| | | | | | | |
|----|---------|-------|------|------|----|----|
| 12 | 56.000 | event | .694 | .085 | 9 | 20 |
| 13 | 60.000 | event | .659 | .088 | 10 | 19 |
| 14 | 62.000 | alive | . | . | 10 | 18 |
| 15 | 67.000 | alive | . | . | 10 | 17 |
| 16 | 71.000 | alive | . | . | 10 | 16 |
| 17 | 78.000 | alive | . | . | 10 | 15 |
| 18 | 79.000 | event | .615 | .092 | 11 | 14 |
| 19 | 79.000 | alive | . | . | 11 | 13 |
| 20 | 79.000 | alive | . | . | 11 | 12 |
| 21 | 80.000 | alive | . | . | 11 | 11 |
| 22 | 81.000 | alive | . | . | 11 | 10 |
| 23 | 82.000 | alive | . | . | 11 | 9 |
| 24 | 84.000 | event | .547 | .104 | 12 | 8 |
| 25 | 84.000 | alive | . | . | 12 | 7 |
| 26 | 88.000 | alive | . | . | 12 | 6 |
| 27 | 101.000 | alive | . | . | 12 | 5 |
| 28 | 104.000 | event | .438 | .129 | 13 | 4 |
| 29 | 108.000 | alive | . | . | 13 | 3 |
| 30 | 111.000 | alive | . | . | 13 | 2 |
| 31 | 113.000 | alive | . | . | 13 | 1 |
| 32 | 114.000 | alive | . | . | 13 | 0 |

c) Polymorphism Overall Survival Table

| polymorphism | Time | Status | Cumulative Proportion Surviving at the Time | | N of Cumulative Events | N of Remaining Cases | |
|--------------|------|---------|---------------------------------------------|------------|------------------------|----------------------|----|
| | | | Estimate | Std. Error | | | |
| A147T | 1 | 29.000 | event | .964 | .035 | 1 | 27 |
| | 2 | 48.000 | event | .929 | .049 | 2 | 26 |
| | 3 | 63.000 | Alive | . | . | 2 | 25 |
| | 4 | 65.000 | Alive | . | . | 2 | 24 |
| | 5 | 67.000 | event | .890 | .060 | 3 | 23 |
| | 6 | 67.000 | Alive | . | . | 3 | 22 |
| | 7 | 69.000 | Alive | . | . | 3 | 21 |
| | 8 | 75.000 | Alive | . | . | 3 | 20 |
| | 9 | 77.000 | Alive | . | . | 3 | 19 |
| | 10 | 78.000 | event | .843 | .073 | 4 | 18 |
| | 11 | 78.000 | Alive | . | . | 4 | 17 |
| | 12 | 83.000 | Alive | . | . | 4 | 16 |
| | 13 | 86.000 | event | .790 | .085 | 5 | 15 |
| | 14 | 88.000 | Alive | . | . | 5 | 14 |
| | 15 | 89.000 | Alive | . | . | 5 | 13 |
| | 16 | 89.000 | Alive | . | . | 5 | 12 |
| | 17 | 90.000 | Alive | . | . | 5 | 11 |
| | 18 | 90.000 | Alive | . | . | 5 | 10 |
| | 19 | 92.000 | Alive | . | . | 5 | 9 |
| | 20 | 93.000 | Alive | . | . | 5 | 8 |
| | 21 | 94.000 | Alive | . | . | 5 | 7 |
| | 22 | 95.000 | Alive | . | . | 5 | 6 |
| | 23 | 114.000 | Alive | . | . | 5 | 5 |
| | 24 | 115.000 | Alive | . | . | 5 | 4 |
| | 25 | 115.000 | Alive | . | . | 5 | 3 |
| | 26 | 116.000 | Alive | . | . | 5 | 2 |
| | 27 | 118.000 | Alive | . | . | 5 | 1 |
| | 28 | 118.000 | Alive | . | . | 5 | 0 |
| normal | 1 | 6.000 | event | .955 | .044 | 1 | 21 |
| | 2 | 34.000 | event | .909 | .061 | 2 | 20 |
| | 3 | 39.000 | event | . | . | 3 | 19 |
| | 4 | 39.000 | event | .818 | .082 | 4 | 18 |
| | 5 | 54.000 | event | .773 | .089 | 5 | 17 |
| | 6 | 63.000 | Alive | . | . | 5 | 16 |
| | 7 | 66.000 | Alive | . | . | 5 | 15 |
| | 8 | 70.000 | Alive | . | . | 5 | 14 |
| | 9 | 73.000 | Alive | . | . | 5 | 13 |
| | 10 | 75.000 | Alive | . | . | 5 | 12 |

| | | | | | | |
|----|---------|-------|------|------|---|----|
| 11 | 75.000 | Alive | . | . | 5 | 11 |
| 12 | 82.000 | Alive | . | . | 5 | 10 |
| 13 | 83.000 | Alive | . | . | 5 | 9 |
| 14 | 83.000 | Alive | . | . | 5 | 8 |
| 15 | 85.000 | event | .676 | .119 | 6 | 7 |
| 16 | 86.000 | Alive | . | . | 6 | 6 |
| 17 | 90.000 | Alive | . | . | 6 | 5 |
| 18 | 92.000 | Alive | . | . | 6 | 4 |
| 19 | 93.000 | Alive | . | . | 6 | 3 |
| 20 | 93.000 | Alive | . | . | 6 | 2 |
| 21 | 105.000 | Alive | . | . | 6 | 1 |
| 22 | 111.000 | Alive | . | . | 6 | 0 |